

# Investigation Of Energetic Cosmic Explosions and their after-effects



Rupak Roy

Aryabhata Research Institute of observational sciences (ARIES)

Department of Physics, Kumaun University

A thesis submitted for the degree of

*Doctor of Philosophy*

DD - MM - YYYY

# Investigation of Energetic Cosmic Explosions and their after effects

A THESIS SUBMITTED TO  
**THE KUMAUN UNIVERSITY**  
FOR THE DEGREE OF  
**DOCTOR OF PHILOSOPHY**  
IN PHYSICS

*By*

**Rupak Roy**

**Aryabhata Research Institute of observational  
sciencES (ARIES)**

**Manora Peak, Nainital 263 129, India**

**December 2012**

---

## DECLARATION

I hereby declare that the work presented in this thesis is a result of the investigation carried out by me at the Aryabhata Research Institute of observational sciences (ARIES), Nainital, under the supervision of Dr. Brijesh Kumar (Scientist E, ARIES, Manora Peak, Nainital) and Co-Supervision of Prof. H. C. Chandola (Department of Physics, Kumaun University, Nainital). This thesis has not been submitted for the award of any degree, diploma, associateship or fellowship of any University or Institute.

Place : Nainital

Date :

(Rupak Roy)

---

## CERTIFICATE FROM THE SUPERVISORS

This is to certify that

The synopsis of the thesis entitled “**Investigation of Energetic Cosmic Explosions and their after effects**” for the award of the degree of Doctor of Philosophy in Physics was approved by the Kumaun University, Nainital (Letter no.-Res/43/Physics-2011, dated 12/11/2011).

This thesis embodies the work of Mr Rupak Roy himself.

Mr Rupak Roy worked under our joint supervisions for this thesis as a Research Fellow at the Aryabhata Research Institute of observational sciences (ARIES), Nainital. He has put in more than 200 days of attendance at ARIES, Nainital during this period.

This thesis has not been submitted before for the award of any degree, diploma, associateship or fellowship of any University or Institute.

Dr. Brijesh Kumar  
(Supervisor)  
ARIES,  
Manora Peak  
Nainital

Prof. H. C. Chandola  
(Co-Supervisor)  
Department of Physics  
Kumaun University  
Nainital



*To my family*



**Ancient mythology:** A Flammarion wood engraving by an unknown artist that first appeared in Camille Flammarion's *L'atmosphère: météorologie populaire* (1888). The image depicts a man crawling under the edge of the sky, depicted as if it were a solid hemisphere, to look at the mysterious Empyrean beyond.

Flammarion was a French astronomer and author of more than 70 books, who did more to encourage public interest in the subject than anyone else of his day, although many of his scientific and philosophical arguments were eccentric. His studies were especially on double and multiple stars and on the Moon and Mars.

---

## ACKNOWLEDGMENTS

31st May, 2006, still I can remember, when Howrah-Kathgodam Express train ends its journey at Kathgodam, and then a new journey of a mediocre student graduated from Delhi University was silently started there with lot of hopes and uncertainties, which he had started from a small city ‘Durgapur’ near Kolkata in West Bengal. After two consecutive days train journey he was tired and dejected but he had strongly determined attitude that not to give up and not to give in under any circumstances. He availed a local bus to reach 34 km. away to his destination an institution (ARIES) by the name of great Mathematician Aryabhata, situated on one of the mountaintops Nainital in order to attend ‘PhD interview call’. Soon, he realized in the bus that he was not alone in this journey to ARIES, there are some more passengers. Strong determination and positive attitude motivated him to give the best in the interview. So far nothing was special.

This is probably a very common pre-interview scenario for all educated youths throughout the world whether they are meritorious or not. Anyway, in the next morning, without having any clue about forthcoming destination he had to stand in the next morning before an ‘Experts panel in order to face the extreme reality of life. At last he was shortlisted and selected by the ‘Expert Panel’ who made him an offer joining-offer within next two months. This was the first step in the journey of thousand miles by a young Delhi University graduate from Durgapur.

Oh... I forgot to introduce this young man. People know him as Rupak Roy, a man who never had thought seriously to be an academician during his early school days. Rather, motivated by the art of soccer legends like Diego Armando Maradona, he always became fascinated in football and was closely associated with this game till the end of his school life. Although he had a little affection in mathematics and basic sciences, but it was a series of popular books on physics, published from Russia (former Soviet-Union), which transformed the way of his thinking. It is well known that sowing a seed in a well fertilized soil is not enough for its germination and growth – proper arrangement for sunlight, water along with airflow, are also essential. Being the youngest member of the family, he was fortunate enough to get all these three essential elements from his great parents who helped him to grow with proper care and nourishment in a healthy and congenial family atmosphere.

---

His parents: Mr. Ranjan Roy and Mrs. Gauri Roy, are always a source of his inspiration. His elder sister Sonali Roy (now Sonali Chatterjee) and her husband Sanjib Chatterjee are not only his close friends but also they are like his guardians. In fact, his sister Sonali never distinguished him from her son – Kaustav (he calls him Reet) and surprisingly Kaustav also mingles with him just as a friend without considering any generation gap. It is needless to say that without the motivation and mental supports of the family members and other relatives Rupak might not be able to reach his goal of higher education.

Establishing an institute or an organization with larger facility at a hilly area certainly has some logistical challenge. On the other hand, decentralization of higher education and research facility with a direct governmental funding is essential to produce high quality research output from every corner of the country. Probably this was one of the reasons for which in the year 2004, Department of Science and Technology (DST), Govt. of India took this challenge and undertook ‘Uttar Pradesh State Observatory’ (UPSO) as a new DST-wing – ‘Aryabhata Research Institute of observational Sciences (ARIES). I personally would like to gratitude all the members of UPSO, ARIES and DST and especially Prof. Ram Sagar, Director ARIES who came forward to make this quantum jump and bring this place in the limelight of world-class astrophysical and atmospheric research. As a researcher, he is one of the witnesses of the infrastructural development in ARIES over last 5–6 years. ARIES has already made a significant progress and we look forward for a betterment in logistic and research environment in this mountaintop – ‘Manora Peak’.

Rupak has spent an important part of his life in this ‘Kumaun range’ of Himalaya – far away from his native city. It is sure for him that in the rest part of his life, this place and time will remain to him as a nostalgia. The calm and quite behaviour of the people along with its scenic beauty makes this hill station memorable forever which any one must retain in his golden memory. Lush green, calm and quiet environment of the institute is amazing. All the faculties here are so easily approachable and the ‘Teacher-Student relationship’ does not hold for a long time after the pre-PhD coursework. One may criticize, but I would say this also establishes professionalism and highly motivate the juniors.

Rupak must be thankful to his supervisor Dr. Brijesh Kumar for his kind support and guidance throughout his stay in ARIES actually boosted his confidence and his

---

independent thinking ability. Being a researcher of completely different field, he started to work on Supernova keeping him at the front and helped to get a success. Certainly the life was not smooth, there were many ups and downs, but somehow they found their way. A special thanks is honoured to his co-supervisor Prof. H. C. Chandola, Department of Physics, Kumaun University for his invaluable suggestions and cooperation in completing Rupaks research work.

Rupak is also grateful to all the staff members of ARIES and Kumaun University, who extended their valuable support to complete his thesis work. In this regard special thanks must be delivered to the all the staffs of Computer and Library section of ARIES, who were always helpful to solve the issues of computer and library related work required for completion of his thesis. Rupak is also thankful to the staffs of cafeteria that provided him regular food in a homely atmosphere.

Rupak is also indebted to other comembers of his group – Dr. S. B. Pandey, Dr. Kuntal Misra and three juniors Brajesh, Subhash and Vijay for completing his research work. However his hostel life was fabulous. There was no difference between seniors and juniors. Seniors like Saurav, Kumar, Arti, Ramanpreet, Manas, Himali, Jessy, Neelam, Chrisphin, Chavi, Sanjeev, Amitav always were like his close friends. His batch-mets like Eswar, Rajesh, Pankaj and Akash, who shared the Office and Hostel rooms with him during first two years of his PhD, will always be remembered in his golden memory for their love and affection. In the last couple of years many new faces joined the ARIES family. Juniors like Ramkesh, Narendra, Tapaswani, Ravi, Devesh, Haritma, Hema, Archana, Sumit, Rajeev, Krishna, Jai, Pradeep, Piyush, Raman, Abhishek, Subhajeet, Neha, Praveen, Arti, Aditi and Aabha jointly represent a mixed research-squad and the true colour of ARIES. The special attachment with Abhishekh, Snehlata, Bimanda, Indranilda, Pradipda, Soumenda, Samaresh and their families never made him feel lonely.

This research has made use of the NASA/IPAC Extragalactic Database (NED) which is operated by the Jet Propulsion Laboratory (JPL), Caltech, under contract with the National Aeronautics and Space Administration (NASA). Rupak is highly blessed by the uses of NASA's Astrophysics Data System. He is also indebted to the Indo-Russian (DST-RFBR) Project No. RUSP-836 (RFBR-08-02:91314) for the completion of the entire research work and the thesis. This is the time to express his sincere thanks to the staffs of all observing facilities that have helped

---

him by providing data to prepare his thesis. Rupak is also grateful to all supporting and observing staffs of the Optical and near-Infrared telescopes – 0.45m ROTSE; 0.6m REM; 0.6m Lowell, 1m ST; 2m IGO; 2.6m NOT; 2m UKIRT; 3.6m TNG; 3.6m NTT; 6m BTA; 6m MMT; 8m VLT and 9.2m HET who have extended their help to make his effort successful. For this thesis work entire Ultraviolet data was acquired from the archival system of space-based telescope *Swift*/UVOT obtained through the NASA’s ‘High Energy Astrophysics Science Archive Research Center’ (HEASARC) on-line service, provided by the NASA/Goddard Space Flight Center. The National Radio Astronomy Observatory is a facility of the National Science Foundation operated under co-operative agreement by Associated Universities Inc. This is to thank the VLA staffs for easy access to the archival data base.

The author is also highly gratified to Dr. F. Sutaria, Dr. A. Ray, Dr. S. Benetti, Dr. A. Pastorello, Dr. F. Bufano, Dr. V. V. Sokolov, Dr. T. Sokolova, Dr. A. S. Moskvitin, Dr. T. A. Fatkhullin, Dr. G. Leloudas, Dr. J. R. Maund, Dr. J. Hjorth, Dr. C. Gabriel, Dr. A. J. Drake and Dr. P. J. Brown for their kind support and valuable suggestion to carry out this research work. This is also the time to express the thanks to the ‘Committee on Space Research’ (COSPAR), the scientific organization which gave the opportunity to Rupak to explore his research work.

However, this institution brought many surprises in his life, but the turning point that made him more responsible than ever before was the year 2007 when he met Sumana, another research fellow who joined ARIES under a DST project. As both of them had a common native language, they used to share their thoughts, feelings and daily experiences which rather strengthen their friendship into a permanent relationship. None of them knows when they were united and prepared themselves for an everlasting relationship. Both of them were a mental support for each other which made their life more colourful and more beautiful. In this regard Rupak must tender his esteem to Dr. S. G. Nandi (his father-in-law) and Mrs. Arati Nandi (his mother-in-law) and his two beautiful sisters Suranjana and Sudarshana (both of them are research fellow) who at different times have encouraged and motivated him to reach his goal.

Dear friends, you must be wondering and highly eager to exhibit my identity. I had already mentioned about my close association with Rupak over a long time. It is difficult for me to remember exactly the date and time when I met him for the first

---

time but it certainly not before his parents. We first introduced to each other when Rупak was just a baby to realize the external world with his five-sense organs. With course of time our intimacy grew up since we were able to differentiate between good and bad in the society and the people surrounding him started to feel his presence and existence. Yes, you are right to recognize me. I am the consciousness of Rупak that he has gained throughout his life by means of an immense interaction with the world. This thesis is a tribute to all the people who like Rупak and realizes his understanding about the society and believe in his dream.

RUPAK ROY



The great Tycho supernova of 1572. Drawing from 'Astronomie Populaire', by C. Flammarion.

---

## PREFACE

Very massive stars ( $> 10M_{\odot}$ ) undergoes a cosmic explosion at the end of its lifetime. Inner core forms a compact object due to gravitational collapse, while material at the outer shells expelled out in the form of a catastrophic explosion (energy  $\geq 10^{51}$  ergs) through intense flashes of  $\gamma$ -ray and X-ray or UV radiation depending on their initial mass, explosion energy and geometry of explosion mechanism. The ultra compact object may be a ‘Black Hole’ or a ‘Neutron star’ whereas the cosmic explosion leads to the events classified as Gamma Ray Burst (GRBs), X-ray flashes (XRFs) or Supernova (SN) depending on the initial dynamics of the progenitor.

History of Supernova is much older than GRBs and XRFs. Probable first discovery is the birth of Crab nebula in the year 1054, mentioned in Chinese, Japanese and Persian history of astronomy. Second confirmed discovery was done by Tycho Brahe in the year 1572, which was the onset of a supernova, which was later came to be known as ‘Tycho supernova remnant’. Energetics of supernova can vary between  $10^{50}$  to  $10^{51}$  ergs. Depending on the physical scenario, they are categorized in two main sub-classes – (i) Core collapse events and (ii) Thermonuclear events.

In this thesis, a multiwavelength investigation of energetic Core collapse supernovae (CCSNe) explosions have been carried out. Several issues like nature of Type Ibc and II progenitors, the asymmetry scenario in Type Ib burst, the interaction signature of Type Ibc events and nature of Overluminous events have been revisited. In this thesis a set of events have been investigated that show a wide range in luminosity and explosion energy. The sample contain a normal Type IIP event (SN 2008gz), a relatively low-luminous event (SN 2008in), two Type Ib events (SNe 2007uy, 2008D), one nearby Type IIn event (SN 2010jl), an Overluminous Type IIn

---

event (CSS 100217) and an Overluminous Type Ic event (SN 2010kd). In the light of the objectives proposed for this thesis, the following main results are obtained.

Chapter 1 provides a basic introduction about the subject. In this chapter we have discussed different types of cosmic explosions and demonstrate the present understanding about CCSNe. We have also discussed different kinds of peculiarity of these catastrophe that have been discovered and explained by several research groups through out the world. The present issues in this regard have also been discussed and finally we have projected our goal for this thesis and also how it has been organized.

Chapter 2 is fully dedicated to introduce different kinds of tools and scientific techniques that were essential for completion of this research work. For the present thesis data from different telescopes had been acquired. A brief introduction about data acquisition and reductions in Ultraviolet, Optical, near-Infrared and Radio wavebands is presented. Though information gathered from different spectral regimes had been used for this work, but principal emphasize was on Optical data. So, that part has been discussed with a little elaboration. Short descriptions about different kinds of analyzing tools are also presented

In Chapter 3, we have presented *BVRI* photometric and low-resolution spectroscopic investigation of a Type II CCSN 2008gz, which occurred in a star forming, nearby spiral galaxy NGC 3672. The SN event was detected late, and a detailed investigation of its light curves and spectra spanning 200 days suggest that it is an event of type IIP similar to archetypal SNe 2004et and 1999em. However, in contrast

---

to other events of its class, the SN 2008gz exhibits rarely observed visual magnitude drop of 1.5 over the period of a month during plateau to nebular phase. We have estimate synthesized  $^{56}\text{Ni}$  mass of  $0.05 \pm 0.01 M_{\odot}$  and a mid-plateau  $M_V$  of  $-16.6 \pm 0.2$  mag. The photospheric velocity is observed to be higher than that was observed for SN 2004et at similar epochs, indicating explosion energy was comparable to or higher than SN 2004et. Similar trend was also seen for the expansion velocity of H-envelopes. By comparing its properties with other well studied events as well as by using a recent simulation of pre-SN models, we infer an explosion energy range of  $2 - 3 \times 10^{51}$  erg.

In Chapter 4 we have presented the optical photometric and low-resolution spectroscopic observations of the Type IIP SN 2008in, which occurred in the outskirts of the nearly face-on spiral galaxy M 61. Data in the X-rays, ultraviolet and near-infrared bands have been used to characterize this event. The SN field was imaged with the ROTSE-IIIb optical telescope about seven days before the explosion. The duration of the plateau phase, as derived from the photometric monitoring, was  $\sim 98$  days. The spectra of SN 2008in show a striking resemblance to those of the archetypal low-luminosity IIP SNe 1997D and 1999br. A comparison of ejecta kinematics of SN 2008in with the hydrodynamical simulations of Type IIP SNe indicates that it is a less energetic event ( $\sim 5 \times 10^{50}$  erg). However, the light curve indicates that the production of radioactive  $^{56}\text{Ni}$  is significantly higher than that in the low-luminosity SNe. The estimated amount of synthesized  $^{56}\text{Ni} \sim 0.015 M_{\odot}$ . We derived a pre-SN radius of  $\sim 126 R_{\odot}$ , an explosion energy of  $\sim 5.4 \times 10^{50}$  erg and a total ejected mass of  $\sim 16.7 M_{\odot}$ . We concluded the event as a low-energy explosion scenario of a relatively compact, moderate-mass progenitor star that generates a neutron star.

---

In Chapter 5 we have presented the results from a comprehensive analysis of two Type Ib SNe 2007uy and 2008D in a nearby galaxy NGC 2770, using data from space-based *Swift*/UVOT observations along with ground-based follow-up at visible, infrared and radio wave bands. Our study was mainly focused on Type Ib event SN 2007uy. As a complementary part we have also explored the evolution of Type Ib event SN 2008D which occurred in the same galaxy within a gap of 10 days. Spectroscopically, SN 2007uy was not similar to broad lined energetic Type Ibc events, but its peak absolute visual magnitude was  $\sim -18.8$ , which is about 1 mag brighter than the mean value for Type Ibc events. We did not find any evidence of dependency of asymmetry on the distribution of radioactive Ni inside the ejecta, at least for this particular case. Modeling of the optical bolometric light curve shows that about  $0.41 M_{\odot}$  radioactive  $^{56}\text{Ni}$  is produced and roughly  $2.01 M_{\odot}$  material was ejected during this catastrophe with liberated energy  $5.7 \times 10^{51}$  erg. The radio data shows a SSA dominated light curve evolution of SN 2007uy, though the contribution of FFA during the early phase can not be ruled out. We constrained the lower limit of pre-SN mass loss rate at  $\dot{M} \gtrsim 2.03 \times 10^{-5} M_{\odot} \text{ .yr}^{-1}$  and the lower limit of the progenitor mass at  $24 M_{\odot}$ , considering the compact remnant is a neutron star having mass  $1.5 - 2.0 M_{\odot}$ .

In Chapter 6 we have discussed a new class of transients discovered in last decade. We have very few information about these class of catastrophe. Many leading astronomical surveys are trying to catch more and more catastrophe of this kind. They are optically luminous and at least more than 2 mag brighter than normal catastrophe. Most of the time it is believed to be the end of a very massive star  $\gtrsim 60 M_{\odot}$ ,

---

and the explosion mechanism is ‘pair-instability’ process. Though recent investigations show that emergence of heavy magnetar or shock interaction can also produce a prolonged luminous plateau like light curve during a collapsing star. Spectroscopically they may be of Type II or Type I nature. In this present work three this kind of events were observed and their Optical photometric behaviors have been illustrated. CSS 100217 is the most luminous event, whereas peak brightness of SN 2010kd is almost comparable with the CSS event. SN 2010jl is a relatively nearby event and most probably a heavily interacting supernova created from a high mass star (initial mass  $\gtrsim 40 M_{\odot}$ ). At the end of this chapter observations of few other extremely energetic events like GRBs have also been discussed very shortly. The importance of such observations have also been presented.

---

## LIST OF PUBLICATIONS

### In refereed journals

1. **SN 2008gz most likely a normal type IIP event**

**Rupak Roy**, Brijesh Kumar, Alexander S. Moskvitin, Stefano Benetti, Timur A. Fatkhullin, Brajesh Kumar, Kuntal Misra, Filomena Bufano, Ralph Martin, Vladimir V. Sokolov, S. B. Pandey, H. C. Chandola, Ram Sagar

*2011; Monthly Notices of the Royal Astronomical Society; 414; 167; doi: 10.1111/j.1365-2966.2011.18363.x*

2. **The Discovery and Nature of Optical Transient CSS100217:102913+404220**

A.J. Drake, S.G. Djorgovski, A. Mahabal, J. Anderson, **R. Roy**, V. Mohan, S. Ravindranath, D. Frail, S. Gezari, James D. Neill, L.C. Ho, J.L. Prieto, D. Thompson, J. Thorstensen, M. Wagner, R. Kowalski, J. Chiang, J.E. Grove, F.K. Schinzel, D.L. Wood, L. Carrasco, E. Recillas, L. Kewley, K.N. Archana, Aritra Basu, Yogesh Wadadekar, Brijesh Kumar, A.D. Myers, E.S. Phinney, R. Williams, M.J. Graham, M. Catelan, E. Beshore, S. Larson and E. Christensen

*2011; The Astrophysical Journal; 735; 106; doi : 10.1088/0004-637X/735/2/106*

3. **SN 2008in – Bridging the gap between normal and faint supernovae of type IIP**

**Rupak Roy**, Brijesh Kumar, Stefano Benetti, Andrea Pastorello, Fang Yuan, Peter J. Brown, Stefan Immler, Timur A. Fatkhullin, Alexander S. Moskvitin, Justyn Maund, Carl W. Akerlof, J. Craig Wheeler, Vladimir V. Sokolov, Rorbert M. Quimby, Filomena Bufano, Brajesh Kumar, Kuntal Misra, S. B. Pandey, Nancy Elias-Rosa, Peter W. A. Roming and Ram Sagar

*2011; The Astrophysical Journal; 736 ; 76 ; doi : 10.1088/0004-637X/736/2/76*

---

#### 4. **The complex light curve of the afterglow of GRB071010A**

S. Covino, P. D'Avanzo, A. Klotz, D. A. Perley, L. Amati, S. Campana, G. Chincarini, A. Cucchiara, V. DElia, D. Guetta, C. Guidorzi, D. A. Kann, A. Kupcu Yoldas K. Misra, G. Olofsson, G. Tagliaferri, L. A. Antonelli, E. Berger, J. S. Bloom, M. Boer, C. Clemens, F. DAlessio, M. Della Valle, S. di Serego Alighieri, A. V. Filippenko, R. J. Foley, D. B. Fox, D. Fugazza, J. Fynbo, B. Gendre, P. Goldoni, J. Greiner, D. Kocevski, E. Maiorano, N. Masetti, E. Meurs, M. Modjaz, E. Molinari, A. Moretti, E. Palazzi, S. B. Pandey, S. Piranomonte, D. Poznanski, N. Primak, P. Romano, E. Rossi, **R. Roy**, J. M. Silverman, L. Stella, G. Stratta, V. Testa, S. D. Vergani, F. Vitali and F. Zerbi

*2008; Monthly Notices of the Royal Astronomical Society; 388; 347; doi : 10.1111/j.1365-2966.2008.13393.x*

#### 5. **SN 2007uy : Metamorphosis of an asymmetric Type Ib event**

**Rupak Roy**, Brijesh Kumar, Justyn R. Maund, Patricia Schady, Felipe Olivares E., Daniele Malesani, Giorgos Leloudas, Sumana Nandi, Nial Tanvir, Dan Milisavljevic, Jens Hjorth, Kuntal Misra, Brajesh Kumar, S. B. Pandey, H. C. Chandola, Ram Sagar

*Under review in 'Monthly Notices of the Royal Astronomical Society'*

#### 6. **Light curve and spectral evolution of the type IIb SN 2011fu**

Brajesh Kumar, S. B. Pandey, D. K. Sahu, J. Vinko, A. S. Moskvitin, G. C. Anupama, V. K. Bhatt, A. Ordasi, V. V. Sokolov, T. N. Sokolova, V. N. Komarova, Brijesh Kumar, Subhash Bose, **Rupak Roy**, Ram Sagar

*Under review in 'Monthly Notices of the Royal Astronomical Society'*

### **In conference proceedings**

#### 1. **A subluminescent Type IIP Supernova 2008in having properties unknown so far**

---

**Rupak Roy, Brijesh Kumar**

*ASI Conference Series, 2012, Vol. 5, pp 115 – 122*

**2. Spectral and photometric monitoring of distant core-collapse supernovae in the SAO RAS**

A. S. Moskvitin, T. A. Fatkhullin, V. V. Sokolov, V. N. Komarova, A. J. Drake, **R. Roy**, D. Yu. Tsvetkov

*2010; Astrophysical Bulletin; 65; 243; doi: 10.1134/S1990341310030041*

**In Abstract**

**1. SN 2010kd – A Super-luminous, Pair-instability Supernova?**

Jozsef Vinko, W. Zheng, S. B. Pandey, R. Quimby, A. Romadan, **R. Roy**, K. Takats, E. Chatzopoulos, J. C. Wheeler, N. Whallon, F. Yuan, C. Akerlof, D Pooley

*American Astronomical Society, AAS Meeting #219, #436.04*

**2. Optical follow-up of core-collapse supernovae 2010hq and 2010jl**

**Rupak Roy**, Firoza Suturia, Brijesh Kumar, Sayan Chakraborti, Alak Ray, Jose Prieto

*Proceedings of the 29th Meeting of the Astronomical Society of India, held 23-25 February, 2011. ASI Conference Series, Vol. 3, Edited by P. Khare and C. H. Ishwara-Chandra, 2011, p. 124*

**In GCN Circular / CBET**

**1. SUPARNOVA 2012A IN NGC 3239**

**Rupak Roy** and Sayan Chakraborti

*CBET 2975*

---

2. **GRB 090424 : Multiband Optical observation from Nainital**

**Rupak Roy**, Brajesh Kumar, S. B. Pandey and Brijesh Kumar

*GCN Circular 9278*

3. **SUPERNOVAE 2009du – 2009dy**

A. J. Drake, S. G. Djorgovski, A. Mahabal, R. Williams and M. J. Graham, A. S. Moskvitin, T. A. Fatkhullin, V. V. Sokolov, O. I. Spiridonova, A. F. Valeev, E. Sonbas, S. B. Pandey, B. Kumar, **R. Roy**, D. Y. Tsvetkov, M. Catelan, E. C. Beshore S. M. Larson, E. Christensen

*CBET 1791*

4. **SUPERNOVA 2009db**

A. J. Drake, S. G. Djorgovski, A. Mahabal, R. Williams, M. J. Graham, A. S. Moskvitin, T. A. Fatkhullin, V. V. Sokolov, O. I. Spiridonova, and A. F. Valeev, E. Sonbas, S. B. Pandey, B. Kumar, **R. Roy**, D. Y. Tsvetkov, M. Catelan, E. C. Beshore, S. M. Larson, E. Christensen

*CBET 1760*

5. **GRB 081222: Optical afterglow observation**

**Rupak Roy**, Brajesh Kumar, S. B. Pandey

*GCN Circular 8717*

6. **GRB 081128: Optical afterglow observations**

Brajesh Kumar, S. B. Pandey, **Rupak Roy**

*GCN Circular 8628*

7. **GRB 080430: Optical observations**

S. B. Pandey, **Rupak Roy**, Brijesh Kumar

*GCN Circular 7663*

8. **GRB 071013: Optical observations**

**Rupak Roy**, K. Misra and S. B. Pandey

---

*GCN Circular 6913*

9. **GRB 071011: Optical observations**

S. B. Pandey, K. Misra, **Rupak Roy**

*GCN Circular 6899*

10. **Optical observations: GRB 071010A**

**Rupak Roy**, K. Misra and S. B. Pandey

*GCN Circular 6880*

11. **GRB 071003 Optical observations**

K. Misra, S. B. Pandey, **Rupak Roy**,

*GCN Circular 6840*

12. **GRB 070917: R band observations**

K. Misra, S. B. Pandey, **Rupak Roy**,

*GCN Circular 6793*

13. **GRB 070419A, Optical observations**

S. B. Pandey, **Rupak Roy** and Saurabh Sharma

*GCN Circular 6320*

---

# NOTATIONS AND ABBREVIATIONS

The notations and abbreviations which have been used for this thesis are collected here for a quick reference. All these notations and abbreviations have been also explained on their first appearance in the text.

## Notations

$\text{\AA}$	Angstrom (unit of wavelength)
$\alpha$	spectral index
$\alpha_{inj}$	injection spectral index
$'$ , arcmin	arc minute
$''$ , arcsec	arc second
$cm$	centimeter
D	the aperture of the telescope
$Dec.$ , $\delta$	Declination
$^{\circ}$ , deg	Degree
$eV$	Electron Volt
Fig.	Figure
$GHz$	Giga Hertz
$Hz$	Hertz (unit of frequency)
$H_0$	Hubble constant
h, hr	Hour
hrs	Hours
$J2000$	epoch of observation
$km$	Kilo meter
$\lambda$	Wavelength
$Jy$	Jansky
$kpc$	Kilo parsec (unit of distance)
$M_{\odot}$	Mass of the Sun
$Mpc$	Mega parsec
m	meter
mm	milli meter
$\mu m$	micro meter

---

milliarcsec	milli arcsecond
min	Minutes
$\Omega_m$	Matter density of the Universe
$\Omega_\Lambda$	Vacuum energy density
<i>pc</i>	Parsec (unit of distance)
<i>Ref.</i>	References
<i>RA</i>	Right Ascension
rms, $\sigma$	root mean square
s, sec	Seconds
Sect.	Section
W	watt
yr	year
<i>z</i>	Redshift

## Abbreviations

<i>AGN</i>	Active Galactic Nuclei
<i>AIPS</i>	Astrophysical Image Processing System
<i>ARIES</i>	Aryabhata Research Institute of observational sciencES
<i>BTA</i>	Big Telescope Alt-azimuthal
<i>CBET</i>	Central Bureau for Electronic Telegrams
<i>CCD</i>	Charge Coupled Device
<i>CRTS</i>	Catalina Real-Time Transient Surveys
<i>CSM</i>	Circumstellar medium
<i>CSS</i>	Catalina Sky Survey
<i>DAOPHOT</i>	Dominion Astrophysical Observatory Photometry (software)
DST	Department of Science and Technology, Govt. of India
<i>FITS</i>	Flexible Image Transport System
<i>FWHM</i>	Full Width at Half Maximum

---

<i>HCT</i>	Himalayan Chandra Telescope
<i>HEASARC</i>	High Energy Astrophysics Science Archive Research Center
<i>HET</i>	Hobby Eberly Telescope
<i>HST</i>	Hubble Space Telescope
<i>GMRT</i>	Giant Metrewave Radio Telescope
<i>IAO</i>	Indian Institute of Astrophysics
<i>IAU</i>	International Astronomical Union
<i>IAUC</i>	International Astronomical Union Circular
<i>IIA</i>	Indian Institute of Astrophysics
<i>ISM</i>	Interstellar medium
<i>IGM</i>	Inter galactic medium
<i>IGO</i>	IUCAA Girawali Observatory
<i>IRAF</i>	Image Reduction and Analysis Facility
<i>IUCAA</i>	Inter University Center for Astronomy and Astrophysics
<i>JPL</i>	Jet Propulsion Laboratory
<i>LOSS</i>	Lick Observatory Supernova Search
<i>NED</i>	NASA Extragalactic Database
<i>MIDAS</i>	Munich Image and Data Analysis System
<i>NASA</i>	National Aeronautics and Space Administration
<i>NGC</i>	New General Catalogue
<i>NOAO</i>	National Optical Astronomy Observatories
<i>NOT</i>	Nordic Optical Telescope
<i>NRAO</i>	National Radio Astronomical Observatories
<i>NTT</i>	New Technology Telescope
<i>PTF</i>	Palomar Transient Factory
<i>QE</i>	Quantum Efficiency
<i>RFI</i>	Radio Frequency Interference
<i>REM</i>	Rapid Eye Mount
<i>ROTSE</i>	Robotic Optical Transient Search Experiment
<i>ST</i>	Sampurnanand Telescope
<i>TNG</i>	Telescopio Nazionale Galileo
<i>UKIRT</i>	United Kingdom Infra-Red Telescope
<i>UPSO</i>	Uttar Pradesh State Observatory

---

<i>USNO</i>	United States Naval Observatory
<i>UT</i>	Universal Time
<i>UVOT</i>	Ultra-Violet Optical Telescope
<i>VLA</i>	Very Large Array
<i>VLT</i>	Very Large Telescope
<i>WSRT</i>	Westerbrok Synthesis Radio Telescope
<i>XRT</i>	X-ray Telescope

# Contents

<b>Contents</b>	<b>xxv</b>
<b>List of Figures</b>	<b>xxix</b>
<b>List of Tables</b>	<b>xxxix</b>
<b>1 Introduction</b>	<b>1</b>
1.1 Cosmic Explosions . . . . .	1
1.1.1 Types of Cosmic Explosions . . . . .	2
1.2 Supernovae . . . . .	5
1.2.1 Brief History . . . . .	5
1.2.2 Observed properties of SNe and taxonomy . . . . .	6
1.2.3 Supernova rate and detection probability . . . . .	13
1.2.4 Different mechanisms for SNe explosions . . . . .	16
1.3 Core collapse supernovae . . . . .	16
1.3.1 Explosion mechanism of CCSNe . . . . .	18
1.3.2 Interactions with surroundings and after-effects . . . . .	23
1.3.3 Radiations emitted from explosions: light curves and spectra . . . . .	30
1.3.4 Fate of the progenitors . . . . .	43
1.4 Overluminous SNe and Gamma Ray Bursts . . . . .	46
1.4.1 Overluminous Supernovae (OLSNe) . . . . .	47
1.4.2 Gamma Ray Bursts (GRBs) . . . . .	48
1.5 Motivation of the work & organization of the thesis: . . . . .	51
<b>2 Facilities, observations and data reduction</b>	<b>53</b>
2.1 Introduction . . . . .	53
2.2 Data acquisition at optical and near infrared wavebands . . . . .	55
2.2.1 The optical telescopes . . . . .	55
2.2.2 Optical filters for ground-based telescopes . . . . .	56
2.2.3 The detectors for imaging . . . . .	57
2.2.4 The spectrograph . . . . .	60

# CONTENTS

---

2.2.5	The near infrared telescopes . . . . .	62
2.3	Optical and near infrared Photometry . . . . .	62
2.3.1	Pre-processing . . . . .	63
2.3.2	Processing . . . . .	67
2.3.3	Post-processing . . . . .	72
2.4	Optical Spectroscopy . . . . .	76
2.4.1	Aperture Extraction . . . . .	77
2.4.2	Wavelength Calibration . . . . .	78
2.4.3	Flux Calibration . . . . .	79
2.5	Acquisition and reduction of <i>Swift</i> /UVOT data . . . . .	79
2.6	Data acquisition at Radio wavebands . . . . .	80
2.7	Data reduction strategy at Radio wavebands . . . . .	85
2.7.1	Pre-processing . . . . .	86
2.7.2	Data editing . . . . .	87
2.7.3	Calibration . . . . .	88
2.7.4	Imaging . . . . .	90
<b>3</b>	<b>The normal Type IIP SN 2008gz</b>	<b>91</b>
3.1	Introduction . . . . .	91
3.2	Broad band photometry . . . . .	95
3.2.1	Observation & data reduction . . . . .	95
3.2.2	Optical light curve . . . . .	97
3.3	Low resolution spectroscopy . . . . .	100
3.3.1	Data . . . . .	100
3.3.2	Optical spectra . . . . .	100
3.4	Temporal evolution of spectral lines . . . . .	107
3.5	Photospheric and H-envelope velocities of ejecta . . . . .	112
3.6	Distance and extinction of SN 2008gz . . . . .	120
3.7	Temporal Evolution of colour and bolometric luminosity . . . . .	122
3.8	Physical Parameters . . . . .	125
3.8.1	Amount of ejected radioactive Nickel . . . . .	125
3.8.2	Environment of the progenitor . . . . .	128
3.8.3	Properties of progenitor star . . . . .	130
3.9	Comparison with other core collapse supernovae . . . . .	131
3.10	summary . . . . .	135
<b>4</b>	<b>The subluminous Type IIP SN 2008in</b>	<b>137</b>
4.1	Introduction . . . . .	137
4.2	observation and data reduction . . . . .	140
4.2.1	Photometric Observation . . . . .	140
4.2.2	X-ray Observations . . . . .	142

4.2.3	Optical Spectroscopic Observation . . . . .	143
4.3	Light Curve Evolution . . . . .	147
4.3.1	The Rising Phase . . . . .	147
4.3.2	The Plateau and Nebular Phase . . . . .	152
4.4	Spectroscopic Evolution . . . . .	153
4.5	extinction and distance toward SN 2008in . . . . .	164
4.6	Color Evolution and Bolometric Flux . . . . .	166
4.7	Physical Parameters . . . . .	169
4.7.1	Produced Radioactive Nickel . . . . .	169
4.7.2	Explosion Energy and Mass of Progenitor Star . . . . .	171
4.8	Discussion in context of other Type IIP SNe . . . . .	173
4.9	conclusion . . . . .	177
<b>5</b>	<b>The stripped envelope SNe 2007uy and 2008D</b>	<b>181</b>
5.1	Introduction . . . . .	181
5.2	Observation and data reduction . . . . .	186
5.3	Multiband photometry . . . . .	186
5.3.1	SN 2007uy: . . . . .	186
5.3.2	SN 2008D: . . . . .	192
5.4	Optical Spectroscopy of SN 2007uy . . . . .	193
5.4.1	Radio observation of SN 2007uy . . . . .	194
5.5	Photometric evolution of SN 2007uy & SN 2008D . . . . .	195
5.5.1	Evolution of SN 2007uy: NUV, Optical and NIR . . . . .	195
5.5.2	<i>BVRI</i> evolution of SN 2008D . . . . .	196
5.5.3	Early phase: first 40 days . . . . .	199
5.5.4	Late phase: beyond 50 days . . . . .	206
5.6	Distance and extinction toward SN 2007uy and SN 2008D. . . . .	209
5.7	Colour Evolution and Bolometric Flux . . . . .	213
5.8	Spectroscopic Evolution of SN 2007uy . . . . .	216
5.8.1	Evolution of some spectral lines: a message regarding asymmetry in SN 2007uy . . . . .	220
5.9	Modeling of SN 2007uy: Optical and Radio light curve . . . . .	230
5.9.1	Optical data modeling . . . . .	230
5.9.2	Radio data modeling . . . . .	234
5.10	Conclusion . . . . .	240
<b>6</b>	<b>The overluminous SNe – SN 2010jl, CSS 100217, SN 2010kd</b>	<b>243</b>
6.1	Introduction . . . . .	243
6.2	Luminous Type IIn SN 2010jl at redshift, $z = 0.0107$ . . . . .	245
6.2.1	Observational setup and reduction strategy . . . . .	246
6.2.2	Optical photometry and light curves . . . . .	250

# CONTENTS

---

6.3	Over-luminous event CSS 100217 at redshift, $z = 0.147$ . . . . .	254
6.3.1	Reduction and calibration strategy . . . . .	255
6.3.2	Optical photometry and light curves . . . . .	258
6.4	Over-luminous Type Ic event SN 2010kd at redshift, $z \sim 0.1$ . . . . .	261
6.4.1	Photometry and Calibration . . . . .	263
6.4.2	Optical light curve . . . . .	265
6.5	Discussion on photometric properties, comparison with other events .	266
<b>7</b>	<b>Summary, conclusions and future prospects</b>	<b>273</b>
7.1	Summary and conclusions . . . . .	273
7.2	Future Prospects . . . . .	277
7.2.1	Nature of subluminous and overluminous Type II events . . . . .	278
7.2.2	Occurrence rate of peculiar Type IIP events & their progenitors	279
7.2.3	Type II events as a source of cosmic dust . . . . .	280
7.2.4	Asymmetric nature of SN explosion . . . . .	281
	<b>Bibliography</b>	<b>283</b>

# List of Figures

1.1	Observed transient events on the Luminosity-Time diagram (LTD) (left) and Energy-Time Diagram (ETD) (right) produced respectively by Kasliwal [2011] and Soker and Kashi [2011] . . . . .	4
1.2	The current classification scheme of supernovae. The figure has been borrowed from Turatto [2003] . . . . .	7
1.3	The Schematic blue band light curves for SNe of Types Ia, Ib, II-L, II-P, and peculiar Type II SN 1987A, borrowed from Filippenko [1997]. The curve for SNe Ib includes SNe Ic as well, and represents an average. Figure shows the canonical nature of SN light curves. . .	11
1.4	Typical evolution of spectra of different types of supernova – Near maxima, 3 weeks and one year after maxima [Turatto, 2003] . . . . .	12
1.5	<b>Upper-left panel:</b> The plot has been reproduced from Lennarz et al. [2012]. It shows the number of detected SNe per year. The discovery year of SN1987A is marked with a dashed line. The fraction of bright SNe, which have a magnitude at maximum $\leq 15$ mag, is indicated by the hatched area. <b>Upper-right panel:</b> Also taken from Lennarz et al. [2012], showing the ratio between Type Ia and CCSNe as a function of redshift. <b>Lower panel:</b> This plot, taken from Li et al. [2011], shows the observed fractions of the subclasses of SNe in a volume-limited sample, illustrated as pie charts. The fractions of SNe Ic and IIb are upper limits, while that of SN 1991T-like objects is a lower limit. Also, the subclass of SNe Ibc-pec consists of broad-lined SNe Ic, peculiar objects. . . . .	14

## LIST OF FIGURES

---

- 1.6 The sequence of five events in the collapse of a stellar core to a nascent neutron star. It begins with a massive star with an onion-skin structure (1st stage, at the top-left corner), goes through white-dwarf core implosion (2nd stage), to core bounce and shock-wave formation (3rd stage), to the protoneutron-star stage before explosion (4th stage), and finally to the cooling and isolated-neutron-star stage (5th stage) after explosion. This figure is not to scale. The wavy arrows depict escaping neutrinos and the straight arrows depict mass motion. Figure has been taken from [Burrows \[2012\]](#). . . . . 17
- 1.7 The schematic representation of SN evolution after shock breakout. The left panel shows snapshot of the simplest case, where Hugoniot shocks are propagating outward after a point explosion i.e. , dimension of the exploding star is negligible in comparison to the dimension of the expanding ejecta [[Nadezhin, 1985](#)]. The right panel represents a relatively generalized case, where emissions from different regions have been indicated [[Fransson, 1982](#)]. . . . . 25
- 1.8 2D simulation of Rayleigh-Taylor (R-T) instability for a typical SN explosion [[Blondin and Ellison, 2001](#)]. With lower value of of adiabatic index ( $\gamma_{eff}$ ), effect of instability is more pronounced. . . . . 28
- 1.9 **Left panel:** The nuclear decay of radioactive  $^{56}\text{Ni}$  to  $^{56}\text{Co}$  and then to stable  $^{56}\text{Fe}$ . The energy released during this decay process is the main source that power the SNe. The figure has been borrowed from [Colgate and McKee \[1969\]](#). **Right panel:** The proposed shell structure of SN ejecta by [Falk and Arnett \[1977\]](#). The radioactive source was supposed to be at the innermost portion of the ejecta and other heavy elements are radially stratified. The fractions of stellar mass distributed in different shells are also shown. The  $\gamma$ -ray produced was supposed to get absorbed totally by the outer ejecta, that further produces the optical photons. The scenario changed after the occurrence of SN 1987A and the mixing of  $^{56}\text{Ni}$  in the ejecta was proposed. . . . 32
- 1.10 The schematic diagram of Type IIP lightcurve [[Nadyozhin, 2003](#)]. The abscissa is the time, while ordinate shows the log of luminosity. Lightcurve is segmented in three phases, (i)  $0 < t < \delta t$  is the breakout phase, (ii)  $\delta t < t < \delta t + \Delta t$  is called plateau phase, when luminosity of Type IIP events is remain constant, and (iii)  $t > \Delta t$  is called nebular phase.  $M_V$  and  $u_{ph}$  are mid-plateau  $V$ -band absolute magnitude and photospheric velocity in the comparable epoch, measurable from photometry and spectroscopy. There is a strong relation between observed and physical properties of Type IIP events. . . . . 34

- 1.11 **Left panel:** Formation of the inverted P-Cygni line profile. All the material on a vertical plane perpendicular to the observers line of sight has the same component of velocity along the observers line of sight, and hence the same Doppler shift. **Right panel:** The more realistic situation, where the line forming regions may not be attached with each other and distributed in a shell (‘detached’ case). The absorption width will be narrower and the emission peak will be flat. If the regions are ‘undetached’, we will get the inverted P-Cygni profile. 38
- 1.12 **Left panel:** Synthetic spectrum (dotted line) that has photospheric velocity  $v_{ph} = 10,000 \text{ km.s}^{-1}$  and hydrogen lines detached at  $20,000 \text{ km.s}^{-1}$ , where  $\tau_{H\alpha} = 2$ , is compared with a synthetic spectrum (solid line) that has  $v_{ph} = 10,000 \text{ km.s}^{-1}$  and undetached hydrogen lines, with  $\tau_{H\alpha} = 10$  at the photosphere [Branch et al., 2002]. **Right panel:** Velocity of the photosphere, as inferred from Fe II lines, is plotted against time after maximum light. The velocity evolution can be presented mathematically by a power-law fit to the data. The velocity of SN 1998dt at 32 days (open circle) has been excluded [Branch et al., 2002]. . . . . 39
- 1.13 **Left panel:** The Cartoon, not to scale, is borrowed from Weiler et al. [2002]. It represents the schematic diagram of radio supernova and its shocks, along with the stellar wind established circumstellar medium (CSM), the interstellar medium (ISM), and more distant ionized hydrogen absorbing gas (H II region). The radio emission is expected to arise near the blastwave front. **Right panel:** The long term Radio monitoring and “light curves” for SN1988Z. The plot shows the light curves in four wavelengths [2 cm (14.9 GHz, open circles, solid curve), 3.6 cm (8.4 GHz, crosses, dashed curve), 6 cm (4.9 GHz, open squares, dot-dash curve), and 20 cm (1.5 GHz, open triangles, dotted curve)] along with their best fit. The figure has been borrowed from Weiler et al. [2002]. . . . . 42
- 1.14 Different kinds of supernovae (**upper panel**) and the remnants (**lower panel**) generated from nonrotating massive single stars having different initial mass and metallicity. The figures have been borrowed from [Heger et al., 2003]. The sharp lines are the boundaries, segregating the outcomes of different kinds of catastrophe generated from the progenitors of different masses and metallicities. . . . . 44
- 2.1 From left, the 1.04-m Sampurnanand Telescope (ST) at ARIES, Nainital; 2.0-m IUCAA Girawali Observatory (IGO) at Girawali, Pune and the 2.01-m Himalayan Chandra Telescope (HCT) at IAO, Hanle. . . . 55

## LIST OF FIGURES

---

2.2	Response curve of 2k×4k CCD (squares) at $-100^\circ\text{C}$ , 2k×2k CCD at $-120^\circ\text{C}$ (triangles) and 1k×1k CCD at $-100^\circ\text{C}$ (circles). The curve indicates that all the three CCDs peak near $\lambda \sim 6700\text{\AA}$ . . . . .	58
2.3	The necessity of Template subtraction. The <b>upper-left panel</b> shows the field of galaxy NGC 2770, hosting the SNe 2007uy and 2008D (see chapter 5). The <b>upper-right panel</b> shows the field after template subtraction. The effect of galaxy is subtracted. <b>Lower panel</b> shows the visual light curve of SN 2008D. The green points are found without doing the galaxy back-ground subtraction while the red dots represent the light curve after galaxy subtraction. The effect of galaxy is less when the SN is bright (less magnitude) and more when the SN is faint (high magnitude). . . . .	68
2.4	Standardization of SN 2010jl field using the standard stars of the field SA98. The detail properties of this object has been discussed in chapter 6. . . . .	75
2.5	Very Large Array, an interferometric array. (Image courtesy of NRAO)	81
3.1	SN 2008gz in NGC 3672. <i>V</i> band image from 1 m ST, India. Area of about $8 \times 8$ arcmin is shown, with location of SN marked with a cross and reference standard stars marked with circles. . . . .	93
3.2	Light curve in <i>BVRI</i> magnitudes of SN 2008gz. The light curves are shifted for clarity, while for other SNe, they are scaled in magnitude and time to match with SN 2008gz. . . . .	98
3.3	Doppler corrected flux spectra of SN 2008gz from late plateau (+87 d) to nebular phase (+275 d). Prominent Hydrogen and metal lines are marked. . . . .	101
3.4	Line identification for late plateau and deep nebular phases. . . . .	106
3.5	Evolution of some important spectral lines of SN 2008gz, during its transition from late plateau to nebular phase. The dotted line at zero velocity corresponds to the rest wavelength. Upward arrows show emission peaks, while downward arrows show absorption dips. The feature 'A' is a high velocity P-Cygni component of $\text{H}\alpha$ , features 'B' and 'C' are due to NaID absorption from the Milky Way and the host respectively, and the emission feature 'D' is $\text{H}\alpha$ emission due to underlying HII region at SN location. The numbering sequences and resolution are : 1 (+87 d/10 $\text{\AA}$ ), 2 (+115 d/6 $\text{\AA}$ ) 3 (+140d/12 $\text{\AA}$ ), 4 (+171d/6 $\text{\AA}$ ), 5 (+218d/10 $\text{\AA}$ ), 6 (+222d/10 $\text{\AA}$ ), 7 (+231d/10 $\text{\AA}$ ) and 7 (+275 d/14 $\text{\AA}$ ). . . . .	108
3.6	Two component Gaussian fit of $[\text{O I}]$ 6300, 6364 $\text{\AA}$ emission lines. Measurements of their relative intensities quantifies, whether the corresponding line emitting region is optically thick or thin. . . . .	111

3.9	SYNOW modeling of the +87 d spectrum of SN 2008gz. The line identification is done after considering the SN as a spherically expanding fireball and lines are formed in a region moving ahead of the photosphere. Optical depth of individual line is calculated through “Sobolev approximation”. . . . .	113
3.10	SYNOW models for absorption features of H $\alpha$ (left panel) and H $\beta$ & Fe II (right panel). Blending effect due to Sc II, Ti II and Ba II is also incorporated in the models. Spectral evolution corresponds (top to bottom) to +87, +115, +140, +171 +218, +222, +231 and +275. H $\beta$ region is not modeled for +231 d. . . . .	114
3.11	Velocity profiles of different elements in the ejecta of SN 2008gz . . .	115
3.12	Spectrum of nucleus of the host galaxy NGC 3672 taken with 2-m IGO. The spectrum shows H $\alpha$ , N II (6548 Å and 6583Å), and S II (6717Å and 6730Å) lines in emission (similar to Sc spiral galaxies), which can arise from a gaseous component heated by AGN, post-AGB stars, shocks or cooling flows. The Ca II (K and H), H $\gamma$ , H $\beta$ , Mg I T, Fe I (5270Å), Na I D due to Milky Way and the host are seen in absorption. . . . .	118
3.13	Rest wavelength spectra of SN 2008gz (+87 d /10Å and +115 d /6Å) and the centre of host galaxy (+170 d /6Å). Na I D absorption due to interstellar matter of host galaxy ( $\sim$ 5892Å) and the Milky Way ( $\sim$ 5854Å) is indicated. . . . .	119
3.14	Temporal variation of colour of SN 2008gz. Also shown are the other core-collapse supernovae, SN 1987A, SN 1999em and SN 2004et. . . .	123
3.15	Flux contribution in percentage, in <i>BVRI</i> bands of SN 2008gz along with a comparison to SN 1987A . . . . .	123
3.16	<b>Left:</b> Bolometric light curve of SN 2008gz. For comparison, we also show light curves of SN 1987A, SN 1997D, SN 1999em and SN 2004et. <b>Right:</b> Steepness parameter estimation for SN 2008gz. . . . .	126
3.18	Continuum subtracted H $\alpha$ image of NGC 3672. In left panel ( $\sim 3' \times 3'$ ) five bright H II regions are visible. The SN position is marked with a circle. In right panel ( $\sim 1' \times 1'$ ) zoomed in image of SN is shown. SN location is marked with a dot. . . . .	128
3.19	Comparison of absolute V-band light curve of SN 2008gz with other type IIP SNe, like SN 2004et, SN 2004dj, SN 2004A, SN 2003gd, SN 1999em, SN 1999gi, SN 1998A, SN 1997D, SN 1992H, SN 1990E and SN 1987A. The magnitudes have been corrected for distance and reddening. . . . .	132
3.20	Comparison of spectral features of SN 2008gz along with SN 2004et and SN 1998A . . . . .	133

## LIST OF FIGURES

---

- 4.1 SN 2008in in M 61. A 600 s  $V$ -band image taken at phase +32d from the 1-m ST ARIES, India and covering an area of about  $10' \times 10'$  is shown. The location of SN 2008in as well as the local standard stars are marked with circles. North is up and east is to the left. . . . . 144
- 4.2 Measurement procedure of the true SN flux in the nebular phase. Each image shows  $76'' \times 76''$  around SN location. North is up and east is to the left. The leftmost panel shows  $V$ -band image observed on 2010 January 20 with a SN in it. The middle panel shows the template image taken on 2011 January 04, with no SN in it. A small flux enhancement marked with a cross ( $\times$ ) symbol is probably due to a star forming region. This is also present in the pre-SN SDSS image. The rightmost panel shows the subtracted image, where only SN is present. . . . . 146
- 4.3 The ROTSE  $R$ -band light curve of SN 2008in. Reference time for x-axis is the epoch of ROTSE non detection on 2008 December 23.95. The evolution of post shock breakout flux has been modeled by using the simple analytical expressions given in Cowen et al. [2010] and Arnett [1980]. The best fit time for shock breakout is marked with  $t_0$  while the  $\Delta t_0$  shows the duration of uncertainty. The  $t_d$  is the time of discovery reported by Nakano et al. 2008. The  $t_p$  is the time when  $R$  light shows the peak. The  $t_i$  is the time of inflection obtained using the procedure of Elmhamdi et al. [2003a]. . . . . 148
- 4.4 Light curves of SN 2008in in the UV, optical and NIR bands. The light curves of archetypal low-luminosity SN 2005cs are overplotted for comparison [data are taken from Brown et al., 2009; Pastorello et al., 2009]. The light curves of SN 2005cs are scaled in magnitude to match the light curves of SN 2008in. . . . . 150
- 4.5 Doppler corrected flux spectra of SN 2008in observed during +7 d to +143 d. Prominent lines are marked. Telluric features are marked with  $\oplus$  symbol. The sharp absorption dips seen near  $5000 \text{ \AA}$  and  $6500 \text{ \AA}$  in the +7d and +14d spectra are artifacts. The spectra signify the early photospheric phase (+7d,+14d), mid-plateau phase (+54d, +60d), late-plateau phase (+87d, +90d, and +99d) and nebular phase (+118d, +119d, and +143d). . . . . 155

- 
- 4.6 The end plateau spectrum (+99d) of SN 2008in, is compared with five low-luminosity SNe 1997D, 1999br, 1999eu, 2001dc, 2005cs (Pastorello et al. 2009 and references therein); two normal SNe 2004et [Misra et al., 2007b], 2008gz [Roy et al., 2011b] and a peculiar Type II SN 1998A [Pastorello et al., 2005], observed at comparable epochs. The phases quoted for each event are with reference to the moment of inflection ( $t_i$ ; see Left panel of Figure 4.12), which marks the highest rate of decline in the  $V$ -band light curve during the end of the plateau and the beginning of nebular phase [Elmhamdi et al., 2003a]. All the spectra have low spectral resolution ( $\sim 10 \text{ \AA}$ ). The P-Cygni features of Na I D, Ba II  $\lambda$  6142, Sc II  $\lambda$  6248, Ba II  $\lambda$  6497 and H $\alpha$  are marked. 156
- 4.7 The spectral line identifications in a late-plateau phase (+99d) spectra are shown. Spectral features are mainly identified as per previously published line identifications for IIP SNe [Leonard et al., 2002a; Pastorello et al., 2004]. Telluric features are marked with  $\oplus$  symbol. 158
- 4.8 Spectral evolution of H $\beta$ , FeII  $\lambda$ 4924, FeII  $\lambda$ 5018, HeI  $\lambda$ 5876, Na I D  $\lambda$ 5890, 5896, Ba II  $\lambda$ 6148, Sc II  $\lambda$ 6248, Ba II  $\lambda$ 6497 and H $\alpha$  lines of SN 2008in during its transition from plateau to nebular phase. The dotted line at zero velocity corresponds to the rest wavelength, marked at the top of each panel. The sharp absorption dips seen in the H $\alpha$  profile for +7d and +14d spectra are artefacts. 159
- 4.9 Evolution of expansion velocity of SN 2008in. The upper panel shows the velocity of different elements in the ejecta of SN 2008in. The black filled circle shows the estimated value of mid-plateau photospheric velocity, calculated using the relation mentioned in Roy et al. [2011b]. The lower panel shows a comparison of velocity derived from H $\alpha$  with that of low-luminosity event like SN 2005cs [Pastorello et al., 2009] and normal Type IIP SNe 1999em [Elmhamdi et al., 2003b] and 2004et [Sahu et al., 2006]. 160
- 4.10 Forbidden lines during the nebular phases of SN 2008in are compared with the low-luminosity SN 1997D. The lines [O I], [Fe II] and [Ca II] are marked. 161
- 4.11 Colour curve of SN 2008in is shown with filled circles. Also shown are the SNe 1987A (solid line), 1999em (open triangle), 2004et (filled triangle), 2005cs (open circle) and 2008gz (open square). 167
- 4.12 **Left:** Determination of steepness parameter from the apparent  $V$ -band light curve of SN 2008in. See text for details. **Right:** Comparison of the quasi-bolometric light curve of SN 2008in with the low-luminosity SNe 1997D, 2005cs; the normal SNe 1999em, 2004et, 2008gz; and the peculiar Type II SN 1987A. 170

## LIST OF FIGURES

---

4.13	A comparison of the absolute $V$ -band light curve of SN 2008in with the low-luminosity SNe 1997D, 2005cs; the normal SNe 1999em, 2004et, 2008gz, 2004dj, 2004A, 2003gd, 19992H, 1999E, 1999gi; and the peculiar Type II SNe 1987A, 1998A. The decline rate of emission expected from radioactive decay of $^{56}\text{Ni}$ to $^{56}\text{Co}$ to $^{56}\text{Fe}$ is shown with dot-dashed line. . . . .	174
5.1	Identification chart of SN 2007uy field along with SN 2008D. The image is about 10x10 arcmin taken in $V$ -band with the 104-cm Sampurnanand telescope (ST) at ARIES, Nainital. The SNe locations are marked along with the secondary stars used for calibration. North is up and East is to the left. . . . .	187
5.2	The light curves of SN 2007uy in NIR $JHK$ , Optical $UBVRI$ and $uvw2, uvm2, uvw1\&u, b, v$ NUV-Optical UVOT bands. . . . .	197
5.3	$BVRI$ lightcurves of SN 2008D. Filled circles are our observations whereas crosses are taken from literature [Malesani et al., 2009; Mazzali et al., 2008; Modjaz et al., 2009]. Dates are given in days after the burst trigger time in the observers frame. The solid line in different bands represent the polynomial trace to the data points. . . . .	198
5.4	Absolute light curves of SN 2007uy. Comparison with SN 2008D and other Type Ibc events. . . . .	202
5.5	NUV and u band absolute light curves of SN 2007uy. Comparison with Type Ic event SN 2006aj. Data for SN 2006aj have been borrowed from Simon et al. (2010). . . . .	203
5.6	Temporal evolution of observed SED of SN 2007uy. The temperature of each blackbody is mentioned inside the parenthesis, with a temperature-scale 1000K. The one sigma uncertainties are measured by applying the ‘Monte Carlo’ method . . . . .	207
5.7	Color evolution of SN 2007uy. Comparison with other Type Ibc events	214
5.8	The UVOIR bolometric lightcurve of SN 2007uy. Comparison with other Type Ibc events . . . . .	214
5.9	Spectroscopic evolution of SN 2007uy. The +162d and +392d spectra have been multiplied by a factor of 2 to enlarge several tiny features. . . . .	218
5.10	Spectroscopic comparison of SN 2007uy with other Type I events near maxima. . . . .	219
5.11	Temporal evolution of velocities some spectral lines of SN 2007uy. . . . .	221
5.12	Temporal evolution of velocities of SiIII and HeI spectral features in SN 2007uy. . . . .	229

5.13	The modeled UVOIR bolometric light curve of SN 2007uy. The red dots are bolometric luminosity measured from UVOIR observation whereas the dotted curves are theoretical models. The green curve is for photospheric phase, while the blue curve is for nebular phase. See text for more detail. . . . .	233
5.14	The modeled radio light curve of SN 2007uy. The upper panel shows the variation of radio wave with time. Open circles are the data obtained from literature [van der Horst et al., 2011], whereas the field circles are VLA data acquired and processed during the present work. The solid curves represent the best fitted model. The lower panel shows the variation of spectral index with time. . . . .	237
6.1	Identification chart of SN 2010jl field. The image is about 13x13 arcmin taken in V-band with the 1-m ST at ARIES, Nainital. The transient location is marked along with the secondary stars used for calibration. North is up and East is to the left. . . . .	246
6.2	The correlation between counts and Gunn magnitudes of SDSS field of SN 2010jl. . . . .	250
6.3	Light curves of SN 2010jl. Closed circles are the data observed from ST and HCT telescopes, while the open circles are the pre-discovery photometry taken from Stoll et al. [2011]. . . . .	251
6.4	Identification chart of CSS 100217 field. The image is about 13x13 arcmin taken in V-band with the 1-m ST at ARIES, Nainital. The transient location is marked along with the secondary stars used for calibration. North is up and East is to the left. . . . .	254
6.5	Optical photometric light curve of CSS 100217. The light curve is with respect to observer frame and hence not corrected for redshift. JD = 2455256.0 has been assumed as the origin of time axis for this event. . . . .	260
6.6	Identification chart of SN 2010kd field. The image is about 13x13 arcmin taken in B-band with the 1-m ST at ARIES, Nainital. The transient location is marked along with the secondary stars used for calibration. North is up and East is to the left. . . . .	262
6.7	The multiband Light curves of SN 2010kd. . . . .	265
6.8	The comparison of V-band light of SN 2010jl, CSS 100217 and SN 2010kd with other Types of SNe. All these SNe shows a very high brightness in comparison with other events. A pronounced plateau like decline is noticeable . . . . .	268
6.9	The colour evolution of luminous events. The phases are measured with respect to the observer frame. . . . .	269

**LIST OF FIGURES**

---

6.10 *UBVRI* Bolometric light curve of over luminous events. Comparison with other Types of events. The phase axis is with respect to the observer rest frame. . . . . 270

# List of Tables

1.1	Spectroscopic properties of different supernovae and nature of their progenitors. . . . .	7
2.1	Parameters of the used Indian optical telescopes. . . . .	56
2.2	Details of the filter system. The thickness of the glass in mm is indicated in brackets . . . . .	57
2.3	Basic system parameters of Very Large Array (VLA) . . . . .	84
3.1	Properties of the host galaxy NGC 3672 and SN 2008gz. . . . .	94
3.2	Identification number (ID), coordinates ( $\alpha, \delta$ ) and calibrated magnitudes of stable secondary standard stars in the field of SN 2008gz. Errors in magnitude represent RMS scatter in the night-to-night repeatability over entire period of SN monitoring. . . . .	96
3.3	Photometric evolution of SN 2008gz. Errors in magnitude are derived from ISIS and it denote $1\sigma$ uncertainty. . . . .	102
3.4	Journal of spectroscopic observations of SN 2008gz. . . . .	104
3.5	Velocities of photosphere, $H\alpha$ and $H\beta$ for different epochs of SN 2008gz evolution. All the parameters are derived from SYNOW modelling. . . . .	112
3.6	Equivalent width measurement of Na I D absorptions in the spectra of SN 2008gz and the host galaxy. Last row provides the uncertainty weighted EW of Na I D absorption in the direction of SN 2008gz due to Milky Way and the host. . . . .	120
4.1	The <i>swift</i> /UVOT photometric observations of SN 2008in. . . . .	143
4.2	The photometric magnitudes of secondary standard stars in the field of SN 2008in. . . . .	144
4.3	The <i>UBVRI</i> photometry of SN 2008in. . . . .	145
4.4	The REM near-infrared observation of SN 2008in. . . . .	146
4.5	Journal of spectroscopic observations of SN 2008in. . . . .	147
5.1	Properties of the host galaxy NGC 2770 and SN 2007uy. . . . .	184

## LIST OF TABLES

---

5.2	The <i>swift</i> /UVOT photometry of SN 2007uy. . . . .	188
5.3	Photometry of Secondary Standard stars in the field of SN 2007uy and SN 2008D . . . . .	189
5.4	The <i>UBVRI</i> photometry of SN 2007uy. . . . .	191
5.5	The near-infrared <i>JHK</i> photometry of SN 2007uy. . . . .	192
5.6	The <i>BVRI</i> photometry of SN 2008D. . . . .	193
5.7	Journal of spectroscopic observations of SN 2007uy <sup>a</sup> . . . . .	194
5.8	Light curve shape parameters of different core-collapse SNe, measured in <i>BVRI</i> photometric passbands. The post-maxima magnitude decay $\Delta m_{15}$ , peak width $d_{0.25}$ , pre-( $\alpha_1$ ) and post-( $\alpha_2$ ) flattening decay rates are derived from the absolute magnitude light curves. We quote uncertainties in rise time, peak magnitudes and decay rates arising from fitting polynomials. The errors are fitting error. . . . .	201
5.9	The log of radio observation of SN 2007uy from VLA in 4.8 & 8.4 GHz. The Flux errors are measured using the expression $\sigma_f^2 = (\epsilon.S_0)^2 + \sigma_0^2 + \sigma_{S_0}^2$ . Here $S_0$ is the observed flux density, $\sigma_0$ is the RMS noise of the radio sky, $\sigma_{S_0}$ is the error associated with $\sigma_0$ and $\epsilon$ is the fraction that accounts the error in VLA flux calibration. For 4.8 and 8.4 GHz observations value of $\epsilon$ is 0.05. For the epochs where measured flux density is less than 3 times of the corresponding value of $\sigma_f$ , we have considered the flux density as the upper limit for our measurement. . . . .	236
5.10	The parameters derived from the fitting of radio data . . . . .	238
6.1	Identification number (ID), coordinates ( $\alpha, \delta$ ) and calibrated magnitudes of stable secondary standard stars in the field of SN 2010jl. . . . .	247
6.2	Photometric evolution of SN 2010jl. The Phase is measured in days w.r.t. JD = 2455504.06 . . . . .	249
6.3	Identification number (ID), coordinates ( $\alpha, \delta$ ) and calibrated magnitudes of stable secondary standard stars in the field of CSS 100217. . . . .	255
6.4	Photometric evolution of CSS 100217. The Phase is measured in days w.r.t. JD = 2455256.0 . . . . .	257
6.5	Identification number (ID), coordinates ( $\alpha, \delta$ ) and calibrated magnitudes of stable secondary standard stars in the field of SN 2010kd. . . . .	262
6.6	Photometric evolution of SN 2010kd. The Phase is measured in days w.r.t. JD = 2455515.0 . . . . .	264

# Chapter 1

## Introduction

### 1.1 Cosmic Explosions

From the experience of life one can realize that the word ‘explosion’ stands for a violent blowing or bursting in volume caused by rapid energy release from a very fast chemical reaction, a nuclear reaction or the escape of gases under pressure that produces a loud noise, an unusual heat and light.

It is now established that ‘explosion’ has a great role in generation of new stars, planetary bodies and eventually creation of organic elements even at the extreme conditions. We call these catastrophes as “**Cosmic Explosion**”. One or several such explosions were probably associated with the creation of our solar system. The similar catastrophes which occur in far universe are found to be more than billion times intensive than the man made catastrophes on the earth. The nearest explosive event, like extremely energetic X-class solar flares releases about  $10^{32}$  erg energy [Clark, 1983] while in the present work, we would like to discuss the explosions which liberate energies of the order of  $10^{50}$  erg, about  $10^{30}$  times more energetic than ‘*Hi-*

## 1. INTRODUCTION

---

*roshima and Nagasaki explosions* – One of the greatest examples of ‘inhumanity’ where two 4,500 Kg bombs (“Little boy” and “Fat man”) snatched away the lives of about 2,00,000 people. By no-means these extreme conditions can be generated inside the laboratories. Being a passive observer we can only observe, analyze and study the extreme physics associated with Plasmas [Priest, 1984], Shocks, Nucleosynthesis processes and the mechanisms which trigger these explosions [Arnett, 1996; Weiler, 2003] happening in the universe. We discuss below different types of cosmic explosions.

### 1.1.1 Types of Cosmic Explosions

Cosmic explosions known today are basically transient events, having a timescales, ranging from seconds to months. These explosions are generally associated with celestial objects. The radiations emitted from explosions varies with time, i.e., rises to the peak value and fades into the background. Cosmic explosions can be originated either from ‘collision & merging’ or ‘accretion’ or because of ‘collapse’. It may be a combination of these physical processes.

The recent example of merging scenario in our solar system is the collision of comet ‘Shoemaker-Levy-9’, with Jupiter [Weaver et al., 1995]. Formation of the ‘Blue Stragglers’ in old stellar populations like Globular Clusters is also probably due to merging of two or maybe three main sequence stars of mass  $\sim 0.8 M_{\odot}$ . Similarly there are ample examples of merging of compact objects like White Dwarf (WD) or Neutron stars (NS) and galaxy-merging in the universe. A summary on the energetics and related physics merger events are discussed elsewhere [Sivaram 2007 and references therein].

---

About fifty percent of the stars in the universe belongs to a binary system and in such a system, there is a possibility of collapse through accretion, where gravitational potential, called ‘*Roche potential*’ is established in a binary system [Frank et al., 2002] and the matter from the outer surface of a giant star (mainly red-giant) can be accreted by a compact object (mainly WD) through ‘*inner Lagrangian point*’. This is called ‘*Roche lobe overflow*’. Since WD is a thermodynamically stable system with a definite mass, these excess material creates an enormous temperature ( $\sim 2 \times 10^7$  K) and pressure on this object. The excess matter is released through explosion called **Nova**. Energy liberation in Novae explosions is of the order of  $10^{44}$  ergs. For review on Nova see Bode and Evans [2008].

There is another class of explosions called ‘**Supernovae (SNe)**’ which are  $10^5$  to  $10^7$  times more energetics than Novae. They are classified into two classes – Thermonuclear and core-collapse supernovae.

In late sixties Vela satellite serendipitously discovered a new kind of explosions called ‘**Gamma Ray Burst (GRB)**’, which are normally happening in a relatively extragalactic universe and are extremely energetic ( $10^{52}$  erg) in  $\gamma$ -rays for first 10 – 1000 sec and then produce afterglow radiations in almost all wavelengths spanning from X-ray to Radio. They are also found to be associated with extremely energetic Supernovae.(i.e., Hypernovae). The core-collapse supernovae (CCSNe) and Long duration GRBs are believed to be originated through gravitational collapse of a very massive stars.

There is another class of explosions called as “**Overluminous supernovae**”, which are even brighter than SNe. In fact, these events are the most luminous SNe detected so far. Optically they are about one order higher luminous than energetic supernovae generated from the death of massive stars. Theoretical understanding

# 1. INTRODUCTION

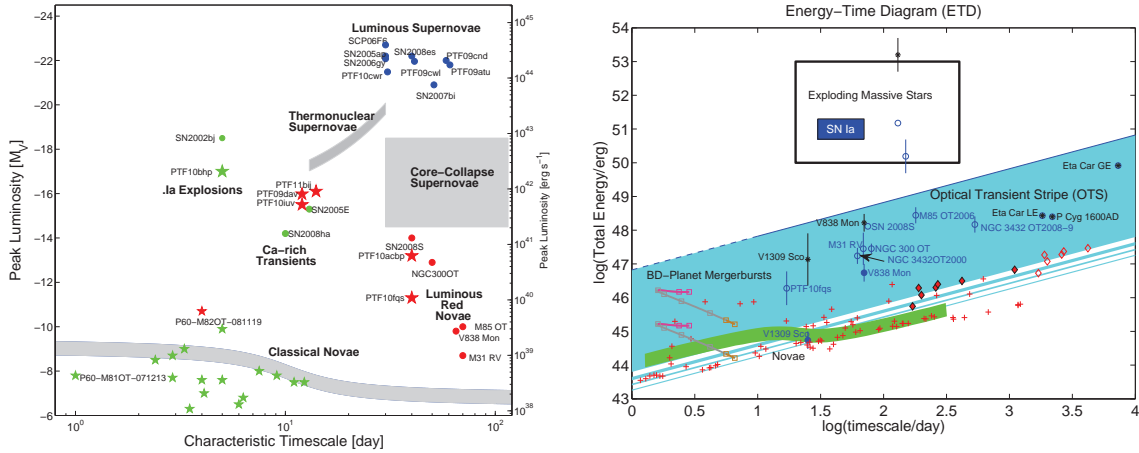


Figure 1.1 Observed transient events on the Luminosity-Time diagram (LTD) (left) and Energy-Time Diagram (ETD) (right) produced respectively by Kasliwal [2011] and Soker and Kashi [2011]

about these events is not very clear. Primarily, they are believed to be a complete disruption of high mass population III stars [the first generation of stars after formation of Universe, Shu 1982], having initial mass  $>60M_{\odot}$ , either by ‘pair instability’ process or by ‘photo-disintegration’ [Bromm et al., 2003; Fryer et al., 2001; Whalen et al., 2012]. Few recent examples are CSS100217 [Drake et al., 2011], SN 2010kd [Vinko et al., 2012], SN 2010gx [Pastorello et al., 2010] and CSS120121 [Smartt et al., 2012].

If the Nove, Supernovae, overluminous events and other catastrophe are placed in Luminosity-Time Diagram (LTD) (that presents peak luminosity against the time in which peak Visual band magnitude reduces by 3 mag), one can find few events that lie between Novae and Supernovae (left panel of Figure 1.1). They are called ‘Intermediate Luminous Transients (ILOT)’ [Kasliwal, 2011; Kulkarni et al., 2007] and there have been very less number of events discovered and probed so far. The location of ILOT also appears distinctly in the Energy-Time diagram (ETD) (right panel of Figure 1.1). The burst mechanism in these objects

---

is not well understood, possible progenitors are likely to be ‘Brown Dwarf-planet merging’, ‘Luminous red Novae’, ‘Ia Explosions’, ‘Calcium-rich halo transients’ and ‘Low velocity transients’.

In this thesis work we focus on core-collapse supernovae (CCSNe) as well as overluminous supernovae (OLSNe) along with a very short discussion on the follow-up of GRB events.

## 1.2 Supernovae

There is approximately one supernova event occurring in the universe in every second. In Milky Way, there is one supernova produced in every, 30–50 years. Supernovae study is a platform to understand nucleosynthesis and particle acceleration in large scale while the use of type Ia SNe as standard candle allows cosmologists to ascertain the geometry and topology of the universe at the very largest scales.

### 1.2.1 Brief History

History of Supernova is older than a thousand years. The first confirmed discovery is the birth of Crab nebula in the year 1054, mentioned in Chinese, Japanese and Persian history of astronomy. It was recorded as a ‘guest star’ on 04 July of the year AD1054 in Chinese literature and remained visible for next two years even at the daylight. Other probable onset of bright SNe noticed by ancient Chinese and Japanese astronomers are ‘guest stars’ of AD1181, AD1006, AD393, AD386, AD369 and AD185 [Green and Stephenson, 2003]. Second confirmed discovery with a detailed monitoring was done by Tycho Brahe in the year 1572, that was the onset of a supernova, which was later came to be known as Tycho supernova remnant. AD1572

## 1. INTRODUCTION

---

was discovered on 06 November, 1972 and it disappeared from sight some time between 21 April and 19 May, 1974. The third well defined and monitored historical supernova was done by Kepler in AD1604. It was discovered on 3rd October. Both Tycho and Kepler events are now confirmed as remnants of two galactic Thermonuclear SNe whereas Crab was a corecollapse event that produced neutron star as a compact object at its core. In recent times, the number of extragalactic supernova detections has grown continuously. This topic has received a major boost with the detection of SN 1987A and the emergence of deep co-ordinated searches for distant supernovae in the last decade. This has allowed us to conduct detailed studies of specific supernova classes and find the common as well as individual properties of supernovae. Also the association of some supernovae with Gamma Ray Bursts in the recent times has generated a substantial interest in the study of supernovae.

### 1.2.2 Observed properties of SNe and taxonomy

A SN is observationally classified by the *absence* (Type I) or by the *presence* (Type II) of Hydrogen (H) in its spectrum at any instant following the explosion<sup>1</sup> [Filippenko, 1997; Minkowski, 1941]. Since SNe are brighter near their maximum light, for most of the time the classification is based on the early spectra, which consist of a thermal continuum and P-Cygni profiles of lines formed by resonant scattering.

Figure 1.2 shows the broad classification of supernovae on the basis of spectroscopy and different ‘branches’ of SN taxonomy. The principle elements, presence or absence of which decides the Types of explosion are also marked in the figure. A short description about the characteristics of different kinds of SNe along with the

---

<sup>1</sup>Contamination by narrow hydrogen emission lines from associated H II region should be excluded from the definition.

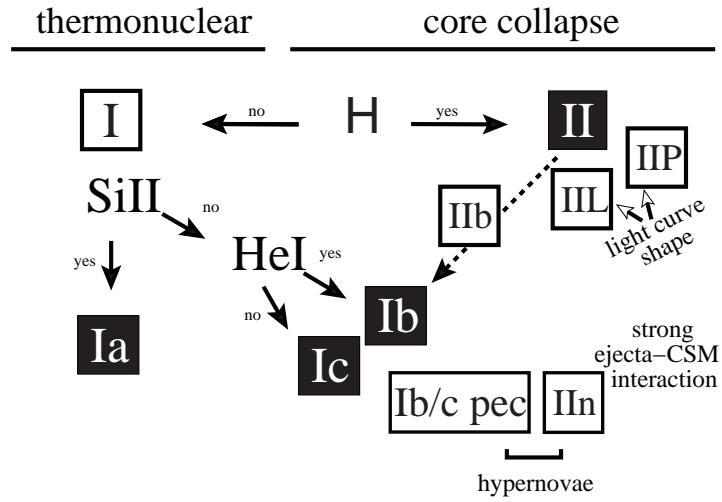


Figure 1.2 The current classification scheme of supernovae. The figure has been borrowed from Turatto [2003]

nature of their progenitors and host environment is presented in table 1.1.

Table 1.1: Spectroscopic properties of different supernovae and nature of their progenitors.

SN Type	Charecteristics	progenitor & its environment
Ia	(i) H lines are not present in the spectrum.	(i) White dwarf of mass $\sim 1.4 M_{\odot}$ accreting matter from its companion in a binary system.
	(ii) Strong Si 6150 Å absorption line near maxima.	(ii) Merger of two white dwarfs.
	(iii) Late time spectrum is dominated by Fe group elements.	(iii) Normally found in elliptical galaxies and never associated with H II regions.

# 1. INTRODUCTION

---

Table 1.1-

continued.

SN Type	Charecteristics	progenitor & its environment
Ib	(i) Nither H & Si lines are present in the spectrum	(i) Core collapse of massive stars ( $\gtrsim 30M_{\odot}$ ) which have stripped off their H envelope, either due to wind or roche-lobe overflow in a binary system.
	(ii) Strong He 5700 Å absorption line can be observed.	(ii) Wolf-Rayet stars are the probable candidates.
	(iii) O I & Ca II lines are present in the nebular spectra.	(iii) Mostly associated with star forming regions.
Ic	(i) Nither H, nor He or Si lines are present in the spectrum.	(i) Core collapse of massive stars, which have stripped off both their H and He envelopes.
	(ii) Strong absorption features of O I & Ca II are present in the spectra.	(ii) Wolf-Rayet stars are the probable progenitors.
		(iii) Always associated with star forming regions.
IIIn	(i) Spectra are dominated by narrow emission lines.	(i) Massive stars ( $\gtrsim 40 M_{\odot}$ ), with huge H-envelope.
	(ii) Rising part is relatively faster, becomes luminous at maximum brightness with a slowly fading light curve.	(ii) Core-collapse is the basic mechanism.

Table 1.1-  
continued.

SN Type	Charecteristics	progenitor & its environment
		(iii) Always associated with the star forming region of the host.
I Ib	(i) prominent H lines are found in the early spectrum, but it disappears at late epochs.  (ii) He, O I, Ca II lines in the late stage of spectrum is noticed.	(i) The progenitors probably loss considerable amount of its outer H layer in a binary system, much before the explosion.  (ii) Core-collapse is the basic mechanism.  (iii) Probably a kind of explosion, bridging Type Ibc with Type IIs.
I IP	(i) P-Cygni profiles of H is noticeable through out the spectral evolution.  (ii) O I, Ca II are present in nebular phae.  (iii) Light curve shows a pronounced plateau of $\sim 100$ days, can be used as a distance indicator.	(i) Mainly Red supergiants having H envelope.  (ii) Here also collapsing core is supposed to be the basic process of triggering.  (iii) Most of the pre-SN imaging shows the progenitors' mass are within $10-20 M_{\odot}$ .
I IL	(i) Featureless early spectrum with a slight impression of H $\alpha$ emission.	(i) Less massive supergiants with a smaller mass H envelope.

# 1. INTRODUCTION

---

Table 1.1-  
continued.

SN Type	Charecteristics	progenitor & its environment
	(ii) Light curve shows a linear uninterrupted decline after maximum.	(ii) Like other Type II events, here also core-collapse is the basic triggering mechanism.  (iii) Associated with star forming regions.
Luminous Type II	(i) These are spectroscopically Type-II SNe, normally shows strong H lines in their spectra.  (ii) Luminosity of these objects are several orders higher than normal Type IIs.	(i) The nature of progenitor is not well understood. One possibility if a progenitor with mass $\gtrsim 60M_{\odot}$ .  (ii) Mostly observed in distant galaxies.
Luminous Type I	(i)These are spectroscopically Type-Ibc events, normally shows the impression of H {II regions in their spectra.	(i) The nature of progenitor is not well understood. One possibility if a progenitor with mass $\gtrsim 140M_{\odot}$ .  (ii) The possibility of the emergence of magnetar can not be ruled out.

The Type Ia SNe are mostly found in the evolved galaxies and also not associated with star forming regions. On the other hand though the spectroscopic characteristics of Type Ib and Ic are different from Type II events, they are found in the same

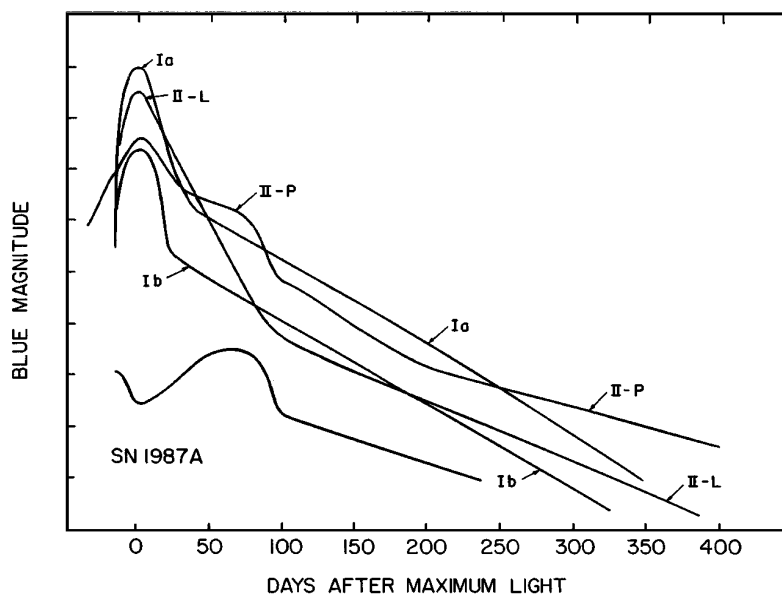


Figure 1.3 The Schematic blue band light curves for SNe of Types Ia, Ib, II-L, II-P, and peculiar Type II SN 1987A, borrowed from Filippenko [1997]. The curve for SNe Ib includes SNe Ic as well, and represents an average. Figure shows the canonical nature of SN light curves.

environment and are also triggered through similar mechanism. Probably Type IIb events, showing very less H during initial stage bridge the gap between Type II and Type Ibc. Few examples are SNe 1993J, 2011dh, 2011fu and 2012P. Recently very minute impression of H is also found in Type Ibc events and it is believed that probably Type IIb and Type Ibc are generated from similar kinds of progenitors. These events are generally called ‘*Stripped-envelope supernovae*’.

Figure 1.3 is a schematic representation of the time evolution of blue light of various SNe. This plot shows the canonical nature of light curve of different SNe along with that of a peculiar Type II SN 1987A. The figure 1.4 shows the temporal evolution of different Types of SN spectra – spectra at the left column are taken around the maximum light curve and normally used to classify the type of the events. Middle column represents the nature of spectra about three weeks after

# 1. INTRODUCTION

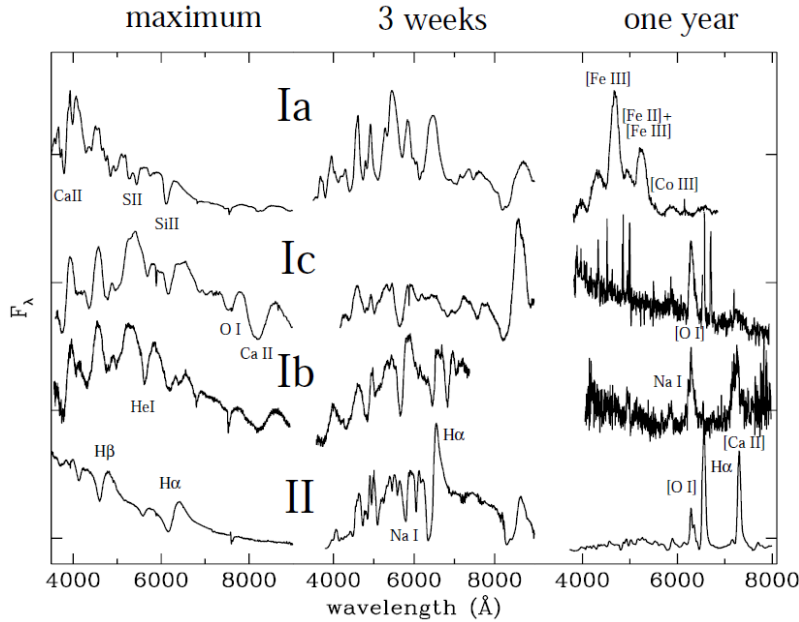


Figure 1.4 Typical evolution of spectra of different types of supernova – Near maxima, 3 weeks and one year after maxima [Turatto, 2003]

maximum. Since maximum light is attained within 20 days after the burst, hence second column can be considered as a representation of spectra of different kinds of SN more than a month after the burst. The third and right most column represents SN spectra taken typically one year after the explosion. In most of the cases only strong emission lines and metal lines (showing inner ejecta) sustain and other are lost due to rarefaction of outer ejecta.

Peculiarity of SNe is either reflected in their light curve or in spectra or in both. This is directly related with the progenitor structure and explosion mechanism. For example, SN 1987A was of this category. Though spectroscopically it was similar to normal Type II events, photometrically it was far different from normal Type IIP and now also called ‘*dome-like*’ event (Type IId)<sup>1</sup> [Utrobin and Chugai, 2011]. Few

<sup>1</sup>In normal Type IIP the bulk of the radiated energy is an internal energy which is deposited during the shock wave propagation. On the other hand for SN 1987A like events the thermal

---

other examples are – SNe 1986G, 1991bg, 1991T, 1997br, 2000cx (Type I); 1997D, 1998A, 1998br, 1999br, 1999eu, 2000cb, 2006V, 2006au, 2009E (Type II) e.t.c.

The events like 1997D [Turatto et al., 1998], 1999br, 1999eu, 1994N, 2001dc [Pastorello et al., 2004], 2009md [Fraser et al., 2011] and many others show very low luminosity in comparison to normal Type IIP events, though their light curves do not show any kind of dome-like structure. These are also rare and peculiar events, but now have been categorized as ‘*low-luminosity events*’.

Arcavi et al. [2012] have studied the possibilities of common origin of Type IIb-IIIL-IIP events on the basis of increasing hydrogen envelope, using a sample of R band light curves of these Types of events, observed during ‘*Caltech Core Collapse Project*’ (CCCP). The core results provides a clear indication for three distinct subclasses of Type II explosions – plateau, slowly and rapidly declining events. The results confirm that these subclasses are unlikely to reflect variance of continuous parameters, but rather might result from physically distinct progenitor systems, strengthening the suggestion of a binary origin for at least some stripped envelope SNe.

### 1.2.3 Supernova rate and detection probability

To understand the stellar death more and more observation and its physical interpretation is required. Few scientific groups like ‘*Catalina Real-Time Transient Surveys*’ (CRTS) [Drake et al., 2009], ‘*Lick Observatory Supernova Search*’ (LOSS) [Leaman et al., 2009], ‘*Palomar Transient Factory*’ (PTF) [Rau et al., 2009], ‘*La Silla-Quest*’ (LSQ) [Hadjiyska et al., 2011] and ‘*Pearth Observatory Supernova Search*’

---

energy is completely exhausted during initial 10–20 days, form a dip in the light curve and then the dome-like part of the light curves are powered by the radioactive decay of  $^{56}\text{Ni}$ , similar to normal Type Ibc events.

# 1. INTRODUCTION

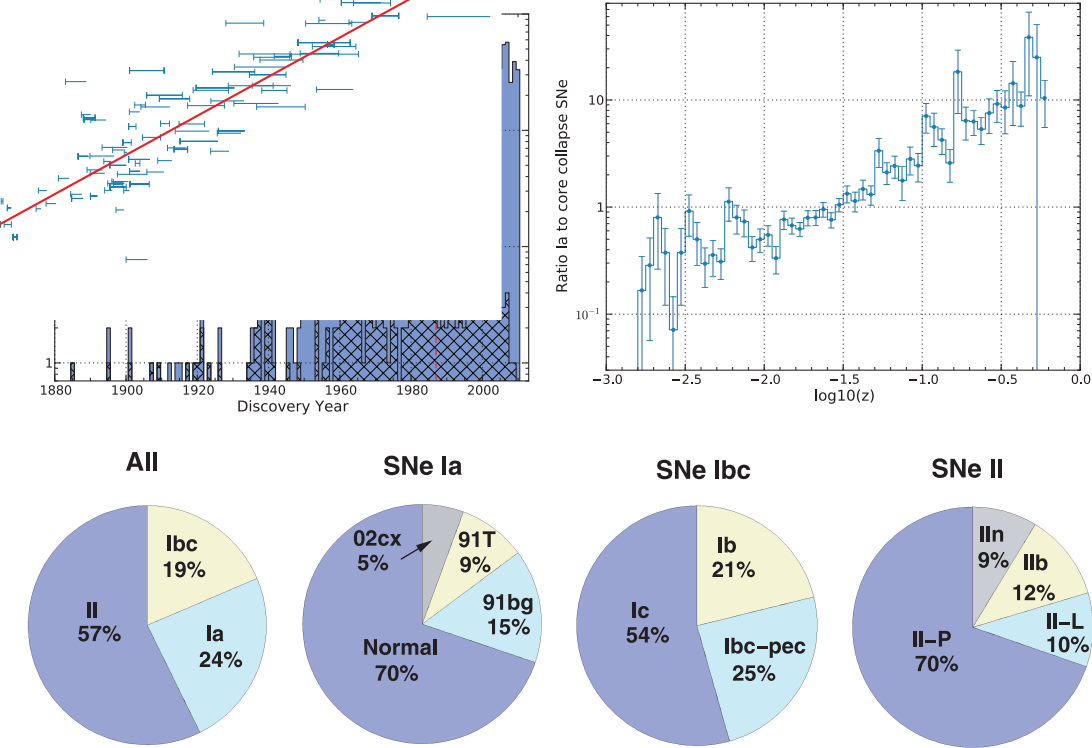


Figure 1.5 **Upper-left panel:** The plot has been reproduced from [Lennarz et al. \[2012\]](#). It shows the number of detected SNe per year. The discovery year of SN1987A is marked with a dashed line. The fraction of bright SNe, which have a magnitude at maximum  $\leq 15$  mag, is indicated by the hatched area. **Upper-right panel:** Also taken from [Lennarz et al. \[2012\]](#), showing the ratio between Type Ia and CCSNe as a function of redshift. **Lower panel:** This plot, taken from [Li et al. \[2011\]](#), shows the observed fractions of the subclasses of SNe in a volume-limited sample, illustrated as pie charts. The fractions of SNe Ic and IIb are upper limits, while that of SN 1991T-like objects is a lower limit. Also, the subclass of SNe Ibc-pec consists of broad-lined SNe Ic, peculiar objects.

---

programs are mainly dedicated to search the luminous and normal SNe in regular fashion. Many robotic telescopes like ‘*Robotic Optical Transient Search Experiment*’ (ROTSE) [Akerlof et al., 2000], ‘*Rapid Eye Mount*’ (REM) [Cutispoto et al., 2004], are also involved for prompt optical observation of GRBs and discovery of new SNe. Amateur astronomy has also a major contribution toward the discovery of new SNe. In near future, two big facilities like ‘*Panoramic Survey Telescope And Rapid Response System*’ (Pan-STARRS) [Hodapp et al., 2004] and ‘*Large Synoptic Survey Telescope*’ (LSST) [Ivezic et al., 2008] which will be continuously busy to scan almost the entire optical sky. The space based missions like *Swift* [Barthelmy et al., 2005] and ‘*GALaxy Evolution eXplorer*’ GALEX [Martin et al., 2005] observatories have their own search programs for X-ray UV and early optical detection of SNe. Similarly ‘*Rossi X-ray Timing explorer*’ RXT [Jahoda et al., 1996], ‘*Monitor of All-sky X-ray Image*’ MAXI [Ueno et al., 2008] and ‘*Fermi Large Area Telescope*’ LAT [Atwood et al., 2009] are used for X-ray counterpart observation.

The rapid improvement in discovery of new supernova is presented statistically in figure 1.5. Detection rate of faint SNe in last decade was improved remarkable, though there is not very considerable change in discovery of bright SNe (brighter than 15 mag). With this sample, Lennarz et al. [2012] found an empirical relation between the ratio of Type Ia to CCSNe and the redshift of the host galaxy. The lower half of figure 1.5 shows a volumetric sample of nearby SNe. The number of Type II events is  $\sim 57\%$ , while that of Type Ibc is  $\sim 19\%$  and Type Ia is  $\sim 24\%$ . Hence the total number of CCSNe is clearly larger than Type Ia SNe.

## 1. INTRODUCTION

---

### 1.2.4 Different mechanisms for SNe explosions

Based on the mechanisms of explosion, SNe are broadly categorised into three types:

(1) *Thermonuclear supernova* – thermonuclear runaway (detonation/deflagration) of a white dwarf in a binary system.

(2) *Core collapse supernova* – gravitational collapse of a massive star.

(3) *Over luminous events* – direct collapse due instability generated through electron-positron pair production from radiation or due to photo-disintegration.

The present thesis mainly focuses on core collapse supernovae, luminous events. Only these mechanisms will be discussed briefly in the subsequent sections.

## 1.3 Core collapse supernovae

Gravitational collapse of a massive star ( $M > 8 M_{\odot}$ ) leads to a core collapse SNe. For simplest case it can be considered as a spherically symmetric phenomena and has been shown schematically in figure 1.6. At the final stage of evolutionary track, these massive stars attain the Red-supergiant phase or more evolved Blue-supergiant phase. A sequence of nuclear fusion reactions takes place before the collapse occurs. Pre-collapse evolutionary stages have been calculated by many workers over the last four decades [e.g. [Woosley 1988](#); [Woosley et al. 2002](#)]. The hydrogen nuclei first fuse to form helium for a few million years in the core of the star until the entire hydrogen is used up. Helium burning sets in when the core contracts, causing an increase in the density and temperature and the Helium fusion forms carbon. Simultaneously the hydrogen burning begins at the surrounding layers. After helium is exhausted, the core contracts further and becomes dense and hot enough to start the carbon burning to form oxygen and neon. Neon further undergoes photo-rearrangement reactions

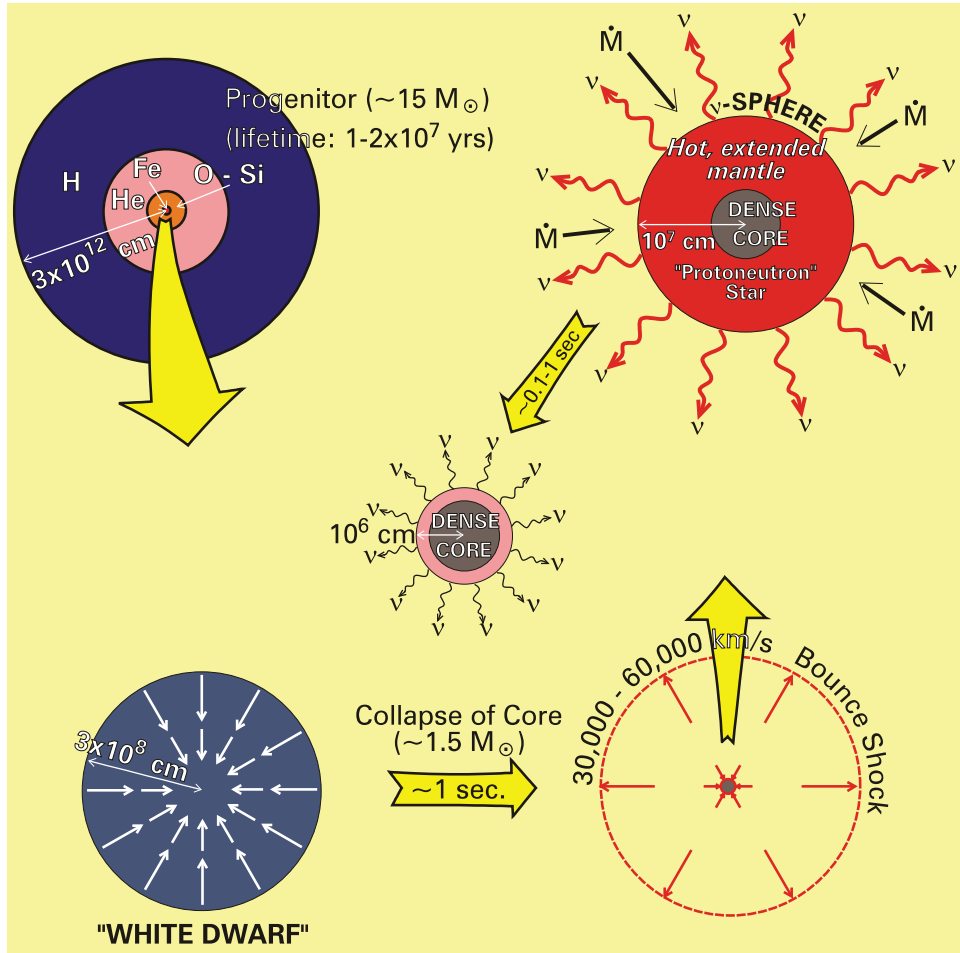


Figure 1.6 The sequence of five events in the collapse of a stellar core to a nascent neutron star. It begins with a massive star with an onion-skin structure (1st stage, at the top-left corner), goes through white-dwarf core implosion (2nd stage), to core bounce and shock-wave formation (3rd stage), to the protoneutron-star stage before explosion (4th stage), and finally to the cooling and isolated-neutron-star stage (5th stage) after explosion. This figure is not to scale. The wavy arrows depict escaping neutrinos and the straight arrows depict mass motion. Figure has been taken from [Burrows \[2012\]](#).

## 1. INTRODUCTION

---

with oxygen and magnesium. Oxygen burns to silicon and silicon burning finally gives iron group elements. Since iron is the most stable nucleus, no further fusion reactions take place. Thus, finally the star has an inert Fe core surrounded by an onion shell structure (First stage of figure 1.6) in which silicon, oxygen, neon, carbon, helium, hydrogen are burning in different layers having progressively lower densities and temperatures. From now onward, the process of collapse within the timescale of one second, many events happen to convert the ‘*implosion*’ to an ‘*explosion*’. The pioneer work in this direction was done by [Bethe and Wilson \[1985\]](#); [Burrows et al. \[1995\]](#); [Hoyle and Fowler \[1960\]](#); [Janka \[1993\]](#); [Janka and Müller \[1993\]](#); [Müller \[1994\]](#); [Myra and Bludman \[1989\]](#); [Wilson \[1983\]](#) and many other fellows. A qualitative description of the process is presented here.

### 1.3.1 Explosion mechanism of CCSNe

#### **The White-Dwarf stage:**

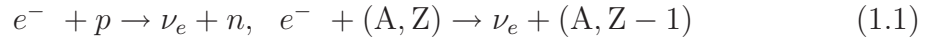
The newly formed Fe core, can not hold its dimension through ‘*electron degeneracy pressure*’ against the collapse under its own gravity. The burned material from the surrounding layers keep increasing the mass of the core. This process continues until the core reaches the ‘*Chandrasekhar mass*’ of about  $1.4 M_{\odot}$  (second stage of the figure). At this point the electrons are relativistically degenerate and can not hold the further contraction and the temperature rises. So it starts to collapse further.

#### **The collapse:**

Prior to achieving the nuclear density, inside an imploding core, pressure continues to come predominantly from relativistic electrons ( $e^{-}$ ) and hence the ratio of

---

specific heats is maintained at  $\Gamma_1 \sim 4/3$ . When the collapsing core attains the density  $\rho \sim 3 \times 10^{11} \text{g.cm}^{-3}$ , electron neutrinos ( $\nu_e$ ) generated mainly through *electron capture* (also called *deleptonization*), are trapped, depending on their energy, within the collapsing core. This physically implies that their outward diffusion time scale exists the collapsing time scale by an order of millisecond. During the collapse, the  $e^-$  capture occurred through the following reactions.



Where  $p$  and  $n$  are single proton and neutron, whereas  $A$  and  $Z$  are respectively the mass number and total number of protons of the bared nucleus. From this stage, the total number of neutrinos plus electrons inside the collapsing core become constant, though the protons are converted to neutrons and the matter inside the collapsing core get neutronized. So,  $\nu_e$ -s are called ‘*neutronization neutrino*’. The typical lepton number density inside the collapsing core becomes,  $n_1 \approx 0.40\rho N_A \text{cm}^{-3}$ , where  $N_A$  is the Avogadro’s number. The radius of this collapsing core is roughly  $10^7$  cm and hence a ‘*proto-neutron*’ star is formed.

### **Formation of bounce-shock:**

The dynamics of collapsing core segregates the imploding core into two regions: (i) an inner subsonic core which collapse homologously ( $v \propto r$ ) with its outer surface falling with local sound speed, and (ii) an outer core (mantle), having a supersonic *infall* velocity ( $v \propto r^{1/2}$ ), roughly 1/2 of the *free fall* velocity. Typical velocity of the infalling outer core is roughly 70,000  $\text{km.s}^{-1}$ . The inner core is tightly bound through sound communication and homology is preserved. Its mass is within the

## 1. INTRODUCTION

---

ranges  $0.5 - 0.7 M_{\odot}$  and mostly depends on various thermodynamic quantities like pressure and adiabatic index of the collapsing gas and how much  $e^{-}$  capture has occurred. When the density ( $\rho_1$ ) of central portion of the collapsing core approaches and exceeds the nuclear density,  $\Gamma_1$  exceeds  $4/3$  and the portion of the homologous core comes to an abrupt halt with peak temperature  $\sim 10 - 15$  MeV and a *super-nuclear* density  $\sim 7 \times 10^{14}$  g.cm $^{-3}$  and rebound as an unit. Because the outer core is out of sonic contact with its inner counterpart, the two regions collide violently. To preserve the *nuclear degeneracy*, a pressure wave is generated that propagates outwards and accumulate where the *Mach number* (ratio between local fluid speed and local sound speed) equals to one and build into a *shock wave* that begins to move out. For simplest case this shock can be considered as a *Rankin Hugoniot Shock wave* [for preliminaries on shock physics please refer [Landau and Lifshitz 1959](#)]. Thus the supernova shock is not formed at the centre of the star, but at around  $0.7 - 0.8 M_{\odot}$  location (measured in *mass coordinate*) from the center, about  $0.2 M_{\odot}$  beyond the unshocked homologous core, roughly 20 km away from the center. This can be considered as the onset of a core collapse supernova, and called '*core bounce*'. The newly formed shock is called '*bounce shock*'. Though the information to the outer world still has to come – first in the form of neutrino and then as an electromagnetic radiation.

### **Neutrino burst and delayed mechanism:**

Near the outer surface of the protoneutron star the matter density becomes so high that even  $\nu_e$  can not escape and a surface of *last-scattering* is formed  $\sim 50 - 150$  km away from the center, that behaves like *neutrinosphere* ( $\nu_e$ -sphere). Though the bounce-shock has an ample energy to onset the entire explosion, but it quickly loses

---

( $\sim 10$  ms) its energy as it reaches out the transparent (w.r.t  $\nu_e$ ) lower density region and hits the  $\nu_e$ -sphere and creates a sharp burst of  $\nu_e$ , liberating energy with peak luminosity  $\sim 10^{53-54}$  erg.s $^{-1}$ . All simulations show that after  $\nu_e$  burst, the prompt shock loses all of its energy and almost dies and is converted to a standing accretion shock, nearly stationary in radius [e.g., see [Burrows 1990](#); [Myra and Bludman 1989](#)], at a distance of 100–300 km from the center, just after passing the  $\nu_e$ -sphere.

After formation of the standing shock, the outer material of the protoneutron star starts to fall through the shock and get settled onto the newly formed compact object. The protoneutron star and  $\nu_e$ -sphere shrink until their radius becomes roughly around 10 km. The time scale of shrink is of the order of 0.1–1.0 sec. This hot collapsing remnant cools down by radiating neutrinos of all kinds, having different *flavours* viz,  $\nu_e$ ,  $\nu_\mu$ ,  $\nu_\tau$  and their antiparticles. These thermally generated neutrinos that cool down the protoneutron star are called ‘*cooling neutrinos*’ having luminosity  $\sim 10^{53}$  erg.s $^{-1}$ . This entire process occurs hours before the first light from the supernova can be seen. For SN 1987A these multiple processes were recorded nicely by the 19 such neutrino events in IMB and Kamiokande II neutrino detectors [[Bionta et al. 1987](#); [Hirata et al. 1987](#) and references therein]. These cooling neutrinos are basically responsible to make the stalled shock energized once again [[Bethe and Wilson, 1985](#)] and known as ‘*delayed explosion mechanism*’. The hot bubbles of high energetic neutrinos generated by infalling matter, create outward pressure to the post-shock material of the standing shock. Only 0.1% of this neutrino energy can be sufficient to power the SN explosion. The time scale to power the shock is equal to the time scale for generation of cooling neutrino i.e.,  $\sim 0.1 - 1.0$  sec.

### **Shock propagation in outer shells and breakout:**

## 1. INTRODUCTION

---

Since the collapsing core was out of sonic-contact from the rest part of the collapsing star, the shockwave generated near the center of the collapsing star will rapidly propagate toward the envelope of the progenitor. The outgoing SN shock wave has a velocity,  $v_s \sim 2 \times 10^3 \text{ km.s}^{-1}$  when it encounters the dense interior of the star, with radiation dominated (rich with photons) post-shock region. While approaching the surface it will accelerate in the steep density gradient up to a velocity roughly  $\sim 10^4 \text{ km.s}^{-1}$  [Chevalier, 1976; Falk and Arnett, 1977; Fransson, 1982]. The thickness of the shock front is  $c/(3.v_s.\sigma_T.n_e)$ , where  $c$  is the speed of light in vacuum,  $\sigma_T$  is the Thompson cross section of  $e^-$ -s and  $n_e$  is the number density of  $e^-$  in the shock location which is roughly equal to that of post shock region. When the optical depth from the photosphere of the star is  $\tau_s \sim c/3.v_s \approx 10$ , the radiation behind the shock starts to escape and for  $\tau_s \lesssim 2/3$  huge amount of photons start to escape giving a very strong burst of UV and soft X-ray radiation. The effective temperature of the burst is roughly  $10^{4-5} \text{ K}$  with duration  $\sim \tau_s^2/(n_e.\sigma_T.c)$ . This is the onset of a supernova that can be seen in terms of electromagnetic radiation and the burst of radiation is called as *shock breakout* phase – a radiation mediated shock is converted to a collisionless shock as the optical depth of the outflow reaches unity. The duration of breakout depends on the optical depth and post shock number density and hence on the nature of the progenitor. For compact objects like the progenitors of Type Ib/c events with steep photospheric density gradient shock breakout time scale  $\sim 1\text{d}$ , while for extended models (progenitors of Type IIP events) with shallow density gradient this time scale is of the order of  $10\text{d}$  Falk and Arnett [1977]. Since the SN event is random in space and time and also the duration of the breakout is  $\lesssim 10\text{d}$ , the direct observation of shock breakout phase is difficult, having technical challenge. So far roughly two events were directly

---

observed, one is Type IIP event SNLS-04D2dc [Schawinski et al., 2008] and other is Type Ib SN 2008D [Mazzali et al., 2008; Soderberg et al., 2008]. There are many events where we have impressions of shock breakout. Few examples are Type IIb SNe 1993J [Prabhu et al., 1995; Ripero et al., 1993; Silvestri et al., 1994], 2008ax [Roming et al., 2010], 2011dh [Tsvetkov et al., 2012] and Type IIP SNe 1999em [Pastorello et al., 2006], 2008in [Roy et al., 2011a]. In addition to this there are now mounting evidence for emergence of CCSNe from extremely energetic catastrophe like GRB/XRFs [XRF 060218/SN 2006aj, Campana et al. 2006; Sonbas et al. 2008; XRF 100316D/SN 2010bh, Cano et al. 2011; Olivares E. et al. 2012].

After breakout, how the SN shock interacts with the surrounding material and how far the hydrodynamics of SN ejecta and its propagation shows impression on the emitted electromagnetic radiations will be discussed in the subsequent sections.

### 1.3.2 Interactions with surroundings and after-effects

The pioneer works on post breakout hydrodynamics were done by Arnett [1973]; Chevalier [1982b]; Fransson [1982]; Grasberg and Nadezhin [1976]; Nadezhin [1985] and Nomoto and Sugimoto [1972]. This was further improved by Nomoto and Hashimoto [1988]; Nomoto et al. [1989] and others.

#### Shock-interaction with Circumstaller Matter

Post breakout propagation of the shock change the entire scenario. The burst environment can be segmented into four different regions. The simplest case has been sketched in left panel of Figure 1.7, where we have considered the propagation of the shock is spherically symmetric. The progenitor must have a pre-explosion wind,

## 1. INTRODUCTION

---

which is the main constituent of circumstellar medium (CSM). As the constituent of ejecta is thermodynamically different from that of CSM, a ‘*surface of discontinuity*’ is produced between outward propagating ejecta and the CSM [for more on ‘surface of discontinuity’, please refer [Shu 1982](#)]. This is ‘*contact discontinuity* (CD)’, having the property of ‘*tangential discontinuity*’. In figure it is marked by the dashed circle ‘c’. Propagation of SN shock wave creates the shocked CSM above the contact discontinuity and a distinct outwardly propagating shock-front is generated between shocked and unshocked CSM. It is marked by the outer circle ‘o’ – this is ‘*forward shock* (FS)’. Since during initial epochs, particle transfer between ejecta and CSM is blocked by CD, the fresh injected matter of the ejecta starts to accumulate behind the CD and makes another ‘shock discontinuity’ ‘i’ at the inner most portion of the ejecta. This is called ‘*reverse shock* (RS)’. These make the entire region in four environments – region ‘1’ is the inner most region, region ‘2’ is shocked ejecta, region ‘3’ is shocked CSM and region ‘4’ is the unshocked CSM. Though the detailed calculation and observations shows that the scenario is more chaotic due to multiple turbulence and internal shocks present in the shocked ejecta and CSM. With respect to CD, FS propagates in the forward direction whereas RS moves in the backward direction, though with respect to the observer in the unshocked ejecta all the surface discontinuities have outward motion. This implies, there is a velocity distribution along the radius of expanding SN shell. This is because the explosion still preserve its homologous nature ( $v \propto r/t$ ).

If  $R(0)$  is the radius of the progenitor, i.e., location of the photosphere just before the burst, then the radius of the homologously expanding spherical shell at

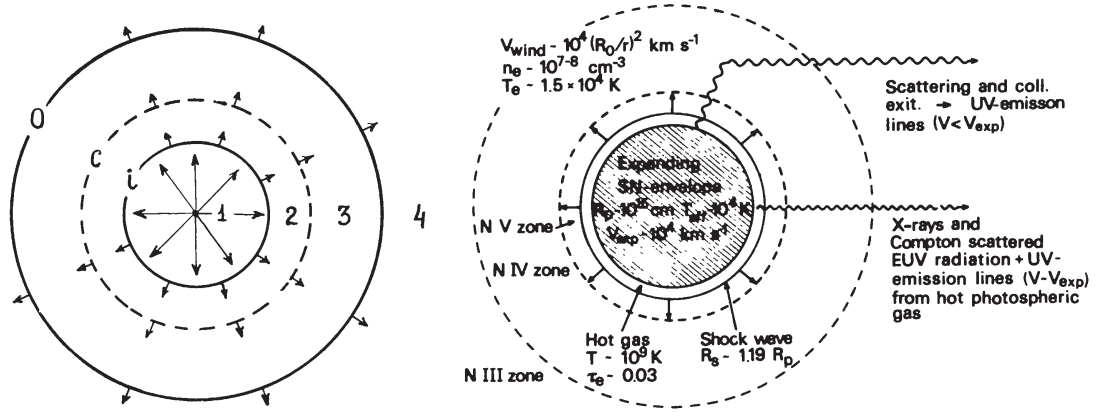


Figure 1.7 The schematic representation of SN evolution after shock breakout. The left panel shows snapshot of the simplest case, where Hugoniot shocks are propagating outward after a point explosion i.e., dimension of the exploding star is negligible in comparison to the dimension of the expanding ejecta [Nadezhin, 1985]. The right panel represents a relatively generalized case, where emissions from different regions have been indicated [Fransson, 1982].

a time ‘ $t$ ’ can be written as [Arnett, 1982],

$$R(t) = R(0) + v_{sc}.t \quad (1.2)$$

In first approximation,  $R(t)$  can be considered as the outer surface of the expanding ejecta i.e. the contact discontinuity. Here  $v_{sc}$  is the ‘velocity scale’ and can be defined as,

$$v_{sc} = v(x)/x \quad (1.3)$$

where,

$$x = r(m, t)/R(t) \quad (1.4)$$

Here ‘ $x$ ’ is a ‘similarity variable’, known as the dimensionless radius of the spherical shell inside the expanding medium that contains a fluid element of mass ‘ $m$ ’ of the

## 1. INTRODUCTION

---

ejecta and normalized by the radius of the expanding photosphere. In a more generalized scenario, the expanding medium can be considered to have a time dependent, power law density profile [Chevalier, 1982b],

$$\rho_{ej} = t^{-3} \cdot (r/t \cdot g)^{-n} \quad (1.5)$$

whereas the CSM has a power-law density profile, without any time dependency.

$$\rho_{CSM} = q \cdot r^{-s} \quad (1.6)$$

Since the CD is a tangential discontinuity, there will not be any exchange of matter across CD. This implies at the position ( $R_{CD}$ ) of CD,

$$\partial\rho/\partial r = 0, \quad \text{i.e.,} \quad (\partial\rho_{ej}/\partial r)_{R_{CD}} = (\partial\rho_{CSM}/\partial r)_{R_{CD}} = 0 \quad (1.7)$$

This corresponds to

$$R_{CD} = [(n/s) \cdot (g^n/q)]^{1/(n-s)} \cdot t^{(n-3)/(n-s)} \quad (1.8)$$

Since CD will accelerate with time ( $\partial^2 R_{CD}/\partial t^2 = 0$ ), then according to above expression we can not get any real solution for  $s \neq 3$ . Moreover for  $n = 5$  we get  $R_{CD} \propto t^{2/(5-s)}$ , which is consistent with the results of point explosion [Sedov, 1959]. Motion of SN shocks and its interaction with surrounding has a self similar nature and investigated by many workers [Chevalier, 1982b; Nadezhin, 1985; Ostriker and McKee, 1988]. If  $R_{FS}$  and  $R_{RS}$  are respectively the radii of forward and reverse shocks at a time  $t$  after explosion, then assuming an adiabatic explosion and neglect-

---

ing the Rayleigh-Taylor instability process one can establish a self similar solution for this expansion that yields a set of three expressions showing the relation between shocked CSM and ejecta in terms of pressure ( $p$ ), density ( $\rho$ ) and bulk velocity ( $v$ ) [Chevalier, 1982b]:

$$\frac{\rho_{RS}}{\rho_{FS}} = \left(\frac{P_{RS}}{P_{FS}}\right) \cdot \left(\frac{R_{FS}}{R_{CD}}\right)^s \cdot \left(\frac{R_{RS}}{R_{CD}}\right)^{-n} \cdot \left(\frac{n-3}{3-s}\right)^2 \quad (1.9)$$

$$\frac{p_{RS}}{p_{FS}} = \left(\frac{P_{RS}}{P_{FS}}\right) \cdot \left(\frac{R_{FS}}{R_{CD}}\right)^{-(2-s)} \cdot \left(\frac{R_{RS}}{R_{CD}}\right)^{-(n-2)} \quad (1.10)$$

$$\frac{v_{RS}}{v_{FS}} = \left(\frac{R_{FS}}{R_{CD}}\right)^{-1} \cdot \left(\frac{R_{RS}}{R_{CD}}\right) \cdot \frac{U_{RS}}{U_{FS}} \quad (1.11)$$

where  $P_{RS}$  and  $P_{FS}$  are the self-similar pressures at reverse and forward shock positions whereas  $U_{RS}$  and  $U_{FS}$  are the self-similar velocities at those shock fronts [Chevalier, 1982b]. Finally, the relation between the masses of swept-up, shocked CSM and shocked ejecta can be given as

$$\frac{M_{ej}}{M_{CSM}} = \left(\frac{P_{RS}}{P_{FS}}\right) \cdot \left(\frac{R_{FS}}{R_{CD}}\right)^{-(3-s)} \cdot \left(\frac{R_{RS}}{R_{CD}}\right)^{-(n-3)} \cdot \left(\frac{n-3}{3-s}\right) \quad (1.12)$$

The above four self-similar expressions are not implicitly dependent on time and represent the hydrodynamical state of SN ejecta expanding within an ambient medium having constant density during any ‘snapshot’. Right panel of figure 1.7 shows more detailed view of a typical snapshot of an expanding SN ejecta near maximum light. The inner-most sphere is the SN-envelope having effective temperature  $\sim 10^4$  K, radius  $\sim 10^{15}$  cm with expansion velocity  $\sim 10^4$  km.s $^{-1}$ . This region is responsible for optical emission. The outer hot gas produces UV radiation due to scattering and collisional excitation, whereas X-ray and Compton scattered FUV radiation along

## 1. INTRODUCTION

---

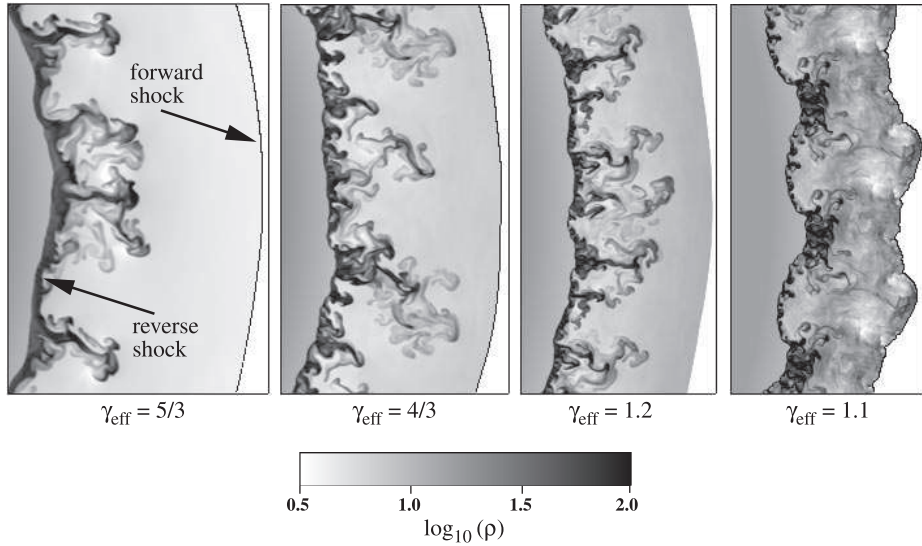


Figure 1.8 2D simulation of Rayleigh-Taylor (R-T) instability for a typical SN explosion [Blondin and Ellison, 2001]. With lower value of of adiabatic index ( $\gamma_{eff}$ ), effect of instability is more pronounced.

with UV emission lines are produced from hot photospheric gas (hot ejecta). The progenitor of Type IIP SNe are red supergiant with mass  $\gtrsim 8 M_{\odot}$  has a very extended envelope ( $\gtrsim 10^{14}$  cm) and wind velocity  $\sim 10 \text{ km.s}^{-1}$ , whereas the precursors of Type Ibc events are more compact Wolf Rayet (WR) stars (radius  $\sim 10^{11}$  cm) with wind velocity  $\sim 10 - 60 \text{ km.s}^{-1}$ . This progenitor wind is the principal component of CSM and the high energy  $e^{-}$ s are produced at the outer-edge of shocked CSM through first-order ‘*Fermi acceleration*’, that further produce synchrotron radiation in the presence of magnetic field.

### Shock-instability:

In actual cases the interaction is occurred through instability. The hydrodynamical instability in supernova ejecta and its importance to understand the mixing of

---

$^{56}\text{Ni}$  in the ejecta (discussed in §1.3.3) as well as the process of particle acceleration were studied by several workers through one, two and recently in three dimensional simulation. A result from [Blondin and Ellison \[2001\]](#) on more generalized 2D hydrodynamical simulation of shock instability has been presented in figure 1.8. The figure shows the effect of Rayleigh-Taylor (R-T) instability for particular density profile of the ejecta ( $n = 7$ ) and CSM ( $s = 2$ ) with different values of ratio of specific heats ( $\gamma_{eff}$ ). The snaps were taken at the end of the simulations, once the instability has reached saturation. Lower value of  $\gamma_{eff}$  produces narrower and denser shell of shocked ejecta with a sharper, denser R-T instability as well as a comparatively shrunked interaction region. With a lower value of  $\gamma_{eff}$  the instability can reach upto forward shock and can distort its geometry from spherical symmetry. Hence the mixing will be more and the effect of radioactive elements on the emitted electromagnetic radiation will be different from the simplest cases.

This is worth mentioning that though it is assumed that during early epochs (first 50 days after explosion) SN photosphere (especially of Type IIP) is optically thick, but actually this assumption does not hold beyond the maximum light ( $\sim 15$  days after burst) [[Wagoner, 1982](#)]. The photosphere of a star is defined as the last electron-scattering surface (where  $\tau_s \lesssim 2/3$ ) from where continuum spectrum is created. [Eastman et al. \[1996\]](#) proposed that in an expanding photosphere the continuum spectrum that is ultimately released from the electron-scattering surface is produced in the deeper layer at which the radiation field thermalizes to the local gas temperature, known as the ‘*thermalization depth*’ and this smaller radius is the location where thermal continuum is generated. Hence the true blackbody continuum basically comes from more inner surface and the SN photosphere behaves like a ‘*diluted blackbody*’ and the ‘*dilution factor*’ is defined as  $\zeta = R_{ther}/R_{phot}$ . Here

## 1. INTRODUCTION

---

$R_{ther}$  is the radius of ejecta at the thermalization depth,  $R_{phot}$  is the photospheres radius (i.e., the surface of last scattering). Hence the photosphere effectively moves inward and the simple assumptions mentioned above will not hold further. This issue was further arised by [Dessart and Hillier \[2008\]](#); [Hamuy et al. \[2001\]](#); [Leonard et al. \[2002a\]](#) and others while using Type IIP SNe as a distance indicator. Modeling of SN atmosphere has been done to compute correct value of  $\zeta$  for different photometric bands.

### 1.3.3 Radiations emitted from explosions: light curves and spectra

Optical light curves and spectra provide the signatures of explosion mechanism and the interaction of the ejecta with the surrounding. Figures 1.3 and 1.4 demonstrate how the nature of radiation can be changed on the basis of progenitor properties and the environment in which it is formed. Evolution of optical light can be divided into three phases – ‘*Shock breakout phase*’, ‘*Photospheric phase*’ and ‘*Nebular phase*’.

#### Radiations during Shock breakout:

Shock breakout is the brightest radiative phenomenon in a supernova but is difficult to be observed due to the short duration and X-ray and UV-peaked spectra. So far there are only few examples like SNLS-04D2dc [[Schawinski et al., 2008](#)], SNLS-06D1jd [[Gezari et al., 2008](#)], SN 208D [[Soderberg et al., 2008](#)] for which we have a direct observations of shock breakout. Starting from [Arnett \[1980, 1982\]](#); [Colgate and McKee \[1969\]](#); [Pinto and Eastman \[2000\]](#) and others have proposed the early light curve of SNe. Very early ( $\lesssim 1$  day) light curve, temperature and spectral evolution

---

of SN 1987A and SN 1993J were modeled by [Blinnikov et al. \[2000, 1998\]](#). Recently [Tominaga et al. \[2009\]](#) modeled the emerging Type II SN ‘SNLS-04D2dc’ observed by *GALEX* satellite. [Tominaga et al. \[2011\]](#) further predicted the probable nature of UV-optical light curve and spectra of an emerging Type II supernova. The nature of emerging light of Type Ib SN 2008D is still debatable. Majority of the community demonstrated the event as a shock breakout effect [[Soderberg et al., 2008](#)], though the possibility of failed GRB can not be ruled out [[Mazzali et al., 2008](#)]. The emergence of Type Ibc events from GRBs/XRFs were observed for many cases. Recently [Olivares E. et al. \[2012\]](#) was able to model the evolution of luminous Type Ic SN 2010bh from XRF 100316D – emergence of blackbody SN light from so called non-thermal radiation of XRF was clearly visible.

### **Generation of optical-IR light curves:**

Since large number of photons are lost during shock breakout process, only shock physics can not explain the long lasting optical light curve of SNe. This is the radioactive power that drives the SN evolution from around peak photospheric light. It was proposed long back by [Colgate and McKee \[1969\]](#) and shown schematically in left panel of figure 1.9. During the radioactive decay,  $^{56}\text{Ni}$  produces  $^{56}\text{Co}$  through  $e^-$  capture and  $\gamma$ -ray emission with a half-life time  $\sim 6.1$  days, that further converted to stable  $^{56}\text{Fe}$  through several  $e^-$  capture and positron ( $\beta^+$ ) transition with half-life time  $\sim 77.0$  days. It was believed that all the heavy elements are radially stratified inside the ejecta and the radioactive elements are concentrated at the central region of the ejecta [[Falk and Arnett, 1977](#)] as shown at the right panel of figure 1.9. The  $\gamma$ -rays and  $\beta^+$  energy are fully trapped inside the optically thick ejecta and re-emitted in the form of optical radiation that illuminates the SN. This is known as ‘*photospheric phase*’. After couple of months ( $\sim 100$  days for Type IIP events and

# 1. INTRODUCTION

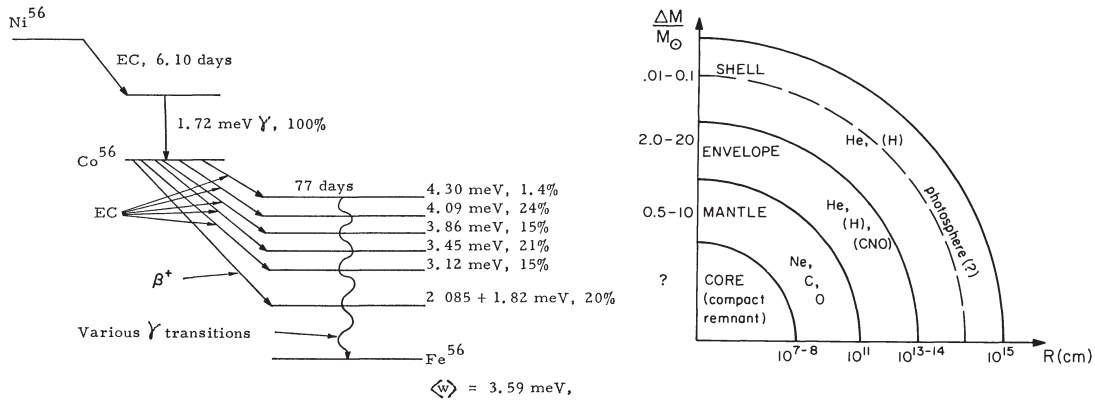


Figure 1.9 **Left panel:** The nuclear decay of radioactive  $^{56}\text{Ni}$  to  $^{56}\text{Co}$  and then to stable  $^{56}\text{Fe}$ . The energy released during this decay process is the main source that power the SNe. The figure has been borrowed from Colgate and McKee [1969]. **Right panel:** The proposed shell structure of SN ejecta by Falk and Arnett [1977]. The radioactive source was supposed to be at the innermost portion of the ejecta and other heavy elements are radially stratified. The fractions of stellar mass distributed in different shells are also shown. The  $\gamma$ -ray produced was supposed to get absorbed totally by the outer ejecta, that further produces the optical photons. The scenario changed after the occurrence of SN 1987A and the mixing of  $^{56}\text{Ni}$  in the ejecta was proposed.

$\sim 50$  days for Type Ibc events), when the ejecta become optically thin,  $\gamma$ -rays and  $\beta^+$  particles start to leak-out. A decline in optical light is observed with constant decline rate  $\sim 0.0098 \text{ mag.d}^{-1}$ , comparable with  $^{56}\text{Co} \rightarrow ^{56}\text{Fe}$  nuclear transition rate. This is the ‘*nebular phase*’.

Based on above shell model,  $\gamma$ -rays [Chan and Lingenfelter, 1987] and X-rays [McCray et al., 1987] were expected to emerge nearly 9 months after the burst of SN 1987A, but only after  $\sim 5$  months, X-ray stars to appear. To explain this discrepancy, an *ad hoc* assumption of ‘*mixing*’ was proposed [Arnett and Fu, 1989; Fu and Arnett, 1989; Pinto and Woosley, 1988; Shigeyama et al., 1988], in which the  $^{56}\text{Co}$  and other heavy elements are stratified throughout the ejecta. It was proposed that dynamical instability (see figure 1.8) may be a cause for this mixing

---

[Arnett et al., 1989; Chevalier, 1976; Ebisuzaki et al., 1989]. The instability along with asphericity can also be introduced due to initial rotation of the collapsing core [Burrows et al., 2005a].

Observations and theoretical exercises carried out over last five decades have developed our understanding about electromagnetic signatures of these catastrophe. Multi-band optical light curves of Type I events demonstrate that high energy and high frequency photons can quickly come-out from the ejecta environment than the low energy and low frequency light. On the other hand Type II events (except Type IIb) are almost equally opaque to entire optical light. The analytical models were initially developed by Arnett [1980, 1982]; Chugai [2000]; Litvinova and Nadezhin [1985]. The nature of late time nebular light curve was further investigated by Jeffery [1999]; Maeda et al. [2003]; Valenti et al. [2008a]. The extremely nebular light of Type II SNe were also modeled analytically by Chugai [1992a] assuming *super-wind* environment of SN progenitor. Meanwhile, hydrodynamical modeling of Type I and Type II SNe were also started considering the initial physical properties of the progenitors and final nucleosynthesis processes of the progenitors as the initial boundary condition [Aksenov and Imshennik, 1994; Blinnikov and Bartunov, 1993; Eastman et al., 1994; Hashimoto et al., 1993; Weaver and Woosley, 1993; Woosley, 1993; Woosley et al., 1994]. The two dimensional model is further developed in recent years to determine the explosion parameters and main sequence mass of the progenitors, to understand the polarization properties as well as to establish the connection between Type IIb, Ib and Ic explosions [Bersten et al., 2011; Dessart et al., 2011, 2010; Pumo and Zampieri, 2011].

The left panel of figure 1.10 represents a schematic diagram of Type IIP light curve. The hydrodynamical modeling of Type IIP light curves predict a correlation

# 1. INTRODUCTION

---

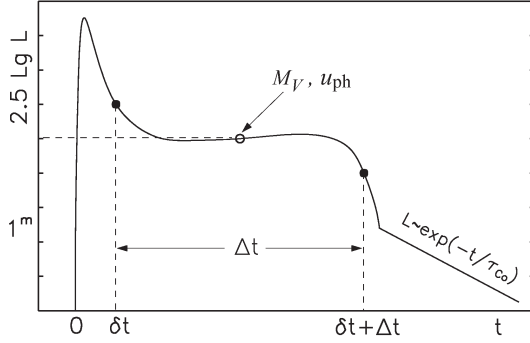


Figure 1.10 The schematic diagram of Type IIP lightcurve [Nadyozhin, 2003]. The abscissa is the time, while ordinate shows the log of luminosity. Lightcurve is segmented in three phases, (i)  $0 < t < \delta t$  is the breakout phase, (ii)  $\delta t < t < \delta t + \Delta t$  is called plateau phase, when luminosity of Type IIP events is remain constant, and (iii)  $t > \Delta t$  is called nebular phase.  $M_V$  and  $u_{ph}$  are mid-plateau V-band absolute magnitude and photospheric velocity in the comparable epoch, measurable from photometry and spectroscopy. There is a strong relation between observed and physical properties of Type IIP events.

between three observable parameters (plateau duration  $\Delta t$ , mid-plateau absolute magnitude  $M_V$  and photospheric velocity  $u_{ph}$ ) and the physical parameters (explosion energy  $E_{exp}$ , ejected mass  $M_{ej}$  and pre-explosion radius of the progenitor  $R(0)$ ) [Litvinova and Nadezhin, 1985; Nadyozhin, 2003]. This is as follows.

$$\text{Log}_{10}(E_{exp}) = -0.135.M_V + 2.34.\text{Log}_{10}(\Delta t) + 3.13.\text{Log}_{10}(u_{ph}) - 4.205 \quad (1.13)$$

$$\text{Log}_{10}(M_{ej}) = -0.234.M_V + 2.91.\text{Log}_{10}(\Delta t) + 1.96.\text{Log}_{10}(u_{ph}) - 1.829 \quad (1.14)$$

$$\text{Log}_{10}(R(0)) = -0.572.M_V - 1.07.\text{Log}_{10}(\Delta t) - 2.74.\text{Log}_{10}(u_{ph}) - 3.350 \quad (1.15)$$

The epochs of transition from breakout to plateau phase and plateau to nebular phase are determined by calculating the point of inflection [Elmhamdi et al., 2003a]. Several analytical expressions were proposed to determine the ejected  $^{56}\text{Ni}$  mass [Elmhamdi et al., 2003a; Hamuy, 2003]. If  $L_t$  is the nebular luminosity of the SN at

---

any time ‘t’, then the amount of radioactive  $^{56}\text{Ni}$  produced in terms of solar mass is given by [Hamuy, 2003]:

$$\frac{M_{Ni}}{M_{\odot}} = (7.866 \times 10^{-44}).L_t.exp \left[ \frac{(t - t_0)/(1 + z) - 6.1}{111.26} \right] \quad (1.16)$$

Where  $t_0$  is the epoch of explosion.

Measurement of progenitor properties of Type I events is not as straight forward as Type IIP. The analytical model, proposed by Arnett [1982] did not consider the heating effect due to  $^{56}\text{Co}$  decay, as a result the theoretical curve does not satisfy the observation after few days beyond maxima. This effect was considered by Clocchiatti and Wheeler [1997]; Jeffery [1999]; Valenti et al. [2008a]. Beyond +60d Type I SN envelope becomes almost transparent, the  $\gamma$ -rays are no more trapped and constant decline in the light curve can be seen. Moreover Maeda et al. [2003] showed that if we assume two components of Type Ibc ejecta then diagnostic tool will be more relevant to the observed properties.

If we neglect the breakout part and only concentrate on the radioactive heating, then light curve can be segmented in two phases. For  $t \lesssim 30$  days past explosion, the ejecta can be assumed as a spherically symmetric homologously expanding medium without any mixing of  $^{56}\text{Ni}$ , constant optical opacity  $k_{opt}$ , initial radius is negligible ( $R(t) \gg R(0)$ ) and the diffusion approximation is valid for photons (optically thick ejecta). With these assumptions, the luminosity evolution in the photospheric phase is described by the following equation.

$$L_{ph}(t) = M_{Ni} \times e^{-x^2} \times \left[ (\epsilon_{Ni} - \epsilon_{Co}) \int_0^x A(z) dz + \epsilon_{Co} \int_0^x B(z) dz \right] \quad (1.17)$$

## 1. INTRODUCTION

---

here

$$A(z) = 2ze^{-2zy+z^2} \quad , \quad B(z) = 2ze^{-2zy+2zs+z^2} \quad (1.18)$$

where  $x \equiv t/\tau_m$ ,  $y \equiv \tau_m/(2\tau_{Ni})$ , and  $s \equiv [\tau_m(\tau_{Co} - \tau_{Ni})/(2\tau_{Co}\tau_{Ni})]$ .  $\epsilon_{Ni}$  ( $= 3.90 \times 10^{10} \text{ erg s}^{-1} \text{ g}^{-1}$ ) and  $\epsilon_{Co}$  ( $= 6.78 \times 10^9 \text{ erg s}^{-1} \text{ g}^{-1}$ ) are respectively the energies produced in one sec by 1 gram of  $^{56}\text{Ni}$  and  $^{56}\text{Co}$ .  $\tau_{Ni}$  ( $= 8.8\text{d}$ ) and  $\tau_{Co}$  ( $= 111.11\text{d}$ ) are respectively the mean life times of  $^{56}\text{Ni}$  and  $^{56}\text{Co}$ , while  $\tau_m$  is called the ‘*diffusion time-scale*’ of the light curve, given by

$$\tau_m = \left(\frac{k_{opt}}{\beta c}\right)^{1/2} \left(\frac{10M_{ej}^3}{3E_k}\right)^{1/4} \quad , \quad (1.19)$$

where  $\beta \approx 13.8$  is a constant of integration [Arnett, 1982]. Equation 1.17 is the modified Arnett’s expression where  $^{56}\text{Co}$  heating is also considered. For  $t \gtrsim 60$  days past explosion, the SN light is fully governed by the energy deposition of radioactive decay  $^{56}\text{Ni} \rightarrow ^{56}\text{Co} \rightarrow ^{56}\text{Fe}$ . According to the results, produced by Cappellaro et al. [1997]; Sutherland and Wheeler [1984], the nebular light is given by,

$$L_{neb}(t) = S^{Ni}(\gamma) + S^{Co}(\gamma) + S_{e^+}^{Co}(\gamma) + S_{e^+}^{Co}(KE), \quad (1.20)$$

where  $S^{Ni}(\gamma)$  is the source energy of the nickel decay,

$$S^{Ni}(\gamma) = M_{Ni}\epsilon_{Ni}e^{-t/\tau_{Ni}} \quad , \quad (1.21)$$

Other terms are the amount of energy deposited by the radioactive decay of  $^{56}\text{Co}$  (81% of the energy is released as  $\gamma$ -rays and 19% of the energy is released as

---

positrons). The rate of energy production ( $\mathcal{E}$ ) by the  $^{56}\text{Co}$  decay is given by,

$$\mathcal{E} = M_{Ni} \epsilon_{Co} (e^{-t/\tau_{Co}} - e^{-t/\tau_{Ni}}) \quad (1.22)$$

The energy  $S^{Co}(\gamma)$  generated by the deposition of  $\gamma$ -rays from  $^{56}\text{Co}$  decay is written as

$$S^{Co}(\gamma) = 0.81 \mathcal{E} (1 - e^{-(F/t)^2}) \quad (1.23)$$

and the amount energy deposited by the  $\gamma$ -rays produced in the positron annihilation  $S_{e^+}^{Co}(\gamma)$  is expressed as

$$S_{e^+}^{Co}(\gamma) = 0.164 \mathcal{E} (1 - e^{-(F/t)^2})(1 - e^{-(G/t)^2}) \quad (1.24)$$

while the source energy due to the kinetic energy of the positrons  $S_{e^+}^{Co}(KE)$  is

$$S_{e^+}^{Co}(KE) = 0.036 \mathcal{E} (1 - e^{-(G/t)^2}) \quad (1.25)$$

The parameters ‘F’ and ‘G’ are functions of the ejected mass, kinetic energy and opacity. According to [Clocchiatti and Wheeler \[1997\]](#),

$$F = \sqrt{\left(C(\rho)k_\gamma M_{ej}^2\right)/E_k} \quad (1.26)$$

$$G = \sqrt{\left(C(\rho)k_{e^+} M_{ej}^2\right)/E_k} \quad (1.27)$$

where  $C(\rho)$  is a function of the density  $\rho$ . For a homogeneous density, one can constrain that  $k_\gamma = 0.027$ , and  $k_{e^+} = 7$  [[Clocchiatti and Wheeler, 1997](#)]. This implies  $F \approx 32.M_{ej}/\sqrt{E_{51}}$  and  $G \approx 515.M_{ej}/\sqrt{E_{51}} = 16.1F$ . Above set of equations can be

# 1. INTRODUCTION

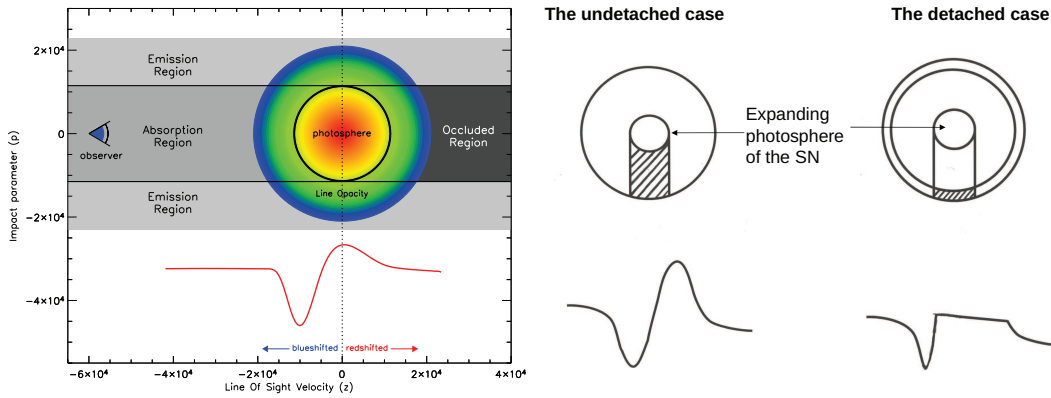


Figure 1.11 **Left panel:** Formation of the inverted P-Cygni line profile. All the material on a vertical plane perpendicular to the observers line of sight has the same component of velocity along the observers line of sight, and hence the same Doppler shift. **Right panel:** The more realistic situation, where the line forming regions may not be attached with each other and distributed in a shell (‘detached’ case). The absorption width will be narrower and the emission peak will be flat. If the regions are ‘undetached’, we will get the inverted P-Cygni profile.

utilized to produce the bolometric light curve and to measure the parameters. For Type Ibc event the effect of segregation is necessary to be introduced to get more correct result [Maeda et al., 2003].

## Evolution of Spectra:

The spectral evolution of supernova provides various information about ejecta composition, structure, velocity profile and optical opacity of the ejecta. A sample of spectra has been shown in figure 1.4. The spectra are mostly dominated by ‘*inverted P-Cygni*’ profiles and also become distorted in late epochs due to heavy ‘*line-blanketing*’. The continuum emission is prominent in early spectra, showing the prominent blackbody nature of the SN. The shape and width of the profile is the natural result of ‘*Doppler shifts*’ arising from the expansion of the supernova

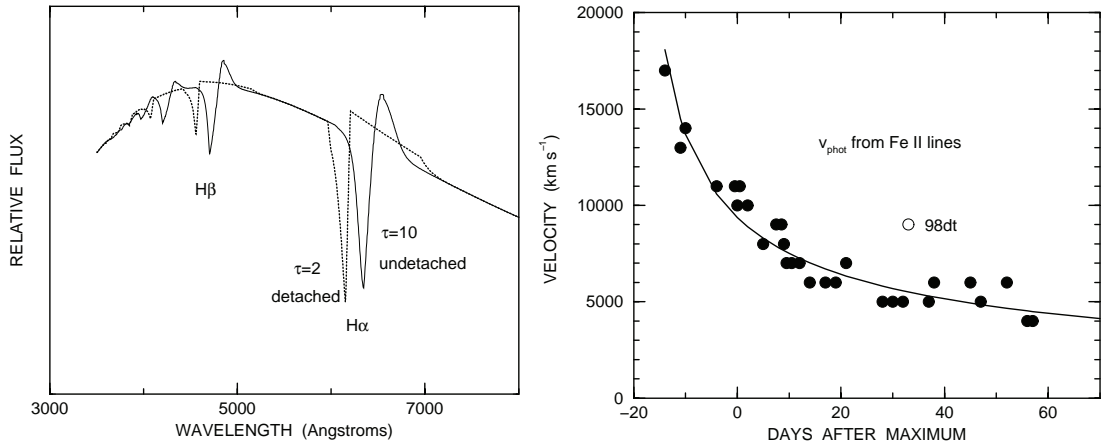


Figure 1.12 **Left panel:** Synthetic spectrum (dotted line) that has photospheric velocity  $v_{ph} = 10,000 \text{ km.s}^{-1}$  and hydrogen lines detached at  $20,000 \text{ km.s}^{-1}$ , where  $\tau_{H\alpha} = 2$ , is compared with a synthetic spectrum (solid line) that has  $v_{ph} = 10,000 \text{ km.s}^{-1}$  and undetached hydrogen lines, with  $\tau_{H\alpha} = 10$  at the photosphere [Branch et al., 2002]. **Right panel:** Velocity of the photosphere, as inferred from Fe II lines, is plotted against time after maximum light. The velocity evolution can be presented mathematically by a power-law fit to the data. The velocity of SN 1998dt at 32 days (open circle) has been excluded [Branch et al., 2002].

ejecta. Creation of inverted P-Cygni profile has been presented in the left panel of figure 1.11. The continuum flux can be thought of as coming from the surface of an ‘*optically thick*’ photosphere. The line formation occurs in the photosphere, which is called as supernova atmosphere. The line opacity in this region, which is directly intervening between the photosphere and the observer, scatters or absorbs flux from the photosphere and creating an absorption feature. As the material in the absorption region is moving toward the observer, the absorption feature is blueshifted. Material outside of the ‘tube’ like ‘absorption region’ does not obscure the photosphere, but rather scatters or emits additional flux into the observer line of sight. This leads to an emission feature that is centered on the line rest wavelength. This is ‘emission region’. The material in the tube behind the photosphere is the ‘occluded region’ and not visible at all. In the present example of P-Cygni profiles

## 1. INTRODUCTION

---

in supernova spectra reflects that the particular line forming region inside the ejecta is moving spherically with velocity  $\sim 10,000 \text{ km.s}^{-1}$  and the breadth of the profiles along the observers line of sight roughly ranges from  $-20,000$  to  $20,000 \text{ km.s}^{-1}$ . In the more realistic situation, where the line forming regions may not be attached with each other and distributed in a shell (*'detached'* case) we may get a different kind of line profile (right panel of figure 1.11) [Branch et al., 2002]. The absorption width will be narrower and the emission peak will be flat. If the regions are *'undetached'*, we will get the inverted P-Cygni profile.

When the ejecta is optically thin, spectra will be mainly governed by the emission lines. The SN ejecta kinematics are described by homologous expansion,  $R(t) = v(R).t$ , where 'R' and  $v(R)$  are respectively the radius (in a spherical coordinate) and the radial expansion velocity of a point in the ejecta. Non-radial velocity components should be negligible. 't' is the time elapsed after burst. The observed wavelength of a photon depends on the point from which it was emitted, as  $\lambda = \lambda_0.(1 - v_{||}/c)$ , where  $\lambda_0$  is the rest wavelength of the line,  $v_{||}$  is the line-of-sight velocity toward the observer, and 'c' is the speed of light. Then, defining 'd' as the projection of R onto the line of sight, it can be shown that  $v_{||} = d/t$ , and this is the same in a given plane perpendicular to the line of sight. This means that, in the late phase, all photons emitted at the same depth along the line-of-sight have the same wavelength. The wavelength of a photon emitted from the near/far side of the ejecta is detected as shorter/longer (blueshifted/redshifted).

The effect of line velocity and structure of the ejecta on the spectrum has been shown in left panel of figure 1.12, the low optical depth in the detached case produces more blueshift in comparison to the undetached case having large optical depth. The right panel of 1.12 shows the photospheric velocity ( $v_{phot}$ ) profile of Type Ib events,

---

measured from absorption dip of Fe II lines, For the simple case of constant opacity and  $v^{-n}$  density profile, the velocity at the photosphere would decrease with time as  $v_{phot} \propto t^{-2/(n-1)}$ . In figure 1.12 it has been shown that  $n = 3.6$  corresponds to the best fit. When the opacity is not really constant, the actual density distribution does not really follow a single power law over a wide range of velocity. Hence, the best power-law index for fitting the spectra will not be well constrained, and that the line optical depths need not have the same radial dependence as the density. Then the above simple scenario will not be preserved.

Many groups are involved individually to model the SN spectra of different kinds. Few of them are ‘**SYNOW**’ [Branch, 1999], ‘**CMFGEN**’ [Dessart and Hillier, 2010], and ‘**PHOENIX**’ [Hauschildt and Baron, 1999]. In this present work few implications of ‘*SYNOW*’ will be discussed.

### **Generation of Radio wave:**

The radio light curve is the signature of shock interaction with the circumstaller medium. The electrons gain their energy through ‘Fermi acceleration’ process during its repeated scattering across the forward shock. The light curves are determined by the shape of the spectrum along with the evolution of the peak, which in turn are determined by the nature and the evolution of ejecta. If the SN is associated with GRB (see §1.4.2) or if we consider the radio emission from the GRB afterglows, then the spectral peak either corresponds to the minimum energy of the synchrotron emitting electrons (with peak frequency  $\nu_m$ ), or it may corresponds to a turnover due to synchrotron self-absorption (with self-absorption frequency  $\nu_a$ ). The spectrum in both cases has a high-energy optically thin spectral index  $\beta$  and a low-energy spectral

# 1. INTRODUCTION

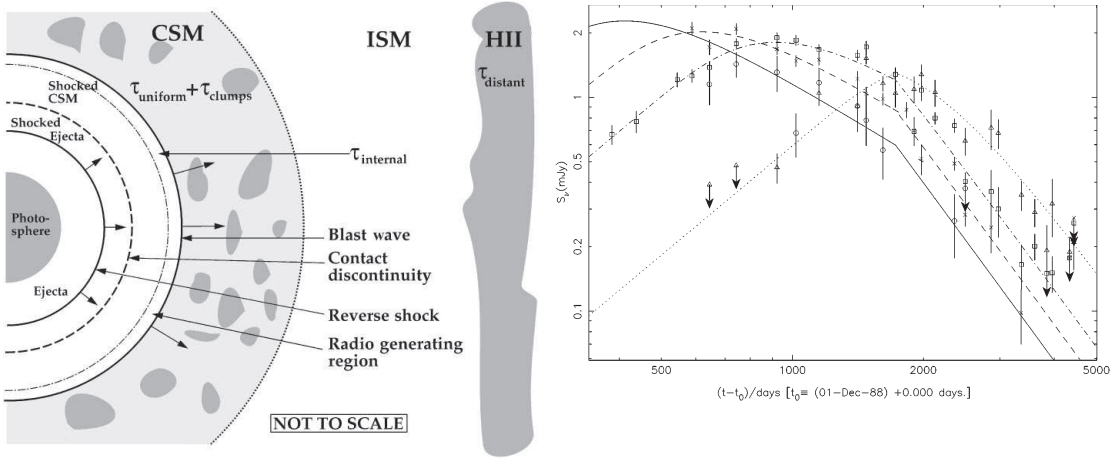


Figure 1.13 **Left panel:** The Cartoon, not to scale, is borrowed from [Weiler et al. \[2002\]](#). It represents the schematic diagram of radio supernova and its shocks, along with the stellar wind-established circumstellar medium (CSM), the interstellar medium (ISM), and more distant ionized hydrogen absorbing gas (H II region). The radio emission is expected to arise near the blastwave front. **Right panel:** The long term Radio monitoring and “light curves” for SN1988Z. The plot shows the light curves in four wavelengths [2 cm (14.9 GHz, open circles, solid curve), 3.6 cm (8.4 GHz, crosses, dashed curve), 6 cm (4.9 GHz, open squares, dot-dash curve), and 20 cm (1.5 GHz, open triangles, dotted curve)] along with their best fit. The figure has been borrowed from [Weiler et al. \[2002\]](#).

---

index with a fixed value of  $1/3$  ( $\nu_a < \nu < \nu_m$ ),  $2$  ( $\nu < \nu_{a,m}$ ) or  $2.5$  ( $\nu_m < \nu < \nu_a$ ) [Sari et al., 1998; Wijers and Galama, 1999].

The other way of explaining Radio SNe is the generation of radio wave due to synchrotron self-absorption [Chevalier, 1998] and/or due to free-free absorption from the ambient medium, causing an exponential cut-off below the peak [Weiler et al., 1986]. This has been shown schematically in the left panel of figure 1.13. The radio generating region is a thin shell just behind the forward-shock, having an internal opacity due to synchrotron self-absorption (SSA) and/or due to free-free absorption (FFA). Beyond that, due to CSM (uniformed/structured) and due to distant H II region there will be excess amount of optical depth. Considering all these effects the radio light curves can be modeled. One such example is presented in the right panel of the figure, where long term radio emission from SN 1988Z has been modeled using the scheme of [Weiler et al., 1986].

### 1.3.4 Fate of the progenitors

At this point the important questions are mainly to know about the stars which give rise to different kinds of SNe and probably leave different types of compact remnant. Though we have a rough understanding about the places where this kind of explosions are happening, above question will provide a test of stellar evolution theory and give information for galactic chemical evolution and predict SNe birth rates and remnant populations. The fate of a massive star is governed chiefly by its mass and composition at birth and by the history of its mass loss. For single stars, mass loss occurs as a result of stellar winds, for which semiempirical estimates are present. De Donder and Vanbeveren [1998, 2003]; Eldridge and Tout [2004]; Heger et al. [2003]

# 1. INTRODUCTION

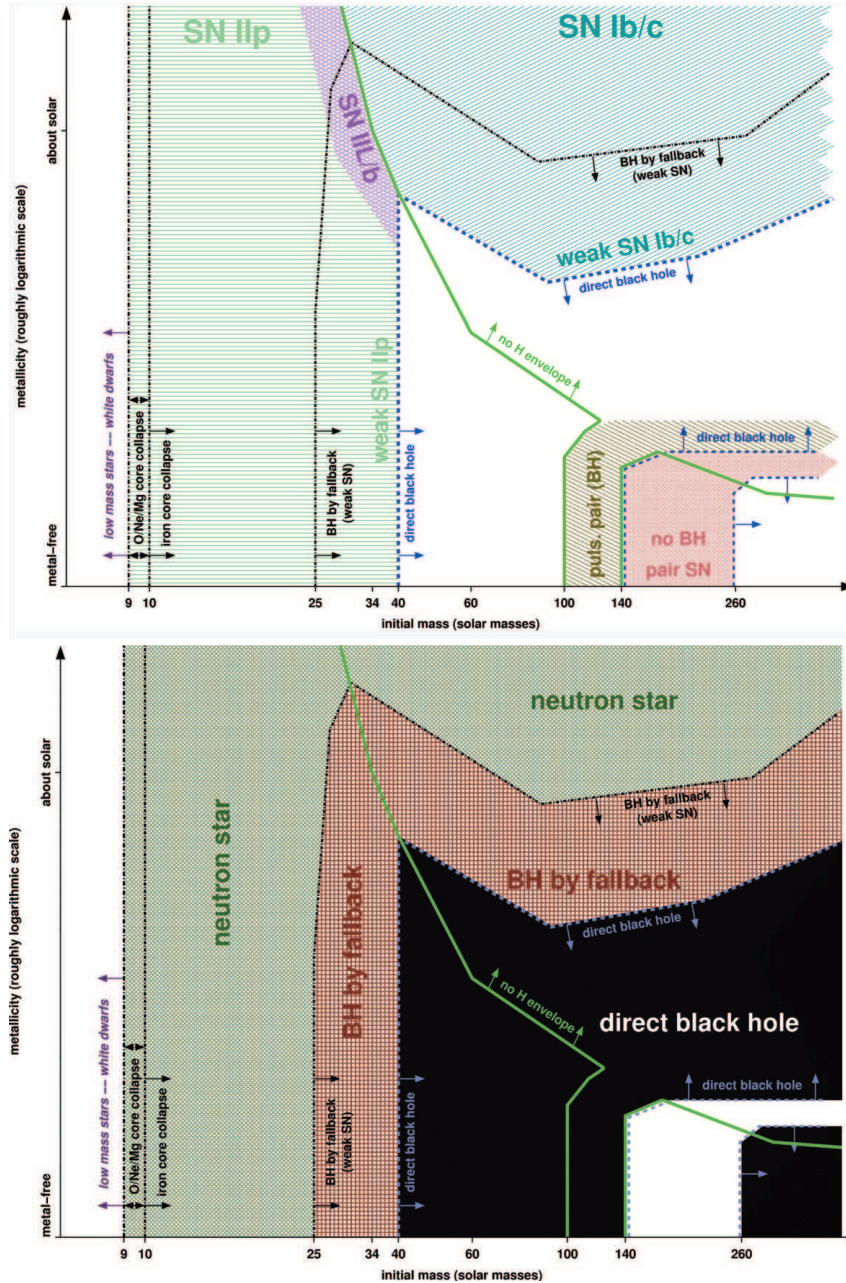


Figure 1.14 Different kinds of supernovae (**upper panel**) and the remnants (**lower panel**) generated from nonrotating massive single stars having different initial mass and metallicity. The figures have been borrowed from [Heger et al., 2003]. The sharp lines are the boundaries, segregating the outcomes of different kinds of catastrophe generated from the progenitors of different masses and metallicities.

---

have used the pre-existing stellar evolution models and evolved the stars up to the point at which they become SNe. They presented the maps of the nature of single star progenitors of supernovae and their remnants in mass and metallicity space.

In figure 1.14 the nature of the explosion (upper panel) and its remnant (lower panel) on the basis of initial mass of the progenitor and metallicity of the environment has been presented in brief. The progenitor is assumed to be non-rotating. The thick green line separates the regimes where the stars keep their hydrogen envelope (left and lower right) from those where the hydrogen envelope is lost (upper right and small strip at the bottom between 100 and 140  $M_{\odot}$ ). In top panel the green horizontal hatching indicates the domain where Type IIP supernovae occur. At the high-mass end of the regime they may be weak and observationally faint because of fallback of  $^{56}\text{Ni}$ . These weak SN Type IIP should preferentially occur at low metallicity. At the upper right-hand edge of the SN Type II regime, close to the green line of loss of the hydrogen envelope, Type IIL/b supernovae that have a hydrogen envelope of  $\lesssim 2 M_{\odot}$  are made (purple cross-hatching). In the upper right-hand quarter of the figure, above both the lines of hydrogen envelope loss and direct black hole formation, Type Ib/c supernovae occur; in the lower part of their regime (middle of the right half of the figure) they may be weak and observationally faint because of fallback of  $^{56}\text{Ni}$ , similar to the weak Type IIP SNe. In the direct black hole regime no ‘normal’ (non-jet-powered) supernovae occur since no SN shock is launched. An exception are pulsational pair-instability supernovae (lower right-hand corner; brown diagonal hatching) that launch their ejection before the core collapses. Below and to the right of this we find the (nonpulsational) pair-instability supernovae (red cross-hatching), making no remnant, and finally another domain where black hole are formed promptly at the lowest metallicities and highest

## 1. INTRODUCTION

---

masses (white) where nor SNe are made. White dwarfs also do not make supernovae (white strip at the very left). The lower panel shows the probable natures of the remnants. The dashed blue line indicates the border of the regime of direct black hole (BH) formation (black). This domain is interrupted by a strip of pair-instability supernovae that leave no remnant (white). Outside the direct black hole regime, at lower mass and higher metallicity, follows the regime of BH formation by fallback (red cross-hatching and bordered by a black dot-dashed line). Outside of this, green cross-hatching indicates the formation of neutron stars. The lowest mass neutron stars may be made by O/Ne/Mg core collapse instead of iron core collapse (vertical dot-dashed lines at the left). At even lower mass, the cores do not collapse and only white dwarfs are made (white strip at the very left).

### 1.4 Overluminous SNe and Gamma Ray Bursts

In the year 1967, a new type of transients were detected by several satellites. These events are extremely luminous in  $\gamma$ -ray and have a very short time scale. They were coined as Gamma Ray Burst (GRB). Similarly, different sky surveys over last decade have revealed several transients in relatively distant universe that are more luminous in UV, Optical and IR bands than normal supernovae and prolonged for a larger time span than normal supernovae. They are now classified as Overluminous Supernovae (OLSNe). In this section a brief introduction on these catastrophe will be presented.

---

### 1.4.1 Overluminous Supernovae (OLSNe)

Research on SNe over the past few years has confirmed that there is a distinct class of events which are much more luminous than canonical CCSNe occurring in nearby universe. The dedicated surveys like ‘*Catalina Real-Time Transient Survey (CRTS)*’, ‘*Lick Observatory Supernova Search (LOSS)*’, ‘*Robotic Optical Transient Search Experiment (ROTSE)*’, ‘*Palomar Transient Factory (PTF)*’, ‘*Panoramic Survey Telescope & Rapid Response System (PanSTARRS)*’ and many other facilities discovered several such events which are 10 times more luminous in near-UV, Optical and near-IR bands than the extremely energetic hypernovic explosions. They are called Overluminous Supernovae (OLSNe). The reason behind these explosions are unknown to a large extent. Many theoretical models have been proposed. It is mostly believe that these kind of events are due to ‘*pair-instability*’ processes in a very heigh mass stars ( $M > 60M_{\odot}$ ), though the possibility of Tidal disruption or emergence of a high mass magnetar [Woodsley, 2010] during SN explosion can not be ruled out. In this section the pair-instability process in context of overluminous events will be briefly discussed.

A pair-instability supernova occurs when pair production, the production of free electrons and positrons in the collision between atomic nuclei and energetic gamma rays, reduces thermal pressure inside the core of a supermassive star. This pressure drop leads to a partial collapse, then greatly accelerated burning in a runaway thermonuclear explosion which blows the star completely apart without leaving a black hole remnant behind. In two individual works Rakavy and Shaviv [1967] and Barkat et al. [1967] first proposed that for stars having more than  $30 M_{\odot}$  core may become unstable due to formation of electron-positron pairs. Fraley [1968] computed

## 1. INTRODUCTION

---

the ejected mass and velocities of the exploding stars having mass 45, 52 and  $60M_{\odot}$  and going through pair-instability process and showed that almost all the mass of the star can be ejected during the explosion process.

After the discovery of SN 2006gy [Frieman et al., 2006] the research on explosion in very high mass stars get intensified. Portegies Zwart and van den Heuvel [2007] proposed the explosion as an effect of collision between two massive stars, whereas Woosley et al. [2007] proposed it as an effect of pair-instability in a star with total mass between 95–130  $M_{\odot}$ . Waldman [2008] also concluded that SN 2006gy was generated by a massive star, having shallow density gradient of the inner shell and about  $3M_{\odot}$  Fe core along with  $10M_{\odot}$  Si group elements were created before the explosion. Many events of similar nature were discovered in recent past, like SNe 2005ap [Quimby et al., 2007a], 2007bi [Gal-Yam et al., 2009], 2010gx [Pastorello et al., 2010], CSS100217 [Drake et al., 2011] and 2010kd [Vinko et al., 2012]. Even after this much progress, the basic understanding about the nature of such explosions is not fully established.

### 1.4.2 Gamma Ray Bursts (GRBs)

Gamma-ray bursts (GRB) are the catastrophe which are occurring at an average rate of a few per day throughout the universe, having a duration of the order of 10–1000 seconds. They are the brightest electromagnetic events in an otherwise almost dark gamma-ray sky. While they are on, they far outshine all other sources of gamma-rays in the sky, including the Sun. GRBs are detected at the rate of about once a day and release energy  $\sim 10^{51}$  to  $10^{52}$  erg within a time span of few seconds, making them the most luminous events in the universe.

---

It was discovered serendipitously in the year 1967 by *VELA* series satellite [Klebesadel et al., 1973]. In 1974, the cosmic origin of GRBs was further confirmed by soviet Konus satellites and in 1976 first satellite Helios 2 dedicated for GRB observation was launched. Till date many astronomical satellites have been dedicated to monitor the  $\gamma$ -ray, X-ray and also optical photons from GRBs, some of them are – ISEE3, CGRO/BATSE, BeppoSAX, Integral, *Swift* and *Fermi*.

Though origin of GRBs has not yet been completely understood, theories predict that, such energetic explosions may arise due to core collapse of massive stars or due to merging of two compact objects, such as a Neutron Star – Neutron Star, Neutron Star – White Dwarf, Neutron Star – Black Hole, White Dwarf – Black Hole, White Dwarf – White Dwarf or Black Hole – Black Hole merger [Fryer et al. 1999 and references there in].

### **Basic characteristics of GRBs and its Afterglows**

The bursts have complicated and irregular time profiles which vary drastically from one burst to another though the typical profile of such a pulse can be described as a Fast Rise and Exponential Decay (*FRED*). The typical variation of each pulse takes place on a time scale, significantly smaller than the total duration of the burst and each pulse behaves as a ‘*building block*’ of the overall GRB light curve. GRB light curves exhibit a tremendous variety ranging from single featureless spikes to completely erratic sequence of pulses.

A clear bimodal behaviour was noticed in the duration distribution of GRBs According to the *BATSE* classification scheme, the bursts are termed as long and short based on the  $T_{90}$  duration [Kouveliotou et al., 1993]. For long duration GRBs  $T_{90} > 2$  sec whereas for short bursts  $T_{90} < 2$  sec. Here  $T_{90}$  is the time needed

## 1. INTRODUCTION

---

to accumulate 90% of the counts in the 50–300 keV band of *BATSE*. It was also suggested that there is a third intermediate class with  $2.5 \text{ sec} < T_{90} < 7 \text{ sec}$  [Horváth, 1998; Horváth et al., 2006; Mukherjee et al., 1998]. Since the duration of the burst is very small, the understanding of GRB physics from received radiation is rather difficult. Afterglows, are relatively long duration phenomena, and these are the important tool to study these multi-wavelength energetic cosmic explosions. The ultra-relativistic shocks emit radiation in the form of huge  $\gamma$ -rays due to some internal process, such as collisions between *internal-shocks* within the outflow and known as GRB [Narayan et al., 1992; Rees and Meszaros, 1994]. When the shocks interacts with relatively low density circumburst material, the remaining kinetic energy is dissipated via *external-shocks* that produce an ‘afterglow’ observable in different wavelengths – from X-ray to radio under different circumstances. Present theoretical understanding shows that afterglow flux is mainly the manifestations of Synchrotron and Inverse-Compton radiation.

Launching of *Swift*<sup>1</sup> satellite in November 2004, gave a major breakthrough in GRB-afterglow physics. In a recent work Kann et al. [2010] showed that that the nature of Optical and X-ray light curve is completely miss-matched among each other. Through spectroscopy the presence of continuum with a power law profile along with the presence of strong Fe lines are mostly detected in GRB spectra. In late epoch, emergence of SN can also be noticed [Matheson et al., 2003]. Among many proposed models on GRB-afterglows, ‘*Fireball model*’ is the most popular theory for this mysterious catastrophe Mészáros [2002]; Piran [1999, 2005].

---

<sup>1</sup><http://swift.gsfc.nasa.gov/docs/swift/swiftsc.html>

---

## 1.5 Motivation of the work & organization of the thesis:

In general CCSNe are a heterogeneous class of events displaying a wide range of physical parameters depending on the nature of progenitors – their initial masses, evolutionary histories, pre-explosion compositions, hydrogen content, dimensions of the progenitors, the nature of explosion and the way the exploded material interacts with the surroundings. Many of them show peculiarity in their light curves or very low luminosity during their evolution. After statistical analysis [Arcavi et al. \[2012\]](#) have proposed that Type IIb, IIL and IIP are originated from different kinds of progenitors, though it is not so far clear whether the normal and low luminosity Type IIPs are originated from same kind of progenitor or not. Moreover, we do not have sufficient understanding about the range of energetics which can be produced by such collapse mechanisms at the interior of massive stars and the nature of the exploded debris with the surroundings. To understand these issues, monitoring of different kinds of highly-energetic cosmic explosions along with their physical interpretation is required.

In this thesis a set of events have been investigated that show a wide range in luminosity and explosion energy. The sample contain a normal Type IIP event (SN 2008gz), a relatively low-luminous event (SN 2008in), two Type Ib events (SNe 2007uy, 2008D), one nearby Type IIn event (SN 2010jl), an overluminous Type IIn event (CSS 100217) and an overluminous Type Ic event (SN 2010kd).

In Chapter 2 the observing facilities along with data reduction procedures have been described. The spectroscopic and photometric properties of normal Type IIP event SN 2008gz and low-luminous Type IIP supernova 2008in have been dis-

## 1. INTRODUCTION

---

cussed respectively in chapters 3 and 4. The near-UV and near-IR properties of low-luminous event SN 2008in have also been described in chapter 4. Chapter 5 demonstrates the near-UV, optical, near-IR, radio properties as well as optical spectroscopic properties of Type Ib events SNe 2007uy. A comparison of this event along with other Type Ib event SN 2008D has also been drawn in this chapter. The optical properties of nearby Type IIn SN 2010jl along with overluminous Type IIn event CSS 100217 and overluminous Type Ic SN 2010kd have been described in chapter 6. The conclusion and future prospects have been drawn in chapter 7.

# Chapter 2

## Facilities, observations and data reduction

### 2.1 Introduction

Early and deep observations of supernovae are crucial to understand the physics of these events. Because of their transient nature and relatively fast decay of flux after discovery, quick follow up observations of such objects are required. The supernovae are randomly discovered by different groups of amateur astronomers and being reported as IAU and/or CBET circulars. The events are now also discovered and monitored in a much more systematic way through different survey programs like ‘*Catalina Real-Time Transient Surveys*’ (CRTS), ‘*Lick Observatory Supernova Search*’ (LOSS), ‘*Robotic Optical Transient Search Experiment*’ (ROTSE), ‘*Palomar Transient Factory*’ (PTF), ‘*MASTER robotic Net*’ and many other survey programs. Our primary-goal is to perform a systematic and extensive follow-up of different proximate and bright events reported in IAU and CBET circulars. The multiwave-

## 2. FACILITIES, OBSERVATIONS AND DATA REDUCTION

length campaign of these events along with optical spectroscopic monitoring are essential to probe the dynamics of the event and the burst mechanism, to estimate the energetics and to understand the nature of the progenitors and its environment.

For a dense and extended coverage of a transient at optical wavebands, getting an access of an optical telescope with moderate light gathering power along with a high efficiency detector is required. For the entire thesis, the optical data were primarily acquired from three Indian telescopes namely 1.04-m Sampurnanand Telescope (ST) at Aryabhata Research Institute of Observational sciencES (ARIES), 2.0-m IUCAA Girawali Observatory telescope under Inter University Center for Astronomy and Astrophysics (IUCAA) near Pune and 2.01-m Himalayan Chandra Telescope (HCT) at Indian Astronomical Observatory (IAO), Hanle. Additionally, the optical observations were also conducted from 3m to 6m optical telescopes outside India, through different active scientific collaborations between ARIES and other observatories over the globe. The optical telescopes, out side India, that have been used for this work are: (i) 0.61-m Lowell telescope, Perth Observatory, Australia; (ii) 0.45-m ROTSE III telescope, McDonald Observatory, USA; (iii) 0.6-m REM telescope, la Silla, Chile; (iv) 3.5-m Telescopio Nazionale Galileo (TNG), Canary Islands, Spain; (v) 3.6-m New Technology Telescope (NTT), ESO, Chile; (vi) 6.0-m Big Telescope Alt-azimuthal (BTA), Special Astrophysical Observatory, Russia and (vii) 9.2-m Hobby Eberly Telescope (HET), McDonald Observatory, USA.

To understand the multi-wavelength characteristics of these objects Near-ultraviolet (NUV) X-ray and Radio data have also been acquired, reduced and analysed. For NUV and X-ray data, archives of space-based telescopes like *Swift*/UVOT and XRT were used. For radio analysis, archival data of radio telescope ‘Very Large Array (VLA)’ has been used. This facility is situated at the Maxican Desert and oper-

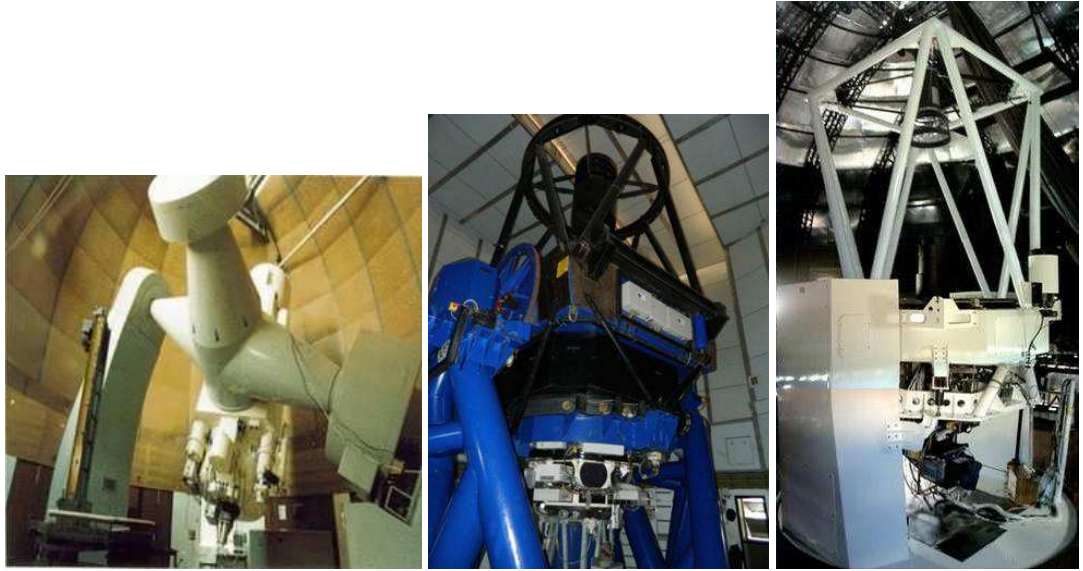


Figure 2.1 From left, the 1.04-m Sampurnanand Telescope (ST) at ARIES, Nainital; 2.0-m IUCAA Girawali Observatory (IGO) at Girawali, Pune and the 2.01-m Himalayan Chandra Telescope (HCT) at IAO, Hanle.

ated by NRAO, USA. For complete analysis of several events, data from published literatures have also been used.

## 2.2 Data acquisition at optical and near infrared wavebands

The characteristics of optical telescopes and the back-end instruments used for collecting the photometric and spectroscopic data discussed here.

### 2.2.1 The optical telescopes

India lies in the middle of the  $180^\circ$  wide longitude belt between Canary Islands ( $\sim 20^\circ$  W) and Eastern Australia ( $\sim 160^\circ$  E), thus filling in an important temporal

## 2. FACILITIES, OBSERVATIONS AND DATA REDUCTION

---

Table 2.1 Parameters of the used Indian optical telescopes.

Telescope	ST	HCT	IGO
Site	Nainital	Hanle	Pune
Longitude	79° 27' E	78° 57' E	73° 40' E
Latitude	29° 21' N	32° 46' N	19° 05' N
Altitude	1951 m	4500 m	1000 m
System	Ritchey-Chrétien	Ritchey-Chrétien	Ritchey-Chrétien
Focal length	Cassegrain: f/13	Cassegrain: f/9	Cassegrain: f/10
Primary Mirror			
Diameter	1.04-m	2.01-m	2.0-m
Plate scale	0.37'' /pix	0.17'' /pix	0.31'' /pix

gaps in the observations of transient events. The photometric and spectroscopic observations of supernovae are carried out using the 1.04-m ST at ARIES<sup>1</sup>, 2.01-m HCT at IAO, Hanle<sup>2</sup> and 2.0-m IGO<sup>3</sup>, IUCAA, Pune, India. Figure 2.1 shows three Indian Optical facilities used for this work, whereas their basic parameters are listed in table 2.1.

### 2.2.2 Optical filters for ground-based telescopes

In optical astronomy filters are used mainly two reasons: (i) either to reduce the overall intensity of light or (ii) to restrict the wavelength range of the incoming light. Nowadays detectors have a wider wavelength response and an improved sensitivity in comparison to previous detectors. Hence the filters are important for the flux measurement of various astronomical objects at different wavelengths. The broad band filters used for this study are Johnson UBV and Cousins RI with ST, Nainital and Bessell UBVRI filter system with HCT, Hanle. Details about the filter system

---

<sup>1</sup><http://aries.res.in>

<sup>2</sup>[http://www.iiap.res.in/centres\\_iao.htm](http://www.iiap.res.in/centres_iao.htm)

<sup>3</sup><http://iucaa.ernet.in>

Table 2.2 Details of the filter system. The thickness of the glass in mm is indicated in brackets

Telescope	Filters	$\lambda_{eff}$	Band Width	Glass combination
		Å	Å	
ST	<i>U</i>	3650	680	UG 1(2) + CuSO4 Solution(5)
	<i>B</i>	4400	980	GG 385(2) + BG 18(1) + BG 12(1) + KG 3(2)
	<i>V</i>	5500	890	GG 495(2) + BG 12(2) + KG 3(2)
	<i>R</i>	6500	2200	OG 570(2) + KG 3(3)
	<i>I</i>	8000	2400	RG 9(3) + WG 305(2)
	H $\alpha$ *	6565	80	–
HCT	<i>U</i>	3500	500	UG 1(1) + S8 612(2) + WG 295(2)
	<i>B</i>	4400	900	BG 37(3) + BG 39(1) + GG 395(2)
	<i>V</i>	5500	800	BG 40(3) + GG 495(2)
	<i>R</i>	6500	1500	OG 570(3) + KG 3(2)
	<i>I</i>	7900	1100	RG 9(2) + WG 305(3)

\*This is a Narrow Band filter. For continuum subtraction R-band image has been taken.

are given in Table 2.2. The filters used are basically combination of coloured glasses of WG, GG (Sulphur and Cadmium sulfide) and OG (Cadmium selenide) which absorb light of quite sharply defined wavelengths. The UG (violet) and BG (blue) are made of ionic glasses.

### 2.2.3 The detectors for imaging

Detectors are the indispensable part of modern telescopes and research facilities. We have used **Charge Coupled Device** (CCD) as a detector for our observations. This device, which replaced the photographic film as well as photomultiplier tubes – is an ultra-sensitive, silicon semiconductor, ‘chip’-based optical detector is composed of an array of thousands or millions of individual, tiny picture elements that almost

## 2. FACILITIES, OBSERVATIONS AND DATA REDUCTION

---

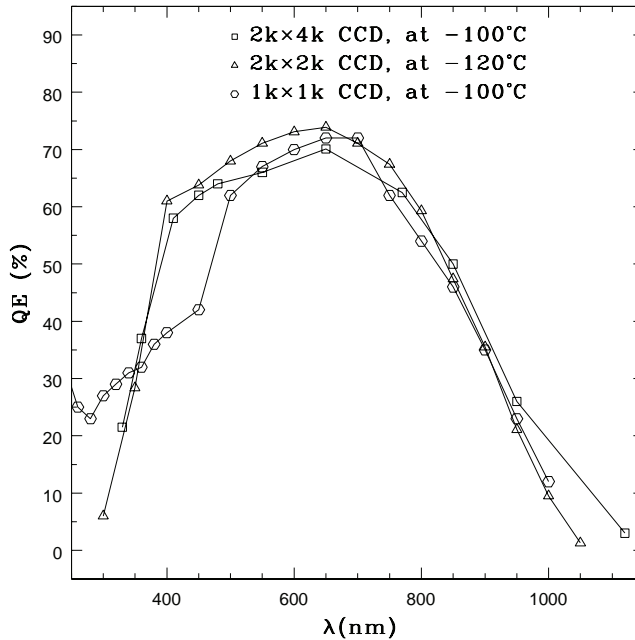


Figure 2.2 Response curve of 2k×4k CCD (squares) at  $-100^{\circ}$  C, 2k×2k CCD at  $-120^{\circ}$  C (triangles) and 1k×1k CCD at  $-100^{\circ}$  C (circles). The curve indicates that all the three CCDs peak near  $\lambda \sim 6700\text{\AA}$ .

touch each other and are called ‘pixels’. This was able to produce a two dimensional detection as an integrating mode, good linear response, dynamic range ( $\sim 10^5$ ) and quantum efficiency ( $\gtrsim 80\%$  at  $\lambda \sim 6900\text{\AA}$ ) which permit to image much fainter objects in relatively lesser time with a large dynamic range of recording over a vastly different levels of brightness. CCDs are nowadays used as detectors in most of the X-ray, NUV, optical and NIR imaging astronomical instruments. CCD operates on the principle of photoelectric effect.

The CCD camera used for astronomical purpose consists of a two dimensional array of photon detectors in a layer of semi-conducting material silicon. Its operation is based on **photoelectric effect** which can be described as follows. When the incident photons having energy 1.1–4 eV, hit the silicon chip within a pixel, it

---

generate single electron-hole pairs inside the chip, whereas those of higher energy produce multiple pairs. Each individual pixel is capable of collecting the photons and storing its energy in the form of produced electrons which can be read out from the CCD array to a computer in the form of a digital image of varying intensities of light detected by the CCD. The potential well of each pixel is capable to collect a definite number of electrons and it behaves like a *bucket* when it is exposed to collect the light. For a faint object, the shutter of the camera can be opened for a longer timespan, to generate and collect more number of  $e^-$  (*integrated*) inside each pixel of the CCD and that can be readout after completion of exposure. In effect, the faint object becomes more prominent in the processed digital image. Depending on the capacity of CCD pixels (known as '*Full-well capacity*'), one can increase the time duration (known as '*integration time*') to collect more photons.

The information from the rows of pixels move down to a single parallel row (the serial register) which is read out sequentially by Analog-to-Digital (A/D) converter where it is measured and then recorded. The measuring device is emptied and once again the process is repeated. This process continues until all of the pixels have been measured (read out). The time required to read out the informations of a CCD by its associated electronic equipments is coined as *readout time* of that CCD.

The pixel size of the CCDs used in the ST and HCT is  $24 \mu\text{m}$ . Particularly, for ST, the CCD is mounted at the f/13 Cassegrain focus of the telescope. Plate scale of the CCD chip is 0.38 arcsec per pixel, and the entire chip covers a field of  $13 \times 13$  square arcmin on the sky. The gain and readout noise of the CCD camera are  $10 e^-$  per analog-to-digital unit and  $5.3 e^-$  respectively.

At room temperature and for a longer integration time (more than hundred milliseconds) thermal noise is created by the random generation of dark current.

## 2. FACILITIES, OBSERVATIONS AND DATA REDUCTION

---

Therefore, CCD must be cooled if the integration time is more than a few seconds to avoid the silicons self-generated dark signal filling the potential well. CCDs used for the present observations were cooled to about  $-110^{\circ}\text{C}$  in a liquid nitrogen dewar. The typical CCD response is presented in Figure 2.2. The Quantum efficiency (QE) which is a function of wavelength seems to be an important characteristic of CCD. The figure shows that the response curves of CCDs used in this study all are peaked near  $\lambda \sim 6700\text{\AA}$ .

Astronomical data are usually archived in a universally accepted common format, namely the ‘*Flexible Image Transport System*’ or FITS. However, because of different technical reasons the recorded data for different telescopes may vary. For e.g., in Sampurnanand Telescope the output comes in FTS – format. This FTS format is converted to FITS format using a routine ‘*WR2FITS*’.

### 2.2.4 The spectrograph

For the present study, two Indian facilities – Hanle Faint Object Spectrograph Camera (HFOSC) and IUCAA Faint Object Spectrograph & Camera (IFOSC) have been used along with other optical facilities through out the world. Here HFOSC and IFOSC instruments will be briefly discussed.

IFOSC is the principal instrument currently mounted on the direct ‘*Cassegrain-port*’ of 2.0-m IGO telescope. This instrument was designed on the principle of very successful FOSC model [for detail see [Buzzoni et al. 1984](#)] which was developed at the Copenhagen University Observatory for the ‘*European Southern Observatory*’ (ESO) and ‘*Nordic*’ Telescopes. This technology is capable to take spectrum as well as images of the objects without changing the detector at the Cassegrain-

---

port. Either images or the spectra are produced on an EEV<sup>1</sup> 2048×2048, thinned, back-illuminated CCD with 13.5μm pixel size. The field of view is about 10.5′. Apart from Bessell *B, V, R, I* imaging filters and photometric equipments, a set of *Grisms*<sup>2</sup> with resolutions ranging from 190 to 3700 covering the wavelength between 3500–9000Å are also placed in the IFOSC instrument. For spectroscopy of a single object, the light coming from the object is allowed to pass through a slit and then it falls on the dispersive element like Grism (consisted with Grating and Prism), which disperses the light and produce spectrum on the CCD. The quality of produced spectrum is highly dependent on the convolved response of CCD and Grism along with the efficiency of the telescope and exposure-time. For present work a *long-slit*, with *slit-width* 1.5″ has been used along with three different grisms – *IFORS5* (range: 3300–6300Å), *IFOSC7* (range: 3800–6840Å) and *IFOSC8* (range: 5800–8300Å).

The basic principle of HFOSC is similar to other FOSC instruments. HFOSC is a focal reducer, allowing for a larger field coverage for a given detector along with low and medium resolution grism spectroscopy by inserting dispersive elements between the collimator and camera. The CCD camera has 2048×2048 pixel elements, each of size 15μm, working within the wavelength range 3500–9500Å. The spatial resolution 0.30″/pixel, whereas the spectral resolution is ∼ 1.6Å (medium resolution) to 50Å (low resolution) for a 1″ slit. Mainly two grisms – *Gr.7* (range: 3800–8000Å) and *Gr.8* (range: 5800–9200Å) have been used for spectroscopic monitoring of the supernovae.

---

<sup>1</sup>The acronym stands for ‘English Electric Valve company ltd.’, who is developing these devices.

<sup>2</sup><http://www.iucaa.ernet.in/~itp/etc/ETC/help.html#grism>

## 2. FACILITIES, OBSERVATIONS AND DATA REDUCTION

---

### 2.2.5 The near infrared telescopes

For several supernovae near-Infrared (NIR) data have been acquired from different telescopes through scientific collaboration with different groups through out the world. Mainly 0.6-m ‘*Rapid Eye Mount* (REM) telescope at La Silla, Chile [Zerbi et al., 2004] and 3.8-m ‘*United Kingdom Infrared Telescope*’ (UKIRT) located on the summit of Hawaii’s Mauna Kea [Hirst et al. 2006 and references therein] have been used to observe these catastrophe in  $J$  (central wavelength  $\sim 12200\text{\AA}$ , bandwidth  $\sim 1620\text{\AA}$ )  $H$  (central wavelength  $\sim 16300\text{\AA}$ , bandwidth  $\sim 2510\text{\AA}$ ) and  $K$  (central wavelength  $\sim 21900\text{\AA}$ , bandwidth  $\sim 2620\text{\AA}$ ) bands. In REM telescope, ‘REMIR’ camera is used for imaging while ‘Wide Field Camera’ (WFCAM) is used as a detector for UKIRT telescope.

## 2.3 Optical and near infrared Photometry

For Optical and NIR image processing several softwares such as *IRAF*<sup>1</sup>, *MIDAS*<sup>2</sup>, *DAOPHOT*<sup>3</sup> etc. have been developed by different observatories to carry out different tasks. The images acquired from CCDs are contaminated by the combination of atmosphere, telescope, filter, the CCD response and the associated electronics and certainly need to be processed to upgrade the image quality before using for scientific work. Strong atmospheric turbulence, poor focusing and deformed optical system (geometric distortion) and charge diffusion in the detector can also generate

---

<sup>1</sup>*IRAF* stands for Image Reduction and Analysis Facility distributed by the National Optical Astronomy Observatories which is operated by the Association of Universities for research in Astronomy, Inc. under co-operative agreement with the National Science Foundation

<sup>2</sup>*MIDAS* stands for Munich Image and Data Analysis System designed and developed by the European Southern Observatory *ESO* in Munich, Germany

<sup>3</sup>*DAOPHOT* stands for Dominion Astrophysical Observatory Photometry

---

a poor quality and distorted image. Image processing helps partially to compensate these deformation and to restore the original cleaned image. The softwares, mentioned above are also used to extract several physical parameters from the images. The three basic stages for image processing and optical photometric measurements are usually referred to as *Pre-processing*, *Processing* and *Post-processing*. Detail descriptions of these techniques are presented by [Howell \[2006\]](#).

### 2.3.1 Pre-processing

The patch of sky observed for scientific work is known as the raw frame. Apart from the raw frames it is also necessary to have bias frames (frames taken with zero second exposure to determine the noise level of the CCD) and flat frames (frames taken after exposing CCD for few seconds to correct for pixel-to-pixel variations in the CCD response as well as any non-uniform illumination of the detector itself). During pre-processing, bias-subtraction and flat-fielding of the object frames are done. A median of several bias images taken during observation is first subtracted from the raw object and flat frames. A median flat image in each filter is produced after taking several bias-subtracted flat frames. Since for median of a sample at least 3 parent elements are required, the acquired number of bias and flat frames in each filter should be  $\gtrsim 3$ . The bias corrected object frame is flat fielded using the median flat field image. These two step correct the object frame for bias level and non-uniformity within pixel response due to atmosphere and observing system. Pre-processing has been done using *IRAF* task and briefly described below.

#### **Bias frame subtraction**

## 2. FACILITIES, OBSERVATIONS AND DATA REDUCTION

These frames are acquired after taking exposure for zero seconds when the shutter remains closed and the CCD is simply readout. These frames are used to determine the underlying noise level of the CCD during observing span. The bias value in a CCD image is usually a low spatial frequency variation throughout the array, caused by the CCD on-chip amplifiers. Bias frame contains both the DC offset level and the variations on that level. For a better statistical estimate, a median bias frame is generated from 3 or more raw bias frames. The *IRAF*-routine ‘*ZEROCOMBINE*’ is used to obtain a median bias frame.

### **Flat fielding**

In practice all the pixels in a CCD do not show same response. With due course of time, dust and other physical distortion can appear on the exposed side of the CCD. Moreover, during opening and closing of the shutter, the central portion of the CCD gets more light in comparison to the edge. It is thus necessary to bring all the pixels to an uniform response level after considering these artifacts. For this, flat frames are obtained by illuminating the CCD with a uniform source of light in different filters. Flat field calibration frames are needed for each passband and different instrumental setup used for which object frames are taken. For a better statistical estimate, a median flat frame is generated from 3 or more bias subtracted flat frames and then further normalized after dividing the median flat by its median response. This is called normalized flat. Bias subtracted object frames are divided by normalised flat frame to correct for pixel-to-pixel variations in the CCD response. ‘*FLATCOMBINE*’ task in *IRAF* is used to get a median flat frame, ‘*IMSTAT*’ and ‘*IMARITH*’ routines are used to get median response and generation of normalized flat and flat fielded object frames. After *FLATCOMBINE*, the remaining

---

part of preprocessing can also be done through ‘*CCDPROC*’ task to get a cleaned object frame free from CCD noise and non-uniform pixel variations.

### **Removing the cosmic hits**

Even after getting object frames free from CCD noise and non-uniform pixel variations usually bright specks in intensity, not spread over more than one pixel, are noticed in addition to stars in an object frame. These are because of cosmic rays. Stellar and cosmic ray intensity profiles are different from each other which is the underlying property used for the removal of cosmic rays from the object frames. ‘*COSMICRAYS*’ task is used for the removal of cosmic rays from the object frames free from CCD noise and non-uniform pixel variations.

### **Producing dethard image for NIR imaging**

Since the earth radiates in infrared band, the near-IR sky is highly fluctuating. To remove this random fluctuation from near-IR images, always a number of images ( $\gtrsim 3$ ) are acquired after shifting the telescope little bit around the object. For a particular band, the median of the bias subtracted images gives a median profile of the sky fluctuation, which can be subtracted from every individual image to get clean NIR images. This process is called ‘*detharing*’. The other processes of data reduction are similar to optical photometry. Thus, for NIR imaging FLAT frames are not required, the median combined image itself behaves like a flat response. ‘*IMCOMBINE*’ task is used to get a median image and ‘*IMARITH*’ is used for individual subtraction.

### **Alignment and stacking**

## 2. FACILITIES, OBSERVATIONS AND DATA REDUCTION

---

To improve the signal-to-noise ratio for faint objects, sometimes several frames are acquired with different exposures and then co-added. To do this, individual frames in a particular filter are first aligned with respect to each other and then either added or averaged (stacking), depending on the science objective. The alignment is done using the task ‘*IMALIGN*’ or ‘*GEOMAP*’ and ‘*GEOTRAN*’ tasks in *IRAF*. The stacking is done using task ‘*IMCOMBINE*’.

### Template subtraction – for supernova photometry

When the supernova is embedded inside its host, the SN flux is expected to have a substantial contribution from the host-galaxy background. At early phases the SN flux dominates the total flux, thus with a PSF-fitting method (discussed below) gives more or less correct estimation of flux. At later epochs, the galaxy flux may brighten the SN light curves depending on its location in the galaxy. To remove the galaxy contribution, pre-SN image of the host or very late post-SN image of the host (when SN contribution becomes negligible), can be utilized as a template to map and estimate the background flux due to host. This technique is also used to discover the new transients and known as ‘*Template subtraction technique*’ [Alard, 2000; Alard and Lupton, 1998]. Self-written scripts employing IRAF tasks which included alignment, *PSF* and *intensity* matching of the galaxy template and SN images and subtraction of the template from the SN images were used to do this task and also verified with widely used *ISIS* tool. The effect of galaxy subtraction to get the true SN flux has been shown pictorially in figure 2.3. This has been applied on the field of galaxy NGC 2770 to determine the true fluxes (and hence the magnitudes) of two SNe 2007uy and 2008D. The detail discussion on the behaviour of these two SNe has been presented in chapter 5. The different kinds of host galaxy

---

subtraction will be discussed in different chapters according to their applicability.

### 2.3.2 Processing

Now, the cleaned and aligned images can be used for the main scientific work – to measure the observed flux of different objects from the images. The main processing is termed as photometry and involves the extraction of stellar positions and magnitudes from a given CCD image. *DAOPHOT II* [Stetson, 1987] is used to perform the photometry of individual stellar images recorded on the object frames. The different steps involved in processing are as follows.

#### Object detection

The automatic detection algorithm ‘*FIND*’ of *DAOPHOT II* package is used to detect star like objects above a certain user defined detection level, rejecting bad pixels, rows and columns in the object frame. The detection level is normally constrained as 3 times of the standard deviation of sky fluctuation. This routine detects and locates small, positive brightness enhancement within an image and able to distinguish stellar profile from galaxy or any other extended objects profiles, cosmic rays or any other high energy particle profile. The image is convolved with analytical stellar profile – either Gaussian/Lorentzian/Moffat/Penny with a given FWHM, provided by user to locate a star in a pixel by fitting the profile to the brightness values of surrounding sub-array of pixels. The stars are located by performing a pixel by pixel search and selecting locations where the Gaussian profile fit is good i.e. where the central height of the best fitted Gaussian model achieves a large, positive value possibly lying near the center of star image. The output of *FIND*

## 2. FACILITIES, OBSERVATIONS AND DATA REDUCTION

---

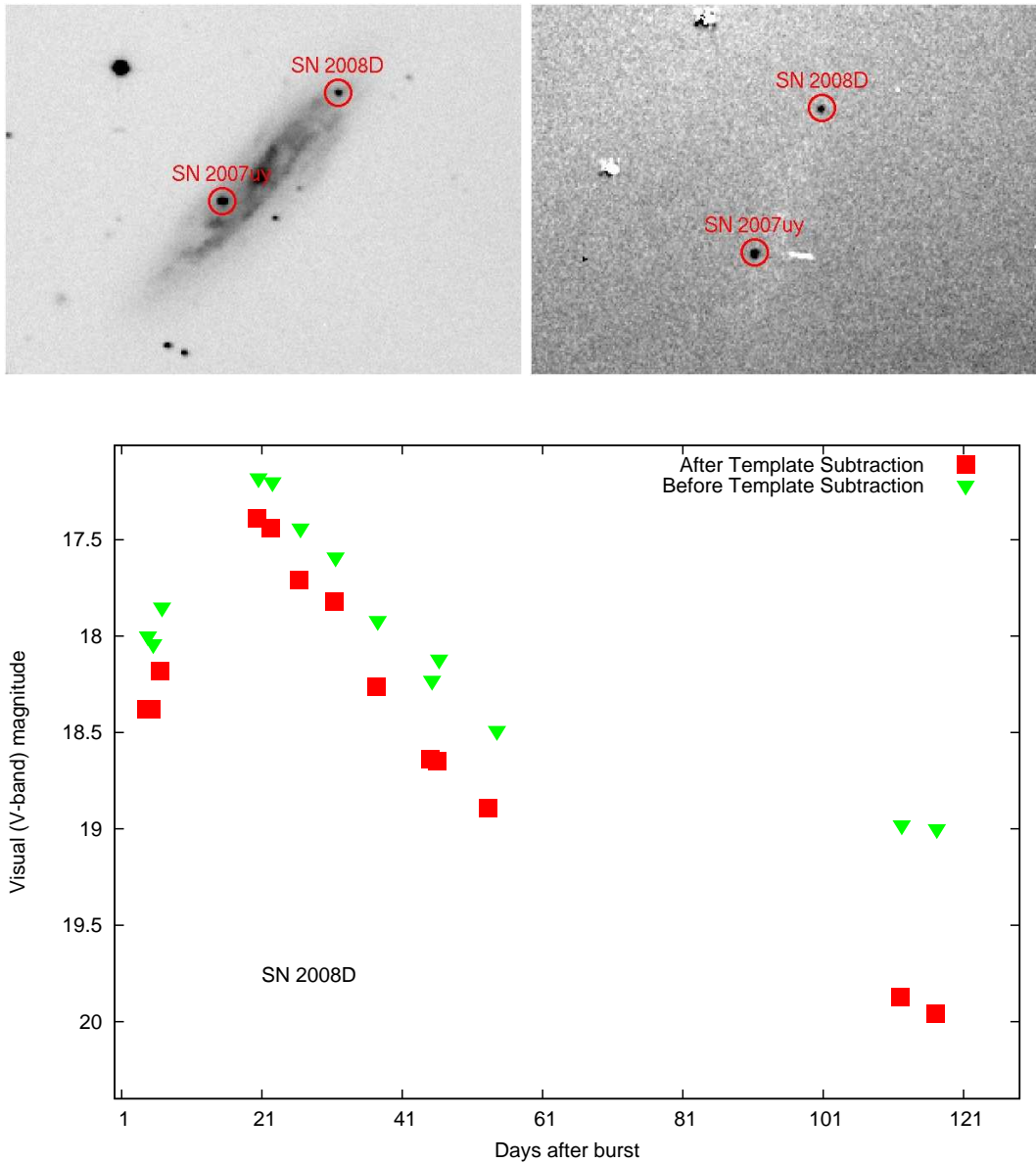


Figure 2.3 The necessity of Template subtraction. The **upper-left panel** shows the field of galaxy NGC 2770, hosting the SNe 2007uy and 2008D (see chapter 5). The **upper-right panel** shows the field after template subtraction. The effect of galaxy is subtracted. **Lower panel** shows the visual light curve of SN 2008D. The green points are found without doing the galaxy back-ground subtraction while the red dots represent the light curve after galaxy subtraction. The effect of galaxy is less when the SN is bright (less magnitude) and more when the SN is faint (high magnitude).

---

catalogues the stars of the frame by mentioning their X and Y positions.

## **Photometry**

The next step is to get the observed flux in the form of instrumental magnitude of the stars detected by *FIND*. By photometry, a quantitative (numerical) values for the brightness of objects are obtained. Two basic steps for obtaining photometric data from CCD are : ‘*Aperture Photometry*’ and ‘*Profile Fitting Photometry*’. For bright objects and less-crowded field Aperture Photometry is preferred, while for faint object and crowded field Profile Fitting Photometry is essential.

### *Aperture Photometry*

Aperture photometry is used to measure the brightness of an object without considering the possible contaminations due to sources such as sky, pixel defects or other nearby stars and galaxies. If a CCD frame contains few stars, it is possible to perform photometry of individual stars by simply defining a circular geometric region as an ‘*aperture*’. Total photons detected within an aperture centered around a star is calculated after summing-up the counts within the aperture. Similarly the sky photons detected within a star free region of the same area elsewhere in the frame is counted. The difference between these two numbers corresponding to a particular star are converted into magnitude scale. For this ‘*PHOT*’ routine in DAOPHOT II is used. This routine calculates the star counts within a series of increasing concentric apertures and also in an annulus to evaluate the count of star free sky region that are defined by user. Similar routine PHOT in IRAF can also be used to do aperture photometry with equivalent results. The output lists the magnitude of the star in different apertures. For the faint stars and in crowded regions, aperture

## 2. FACILITIES, OBSERVATIONS AND DATA REDUCTION

---

photometry does not work properly.

### *Profile Fitting Photometry*

This technique is essential for faint objects and crowded field, where outer sky is not well defined or contamination due to nearby sources is highly possible. This technique offers the best possible recovery of photometric information for stellar objects. In an optical image all the stars are effected due to identical observing conditions and have the same profile and would differ from one another only by an intensity scaling ratio. This property is the basic principle of the profile fitting photometry. In a perfect telescope having no instrumental defect and in the absence of atmospheric turbulence the image can be represented by the profile governed by the diffraction pattern of the telescope optics. In practice, the stellar image is affected by the irregularities of the instrument (telescope observations, tracking errors, optics etc.) and the seeing during ground based observations. So, a model of ‘*point spread function*’ (PSF) is determined from several stars in a given frame. PSFs can be modeled by a number of mathematical functions to describe the stellar brightness profile. Mostly Gaussian, modified Lorentzian or Moffat functions are used in this regard [Stetson et al., 1990].

Thus, the analytical functional forms of PSF can be used to model the PSF for a star within an image, assuming that they provide a good representation of the data itself. Sometimes a combination of one or more of these functions is used to obtain a better fit. However, we see that for CCD frames having good image quality observed under good seeing, the  $\chi^2$  value in fitting Gaussian analytical function is better than that obtained from other two functions. The analytical method has the advantage of integrating numerically over the entire stellar image but the disadvantage being

---

that the function used to fit the profile can only be approximated. Other method of PSF determination is empirical, where it is possible to simply store the observed profile of several bright stars as data array  $O(i,j)$ . The empirical method has the advantage that it uses the observed profile, but the drawback in this case is that near the central region of the stellar image, the brightness varies too rapidly between the adjacent pixels to be interpolated correctly. Better results can be obtained by combining these two methods. In DAOPHOT II model PSF is generated using the routines ‘*PEAK*’ and ‘*PSF*’.

To get magnitude of all the stars in a field, the modeled PSF is applied to all the stars of the frame with the help of ‘*ALLSTAR*’ routine. It is a standalone programme which performs a multiple-profile fit to all the stars in a frame. This routine returns the positions, magnitudes, error in magnitudes, sky brightness, no. of iterations,  $\chi^2$  values and sharpness values of all stars present in the CCD frame. PSF and ALLSTAR tasks in IRAF are also used sometimes to do PSF photometry with equivalent results.

### **Conversion of counts to magnitude**

During both aperture and profile fitting photometry the flux are at first measured in terms of counts (in ADU) and then converted to magnitudes. As stated above, in aperture photometry, the magnitude of the star corresponding to any aperture is determined by summing the data inside that aperture and from the relation,  $m = zpt - 2.5 \log_{10} I$ , where  $zpt$  is the arbitrary zero-point and  $I$  is the true counts of the stars, after subtracting the sky contribution and expressed as  $I = (\Sigma I_{ij} - n_{pix} \cdot i_{sky})$ , where  $n_{pix}$  is the number of sky pixel,  $i_{sky}$  is the count of individual sky pixel and  $I_{ij}$  is the total count of a particular aperture. The similar

## 2. FACILITIES, OBSERVATIONS AND DATA REDUCTION

---

approach is also adopted for profile fitting, where pixels within the PSF profile are considered. Similar algorithm is also applied in *IRAF* tasks. In DAOPHOT II assumes  $zpt = 25.0$  mag which corresponds to 1 ADU.

### 2.3.3 Post-processing

The output of the processed frame provides the instrumental magnitude of the star like objects of that frame. To convert them to the standard magnitude indices Post-processing is done. The steps are as follows.

#### Aperture correction

Aperture photometry is performed for several selected, bright, isolated stars in each observed frame using a series of apertures of increasing size. In PSF photometry, the instrumental magnitude of a star comes from the height of a model point-spread function for that frame scaled to the intensity values recorded inside the stars image. This magnitude is restricted to the aperture chosen and has to be corrected for the counts left out in the wings of the stellar profile. The correction from profile fitting magnitudes to aperture magnitudes is carried out by the process of determining aperture growth curve. This correction is known as ‘*aperture correction*’ and applied to the PSF magnitudes to get the aperture instrumental magnitudes. This is done by ‘*DAOGROW*’ routine [Stetson et al., 1990].

#### Cross Identification

To determine the standard magnitudes and colours, cross identification of the stars of different frame and filters is required. This is performed after using ‘*DAOMATCH*’

---

programme of DAOPHOT II. This routine considers about 30 brightest stars between the two frames and provides the coordinate transformation equations between the various frames with respect to a reference frame. Using the approximate transformation equation provided by *DAOMATCH*, another programme ‘*DAOMASTER*’ is then used to identify all the stars in a field and to cross-match all the stars by spatial proximity. If, after transformation to the coordinate system of the master frame, a star lies within the specified distance of a star in the master list, it is provisionally identified with that star; if it lies near no star in the master list it is added to the list as a possible new detection.

### **Transformation to the standard system**

To transform the instrumental magnitudes to the standard magnitudes a set of transformation equations are used.

$$u_{CCD} = U + a_0 + a_1.(U - B) + a_2.X$$

$$b_{CCD} = B + b_0 + b_1.(B - V) + b_2.X$$

$$v_{CCD} = V + c_0 + c_1.(B - V) + c_2.X$$

$$r_{CCD} = R + d_0 + d_1.(R - I) + d_2.X$$

$$i_{CCD} = I + e_0 + e_1.(V - I) + e_2.X$$

Here  $a_0, b_0, c_0, d_0, e_0$  are the zero points;  $a_1, b_1, c_1, d_1, e_1$  are the colour coefficients;  $a_2, b_2, c_2, d_2, e_2$  are the earths atmospheric extinction coefficients and  $X$  is the air mass.  $U, B, V, R$  and  $I$  are the standard magnitudes and  $u_{CCD}$ ,

## 2. FACILITIES, OBSERVATIONS AND DATA REDUCTION

---

$b_{CCD}$ ,  $v_{CCD}$ ,  $r_{CCD}$  and  $i_{CCD}$  are the corresponding aperture instrumental magnitudes. The second order colour correction terms are ignored as they are generally small in comparison to other errors present in the photometric data reduction.

The light of celestial objects get reduced during its propagating through the terrestrial atmosphere due to absorption and scattering. The reduction of incident flux is called *atmospheric extinction*. It depends on the atmospheric path length through which the light is travelling and hence on the zenith angle ( $Z$ ) of the object, wavelength of radiation, atmospheric conditions during the observation and altitude of the observatory. Atmospheric extinction correction is an integral part of photometric data reduction. For this, the air mass ( $X$ ), i.e., the thickness of the atmosphere crossed by the light rays along the line of site, is calculated using the equation [Hardie and Ballard, 1962]

$$X = \sec Z - 0.0018167.(\sec Z - 1) - 0.002875(\sec Z - 1)^2 - 0.0008083.(\sec Z - 1)^3$$

and

$$\sec Z = [\sin(\phi).\sin(\delta) + \cos(\phi)\cos(\delta)\cos(h)]^{-1}$$

Where,  $\phi$ ,  $\delta$  and  $h$  are observers latitude, the declination and the instantaneous hour angle of the star respectively. By definition, air mass value is 1 at the zenith and increases with the zenith angle. The atmospheric extinction coefficients for each filter are determined from the plot of aperture magnitudes observed versus air mass for the comparison stars on each night using the method of linear least square fit.

The transformation equations and DAOPHOT II routines ‘COLLECT’, ‘CCDSTD’ are used to determine the values of transformation coefficients. Using the obtained

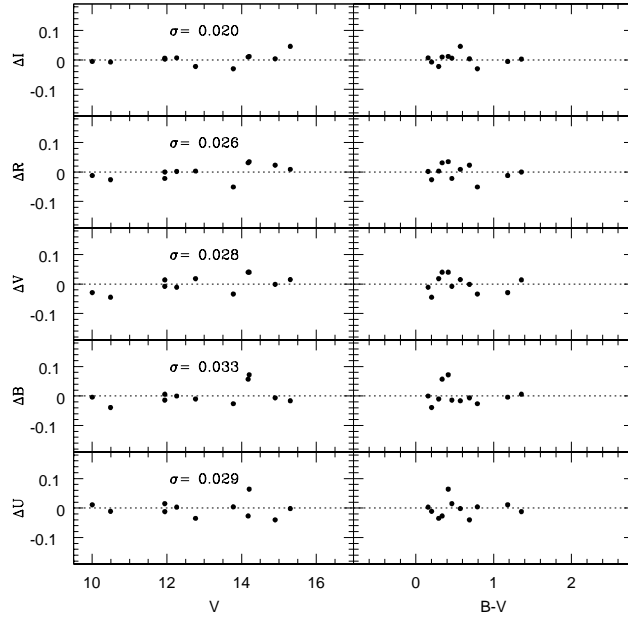


Figure 2.4 Standardization of SN 2010jl field using the standard stars of the field SA98. The detail properties of this object has been discussed in chapter 6.

transformation coefficients and the standard magnitude values from [Landolt \[1992\]](#), secondary standards in the object frame can be generated. ‘*CCDAVE*’ program in DAOPHOT II is used to generate the secondary standards. The final transformation of all the stars in the object frame is done by the ‘*FINAL*’ routine. This program determines a single consistent photometric zero point using all the frames from the local secondary standard stars. Thus, a list of stars and the corresponding positions, standard magnitudes and colours for a given CCD frame of interest is obtained.

After performing the standardization of the observed field, it is necessary to check the quality of this performance. The best way is to check how much accurately we are able to reproduce the magnitudes of the photometric standard found by [Landolt \[1992\]](#). This can be concluded by plotting the difference between standard

## 2. FACILITIES, OBSERVATIONS AND DATA REDUCTION

---

magnitudes and the reproduced magnitudes of these photometric standards against their standard mags and colours. Normally these are plotted against  $V$ -band mag and  $(B - V)$  colours. If the standardization process goes well all the differences should be around zero and within a scatter (standard deviation)  $\sigma \lesssim 0.05$  mag. For all the objects, discussed in this work this process have been performed. Figure 2.4 represents the typical nature of this plot. Field of CSS 100217 (see chapter 6) has been calibrated using the stars from the Landolt standard field SA98. The plot shows that the calibration process went very perfectly.

### 2.4 Optical Spectroscopy

During acquisition, optical spectra are also obtained in the form of two-dimensional CCD images. Like photometric data, the long slit spectroscopic data also consists of bias frames, flat frames and object frames along with other calibration frames. These frames are acquired for each observing night. The object frame contains the image of the particular object under interest, focussed at a slit. Unlike photometry, this image is binned over the entire wavelength regime of the optical band (of course, dependent on instrument setup). This image is made by dispersing the light rays of the target on the CCD frame along a particular direction known as ‘*dispersion axis*’, This normally lies either x-axis or y-axis of the CCD when it is properly aligned with the slit axis. In order to avoid any degradation of resolution as well as the sky background contribution, the slit widths are usually kept equal to the FWHM of the stars seeing limited image. Thus, the spatial profile of the star is governed by the seeing. So, after reduction, the pixels along the dispersion axis give a measurement of wavelength, while the pixels along the spatial axis give a

---

measurement of counts/flux. To convert these pixels and counts in wavelength and flux respectively, calibration frames are required. ‘*Arc*’ and ‘*standard star*’ frames are required for wavelength and flux calibration respectively.

Spectroscopic data reduction has been done using the routines of ‘*SPECRED*’ package provide in ‘*IRAF*’. The basic pre-processing is similar to photometric reduction (except detharing and template subtraction). The cosmic ray rejection task can be improved using the Laplacian kernel detection method [van Dokkum, 2001]. After getting a cleaned 2D frame, the 1D spectrum is extracted and then calibrated. The three main steps are ‘*Aperture Extraction*’, ‘*Wavelength Calibration*’ and ‘*Flux Calibration*’. These are briefly discussed here.

### 2.4.1 Aperture Extraction

The one dimensional spectra are extracted using ‘*APALL*’ task. This is based on the extraction algorithm proposed by Horne [1986]. *APALL* is a collection of many tasks. After selecting the aperture around the object part and background, which comes from sky regions, it traces the spectrum along the dispersion axis and sums it along a one-dimensional line. This routine eliminates the sky noise, delivers maximum possible signal-to-noise ratio and takes care of the effects of moderate geometric distortion and cosmic ray hits. The output comes as an one dimensional spectrum in the form of pixel vs intensity values.

In order to calibrate the pixel number in terms of wavelength, it is necessary to take spectra of a laboratory standard source (e.g., Fe-Ar and Fe-Ne, He-Ne Arc-lamp). Similarly to convert the counts to flux spectra of spectroscopic-standard stars [Hamuy et al., 1994; Massey et al., 1988] are taken during the same observing

## 2. FACILITIES, OBSERVATIONS AND DATA REDUCTION

---

night. Extraction of 1D-spectra of spectroscopic-standard star and that of Arc-lamp are also done through *APALL*.

### 2.4.2 Wavelength Calibration

The 1D spectrum of the Arc-lamp is now used to convert the pixel to wavelength for both 1D spectra of object and standard star. Since Arc-lamp is a laboratory standard source, wavelength of different spectral features such as emission in Arc-spectrum is known and provided by the observatory as an ‘*Arc Atlas*’. The emission lines of 1D extracted spectrum of the Arc is then identified using that atlas by running the ‘*IDENTIFY*’ task which calculates the pixel-to-wavelength solution for Arc spectrum. ‘*HEDIT*’ task is used to incorporate this information in 1D extracted spectra of object as well as of standard. Task ‘*DISPCOR*’ is then executed to apply this solution on the spectra of standard and object simultaneously. It gives dispersion-corrected spectra for object and standard. Usually a high order polynomial is employed to fit the identified pixels against wavelength. It is always better to check the wavelength calibration before going for flux calibration. For this the standard atmospheric emission lines like 5577Å, 6300Å and 6364Å are used. If any correction is required then the necessary offset can be applied to dispersion-corrected standard and object spectra using the task ‘*SPECSHIFT*’ or by applying the offset to the *header – adverb* ‘*CRVAL1*’ mentioned in the header of dispersion-corrected spectra. ‘*HEDIT*’ task is used for this purpose.

---

### 2.4.3 Flux Calibration

After getting the wavelength calibrated spectra of standard and object, they are calibrated in flux after knowing the standard-flux of spectroscopic standards. These standard fluxes are provided in *IRAF* itself and can also be found in the web interface of several observatories like ESO. Flux calibration is performed using the tasks ‘*STANDARD*’, ‘*SENSFUNC*’ (used to fit a polynomial to the observed magnitude as a function of wavelength after applying extinction correction in the standard and programme star spectra) and ‘*CALIBRATE*’. The final flux calibrated one-dimensional spectra give distribution of flux over wavelength.

## 2.5 Acquisition and reduction of *Swift*/UVOT data

The Ultraviolet Optical Telescope (UVOT), on-board the *Swift* satellite, is a 30 cm modified Ritchey-Chretien Ultraviolet (UV)/Optical telescope Co-aligned with the X-ray Telescope and mounted on the telescope platform common to all instruments of *Swift*. The photometric data from UVOT, was used to access the UV and Optical data. This is the only space-based facility that has been used for this work. UVOT provides simultaneous ultraviolet and optical coverage (170–650 nm) in a  $17' \times 17'$  field. Despite its limited aperture, UVOT is a powerful complement to other instruments because of its UV capabilities and the absence of atmospheric extinction, diffraction, and background.

UVOT has six photometric filters, three near-UV (NUV) bands –*uvw2*, *uvm2*, *uvw1* and three Optical bands –*u*, *b*, *v*. It is also equipped with a *White filter*, having a response curve extended between NUV and NIR. The detail information of UVOT filter system can be found at [Poole et al. \[2008\]](#). The UVOT data has be obtained

## 2. FACILITIES, OBSERVATIONS AND DATA REDUCTION

---

from the *Swift* Data Archive through NASA’s *High Energy Astrophysics Science Archive Research Center* (HEASARC) on-line services. The photometry was done using standard processes of HEASOFT routines.

The *Swift* data have had bad pixels identified, mod-8 noise corrected, and have been transformed into FK5 coordinates. We used the standard UVOT data analysis software distributed with HEASOFT 6.10 along with the standard calibration data. As long as the source had a count rate greater than 0.5cts/s, photometry was done using the command ‘*uvotsource*’ with a standard circular aperture of radius 5'' and a circular background region with a radius of 15''. Below this threshold, a 3.5'' radius was used and an aperture correction was applied. The background region was selected to have similar background properties to those at the location of the transient, and to be free of contaminating sources. The photometry was calibrated to the UVOT photometric system following the procedure described in [Poole et al. \[2008\]](#). To remove the contribution from the underlying host galaxy we measured the host galaxy flux at the position of the SN from late UVOT observations, where there was no longer a contribution from the SN. This additional flux was then subtracted from SN photometric measurements. For all observations the source was close to the centre of the field-of-view, and differences in the PSF between observations were, therefore, negligible. A detail description of UVOT photometry can also be found elsewhere [[Brown, 2009](#)].

### 2.6 Data acquisition at Radio wavebands

The archival radio data have been used for analysis of Type Ib SN 2007uy. Mainly archival data from radio telescope VLA has been used in this regard. VLA [[Thomp-](#)



Figure 2.5 Very Large Array, an interferometric array. (Image courtesy of NRAO)

[son et al., 1980](#)] is a radio astronomy observatory located on the Plains of San Agustin, between the towns – Magdalena and Datil, about fifty miles (80 km) west of Socorro, New Mexico, USA (Latitude =  $34^{\circ} 04' 43.497''$  N, longitude =  $107^{\circ} 37' 03.819''$  W). It is consisted with 27 independent antennas, arrayed along the three arms of a Y-shape, each of which measures  $\sim 21$  km/13 miles long. Each antenna is 25 m in diameter and the weight of each solid dish is about 230 tons (see figure 2.5). There are four array configurations. The maximum antenna separations are respectively 36 km, 10 km, 3.6 km and 1 km for A array, B array, C array and D array. These configurations change in every four months or so.

The earth atmosphere is transparent with respect to radio waves having wavelength range between  $\sim 1$  cm to few tens of metre. So, by principle big reflecting telescopes can be used to get an image of distant celestial objects emitting in radio waves. The procedure for image production at different frequencies will be of

## 2. FACILITIES, OBSERVATIONS AND DATA REDUCTION

course different from optical telescopes, though they are mathematically identical. In fact, many such huge reflectors had been used (and still being utilized) to image the radio sky. Some of them are – 300-m Arecibo radio telescope, USA; 600-m RATAN radio telescope, Russia; 530 m long and 30 m wide cylindrical-paraboloid radio telescope at Ooty (ORT), India; 10.4-m Caltech Submillimeter Observatory (CSO), USA etc. On the other hand according to *Rayleigh's criterion* the angular resolution of a telescope is ultimately diffraction limited by the expression  $\theta \sim \lambda/D$ . Where  $\lambda$  is the observed wavelength and 'D' is the measure of aperture size (size of reflector/refractor) (The actual resolution of optical telescopes is however limited by atmospheric fluctuation, known as '*seeing*'). Hence, to get a better angular resolution at higher wavelength, larger aperture size is required. For e.g., while the human eye has a diffraction limit of  $\sim 20''$  and the modest optical telescopes have this value as low as  $0.1''$ , the large ( $\sim 300$ -m) single dish radio telescope has angular resolution of only  $\sim 10'$  at 1 metre wavelengths. To increase the angular resolution in radio wave, interferometry technique is adopted.

The telescopes like VLA, Giant Metrewave Radio Telescope (GMRT), Westerbork Synthesis Radio Telescope (WSRT) and all other upcoming radio telescopes work / will work on the basis of interferometry. In this technique, each single dish antenna behaves like a slit and each combination of two antennas behaves like a setup producing double-slit diffraction pattern, where the projected distance between two antennas toward the object is equivalent to slit separation. A very large area is covered by several small antennas and after interferometry, they act coherently like a big telescope. The observed quantities in a radio-interferometric observations are the complex visibilities which is the fourier transformation of the sky brightness distribution. A radio-interferometer consists of several antennas (say N antennas)

---

and each pair records one fourier component. Hence at any given instant of time only  ${}^N C_2$  fourier components are recorded. With the motion of the object on the sky from east to west, projected separations between pair of antennas changes and within a moderate time span, a considerable number of discrete samples of visibilities are observed and hence the sky brightness distribution can be reconstructed. This procedure is known as ‘*earth rotation aperture synthesis*’ and is used widely to synthesize large aperture telescope even with a finite number of antennas. The basic parameters for VLA are mentioned in table 2.3. For the analysis of SN 2007uy radio data mainly ‘C’ and ‘X’ band VLA archival data, along with other literature data have been used.

Table 2.3 Basic system parameters of Very Large Array (VLA)

Chareteristic	4 Band	P Band	L Band	C Band	X Band	U Band	K Band	Q Band
Freq (GHz)	0.07–0.074	0.30–0.34	1.34–1.73	4.5–5.0	8.0–8.8	14.4–15.4	22–24	40–50
Wavelength (cm)	400	90	20	6	3.6	2	1.3	0.7
Primary beam (')	600	150	30	9	5.4	3	2	1
Highest resolution (")	24.0	6.0	1.4	0.4	0.24	0.14	0.08	0.05
System Temperature ( $^{\circ}$ K)	1000–10,000	150–180	37–75	44	34	110	50–190	90–140

---

## 2.7 Data reduction strategy at Radio wavebands

In terms of mathematical-algorithms, the processing and analysis of Radio data is similar to Optical, though due to a completely different ‘*receiver/detector – technology*’ and presence of different kinds of artifacts than optical, reduction process and used softwares are different from optical. The software that is widely used to reduce and analysis of ‘*radio interferometric data*’ is ‘*Astrophysical Image Processing System*’ (*AIPS*)<sup>1</sup>. Unlike *IRAF*, working with radio interferometric data, requires to bring the data under *AIPS*-environment, before starting any processing. To bring the processed data, outside *AIPS* also requires particular task, so that it can be fetched from *AIPS*-environment.

The radio data may or may not be in the FITS format and provided by the observatories mostly in the form of a ‘*data – cube*’, containing data and informations of multiple observations. In VLA archive, the data are not provided in completely binary format. This data have been downloaded to do further analysis. In principle the spatial correlation function or the visibility,  $V(u,v)$ , measured across several baselines using an interferometer can be inverse Fourier transformed to reconstruct the sky brightness distribution  $I(l,m)$ . However, the measured visibilities are affected by man made interferences and is scaled by the antenna gains etc. Because of these a series of analysis techniques has to be applied on them before any scientific analysis.

To calibrate the flux of a radio source and its brightness distribution over the sky plane, a standard calibrator is required. After several measurements, NRAO/VLA had chosen few point like objects (not resolvable in the VLA operating radio frequencies) in the radio-sky as *flux calibrator*. On the other hand, the radio wavelength

---

<sup>1</sup>Astrophysical Image Processing System (*AIPS*) has been developed by the National Radio Astronomical Observatories (NRAO), USA

## 2. FACILITIES, OBSERVATIONS AND DATA REDUCTION

---

is affected due to earth's ionospheric turbulence. These turbulences are distributed in the form of patches and every radio observation is scattered when it passes these turbulent zones. This is similar to atmospheric extinction for optical observations. Angular dimensions of these turbulent zones are within few degrees. Since the number of flux calibrators are limited, a secondary calibrator (also listed by NRAO) is used to calibrate the target object. These secondary calibrators are called *phase calibrator*. While observing, the phase calibrators are chosen in such a way that their angular separation from the object remains within a few degrees. This confirms that both the phase calibrator and the target are affected by the same turbulent zone. The phase of this secondary calibrator is well known for a given VLA frequency. During calibration the secondary (phase) calibrator is calibrated in flux by the flux calibrator and then the target source can be calibrated in both flux and phase using flux and phase calibrators. If the flux calibrator is located within a few degrees away from the target object, then for that object the use of a phase calibrator is not required; only a flux calibrator can be used for this purpose.

VLA provides preliminary calibrated data. This will be discussed further in subsequent sections. The SN radio data reduction in *AIPS* can broadly be divided into four categories – ‘*Pre-processing*’, ‘*Data editing*’, ‘*Calibration*’, ‘*Imaging*’.

### 2.7.1 Pre-processing

The Radio data are first loaded in *AIPS*-environment. If the data is in FITS-format task ‘*FITLD*’ is used. For the VLA data, which was not in FITS format, task ‘*FILLM*’ is applied. Thus, the basic purpose of these two tasks is the same – to bring the Radio data into the *AIPS*-environment.

---

For loading the data, indexing and a primary calibration may be required for few cases, like low frequency GMRT data. For this task ‘*INDXR*’ is used. For VLA data, primary calibration is provided by the observatory, so this task is not required. The listing of all the individual data present in the loaded data cube is done through the task ‘*LISTR*’. The list should indicate the object data, flux and phase calibrators (surveyed and listed by NRAO in VLA website), their coordinates, observing sequence over time, the observing frequency along with bandwidth and the polarization. So, the data is now ready for further processing.

### 2.7.2 Data editing

Radio astronomical measurements particularly at low frequencies are highly affected by the man made radio signals like satellite and mobile phone communication and use of radio receivers near the observatory. These signals basically create ‘*Radio Frequency Interference*’ (RFI) with the radio-signal coming from the celestial object and makes the data noisy. A good quality image is possible only when the data is fully free from RFI. The process of editing the radio data to remove the RFIs is commonly known as ‘*flagging*’. Many tasks like ‘*UVPLT*’, ‘*UVFLG*’, ‘*TVFLG*’, ‘*VPLOT*’, ‘*WIPER*’ are used to look the UV data and to identify the bad signals and RFIs. This is usually done minutely to preserve the good data after removing the bad portion. The defects of data set comes in different form - antenna or baseline based or time based (and also channel based for GMRT). The data editing is first applied on the point sources – flux and phase calibrators and finally on target if required. The visibility amplitude of an unresolved point source should remain constant as a function of baseline length. By the task *UVPLT* visibility

## 2. FACILITIES, OBSERVATIONS AND DATA REDUCTION

---

amplitude vs UV distance can be plotted to locate the inconsistent data points. Using task *V PLOT* the particular antennas or baselines which are responsible for those discrepant points can be located and the task *UVFLG* can be used to flag the contribution of those antennas or baselines either for whole or particular time range within which they were behaving abruptly. If any antenna or baseline remain dead through out the observation of both flux and phase calibrator then it has to be removed from entire data set by the task *TVFLG* as well. Sometime, first few minute data of a scan get corrupted. Task ‘*QUACK*’ is used to remove this corrupted part from entire data set.

### 2.7.3 Calibration

Through calibration, observed visibilities are corrected to the true visibilities. At the time of observation we observe flux calibrator ( $\sim 15$  minutes) in the beginning and at the end of the observation and the target source observations are interspersed with observations of the secondary phase calibrator. The desirable flux density calibrators have to be unresolved so that they will appear same in all baselines. Furthermore flux density has to be known and be constant with time which helps to find out any systematic atmospheric or instrumental errors [Fassnacht and Taylor, 2001]. Inhomogeneous and dynamic earth ionosphere is responsible for rapid change of refractive index with time and position for radio waves. The ionosphere adds an differential phase rotation to the complex visibilities. To calibrate this atmospheric phase fluctuations we need a secondary calibrator which is near ( $\lesssim 20^\circ$ ) to the target source and whose true visibility is known. In calibration process observed visibility is to be divided by the true visibility to get the gain factor. This is applied as a

---

correction to the visibilities of the target source. To get the gain values in between calibrator observations interpolation needs to be done. However if a flux calibrator is near by our target source then secondary phase calibrator is not needed.

The calibration process starts with setting the flux density of the flux calibrator using the task ‘*SETJY*’. This task follows standard [Baars et al. \[1977\]](#) formulae and takes frequency information from the header to determine the flux densities of primary calibrators. The task ‘*CALIB*’ is used for the selected single channel to determine the antenna based complex gains for the calibrators. This creates a solution (*SN*) table which contains the complex gain solutions. The SN table can be plotted by the task ‘*SNPLT*’ to check the gain solutions. If the solutions are not reasonable then one can repeat the same process starting from the flagging. The flux density of the phase calibrator was computed by the task ‘*GETJY*’. This creates a *SU* table and corrects the amplitude in the *SN* table. The flux density of the phase calibrator are cross checked with value given by VLA calibrator list. If it differs too much then more flagging is needed for the phase calibrator. The task ‘*CLCAL*’ is used to interpolate the gains of the target with time. This creates *CL* table version two which contains solutions derived from SN table by linear vector interpolation. The amplitude and phase deviations of all the flux and phase calibrator has to be checked applying *CL* table in ‘*UVPLT*’. If there is any significant deviation then one has to identify the bad data and flag them. Deleting the *SN* tables and *CL* table 2 same calibration process has to be repeated again.

The calibration and flagging are repeatedly done in an iterative way to remove the RFI and calibrate the good data in flux and phase. After a complete calibration the target data is fetched out from the data cube using the task ‘*SPLIT*’. This is further utilized to make a radio image.

## 2. FACILITIES, OBSERVATIONS AND DATA REDUCTION

---

### 2.7.4 Imaging

The visibilities measured by all antennas are all discrete points in uv-plane. ‘*Dirty beam*’ is the Fourier transform of uv sampling function or uv tracks during our observation. ‘*Dirty map*’ is convolution between real brightness distribution of the source and Dirty beam. The Dirty beam and the Dirty map comes from fourier transformation of sampling function and visibilities by ‘*Fast Fourier Transform*’ (FFT) algorithm. The true image can be achieved by deconvolution of Dirty map. The most popular deconvolution algorithm *CLEAN* was proposed by Högbom [1974] and widely used for imaging of point sources like supernova. The task ‘*IMAGR*’ is used to make the Cleaned image from a Dirty image.

The supernova flux can be measured from the cleaned image, obtained after running *IMAGR*.

# Chapter 3

## The normal Type IIP SN 2008gz

### 3.1 Introduction

Core-collapse supernovae (CCSNe) occur in late type galaxies and their locations are usually associated with the regions of high stellar surface brightness or recent/ongoing star formation, suggesting that they represent the end stages of massive stars ( $M > 8-10M_{\odot}$ ) [Anderson and James, 2008; Hakobyan et al., 2009]. Observationally it has been found that, Type II SNe constitute about 70% of all the CCSNe [Cappellaro et al., 1999; Smith et al., 2011a] and their light curves and spectra differ significantly. Out of them, Type IIP, the optical light is featured with  $\sim 100$  days plateau and strong P-cygni profiles whereas others have different properties and briefly discussed in chapter 1 [Filippenko, 1997; Smartt et al., 2009]. Theoretically, in H-rich events, after shock breakout the shock-heated expanding stellar envelope cools down, by recombination of H and sustains the plateau phase of IIP SNe, while the post-maxima/plateau light curves are powered by the radioactive decay of  $^{56}\text{Co}$  into  $^{56}\text{Fe}$ . Though the explosion mechanism is similar to these events,

### 3. THE NORMAL TYPE IIP SN 2008GZ

---

they differ largely in energetics, e.g. IIP SNe are observed to form a sequence from low-luminosity, low-velocity, Ni-poor events to bright, high-velocity, Ni-rich objects [Hamuy, 2003]. Thus, a detailed investigation of individual CCSNe is important for understanding the nature and environment of progenitors. Type IIPs generally probe the star formation processes, galactic chemical evolution and constrain the stellar evolutionary models [Haberman et al., 2010; Heger et al., 2003; Smartt, 2009] and also turned out to be good standardizable candles [Hamuy and Pinto, 2002; Olivares E. et al., 2010; Poznanski et al., 2009]. In this chapter, the evolution of a normal Type IIP event will be discussed.

The SN 2008gz event was discovered on November 5.83 UT, 2008 by Koichi Itagaki using a 0.6m telescope in the spiral galaxy NGC 3672 at an unfiltered magnitude of about 16.2. On November 7.84 and 8.84 UT, an independent discovery of this new transient was reported by R. Martin from Perth Observatory as a part of “Perth Automated Supernova Search Program” by using 0.6m Lowell Telescope. The red magnitude of this new object was about 15.5 [Nakano and Martin, 2008]. On November 11.25 UT, Benetti et al. [2008] took the first spectra of this event with the 3.5m TNG (+ DOLORES; range 340-800 nm, resolution 1.0 nm) and showed that it is a type II supernova event and by using GELATO tool [Harutyunyan et al., 2008], they found that the spectrum of SN 2008gz resembles best with that of a II-peculiar event SN 1998A, taken at 62 days after explosion [Pastorello et al., 2005]. Assuming the recession velocity of the host galaxy  $\sim 1862 \text{ km s}^{-1}$ , they found the expansion velocity of hydrogen layer was about  $6600 \text{ km s}^{-1}$ . An independent regular *BVRI* CCD photometric monitoring of SN 2008gz was carried out since November 10, 2008 by using 1m Sampurnanand Telescope at Nainital, India. We also collected spectra in optical ( $0.4 - 0.9 \mu\text{m}$ ) with 2m IUCAA, India; 3.6m NTT, Chile; 6m BTA, Russia;

---

3.6m TNG, Spain.

In this work, the results of optical photometric and low-resolution spectroscopic investigation of SN 2008gz have been presented. We adopt time of explosion to be August 20.0, 2009 or JD 2454694.0 having uncertainty of a few days (see §3.2.2 for details). Hence the time of post/pre-explosion are rounded off to nearest day and they are referred with + and – signs respectively. Basic properties of SN 2008gz and its host galaxy NGC 3672 are given in Table 5.1.

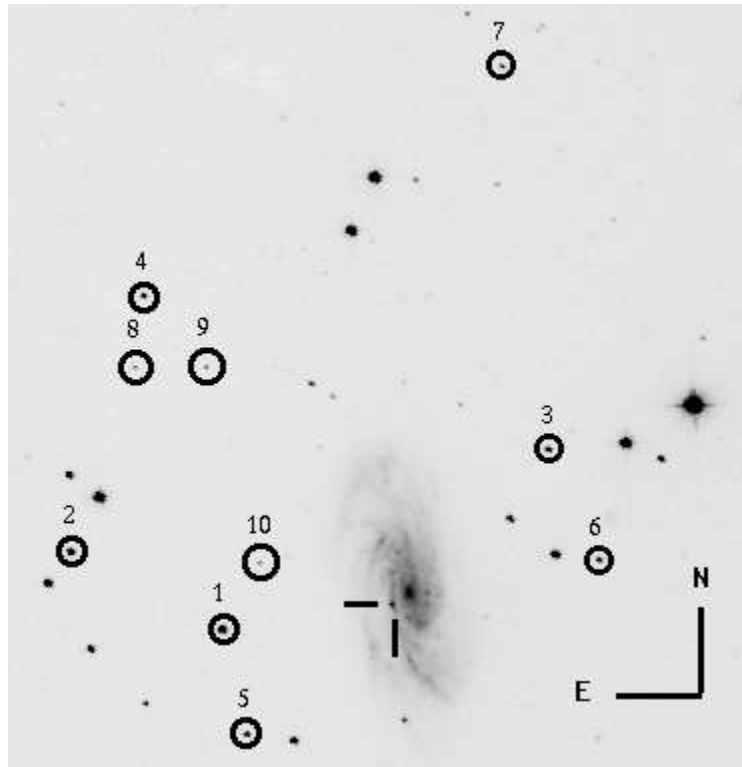


Figure 3.1 SN 2008gz in NGC 3672. *V* band image from 1 m ST, India. Area of about  $8 \times 8$  arcmin is shown, with location of SN marked with a cross and reference standard stars marked with circles.

### 3. THE NORMAL TYPE IIP SN 2008GZ

---

Table 3.1 Properties of the host galaxy NGC 3672 and SN 2008gz.

Parameters	Value	Ref. <sup>a</sup>
<b>NGC 3672:</b>		
Type	SAC	1
RA (J2000)	$\alpha = 11^{\text{h}}25^{\text{m}}2.^{\text{s}}48$	1
DEC (J2000)	$\delta = -09^{\circ}47'43.''0$	1
Abs. Magnitude	$M_B = -20.59$ mag	1
Distance	$D = 25.5 \pm 2.4$ Mpc	§3.6
Scale	$1'' \sim 123$ pc, $1' \sim 7.4$ kpc	
Distance modulus	$\mu = 32.03 \pm 0.21$	
Apparent radius	$r_{25} = 1.'4$ ( $\sim 10.4$ kpc)	1
Inclination angle	$\Theta_{\text{inc}} = 56.^{\circ}2$	1
Position angle	$\Theta_{\text{maj}} = 6.^{\circ}5$	1
Heliocentric Velocity	$cz_{\text{helio}} = 1864 \pm 19$ km s <sup>-1</sup>	1
<b>SN 2008gz:</b>		
RA (J2000)	$\alpha = 11^{\text{h}}25^{\text{m}}3.^{\text{s}}24$	2
DEC (J2000)	$\delta = -09^{\circ}47'51.''0$	2
Location	13'' E, 7'' S	2
Deprojected radius	$r_{\text{SN}} = 23.''37$ ( $\sim 2.81$ kpc)	§3.8.2
Explosion epoch (UT)	20.0 August 2008 (JD 2454694.0)	§3.2.2
Discovery date (UT)	5.83 November 2008	2

<sup>a</sup> (1) HyperLEDA - <http://leda.univ-lyon1.fr>; (2) [Nakano et al. \[2008b\]](#)

---

## 3.2 Broad band photometry

### 3.2.1 Observation & data reduction

Initial pre-SN images ( $-403\text{d}$ ) of the host galaxy NGC 3672 at *VRI* bands were obtained from Perth Observatory, as a part of supernova search program for another type Ia SN 2007bm, which occurred in the same galaxy. Images were taken with  $512 \times 512$  CCD camera mounted on a 0.6m Lowell Telescope, covering around  $5 \times 5$  square arcmin on the sky.

SN 2008gz was observed at different epochs from different observatories around the world. The major part of monitoring was carried out in Johnson *BV* and Cousins *RI* bands from 1m *Sampurnanand* Telescope (ST) at the Aryabhata Research Institute of Observational Sciences (ARIES), Nainital, India. SN 2008gz was observed during 10 November 2008 ( $+87\text{d}$ ) to 17 May 2009 ( $+275\text{d}$ ). We could not detect SN in the observations of 19 November ( $+462\text{d}$ ) in *B*, of 13 February 2010 ( $+547\text{d}$ ) in *VRI* and of 14 February 2010 ( $+548\text{d}$ ) in *BVRI*. In addition to 1m ST, observations of SN 2008gz at *BVRI* bands were also obtained on 21, 22, 24 and 25 March 2009, with IFOSC mounted on 2m IGO, IUCAA, India and on 17 May 2009 with EFOSC2 mounted on 3.6m NTT, ESO, Chile.

Fig. 5.1 shows the location of SN 2008gz in the galaxy NGC 3672. The SN flux is expected to have substantial contribution from the host galaxy background, due to its proximity to the galaxy centre, its location in a spiral arm and a high inclination angle ( $56.2^\circ$ ; Table 5.1) of the galaxy. At early phases, SN flux dominates the total flux, thus with a PSF-fitting method we were able to remove the galaxy contribution. At later epochs (e.g. end of plateau in case of type IIP events), galaxy flux may brighten the SN light curves by 0.5 to 1 mag depending on its location in the

### 3. THE NORMAL TYPE IIP SN 2008GZ

---

Table 3.2 Identification number (ID), coordinates ( $\alpha, \delta$ ) and calibrated magnitudes of stable secondary standard stars in the field of SN 2008gz. Errors in magnitude represent RMS scatter in the night-to-night repeatability over entire period of SN monitoring.

Star ID	$\alpha_{J2000}$ (h m s)	$\delta_{J2000}$ ( $^{\circ}$ $'$ $''$ )	$B$ (mag)	$V$ (mag)	$R$ (mag)	$I$ (mag)
1	11 25 11.27	-09 48 04.4	15.36 $\pm$ 0.01	14.36 $\pm$ 0.03	13.99 $\pm$ 0.01	13.49 $\pm$ 0.01
2	11 25 18.34	-09 47 03.0	15.70 $\pm$ 0.01	14.92 $\pm$ 0.02	14.68 $\pm$ 0.01	14.25 $\pm$ 0.01
3	11 24 55.62	-09 46 07.9	16.50 $\pm$ 0.01	15.82 $\pm$ 0.03	15.64 $\pm$ 0.01	15.26 $\pm$ 0.01
4	11 25 14.22	-09 44 04.7	16.91 $\pm$ 0.01	16.15 $\pm$ 0.01	15.93 $\pm$ 0.01	15.50 $\pm$ 0.01
5	11 25 10.47	-09 49 17.0	17.00 $\pm$ 0.02	16.23 $\pm$ 0.03	15.98 $\pm$ 0.01	15.52 $\pm$ 0.04
6	11 24 53.17	-09 47 25.1	17.09 $\pm$ 0.02	16.42 $\pm$ 0.03	16.22 $\pm$ 0.01	15.83 $\pm$ 0.03
7	11 24 56.67	-09 41 35.1	17.80 $\pm$ 0.02	16.99 $\pm$ 0.02	16.66 $\pm$ 0.01	16.19 $\pm$ 0.04
8	11 25 14.78	-09 44 54.3	18.50 $\pm$ 0.07	17.70 $\pm$ 0.07	17.49 $\pm$ 0.06	17.12 $\pm$ 0.03
9	11 25 11.40	-09 44 54.5	18.28 $\pm$ 0.04	17.75 $\pm$ 0.03	17.62 $\pm$ 0.02	17.22 $\pm$ 0.04
10	11 25 09.31	-09 47 16.4	18.83 $\pm$ 0.09	17.92 $\pm$ 0.07	17.63 $\pm$ 0.03	17.08 $\pm$ 0.06

galaxy [Pastorello et al. 2005, also see Figure 2.3]. We applied the self written code (as discussed in §2.3.1) to correct the measurement of SN flux through Template subtraction method and also checked its performance by comparing the results with other widely used code like *ISIS*<sup>1</sup> [Alard and Lupton, 1998]. Late time *BVRI* images (with high S/N ratio and SN impression is absent) have been used as templates [see also Roy et al. 2011b].

Calibration of the field was done in regular fashion (as discussed in §2.3.3). SN 2008gz was observed along with Landolt [2009] standard fields SA92 and PG0231 in *BVRI* with 1m ST on 15 November 2008 under good night conditions (transparent sky, FWHM seeing in  $V \sim 2''$ ). The data reduction of SN and Landolt fields were done using profile fitting technique and the instrumental magnitudes were converted into standard system following least-square linear regression procedures outlined in Stetson [1992b] and mean values of atmospheric extinction coefficients

---

<sup>1</sup><http://www2.iap.fr/users/alard/package.html>

---

of the site viz. 0.28, 0.17, 0.11 and 0.07 mag per unit airmass for the  $B$ ,  $V$ ,  $R$  and  $I$  bands respectively [Kumar et al., 2000]. A typical scatter in the photometric solutions to the Landolt standard stars is found to be  $\sim 0.03$  mag. Table 4.2 lists the calibrated magnitudes for a set of ten stable secondary standards in the SN field, while calibrated  $BVRI$  magnitudes of SN 2008gz are presented in Table 4.3. For SN, we quote ISIS derived errors ( $1\sigma$  uncertainty), which is consistent with the RMS scatter in the magnitude of standard stars determined from night-to-night repeatability over entire period ( $\sim 215$ d) of SN monitoring. Large errors in 2m IGO and 3.6m NTT data arises due to mismatch in the PSF and pixel scale.

### 3.2.2 Optical light curve

Fig. 4.4 shows  $BVRI$  light curves of SN 2008gz ranging from +87d to +275d since the time of explosion. We also present the light curves of other well studied nearby ( $D < 12$  Mpc) type IIP SNe viz. 2004et [Misra et al., 2007b; Sahu et al., 2006], 1999em [Elmhamdi et al., 2003b] and 1999gi [Leonard et al., 2002a], scaled in time and magnitude to match the transition between plateau to nebular phases. It is seen that SN 2008gz was detected close to the end of its plateau phase and its light curve resembles well with the above three template IIP events and hence we could determine (and adopt) the time of inflection (plateau to nebular),  $t_i$  of  $115 \pm 5$  d, by adjusting the template light curves to get the best match to SN 2008gz data points. This derived plateau duration is typical for type II P events [Elmhamdi et al., 2003a] and it is also consistent with the fact that SN 2008gz was not visible around three months before the discovery date (November 5.83, 2008) at the level of unfiltered magnitude of 19.0 [Nakano and Martin, 2008]. Further, similarities

### 3. THE NORMAL TYPE IIP SN 2008GZ

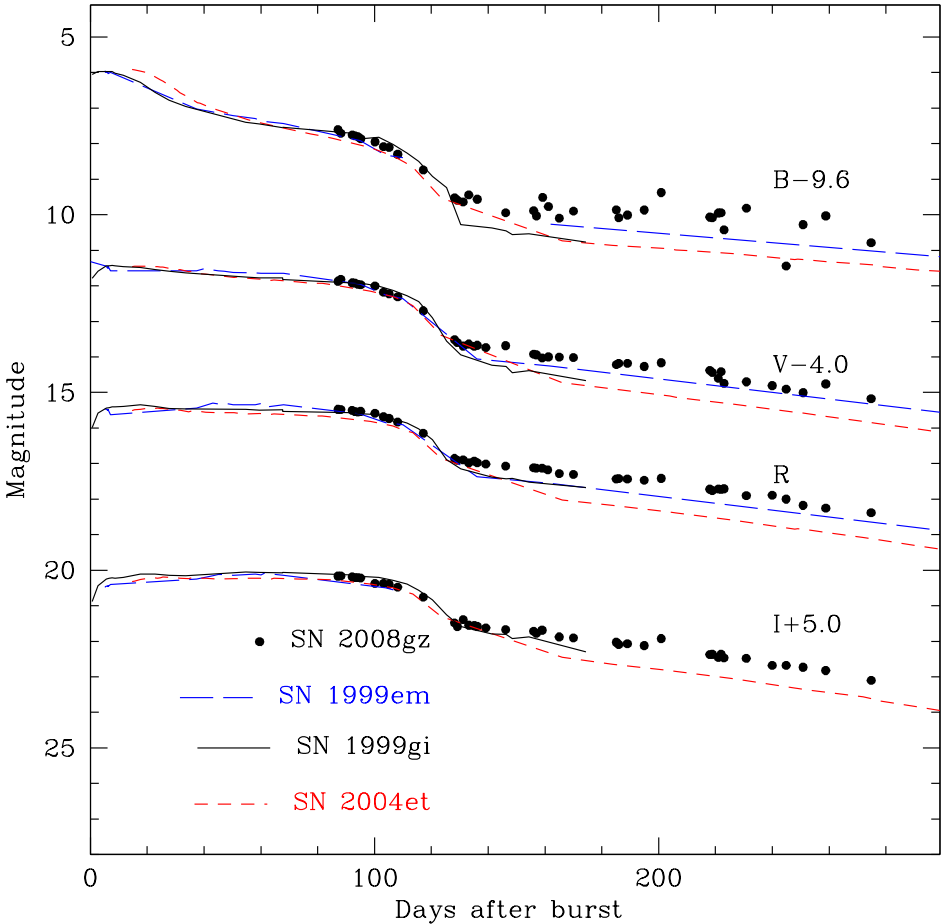


Figure 3.2 Light curve in *BVRI* magnitudes of SN 2008gz. The light curves are shifted for clarity, while for other SNe, they are scaled in magnitude and time to match with SN 2008gz.

---

between bolometric tail luminosity of SN 2008gz (see §3.7) with that of SN 2004et and SN 1999em indicates that probably explosion happened about 82 days before the discovery date. Analysis of first spectrum of SN 2008gz (see §3.3.2) also revealed few similarities between the kinematical properties of its ejecta to that of SN 2004et observed nearly 80 days after the burst. We therefore adopt time of SN explosion to be  $82 \pm 5$  days before the discovery date and this corresponds to burst time,  $t_0$  of JD 2454694.0, however, we note that based on the first spectrum (November 11.25 UT, 2008) and its similarity with +62d spectrum of SN 1998A [Benetti et al., 2008] suggesting a time of explosion of nearly 56 days before the discovery date (corresponding to plateau phase of  $\sim 90$ d) cannot be ruled out.

In the late plateau phase ( $\sim +90$ d) flatness behaviour in  $RI$  and decline trend in  $BV$  are clearly seen, which are similar to other IIP events. The  $V$  magnitude drop of 1.5 mag from plateau phase ( $V \sim 16$  mag at +100d) to nebular phase (17.5 mag at +130d), is slightly lower than 2-3 mag drop for a typical IIP event [Olivares E. et al., 2010]. This shallow decline which is seen in  $BRI$  also, indicating production of large  $^{56}\text{Ni}$  mass (see §3.8.1). In contrary to this, very steep brightness decline at  $V$  has also been observed, e.g. 4.5 mag for SN 2007od [Andrews et al., 2010]. The nebular phase starts at  $\sim +140$ d, and it roughly follows the decay slope of  $^{56}\text{Co}$  to  $^{56}\text{Fe}$ :  $0.98 \text{ mag } (100\text{d})^{-1}$ . A linear fit to the tail from +150d to +275d gives the following decline rates [in  $\text{mag } (100\text{d})^{-1}$ ]:  $\gamma_B \sim 0.51$ ,  $\gamma_V \sim 0.98$ ,  $\gamma_R \sim 1.12$ ,  $\gamma_I \sim 1.13$  at  $B$ ,  $V$ ,  $R$ ,  $I$  which is typical to the values found for IIP SNe. The flattening seen in  $B$  band light curve, though non-conclusive due to large scatter of the measurements, has also been observed in other events, e.g. in 1999em [Elmhamdi et al., 2003b] and 1987A [Suntzeff et al., 1988] until +400d.

## 3.3 Low resolution spectroscopy

### 3.3.1 Data

Long-slit low resolution spectra ( $\sim 6$  to  $14 \text{ \AA}$ ) in the optical range ( $0.33 - 1.0 \text{ \mu m}$ ) were collected at eight epochs during  $+87\text{d}$  to  $+275\text{d}$ ; five epochs from 2m IGO, and one epoch each from 3.5m TNG, 6m BTA and 3.6m NTT. Journal of spectroscopic observations are given in Table 5.7.

At 2m IGO, observations were carried out using IFOSC (IUCAA Faint Object Spectrograph and Camera) mounted at the cassegrain end of f/10 reflector [Chakraborty et al., 2005; Gupta, 2002]. Slit spectra were recorded using  $2048 \times 2048$  EEV CCD camera with  $13.5 \text{ \mu m}$  pixel, having a gain of  $1.8 e^-$  per analog-to-digital unit, and readout noise of  $6.3 e^-$ . Grism 7 with peak sensitivity at  $500 \text{ nm}$  and a slit width of  $1.''5$  were used. The spectroscopic observation was done in a canonical fashion and the reduction was done under *IRAF* as described in §2.4. Spectroscopic data reduction for DOLORES on 3.6m TNG, EFOSC2 on 3.6m NTT, and SCORPIO on 6m BTA were done in similar fashion and at around  $6000 \text{ \AA}$  it had a resolution of  $10 \text{ \AA}$ ,  $14 \text{ \AA}$  and  $12 \text{ \AA}$  respectively.

### 3.3.2 Optical spectra

Fig. 3.3 and Fig. 3.4 show the rest frame spectra of SN 2008gz, corrected for recession velocity ( $1864 \text{ km s}^{-1}$ ) of the host galaxy NGC 3672. We identify all the spectral features as per previously published line identifications for IIP events [Leonard et al., 2002a; Sahu et al., 2006]. In Fig. 3.3, end of the plateau phase ( $+115\text{d}$ ) and beginning of nebular phase ( $+140\text{d}$ ) is clearly evident in the spectral evolution.

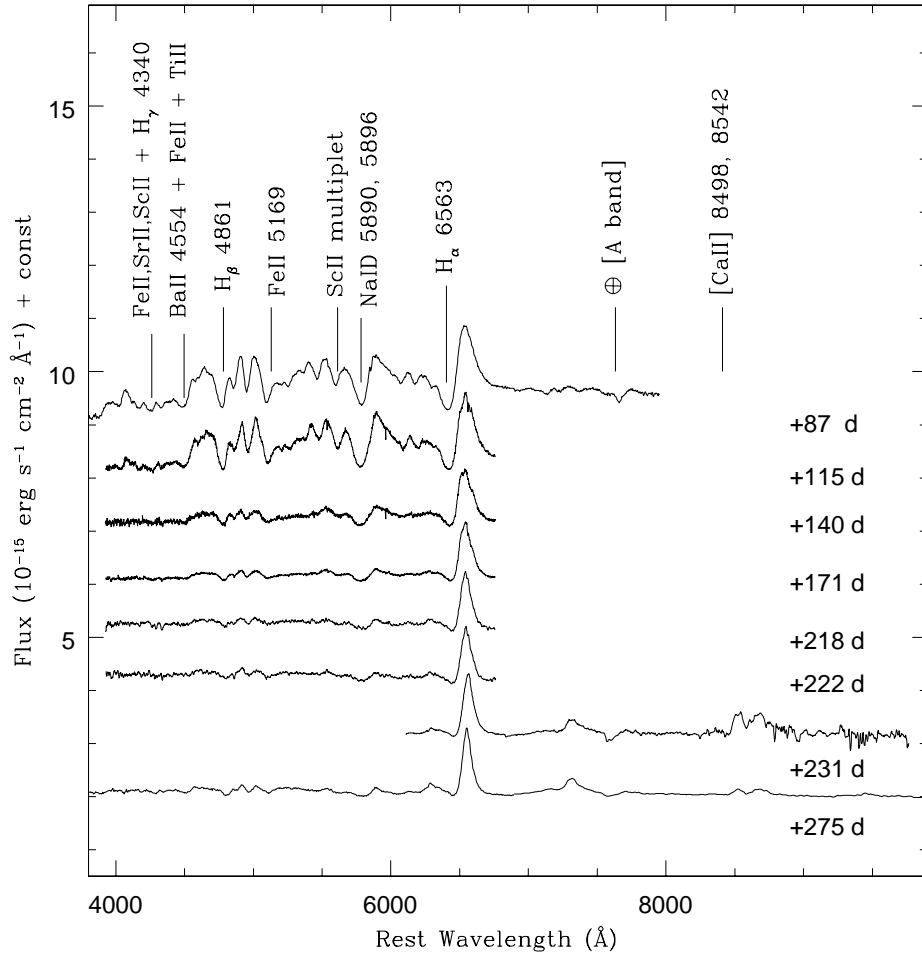


Figure 3.3 Doppler corrected flux spectra of SN 2008gz from late plateau (+87 d) to nebular phase (+275 d). Prominent Hydrogen and metal lines are marked.

### 3. THE NORMAL TYPE IIP SN 2008GZ

Table 3.3 Photometric evolution of SN 2008gz. Errors in magnitude are derived from ISIS and it denote  $1\sigma$  uncertainty.

UT Date (yy/mm/dd)	JD 2454000+	Phase <sup>a</sup> (day)	<i>B</i> (mag)	<i>V</i> (mag)	<i>R</i> (mag)	<i>I</i> (mag)	Telescope <sup>b</sup>	Seeing <sup>c</sup> (")
2008/11/10	781.47	+87	17.205±0.016	15.871±0.012	15.475±0.008	15.168±0.015	ST	2.4
2008/11/11	782.49	+88	17.312±0.030	15.819±0.014	15.477±0.010	15.164±0.013	ST	2.6
2008/11/15	786.47	+92	17.355±0.040	15.918±0.019	15.501±0.013	15.189±0.017	ST	2.7
2008/11/16	787.47	+93	17.376±0.033	15.920±0.017	15.537±0.011	15.210±0.014	ST	2.4
2008/11/17	788.48	+94	17.402±0.030	15.957±0.017	15.552±0.011	15.207±0.016	ST	2.4
2008/11/18	789.46	+95	17.457±0.037	15.966±0.021	15.533±0.012	15.219±0.015	ST	3.3
2008/11/23	794.47	+100	17.550±0.033	16.002±0.020	15.587±0.015	15.373±0.019	ST	3.5
2008/11/26	797.47	+103	17.684±0.014	16.182±0.008	15.685±0.003	15.373±0.005	ST	2.7
2008/11/28	799.45	+105	17.703±0.029	16.228±0.018	15.732±0.014	15.397±0.021	ST	3.0
2008/12/01	802.49	+108	17.900±0.028	16.311±0.017	15.830±0.011	15.475±0.017	ST	2.5
2008/12/10	811.49	+117	18.342±0.037	16.702±0.027	16.151±0.017	15.761±0.026	ST	2.9
2008/12/21	822.49	+128	19.125±0.094	17.519±0.047	16.857±0.026	16.480±0.040	ST	2.6
2008/12/22	823.46	+129	19.190±0.073	17.597±0.043	16.909±0.023	16.583±0.029	ST	2.3
2008/12/24	825.53	+131	19.242±0.174	17.695±0.058	16.893±0.022	16.393±0.026	ST	3.6
2008/12/26	827.52	+133	19.044±0.176	17.638±0.036	16.982±0.017	16.546±0.024	ST	3.1
2008/12/28	829.44	+135	–	17.704±0.037	16.928±0.020	16.559±0.026	ST	2.7
2008/12/29	830.49	+136	19.165±0.085	17.674±0.039	16.976±0.021	16.582±0.041	ST	3.2
2009/01/01	833.52	+139	–	17.738±0.047	17.016±0.021	16.623±0.030	ST	2.7
2009/01/08	840.48	+146	19.547±0.121	17.684±0.043	17.069±0.024	16.671±0.049	ST	3.1
2009/01/18	850.36	+156	19.489±0.168	17.920±0.082	17.118±0.040	16.717±0.055	ST	3.1
2009/01/19	851.32	+157	19.631±0.156	17.941±0.068	17.128±0.033	16.779±0.061	ST	3.1
2009/01/21	853.48	+159	19.115±0.069	18.027±0.078	17.128±0.038	16.688±0.049	ST	3.2
2009/01/23	855.51	+161	19.373±0.077	18.000±0.102	17.178±0.036	–	ST	3.1
2009/01/27	859.36	+165	19.699±0.096	18.002±0.054	17.279±0.029	16.877±0.045	ST	2.2
2009/02/01	864.35	+170	19.498±0.093	18.019±0.062	17.305±0.032	16.903±0.047	ST	2.5
2009/02/16	879.42	+185	19.461±0.096	18.217±0.065	17.434±0.032	17.029±0.046	ST	2.4
2009/02/17	880.27	+186	19.684±0.095	18.181±0.064	17.420±0.030	17.087±0.046	ST	2.9
2009/02/20	883.34	+189	19.609±0.124	18.179±0.075	17.434±0.039	17.071±0.058	ST	3.2
2009/02/26	889.27	+195	19.467±0.113	18.269±0.093	17.468±0.045	17.121±0.068	ST	3.6
2009/03/04	895.23	+201	18.976±0.118	18.163±0.111	17.417±0.052	16.924±0.070	ST	3.0 <sup>d</sup>
2009/03/21	912.33	+218	19.665±0.877	18.380±0.341	17.720±0.125	17.373±0.181	IGO	1.6
2009/03/22	913.24	+219	19.681±0.775	18.441±0.335	17.762±0.128	17.366±0.196	IGO	1.6
2009/03/24	915.32	+221	19.552±0.712	18.601±0.292	17.714±0.104	17.449±0.165	IGO	1.5
2009/03/25	916.30	+222	19.545±0.727	18.416±0.320	17.723±0.117	17.362±0.171	IGO	1.4
2009/03/26	917.32	+223	20.029±0.188	18.743±0.143	17.710±0.057	17.463±0.107	ST	3.5
2009/04/03	925.20	+231	19.414±0.372	18.701±0.242	17.899±0.083	17.481±0.130	ST	2.8
2009/04/12	934.29	+240	–	18.807±0.257	17.888±0.089	17.680±0.124	ST	2.7
2009/04/17	939.23	+245	21.040±0.270	18.909±0.132	18.000±0.052	17.680±0.080	ST	2.8
2009/04/23	945.16	+251	19.878±0.187	19.005±0.165	18.176±0.093	17.730±0.145	ST	3.1
2009/05/01	953.15	+259	19.633±0.182	18.760±0.199	18.254±0.080	17.822±0.109	ST	2.5
2009/05/17	969.11	+275	20.388±0.984	19.173±0.556	18.383±0.269	18.099±0.281	NTT	0.9

<sup>a</sup> with reference to the explosion epoch JD 2454694.0

<sup>b</sup> ST : 1 m Sampurnanand Telescope, ARIES, India; IGO : 2 m IUCAA Girawali Observatory, IUCAA, India; NTT : 3.6 m New Technology Telescope, ESO, Chile

<sup>c</sup> FWHM of the stellar PSF at *V* band

<sup>d</sup> Flat field problem

---

The late plateau phase (+87d and +115d) spectra are marked by strong P-Cygni features of  $H\alpha$ ,  $O\text{I } 7700\text{\AA}$ ,  $\text{Na I D } 5890, 5896\text{\AA}$ , and singly ionised Sc, Ba, Ti, Fe atoms, while the +140d and later spectra show significant drop in the absorption strength of P-Cygni features. The spectra during +115d to +222d show the spectral evolution of the event from early to mid-nebular stage, while the last two spectra (+231d and +275d) are those typical shown during the late stages of a typical SNIIP. In Fig. 3.4, the +87d spectrum shows various atomic absorption lines over the weak continuum. These lines are mainly due to elements present in the SN ejecta along with some earth atmospheric molecular lines (marked with  $\oplus$ ) and absorption due  $\text{Na I D}$  of Milky Way and host galaxy. On the other hand, the +275d spectrum shows a typical nebular phase spectrum dominated by emission lines.

Table 3.4 Journal of spectroscopic observations of SN 2008gz.

UT Date (yy/mm/dd/hh.hh)	JD 2454000+	Phase <sup>a</sup> (days)	Range $\mu\text{m}$	Telescope <sup>b</sup>	Grating (gr mm <sup>-1</sup> )	Slit width ( $''$ )	Dispersion ( $\text{\AA pix}^{-1}$ )	Exposure (s)	S/N <sup>c</sup> (pix <sup>-1</sup> )
2008/11/11/06.049	781.88	+87	0.34–0.80	TNG	500	1.5	2.5	1200	80
2008/12/08/23.346	809.46	+115	0.38–0.68	IGO	600	1.5	1.4	2x1800	50
2009/01/03/00.333	834.52	+140	0.38–0.68	IGO	600	1.5	1.4	2x1800	26
2009/02/01/22.208 <sup>d</sup>	864.40	+170	0.38–0.68	IGO	600	1.5	1.4	2x1800	20
2009/02/02/21.400	865.40	+171	0.38–0.68	IGO	600	1.5	1.4	3x1800	24
2009/03/22/18.303	913.27	+218	0.38–0.68	IGO	600	1.5	1.4	1800	8
2009/03/25/19.673	916.33	+222	0.38–0.68	IGO	600	1.5	1.4	1800	7
2009/04/03/22.643	924.50	+231	0.61–1.00	BTA	550	2.1	3.5	3x900	70
2009/05/17/00.543	969.04	+275	0.33–0.80	NTT	300	1.0	4.0	2700	16
2009/05/17/01.308	969.07	+275	0.55–1.05	NTT	300	1.0	4.2	2700	24

<sup>a</sup> With reference to the burst time JD 2454694.0

<sup>b</sup> TNG : DOLORES on 3.5m Telescopio Nazionale Galileo, Italy; IGO : IFOSC on 2m IUCAA Girawali Observatory, India; BTA : SCORPIO on 6m Big Telescope Alt-azimuthal, Special Astrophysical Observatory, Russia; NTT : EFOSC2 on 3.6m New Technology Telescope, ESO, Chile.

<sup>c</sup> At 0.6  $\mu\text{m}$

<sup>d</sup> Only center of galaxy observed

---

Temporal evolution of P-Cygni nature of  $H\alpha$  is clearly seen viz. the emission component becomes narrower with a decrease in depth of associated absorption component during the transition of SN from plateau to nebular phase. The FWHM of emission component of  $H\alpha$  decreases from  $\sim 5477 \text{ km s}^{-1}$  at +87d to  $\sim 3526 \text{ km s}^{-1}$  at +275d, indicating decrease in opacity and temperature of H I line emitting regions. For  $H\beta$ ,  $H\gamma$  and  $H\delta$ , the emission components are crowded with numerous metal lines. In Fig. 3.4, we also see impression of an additional P-Cygni component in the absorption profile of  $H\alpha$  and  $H\beta$ . This is speculated as a footprint of high velocity emitting shells in SN ejecta. Similar signatures were also noticed in type IIP SNe 1999em and 2004et [Leonard et al., 2002a; Li et al., 2005; Sahu et al., 2006].

The spectrum, labeled with +275d shows a typical late nebular phase spectrum marked by emission dominated permitted lines of Ca II 8498, 8542, 8662Å and Na I D as well as with the appearance of forbidden emission lines, i.e., [O I] 6300, 6364Å; [Fe II] 7155Å and [Ca II] 7291, 7324Å. These forbidden lines are not observed at Earth due to high density of gas. [Ca II] is already seen in +87d spectrum, [O I] appears at +171d, while the [Fe II] appears in +275d spectrum. Increasing strength of these forbidden lines indicate expansion and rarefaction of SN ejecta with time. The [Fe II] line is also noticed by Pastorello et al. [2005] in +344d spectrum of SN 1998A and +346d spectrum of SN 1987A, whereas for low luminosity SN 1997D it was visible at +417d [Benetti et al., 2001]. We determine relative strength  $I([\text{Ca II}])/I([\text{Fe II}])$  of 2.06 for SN 2008gz, whereas for SNe 1999em and 1987A, values of this ratio are respectively 6.98 and 24.68 at around +400d [Elmhamdi et al., 2003b]. This indicates that the physical conditions of [Fe II] formation in SN 2008gz may be similar to that of SN 1999em rather than SN 1987A.

### 3. THE NORMAL TYPE IIP SN 2008GZ

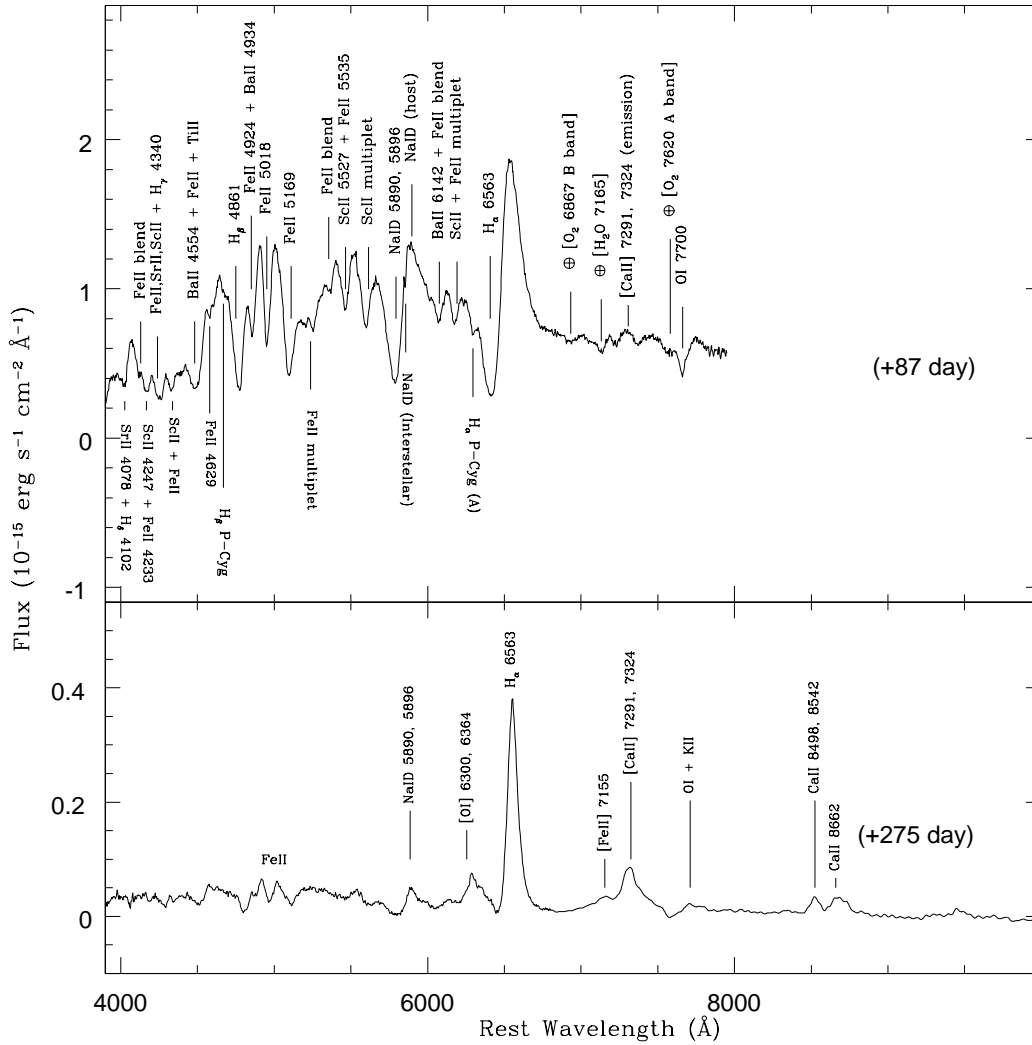


Figure 3.4 Line identification for late plateau and deep nebular phases.

---

### 3.4 Temporal evolution of spectral lines

To further illustrate the nature of burst, we show in Fig. 3.5 (and describe below) the velocity profiles of  $H\alpha$ ,  $H\beta$ ,  $\text{Na I D}$ ,  $\text{Ba II } 6142\text{\AA}$  and  $[\text{O I}] 6300, 6364\text{\AA}$ . The absorption dips and emission peaks due to SN are marked by downward and upward arrows respectively. For a spherically symmetric burst, the emission peak of P-Cygni profiles should be located at the rest wavelength of the corresponding line, while absorption dip will be blueshifted reflecting the instantaneous velocity of corresponding line emitting region. In our rest frame spectra,  $H\alpha$  emission peak is found to be slightly blue shifted by  $\sim 406 \text{ km s}^{-1}$  at +87d. Such blue shift in  $H\alpha$  emission peak at the early epochs was also observed for other type II SNe (i.e., 1987A [Hanuschik and Dachs, 1987], 1988A [Turatto et al., 1993], 1990K [Cappellaro et al., 1995], 1993J [Matheson et al., 2000], 1998A [Pastorello et al., 2005], 1999em [Elmhamdi et al., 2003b], 2005cs [Pastorello et al., 2009], 2007od [Andrews et al., 2010]). It is observed for few low luminosity type II as well, e.g., SN 1999br in their early phases [Pastorello et al., 2004]. On the basis of SN 1987A velocity profile, Chugai [1988] explained this phenomenon as an effect of diffused reflection of resonance radiation by the expanding photosphere. For SN 1987A at the +85d this velocity was about a few hundred  $\text{km s}^{-1}$  and hence comparable with SN 2008gz. On the other hand for SN 1998A and SN 1993J  $H\alpha$  emission peak velocity at comparable epoch were at least one order of magnitude higher than SN 2008gz. At later epoch (+275d)  $H\alpha$  emission peak velocity for SN 2008gz is about  $-200 \text{ km s}^{-1}$  which is considerably different from SN 1987A, where redshifted velocity of  $+600 \text{ km s}^{-1}$  was observed.

In most of our  $H\alpha$  profile, a narrow emission line (marked by ‘D’ in Fig. 3.5) is seen at zero velocity, which is probably due to underlying H II region and this

### 3. THE NORMAL TYPE IIP SN 2008GZ

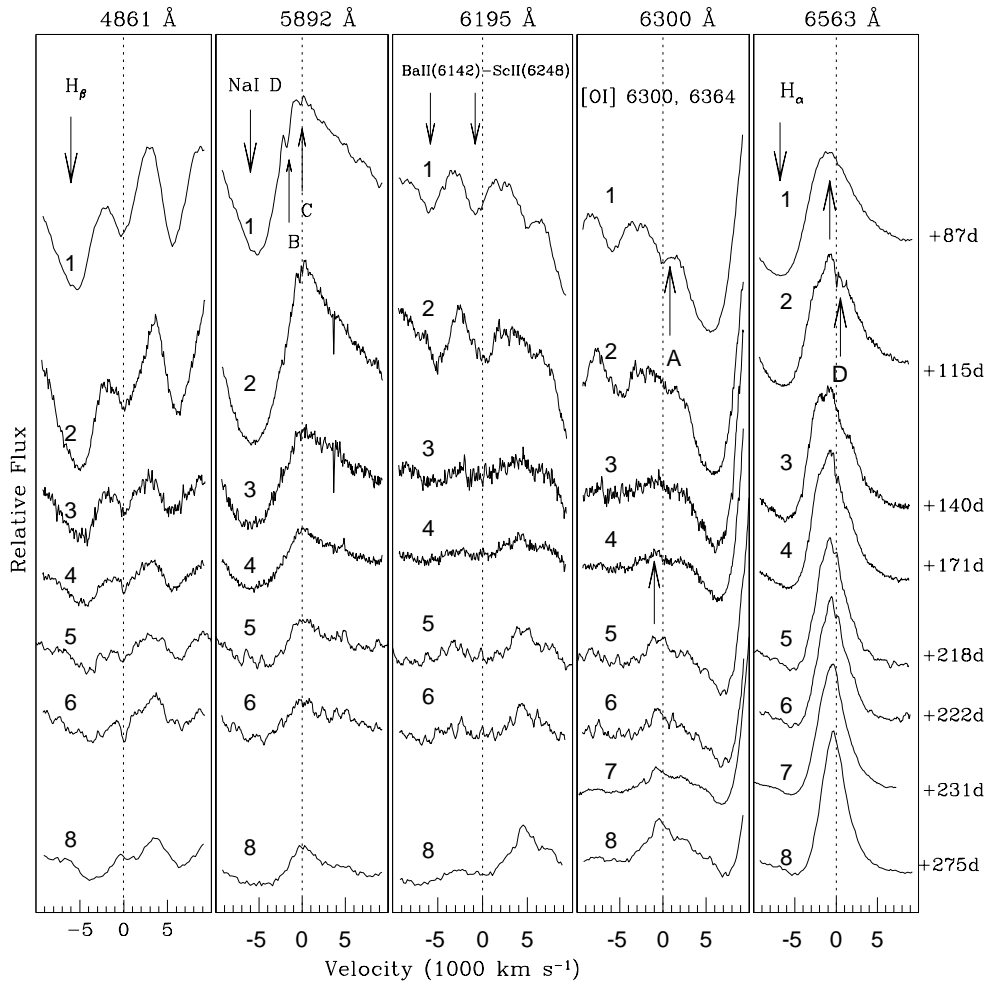


Figure 3.5 Evolution of some important spectral lines of SN 2008gz, during its transition from late plateau to nebular phase. The dotted line at zero velocity corresponds to the rest wavelength. Upward arrows show emission peaks, while downward arrows show absorption dips. The feature 'A' is a high velocity P-Cygni component of  $H\alpha$ , features 'B' and 'C' are due to Na I D absorption from the Milky Way and the host respectively, and the emission feature 'D' is  $H\alpha$  emission due to underlying H II region at SN location. The numbering sequences and resolution are : 1 (+87 d/10Å), 2 (+115 d/6Å) 3 (+140d/12Å), 4 (+171d/6Å), 5 (+218d/10Å), 6 (+222d/10Å), 7 (+231d/10Å) and 7 (+275 d/14Å).

---

is consistent with presence of low-luminosity H II region at SN location revealed by our H $\alpha$  narrow band observation (§3.8.2). Such a feature is not seen in well observed nearby IIP SNe 2004et [Sahu et al., 2006] and 2004A [Gurugubelli et al., 2008], which occurred in the outskirts of their host galaxies.

Na I D 5892Å P-Cygni nature is prominent in the spectra at all epochs with emission peak located at zero velocity, indicating almost spherical distribution of Na ion in the ejected material. In high S/N spectra (+87d and +115d), two peculiar absorption dip in the SN Na I D emission profile is seen at  $-80 \text{ km s}^{-1}$  (marked by B), and at  $-1630 \text{ km s}^{-1}$  (marked by C), respectively. These are identified as Na I D absorption respectively due to the interstellar matter in the host galaxy and the Milky Way (§3.6). In this regard, we note that due to highly inclined host galaxy ( $\Theta_{\text{inc}} = 56.2^\circ$ ), true recession velocity for SN will be different from the adopted ones ( $1864 \text{ km s}^{-1}$ ), and as measured from Na I D absorption at SN location, it should differ by  $\sim 100 \text{ km s}^{-1}$ , however, considering, low dispersion spectra, this will not change any of our conclusions.

The absorption dips due to an s-process element Ba II 6142 Å and for the element Sc II 6248 Å are clearly visible in +87d and +115d spectra, however, they disappeared in the +140d spectrum. This is similar to luminous type IIP SNe 2004et [Sahu et al., 2006] where these lines were prominent at +113d and barely observable at +163d and for 1999em [Elmhamdi et al., 2003b] it was visible up to +166d. In contrary to this, low luminosity IIP SNe 1997D, 2005cs and others [Benetti et al., 2001; Pastorello et al., 2004; Turatto et al., 1998], these features sustain comparatively for longer time and observable till +208d. Low luminous type IIP SNe expand with velocity, much slower than that of normal type IIP events. So, the Ba lines in low luminosity events sustain for longer time just because the ejecta

### 3. THE NORMAL TYPE IIP SN 2008GZ

---

takes more time to cool-down. For luminous type II-peculiar SNe 1987A and 1998A, these features are seen even at later epochs beyond +300d. For SN 2008gz, probably Ba abundance was low and s-process was not so effective like low luminosity events.

Metastable [O I] 6300, 6364 Å lines start to appear at +171d, and its strength increases progressively in spectra at later epochs. A normalized profile for +275d is shown in Fig. 3.6, which is nearly symmetric, indicating a spherically symmetric Oxygen ejecta.

The average FWHM for [O I] lines is  $\sim 2500 \text{ km s}^{-1}$ . Two component Gaussian fit results in ratio of  $I(6300)/I(6364) \approx 1.8$ , which is at deviation from their strength ratio of 3 expected from transitional probability for a rarefied gas at certain temperature. Smaller ratio for SN 2008gz may indicate higher opacity for 6300 Å in comparison to 6364 Å. We however note that the ratio of  $I(6300)/I(6364)$  is not always 3 for type IIP events. For the SN 1988A, [Spyromilio \[1991\]](#) showed that at initial epochs when optical depth of the ejecta is very high, value of  $I(6300)/I(6364) \approx 0.952$ , whereas at late phase, for optically thin ejecta this ratio approaches to 3.03.

Blueshift in [O I] lines, particularly at epochs later than +400d (i.e. in SNe 1999em and 1987A), is interpreted as an effective indicator of dust formation in the SN ejecta due to excessive extinction of redshifted wings of emission lines than the blueshifted ones [[Danziger et al., 1991](#); [Lucy et al., 1991](#)]. Between +300-400d, the observed blueshift in oxygen may be due to contamination from the Fe II multiplet at 6250 Å. The reason of the blue-shift of the oxygen line at early epochs ( $\lesssim 200$  day) is still not clear and several hypothesis have been done. In a recent work [Taubenberger et al. \[2009\]](#) described this as a result of residual opacity that remains in the inner ejecta. This seems to be the most likely explanation for observed blue-shift of oxygen line. Dust formation at an early epoch  $\sim +300$ d is also reported

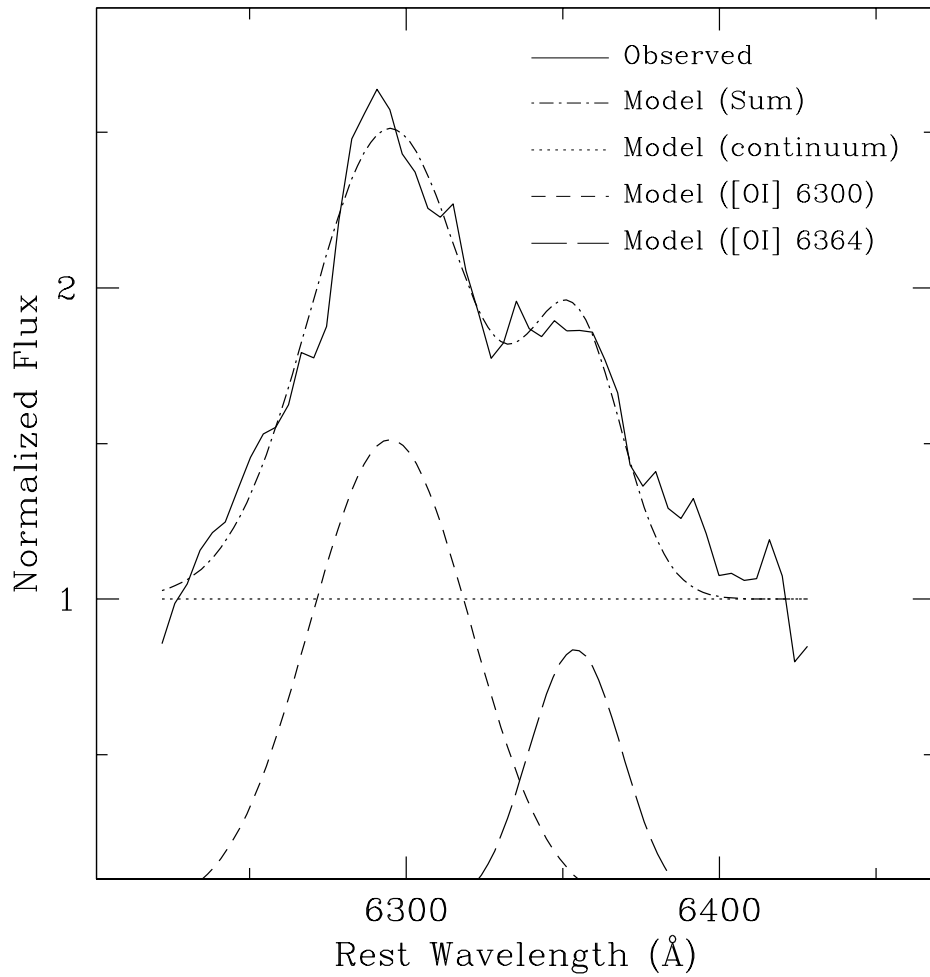


Figure 3.6 Two component Gaussian fit of [O I] 6300, 6364 Å emission lines. Measurements of their relative intensities quantifies, whether the corresponding line emitting region is optically thick or thin.

### 3. THE NORMAL TYPE IIP SN 2008GZ

Table 3.5 Velocities of photosphere, H $\alpha$  and H $\beta$  for different epochs of SN 2008gz evolution. All the parameters are derived from SYNOW modelling.

UT Date (yy/mm/dd/)	Phase (days)	$v_{\text{ph}} = v(\text{Fe II})$ km s $^{-1}$	$v_e(\text{Fe II})$ km s $^{-1}$	$v(\text{H}\alpha)$ km s $^{-1}$	$v_e(\text{H}\alpha)$ km s $^{-1}$	$v(\text{H}\beta)$ km s $^{-1}$	$v_e(\text{H}\beta)$ km s $^{-1}$
2008/11/11	+87	4200 $\pm$ 400	1000 $\pm$ 400	5500 $\pm$ 200	2100 $\pm$ 300	4300 $\pm$ 300	1300 $\pm$ 100
2008/12/08	+115	3200 $\pm$ 400	1500 $\pm$ 500	4700 $\pm$ 300	1500 $\pm$ 200	3800 $\pm$ 600	900 $^{+300}_{-100}$
2009/01/03	+140	4000 $\pm$ 400	2500 $\pm$ 1100	5300 $\pm$ 400	1300 $\pm$ 300	4000 $\pm$ 400	1000 $\pm$ 200
2009/02/02	+171	3500 $\pm$ 300	1600 $\pm$ 800	5100 $\pm$ 200	1300 $\pm$ 200	3500 $\pm$ 300	1000 $\pm$ 200
2009/03/22	+218	3100 $\pm$ 500	1700 $\pm$ 900	4800 $\pm$ 400	1500 $\pm$ 500	3700 $\pm$ 300	1600 $^{+400}_{-800}$
2009/03/25	+222	3100 $\pm$ 700	1200 $\pm$ 800	4900 $^{+700}_{-300}$	1100 $^{+300}_{-500}$	3100 $\pm$ 700	2000 $\pm$ 1000
2009/04/03	+231	< 5400	—	4800 $^{+600}_{-200}$	1600 $^{+200}_{-600}$	—	—
2009/05/17	+275	2000 $^{+200}_{-100}$	1500 $\pm$ 500	3800 $\pm$ 200	600 $\pm$ 200	2000 $\pm$ 100	600 $^{+600}_{-200}$

for SN 2004et. For SN 2008gz we estimate a blueshift of  $\sim 250$  km s $^{-1}$ , in [O I] components at epoch of +275d (see Fig. 3.3 and 3.6), however due to absence of any other evidence, this is not enough to claim dust formation in the SN 2008gz ejecta.

### 3.5 Photospheric and H-envelope velocities of ejecta

We used multi-parametric resonance scattering code SYNOW [Baron et al., 2005; Branch et al., 2003, 2002] for modeling the spectra of SN 2008gz to interpret spectral features and estimate velocities of layers at different epochs. The algorithm works on the assumptions of spherical symmetry; homologous expansion of layers ( $v \sim r$ ); sharp photosphere producing a black-body spectrum and associated at early stages with a shock wave. In photospheric phase, the spectral lines are formed by the shell above the thick photosphere, but in nebular phase all visible regions are optically thin [Branch et al., 2003]. Each of these two phases of SN evolution can be explained with individual approximations and the modeling of observed spectra needed in different synthetic codes.

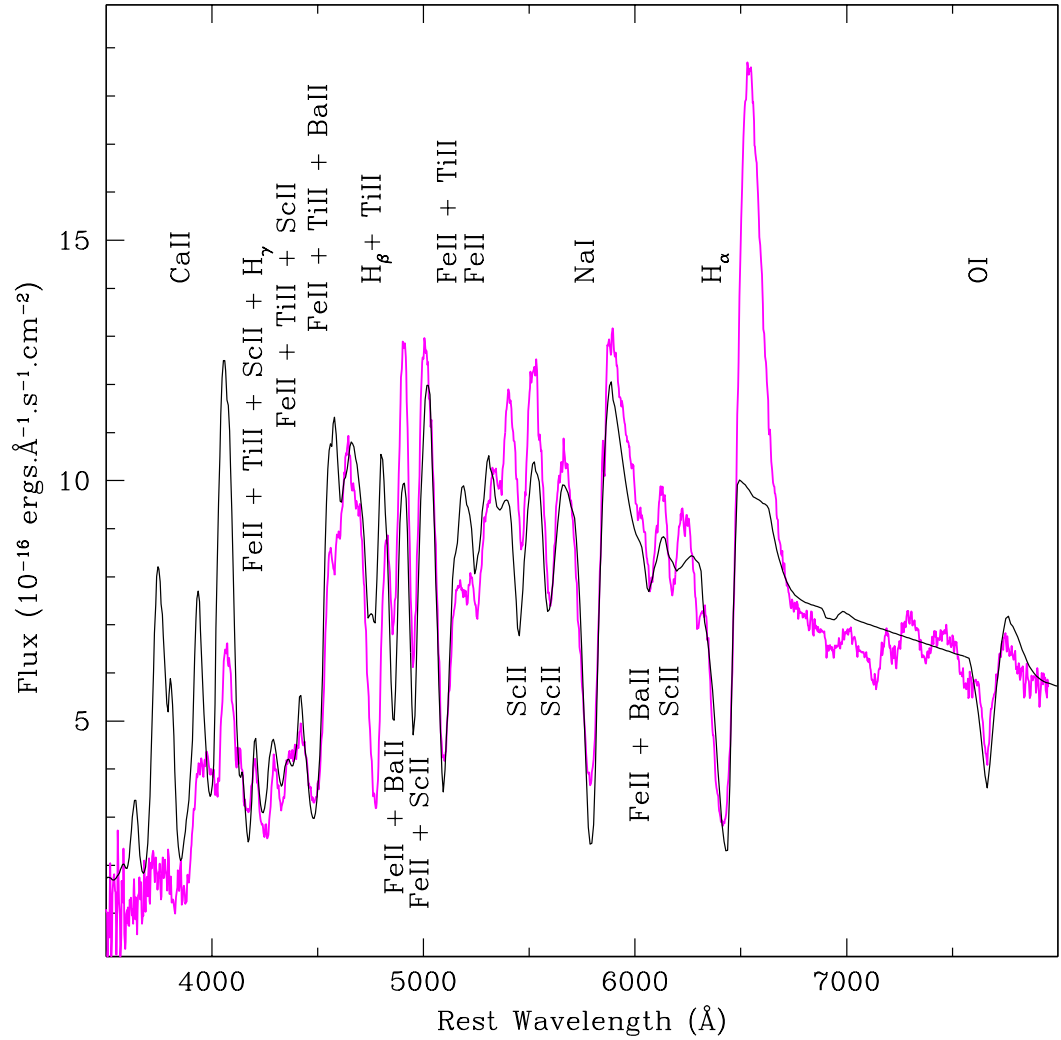


Figure 3.9 SYNOW modeling of the +87 d spectrum of SN 2008gz. The line identification is done after considering the SN as a spherically expanding fireball and lines are formed in a region moving ahead of the photosphere. Optical depth of individual line is calculated through “Sobolev approximation”.

### 3. THE NORMAL TYPE IIP SN 2008GZ

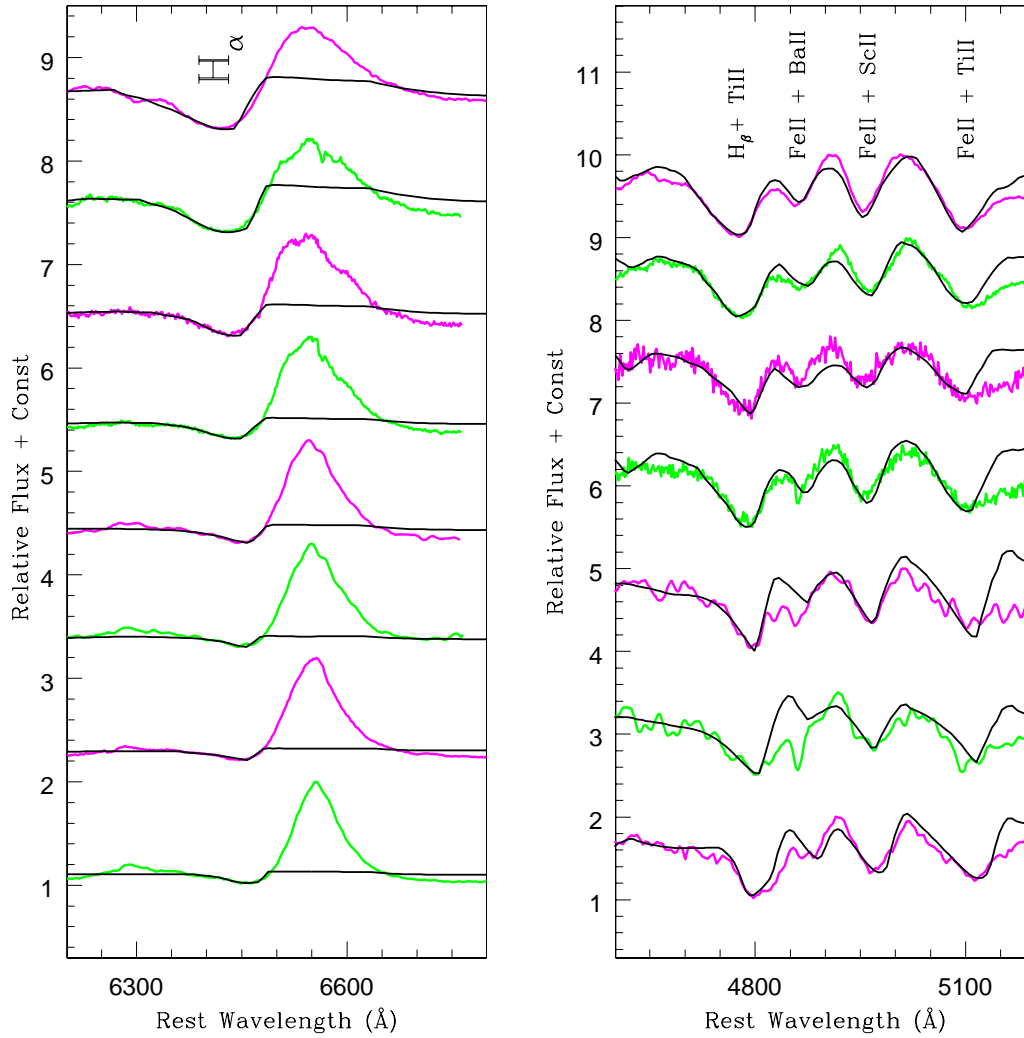


Figure 3.10 SYNOW models for absorption features of H $\alpha$  (left panel) and H $\beta$  & FeII (right panel). Blending effect due to ScII, TiII and BaII is also incorporated in the models. Spectral evolution corresponds (top to bottom) to +87, +115, +140, +171, +218, +222, +231 and +275. H $\beta$  region is not modeled for +231 d.

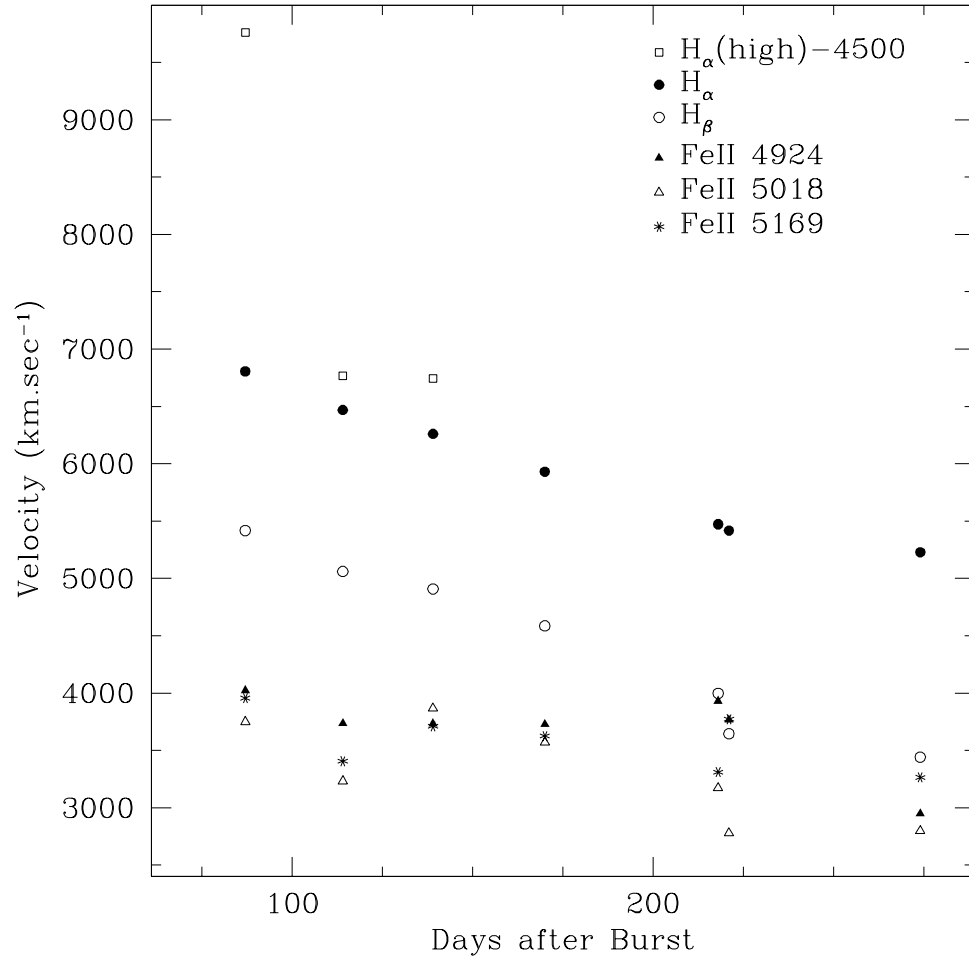


Figure 3.11 Velocity profiles of different elements in the ejecta of SN 2008gz

### 3. THE NORMAL TYPE IIP SN 2008GZ

---

Our main aim in modeling the spectral features is to estimate the velocities of the layers and that of pseudo-photosphere. It was also noted in [Branch et al. \[2003\]](#) there is no sharp division between the photosphere and the nebular phases. We note the presence of absorption components in Iron and Hydrogen lines at the latest spectra, which can be explained as a result of the decreasing resonance scattering mechanism. Although the resonance scattering codes like SYNOW are not used for describing late time spectra [see [Elmhamdi et al. 2006](#)], we use it to describe only the absorption parts of line profiles. It is not our intention to fit the emission part of the line profiles because this procedure needs to make use of other assumptions and other codes.

A preliminary result of SYNOW fit on SN 2008gz is reported by [Moskvitin et al. \[2010\]](#). In [Fig. 3.9](#), we present our model fit for +87d spectrum in detached case, i.e., assuming line forming shells of ionized gases moving ahead of the photosphere. Most of the spectral features (particularly absorption minima and the continuum) are produced well. All the identified spectral features are same as marked in [Fig. 3.4](#). We tried out undetached cases [[Sonbas et al., 2008](#)] as well and also attempted changing density laws (exponential and power) and we found that it had very little effect while fitting the absorption minima. In order to obtain precise velocity measurements of hydrogen layers, we modeled the profiles of H $\alpha$ , H $\beta$  and Fe II independently (see [Fig. 3.10](#)) following  $\tau \sim \exp(-v(r)/v_e)$ , where  $\tau$  is optical depth and  $v_e$  is the e-fold velocity. We also incorporated Ti II, Sc II, and Ba II ions to model multi-minima absorption features around H $\beta$ . For Fe II lines, we noticed that velocities of various absorption features are similar or have insignificant differences and hence we used averaged Fe II values to represent the photospheric velocity ( $v_{\text{ph}}$ ) [[Branch et al., 2003](#); [Elmhamdi et al., 2006](#)]. Estimations of photospheric and envelopes velocities

---

of different layers are given in Table 3.5. Uncertainties in the estimates take into account the noise in the spectra.

We also estimated photospheric and H-envelope velocities using IRAF by directly locating the absorption minima and the same is shown in Fig. 3.11. The velocity for Fe II 4924, 5018 and 5169 lines, range from  $\sim 4000 \text{ km s}^{-1}$  at +87d to around  $3000 \text{ km s}^{-1}$  at +275d. These values are similar to the values estimated above from SYNOW modeling. For H $\beta$  and H $\alpha$  layers our values are consistently higher by about  $1500 \text{ km s}^{-1}$  at all epochs than that derived from SYNOW. This discrepancy may arise due to contamination of true absorption minima by the emission component of P-Cygni profile of H $\alpha$  and H $\beta$  and hence it is likely that the true blueshift would be overestimated while using absorption minima.

For SN 2008gz the H $\alpha$  velocity at +87d is  $\sim 6800 \text{ km s}^{-1}$ , while for SNe 2004et, it is  $\sim 6000 \text{ km s}^{-1}$  [Sahu et al., 2006]. H $\beta$  also shows higher expansion velocity at comparable epochs. Similarly the photospheric velocity at day +50 is  $\sim 3700 \text{ km s}^{-1}$ , while it is  $4000 \text{ km s}^{-1}$  at +87d for SN 2008gz. So, even by considering an overestimate of the plateau period about 25 days (i.e. for  $t_i \sim 95\text{d}$ ), the photospheric and H-envelope velocity for SN 2008gz seem to have comparable or higher values than SN 2004et. The photospheric velocity is a good indicator of the explosion energy [see Dessart et al., 2010] and hence SN 2008gz has explosion energy similar to that of SN 2004et,  $\sim 2.3 \times 10^{51} \text{ erg}$  [Utrobin and Chugai, 2009] or higher. Utrobin [2007] obtains an explosion energy of  $\sim 1.3 \times 10^{51} \text{ erg}$  for SN 1999em, which has comparatively lower expansion velocity than to SN 2004et at similar epochs.

### 3. THE NORMAL TYPE IIP SN 2008GZ

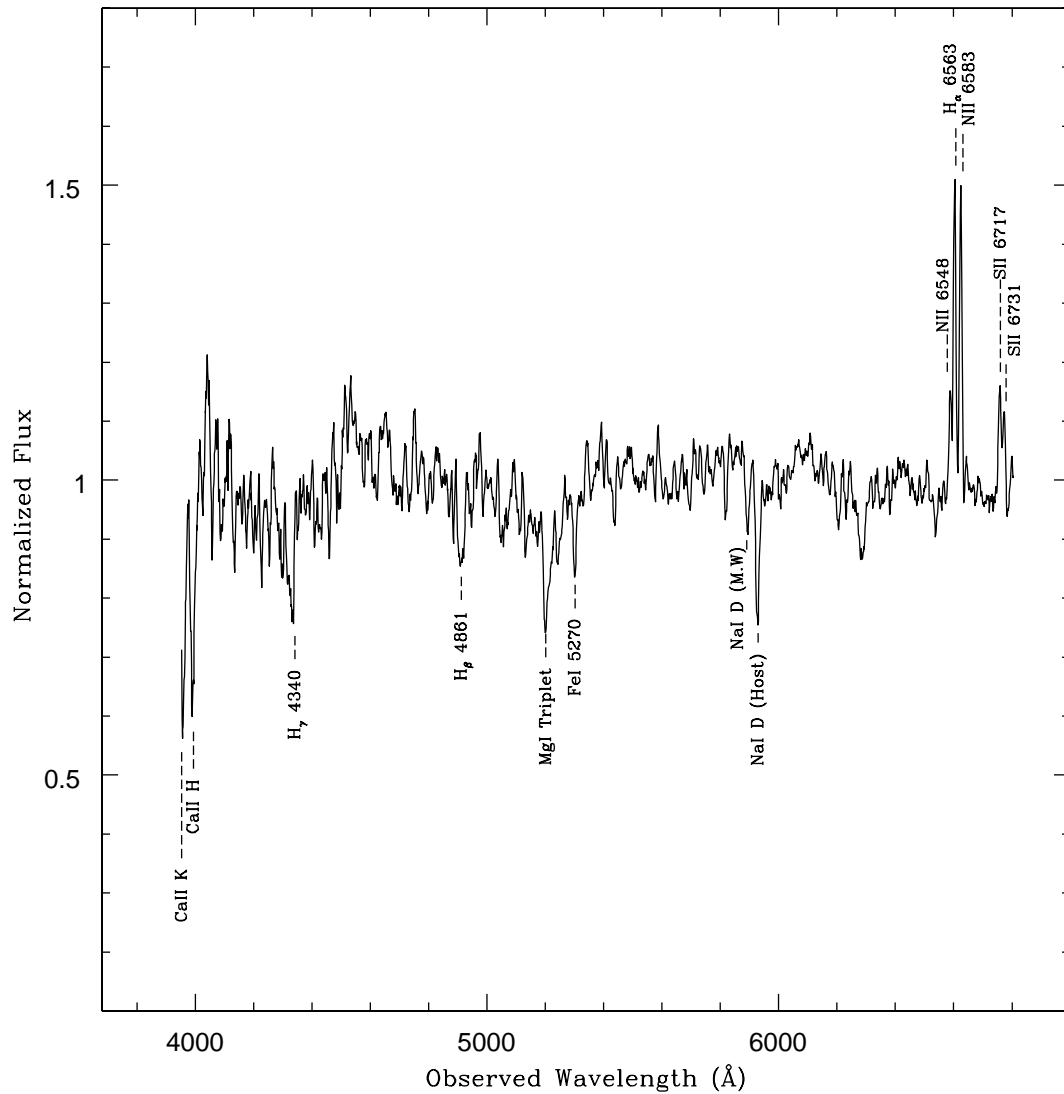


Figure 3.12 Spectrum of nucleus of the host galaxy NGC 3672 taken with 2-m IGO. The spectrum shows H $\alpha$ , N II (6548 Å and 6583Å), and S II (6717Å and 6730Å) lines in emission (similar to Sc spiral galaxies), which can arise from a gaseous component heated by AGN, post-AGB stars, shocks or cooling flows. The Ca II (K and H), H $\gamma$ , H $\beta$ , Mg I T, Fe I (5270Å), Na I D due to Milky Way and the host are seen in absorption.

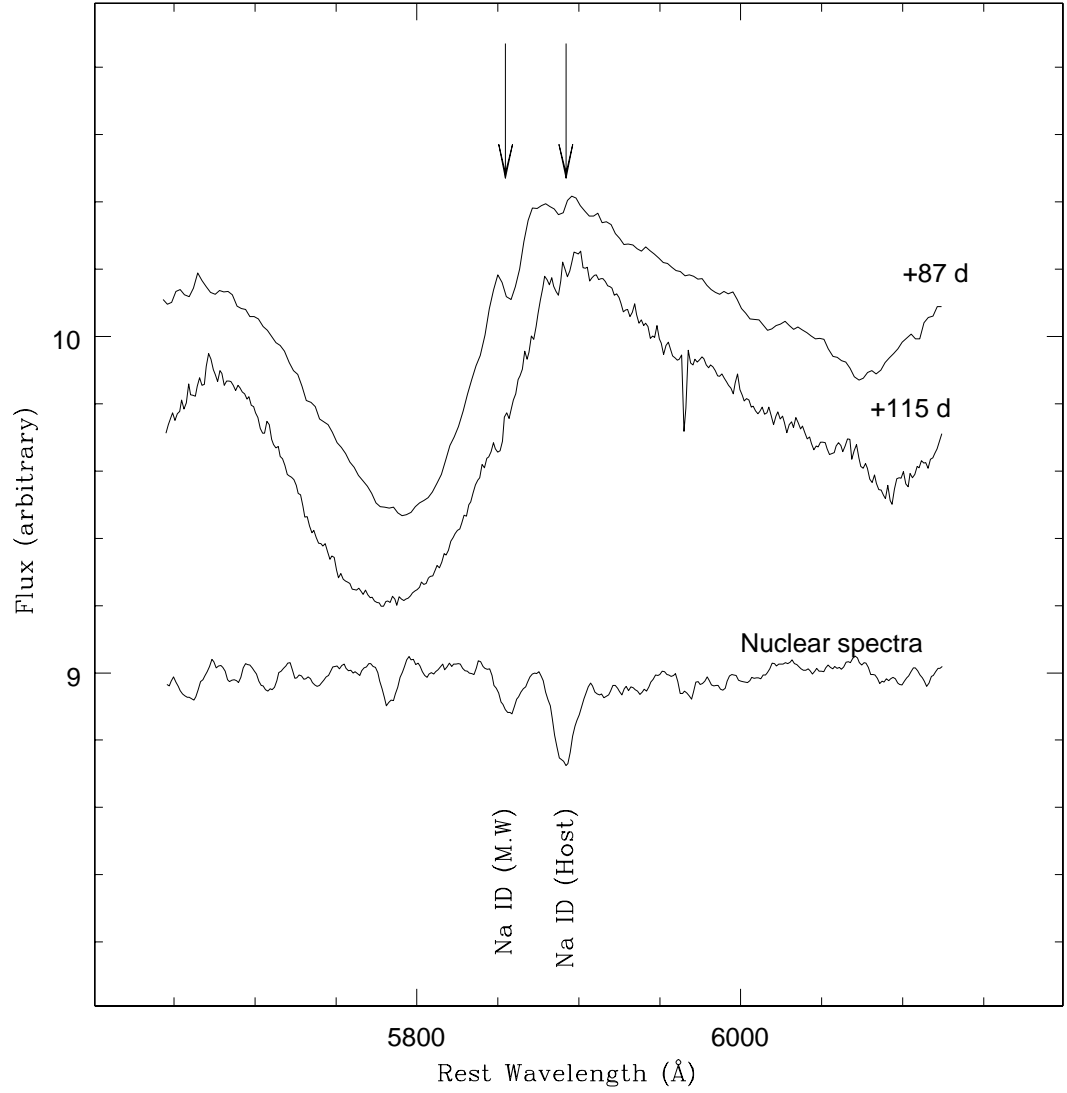


Figure 3.13 Rest wavelength spectra of SN 2008gz (+87 d/10Å and +115 d /6Å) and the centre of host galaxy (+170 d /6Å). Na I D absorption due to interstellar matter of host galaxy ( $\sim 5892\text{\AA}$ ) and the Milky Way ( $\sim 5854\text{\AA}$ ) is indicated.

### 3. THE NORMAL TYPE IIP SN 2008GZ

---

Table 3.6 Equivalent width measurement of NaID absorptions in the spectra of SN 2008gz and the host galaxy. Last row provides the uncertainty weighted EW of NaID absorption in the direction of SN 2008gz due to Milky Way and the host.

UT Date (yy/mm/dd/)	Phase (days)	EW (MW) Å	EW(host) Å
2008/11/11	+87	$1.39 \pm 0.34$	$0.23 \pm 0.28$
2008/12/08	+115	$1.21 \pm 0.69$	$0.28 \pm 0.50$
2009/02/02	+171	$1.32 \pm 1.29$	–
Weighted EW		$1.29 \pm 0.29$	$0.23 \pm 0.24$

### 3.6 Distance and extinction of SN 2008gz

Spectrum of the nuclear region of the host galaxy taken on +170d (see Fig. 3.12) was used to estimate  $cz_{\text{helio}}$ , the heliocentric velocity. Employing five nebular emission lines and prominent absorption features and using the 5577 Å skyline as a reference wavelength, we obtain  $cz_{\text{helio}}$  of  $1891 \pm 14 \text{ km s}^{-1}$ . This is in agreement with 18 other radio and optical measurements of  $cz_{\text{helio}}$  of NGC 3672 (in range of 1400 to 2000  $\text{km s}^{-1}$ ) listed in HyperLEDA<sup>1</sup>. The Combined measurement gives a mean  $cz_{\text{helio}}$  of  $\sim 1864 \pm 19 \text{ km s}^{-1}$  and it corresponds to a corrected (Local Group infall into Virgo) distance of  $\sim 25.65 \pm 2.93 \text{ Mpc}$ <sup>2</sup>. NED<sup>3</sup> lists four distance measurements based on HI Tully-Fisher relation, with a mean of  $25.25 \pm 4.0 \text{ Mpc}$ , which is in agreement with the above kinematic estimate, we therefore, adopt uncertainty weighted distance of  $25.5 \pm 2.4 \text{ Mpc}$  for SN 2008gz.

The Galactic reddening in the direction of SN 2008gz as derived from the 100

---

<sup>1</sup><http://leda.univ-lyon1.fr/>

<sup>2</sup>The cosmological model with  $H_0 = 70 \text{ km.s}^{-1}.\text{Mpc}^{-1}$ ,  $\Omega_m = 0.3$  and  $\Omega_\Lambda = 0.7$  is assumed throughout this work and the uncertainty corresponds to a local cosmic thermal velocity of  $208 \text{ km s}^{-1}$  [Terry et al., 2002].

<sup>3</sup><http://nedwww.ipac.caltech.edu/>

---

$\mu\text{m}$  all sky dust extinction map of [Schlegel et al. \[1998\]](#) is estimated as  $E(B - V) = 0.041 \pm 0.004$  mag. Additionally, we could also determine reddening in the direction of SN 2008gz from equivalent widths of Na I D absorption lines present in the spectra of SN 2008gz (+87d and +115d) and the centre of the host galaxy (see Fig. 3.13). D<sub>1</sub> (5889.95Å) and D<sub>2</sub>(5895.92Å) component of Na I D is not resolved in +87d spectra and it is seen as narrow absorption features overlaid on the broad P-Cygni emission wings of Na I D due to SN. In rest wavelength plot the host galaxy contribution is seen at  $\sim -80 \text{ km s}^{-1}$ , while the Galactic contribution is at  $-1630 \text{ km s}^{-1}$ . In +115d spectrum, both components of Na I D are resolved. Intriguingly, the Galactic component appear to split into two – a stronger component at  $\sim -1896 \text{ km s}^{-1}$  (due to Milky Way ISM) and a weaker component at  $\sim -1021 \text{ km s}^{-1}$ , possibly due to inter-galactic medium. In the +170d spectra, the Galactic Na I D absorption appear as a single component. Estimated total Na I D equivalent widths (EW) are reported in Table 3.6. Quoted errors in EW are photon-noise dominated RMS uncertainty derived following [Vollmann and Eversberg \[2006, see their Eq. 6\]](#). It is seen that the EW contribution due to host ( $0.23 \pm 0.24\text{Å}$ ) is smaller in comparison with the total Galactic contribution ( $1.29 \pm 0.29\text{Å}$ ).

It is known that the EWs of interstellar absorption bands is well correlated with the reddening  $E(B - V)$  estimated from the tail of SNIa colour curves [[Barbon et al., 1990](#); [Richmond et al., 1994](#)] and by employing empirical relations established by [Turatto et al. \[2003\]](#),  $E(B - V) = -0.01 + 0.16\text{EW}$  (where EW is in Å)<sup>1</sup>, we obtain Galactic  $E(B - V)$  contribution as  $0.20 \pm 0.05$  mag and host galaxy as  $0.03 \pm 0.04$  mag. The Galactic  $E(B - V)$  derived in this way is larger than that derived from

---

<sup>1</sup>In [Turatto et al. \[2003\]](#) there are two relations – one is with low slope and other with a high slope. In this work we have considered the lower slope, because it is well sampled and matches with the previous works in this direction [[Barbon et al., 1990](#)].

### 3. THE NORMAL TYPE IIP SN 2008GZ

---

Schlegel map. Considering the normal extinction law ( $R_V = 3.1$ ) and Schlegel value of  $E(B - V) = 0.041$  for the Milky Way; the EW (host/Galactic) ratio would suggest a slightly lower reddening in the host ( $E(B - V) \leq 0.01$  mag). However the host galaxy value of 0.03 mag may not be ruled out in case of a different dust to gas ratio for the host.

For this work, we will adopt a conservative value of  $E(B - V) = 0.07 \pm 0.04$  mag, obtained by adding Galactic (Schlegel) and host galaxy (NaID) contribution. This corresponds to visual extinction ( $A_V$ ) of  $0.21 \pm 0.12$  by assuming ratio of total-to-selective extinction  $R_V = 3.1$  [Cardelli et al., 1989].

## 3.7 Temporal Evolution of colour and bolometric luminosity

Fig. 3.14 shows reddening corrected colour evolution of SN 2008gz. For comparison, we also show reddening corrected colour curve of SN 1987A [Suntzeff and Bouchet, 1990], SN 1999em [Elmhamdi et al., 2003b] and SN 2004et [Sahu et al., 2006], for  $E(B - V)$  of 0.15, 0.10, and 0.41 mag and explosion epochs of JD 2446849.82, JD 2451480.5 and JD 2453275.5 respectively. Though the colour curves of SN 2008gz have large scatter but overall nature of its temporal evolution is prominent. SN 2008gz follows general trend of colour evolution i.e. a steep and rapid decrease from blue (high temperature) to red (low temperatures) colours similar to SNe 2004et and 1999em.  $(B - V)_0$  becomes redder from 1.2 mag at +87d to about 1.7 mag at +140d and it follows trend similar to SNe 2004et and 1999em. The overall trend in colour evolution of SN 2008gz between end of plateau and middle of the tail is

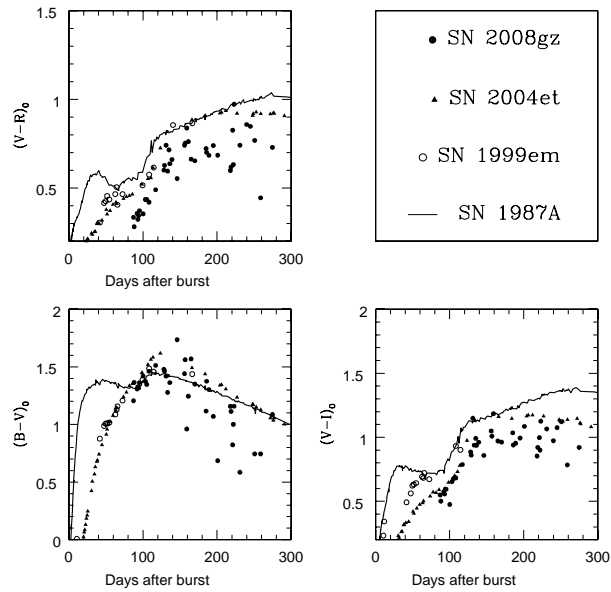


Figure 3.14 Temporal variation of colour of SN 2008gz. Also shown are the other core-collapse supernovae, SN 1987A, SN 1999em and SN 2004et.

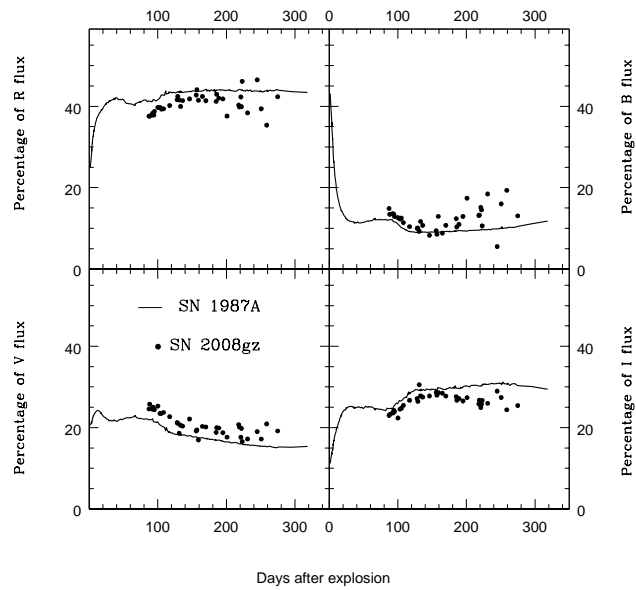


Figure 3.15 Flux contribution in percentage, in *BVRI* bands of SN 2008gz along with a comparison to SN 1987A

### 3. THE NORMAL TYPE IIP SN 2008GZ

---

similar to that of peculiar type II SN 1987A. In nebular phase,  $(B - V)_0$  turns blue rather rapidly,  $-1 \text{ mag (100d)}^{-1}$  and this arises due to suspected flattening in  $B$  light and a shallow decay in  $V$ ,  $R$  and  $I$  bands. The  $(V - R)_0$  colour is found to be consistently bluer than for other IIP SNe. For  $(V - R)_0$  and  $(V - I)_0$ , the increment is quite shallow during the transition from plateau to nebular phase. This is in contrary to the colour evolution of low luminosity type II-peculiar SNe 1997D and 1999eu, where a steep rise and excess in colour has been noticed [Misra et al., 2007b; Pastorello et al., 2004].

Bolometric luminosity is essential to estimate total optical radiant energy in the explosion and also at the tail phase it is a good estimator of radioactive  $^{56}\text{Ni}$  synthesized in the explosion. To a good approximation, the integration of extinction corrected flux in  $UBVRI$  at a given epoch gives a meaningful estimate of bolometric luminosity. The extinction corrected  $BVRI$  magnitudes were converted into fluxes using zeropoints given by Bessell et al. [1998] and the total  $BVRI$  flux is obtained by interpolating and integrating fluxes between 0.4 to 0.85  $\mu\text{m}$ . Fig. 3.15 shows percentage flux contribution in different passbands and the overall trend is found to be similar to that of SN 1987A. From plateau (+87d) to nebular (+140d) phase, the flux contribution declines from  $\sim 15$  to 10% at  $B$ , from  $\sim 25$  to 20% at  $V$ , while it ascends from  $\sim 36$  to 42% at  $R$ , from  $\sim 22$  to 30% at  $I$ . In nebular phase (until +270d), the flux contributions remain constant. For nearby SNe 1987A and 2004et, large ( $\sim 40\%$ ) flux contribution in  $U$  and  $B$  bands are observed at initial epochs, which reduces to a few percent by +60d. Though, towards later epochs, when SN ejecta becomes optically thin, a little enhancement (about 5%) in  $U$  and  $B$  bands is also noticeable [Misra et al., 2007b]. Therefore, for SN 2008gz, we have constructed  $UBVRI$  bolometric light curve after making a constant (5%) contribution from

---

$U$  band over the period of our observation. No correction for flux contributions in the ultraviolet and near-infrared region were made as they become significant respectively in early and late phases of the light curve evolution.

The left panel of Figure. 3.16 shows the  $UBVRI$  bolometric nature of SN 2008gz along with other type II events. Different behavior of these events is clearly evident and it provides constraint on the synthesized radioactive  $^{56}\text{Ni}$  as well as explosion energy of SNe. Tail luminosity of SN 2008gz is similar to SN 2004et, while the plateau luminosity is about 0.2 dex fainter. Explosion parameters for SN 2008gz are estimated in next sections.

## 3.8 Physical Parameters

### 3.8.1 Amount of ejected radioactive Nickel

The nebular phase light curve of type II SNe is mainly governed by the radioactive decay of  $^{56}\text{Ni}$  to  $^{56}\text{Co}$  to  $^{56}\text{Fe}$  having half-life of 6.1 and 111.26 days respectively and hence the tail luminosity is directly proportional to the amount of  $^{56}\text{Ni}$  synthesized by explosive burning of Si and O during shock breakout [Arnett, 1996, 1980].

By using tail luminosity,  $^{56}\text{Ni}$  mass can be derived following the method described by Hamuy [2003] applied under the assumption that all the  $\gamma$ -rays emitted during the radioactive decay make the ejecta thermalised. For SN 2008gz using the  $V$  band magnitude at +200d, corrected for extinction ( $A_V = 0.21 \pm 0.12$  mag; §3.6), a bolometric correction of  $0.26 \pm 0.06$  mag during nebular phase, and a distance modulus of  $32.03 \pm 0.21$ , we derive tail luminosity of  $1.51 \pm 0.29 \times 10^{41} \text{ erg s}^{-1}$  and this, for the plateau duration of 115 days, results in Ni mass  $M_{\text{Ni}} = 0.067 \pm 0.012 M_{\odot}$ .

### 3. THE NORMAL TYPE IIP SN 2008GZ

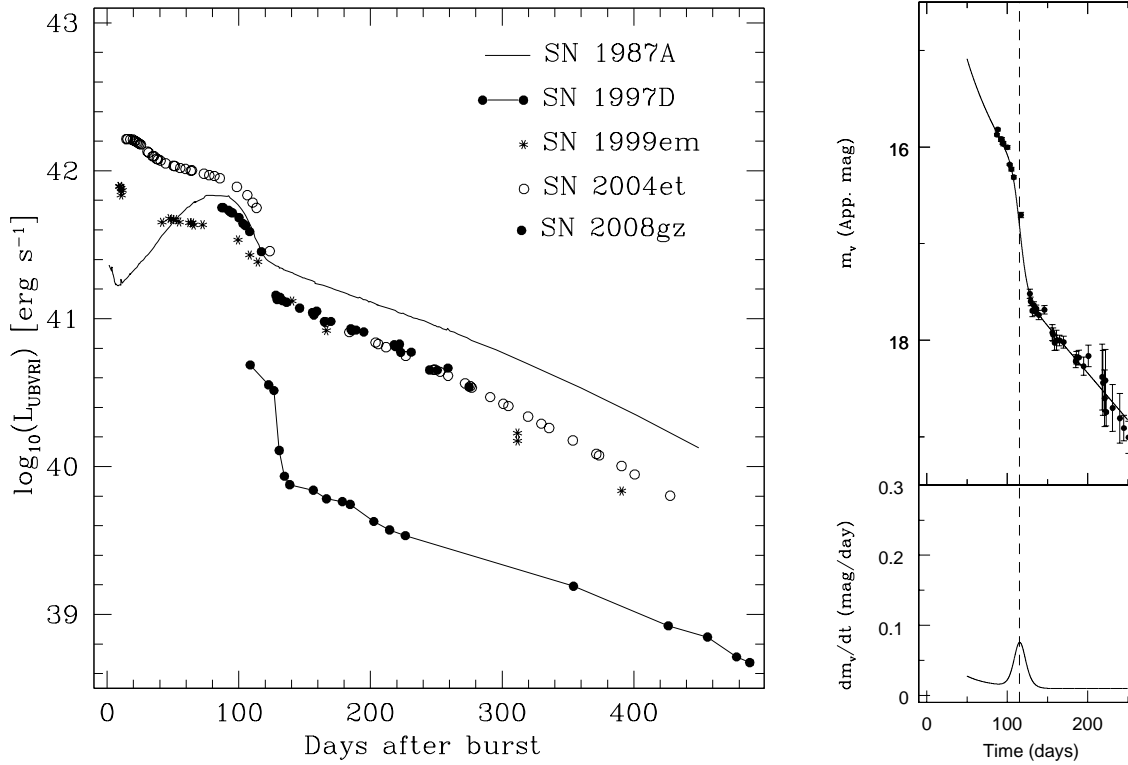


Figure 3.16 **Left:** Bolometric light curve of SN 2008gz. For comparison, we also show light curves of SN 1987A, SN 1997D, SN 1999em and SN 2004et. **Right:** Steepness parameter estimation for SN 2008gz.

---

We can estimate the mass of  $^{56}\text{Ni}$  by a direct comparison with that of SN 1987A for which it is accurately determined as  $0.075M_{\odot}$ . We note that the temporal evolution of flux contribution in different bands for SN 2008gz is comparable with that for SN 1987A (§3.7) and consequently we can safely assume that at a comparable epoch the ratio of their luminosities is equal to the ratio of synthesized  $^{56}\text{Ni}$  mass. SN 2008gz attains the deep nebular phase beyond 150 days after the burst. The last observation was also performed nearly at +275 day. Hence, the mean ratio between tail *UBVRI* bolometric luminosity of SN 2008gz ( $\sim 150\text{--}275$ ) and that of SN 1987A is about 0.539. This implies that for SN 2008gz ejected  $^{56}\text{Ni}$  mass  $[0.539 \times 0.075] \approx 0.041M_{\odot}$ .

By taking a sample of ten IIP SNe, [Elmhamdi et al. \[2003a\]](#) show that the steepness of V-band light curve slope (defined as  $S = dm_V/dt$ ) at the inflection time ( $t_i$ ) is anti-correlated with  $^{56}\text{Ni}$  mass ( $\log M_{\text{Ni}} = -6.2295S - 0.8147$ ). For SN 2008gz we have well sampled transition phase and get a value of  $S = 0.075 \pm 0.036$ ,  $\text{mag d}^{-1}$  (right panel of figure 3.16) which corresponds to  $M_{\text{Ni}} = 0.052 \pm 0.01M_{\odot}$ . Considering the uncertain values of extinction towards SN 2008gz, we note that for SNe 2004A and 2003gd, [Hendry et al. \[2006\]](#) finds that the [Elmhamdi et al. \[2003a\]](#) scheme gives somewhat lower values. Further, based on plateau luminosity, a linear correlation,  $\log M_{\text{Ni}} = -0.438M_V(t_i - 35) - 8.46$  found by [Elmhamdi et al. \[2003a\]](#) provides a value of  $^{56}\text{Ni}$  mass as  $0.051M_{\odot}$  for  $M_V$  of  $-16.37 \pm 0.24$  at +87d ( $t_i - 28$ ). Taking average of above four estimates, we get the amount of produced  $^{56}\text{Ni}$  mass =  $0.05 \pm 0.01M_{\odot}$ . For estimation of other physical quantities we assume that above amount of  $^{56}\text{Ni}$  was produced by SN 2008gz. Though we would like to state that adopting smaller plateau duration (§3.2.2) will reduce the amount of ejected radioactive  $^{56}\text{Ni}$  which will further propagate in determination of progenitor properties (§3.8.3).

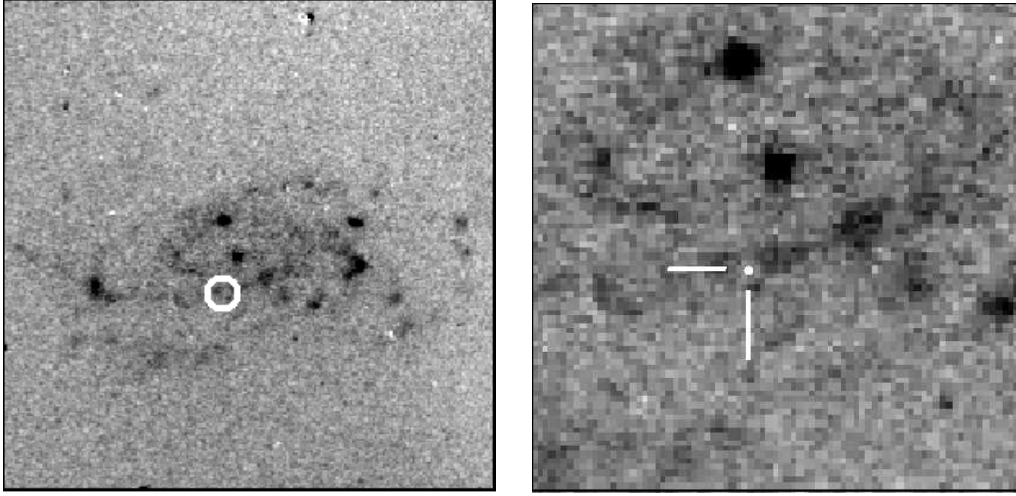


Figure 3.18 Continuum subtracted  $H\alpha$  image of NGC 3672. In left panel ( $\sim 3' \times 3'$ ) five bright H II regions are visible. The SN position is marked with a circle. In right panel ( $\sim 1' \times 1'$ ) zoomed in image of SN is shown. SN location is marked with a dot.

#### 3.8.2 Environment of the progenitor

Constraints on the nature of progenitors of core-collapse SNe are derived from the studies of environments in which they occur. For example, by correlating the position of explosion sites with that of the sites of recent star formation as traced by  $H\alpha$  line emission, it is found [see e.g. [Anderson and James, 2008](#); [James and Anderson, 2006](#); [Kelly et al., 2008](#)] that core-collapse events are excellent tracer of star formation, and type Ib/c are more likely to be associated with regions of high surface brightness or high  $H\alpha$  emission than type II SNe. [Anderson and James \[2009\]](#) found that type IIP events are likely to be more centrally concentrated than other II-subtypes. SN 2008gz occurred in spiral arms of the host galaxy at a deprojected galactocentric distance of 2.8 kpc (within half light radius) and the oxygen abundance ( $[O/H]=12+\log N_O/N_H$ ) of the galactic ISM at the position of SN is estimated as 8.6 (derived from the  $O/H-M_B$  relation proposed by [Pilyugin et al. \[2004\]](#)), which

---

is close to the solar abundance [O/H] of 8.65 [Asplund et al., 2009].

In order to further investigate the level of H $\alpha$  emission level, we observed NGC 3672 in narrow-band H $\alpha$ -line ( $\lambda_c = 6551\text{\AA}$ ) and H $\alpha$ -red ( $\lambda_c = 6650\text{\AA}$ ) having FWHM of  $83\text{\AA}$  and  $79\text{\AA}$  respectively. We used 2k CCD camera mounted with 1m ST, Nainital on 18 February 2010 (+560 d). A total exposure of 1 hr in each H $\alpha$ -line and H $\alpha$ -red filters were taken along with several bias and sky flats. Raw images were corrected for bias and flats using IRAF. FWHM of stellar PSF (seeing) varied from  $1.''8$  to  $2.''2$ . Images were combined to improve signal-to-noise ratio and the continuum subtraction was done using ISIS. Our narrow-band filter-set were not customized for extra-galactic work, and we expected H $\alpha$ -red to contain emission line fluxes, as at the redshifted wavelength ( $\sim 41\text{\AA}$  at H $\alpha$ ) of NGC 3672, the H $\alpha$ -red filter had a transmission of 25%, 40% and 80% respectively for N II  $6548\text{\AA}$ , H $\alpha$  and N II  $6589\text{\AA}$ . We could verify this by subtracting H $\alpha$ -line frame from the broadband  $R$  and  $V$  frames of SN taken on 14 February 2010, which gave no residual, while H $\alpha$ -red frame showed residuals. Fig. 3.18 shows the continuum subtracted image of SN 2008gz showing contributions from H $\alpha$ +N II emissions. A close up view of SN location is also shown. The sky is at level of 0 while the peak flux is around 22 counts. Five prominent regions of H $\alpha$  emission having peak counts above 15 are clearly apparent. SN 2008gz position is at a level of 8 counts, and hence it belongs to a low-luminosity H II regions. This is also evident from the early epoch spectra, in which an emission peak (not so prominent) of zero velocity is seen.

#### 3.8.3 Properties of progenitor star

Accurate estimates of explosion parameters require detailed hydrodynamical modeling of the optical light curves, though the analytical relations (based on a few well modeled IIP events) correlating the physical parameters explosion energy, pre-SN radius and total ejected mass on the one hand and the observable quantities, plateau duration, mid-plateau V-band magnitude ( $(M_V)_{\text{mp}}$ ) and mid-plateau photospheric velocity ( $v_{\text{mp}}$ ) on the other hand are proposed to exist [see e.g. [Litvinova and Nadezhin, 1985](#); [Nadyozhin, 2003](#); [Popov, 1993](#)]. For SN 2008gz, we can only provide an approximation of these observables. The estimates of  $(M_V)_{\text{mp}}$  and  $v_{\text{mp}}$  can be made by using the  $^{56}\text{Ni}$  mass estimate and by employing following empirical relations derived (by minimizing least squares) from the data given in [Hamuy \[2003](#), see their Fig. 3 and 4].

$$\log(M_{\text{Ni}}) = -0.385 \times (M_V)_{\text{mp}} - 7.749$$

$$\log(M_{\text{Ni}}) = 2.771 \times \log(v_{\text{mp}}) - 11.425$$

For  $M_{\text{Ni}} = 0.05 \pm 0.01 M_{\odot}$ , we derive  $(M_V)_{\text{mp}} = -16.7_{+0.3}^{-0.2}$  mag and  $v_{\text{mp}} = 4503_{-348}^{+306}$  km s $^{-1}$ . This value of absolute magnitude is consistent with those obtained from the first photometric V point (§3.9). These estimates, along with a plateau duration of 115 days provides [[Litvinova and Nadezhin, 1985](#)] burst energy  $\sim 2.5_{-0.7}^{+0.8} \times 10^{51}$  erg, ejected mass  $\sim 34_{-8}^{+10} M_{\odot}$  and pre-SN radius  $\sim 167_{-61}^{+106} R_{\odot}$ . The explosion energy derived in this way is consistent with the one expected from photospheric velocity (see §3.5), however, the ejecta mass is larger in comparison to the typical progenitor mass range (8.5-16.5 $M_{\odot}$ ) estimate derived from pre-explosion

---

SN images [Smartt et al., 2009] and this may arise due to uncertainty in above measured parameters.

Dessart et al. [2010] demonstrate that by employing the explosion energy estimate, the observed line width of [O I] and artificially generated radiation hydrodynamic simulations of core-collapse SNe, it is possible to put an upper limit on the main-sequence mass of the progenitor. For SN 2008gz, the Oxygen ejecta velocity of  $\sim 1250 \text{ km s}^{-1}$  (HWHM of [O I] profile, see §3.4) (which is slightly higher than  $\sim 1000 \text{ km s}^{-1}$  observed for SNe 2004et and 1999em at around +330 d) and assuming an explosion energy of  $3 \times 10^{51} \text{ erg s}^{-1}$  provide a main-sequence mass of 15 (12) respectively for non-rotating (rotating) pre-SN models while assuming an ejecta velocity of  $1500 \text{ km s}^{-1}$  for [O I] gives an upper limit of 17(13)  $M_{\odot}$ , which is consistent with that derived using pre-explosion images [Smartt et al., 2009].

### 3.9 Comparison with other core collapse supernovae

A detailed investigation of SN 2008gz indicates that it is a normal type IIP event showing photometric and spectroscopic evolutions similar to archetypal SNe 2004et and 1999em. SN 2008gz occurred in a highly inclined ( $\Theta_{\text{inc}} = 56.2^{\circ}$ ) host galaxy, within deprojected galactocentric radius of  $0.27r_{25}$  (Table 5.1) implying solar metallicity region similar to SNe 1999em and 2005cs, though its explosion and other properties were found to be similar to SN 2004et, which occurred in the outskirts of its host galaxy. Our narrow-band  $H\alpha$  photometry indicates that SN 2008gz was associated with a star forming low luminosity H II region of the galaxy. Thus, the

### 3. THE NORMAL TYPE IIP SN 2008GZ

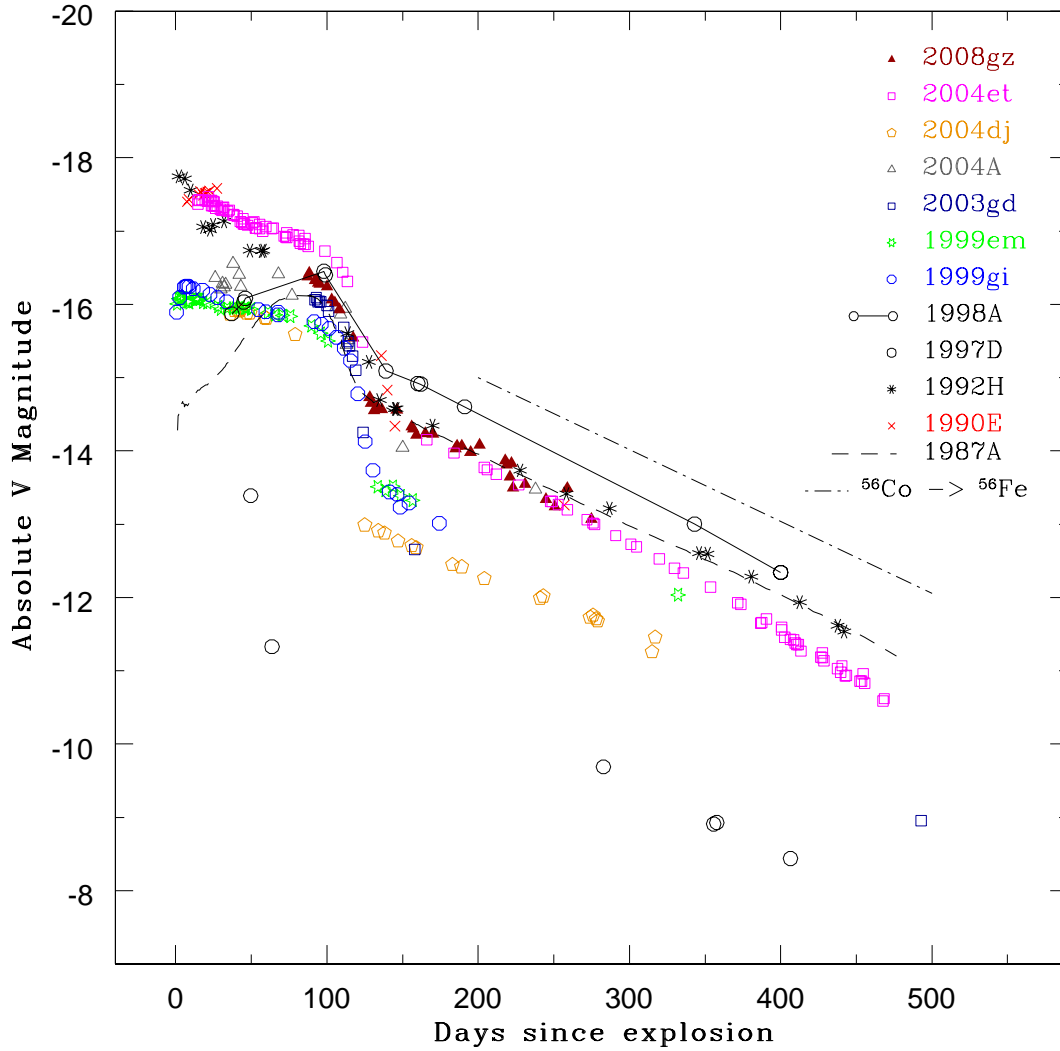


Figure 3.19 Comparison of absolute V-band light curve of SN 2008gz with other type IIP SNe, like SN 2004et, SN 2004dj, SN 2004A, SN 2003gd, SN 1999em, SN 1999gi, SN 1998A, SN 1997D, SN 1992H, SN 1990E and SN 1987A. The magnitudes have been corrected for distance and reddening.

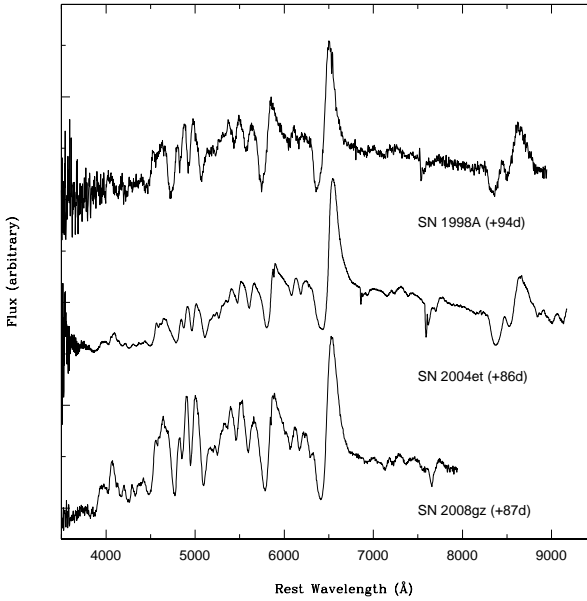


Figure 3.20 Comparison of spectral features of SN 2008gz along with SN 2004et and SN 1998A

metallicity appear to have little effect on the explosion properties of core-collapse SNe.

In Fig. 5.4 we show absolute V-band light curve of well studied core-collapse events collected from literature [see Misra et al., 2007b, for references]. The plateau luminosity ( $M_V \sim -16.6$ )<sup>1</sup> of SN 2008gz is at the similar level as of peculiar SNe 1987A, 1998A and it lies in between to the brighter end of IIP SNe 1990E, 1992H, 2004et ( $\sim -17$  mag) and the fainter end SN 1997D ( $\sim -15$  mag). This shows that SN 2008gz is a normal event, both in energetics and nickel production. These values of plateau luminosity for IIP SNe are lower than  $-17.6 \pm 0.6$  mag which was predicted using theoretical models calculated by Höflich et al. [2001] for IIP

<sup>1</sup>We estimate the value of mid plateau  $M_V$  as  $-16.6 \pm 0.2$  mag, by considering an average decline rate of  $0.006 \text{ mag d}^{-1}$  during the plateau phase of SNe 1999em and 2004et, we found that the mid-plateau magnitude of SN 2008gz was  $\sim 0.2$  mag brighter than that determined at +87d (§3.8.1). We assume  $A_V$  of 0.214 mag.

### 3. THE NORMAL TYPE IIP SN 2008GZ

---

SNe based on wide range of parameters (explosion energy, metallicity, mass loss of progenitor).

SN 2008gz showed rarely observed 1.5 mag drop at  $V$  from plateau to nebular phase and it had tail luminosity comparable (or higher) to SNe 2004et resulting in the synthesised  $^{56}\text{Ni}$  mass in range  $0.05 - 0.1M_{\odot}$ . Large tail luminosity of SN 1998A indicates that the thermalization process for 1998A was more efficient than SN 2008gz. Colour evolution of SN 2008gz has a similar trend like normal IIP and peculiar SNe 1987A and 1998A. Expansion velocity of the SN 2008gz ejecta was comparable to SN 2004et or higher, implying explosion energy of  $\sim 2 \times 10^{51}$  erg. Our calculation for progenitor mass (§3.8.3) of SN 2008gz favours the mass range of  $13 - 18 M_{\odot}$  (i.e., SNe 1999em, 1999gi, 2004dj, 2004et) than to the lower mass range of  $8 - 18 M_{\odot}$  (i.e., SNe 1997D, 2004A, 2005cs). This progenitor mass grouping is also favoured on the basis of radio luminosity [Chevalier et al., 2006]. As an alternative scenario, SN 2008gz can be characterized as a peculiar event. Lack of data in first 1-2 months after the explosion and spectral similarity with SN 1998A [Benetti et al., 2008] also indicates toward the possibility that SN 2008gz is a peculiar type II event. Figure 3.20 shows a comparison of SN 2008gz spectrum with SN 2004et and SN 1998A at comparable epoch. There are many similarities between spectral features of SN 2008gz and SN 1998A. On the other hand, low rates of peculiar type II SN, similarity in late light curve of SN 2008gz with type IIP events and similarity of some particular spectral features, like high velocity  $\text{H}\alpha$  line (§3.4) of this event with that of SNe 2004et and 1999em also indicates that SN 2008gz would be a normal type IIP event.

---

### 3.10 summary

We present *BVRI* photometric and low resolution spectroscopic observations of a supernova event SN 2008gz which occurred in an spiral arm and within half-light radius of a nearby ( $\sim 25$  Mpc) galaxy NGC 3672. As the event was buried the galaxy light, we used template subtract technique to estimate the apparent magnitude of the event. We monitored the event for a period of  $\sim 200$  days. We summarize our results as follows.

1. Photometric and spectral nature of the event is found similar to normal type IIP SNe 2004et and 1999em. The event was discovered by about 82 days after the burst and it has a plateau phase lasted  $115 \pm 5$  days. We monitored the SN evolution from +87d to +275d.
2. We estimate photospheric and H-envelop velocity by using both direct measurements of the absorption minima of H I and Fe II lines and SYNOW modeling of the spectra. Here both values agree well within uncertainties. We estimate the photospheric velocity of  $\sim 4000 \text{ km s}^{-1}$  at +87d, which is higher than that observed for well studied SN 2004et at similar epochs indicating explosion energy comparable to or higher than 2004et. Similar trend was also seen for the expansion velocity of H-envelopes.
3. Using pre-SN models of [Dessart et al. \[2010\]](#) and also by comparing explosion energies (derived by using hydrodynamical models) of well studied IIP SNe, we find that the SN 2008gz had explosion energy of  $2 - 3 \times 10^{51} \text{ erg.s}^{-1}$ . This estimation, coupled with the observed width of the forbidden [O I] line gives an upper limit for the main-sequence progenitor mass of  $17M_{\odot}$ .

### 3. THE NORMAL TYPE IIP SN 2008GZ

---

4. SN2008gz exhibits rarely observed drop of 1.5 mag within 30 days in V-band from plateau to nebular phase, this is higher than the typically observed fall of 2-3 mag in normal IIP SNe. Adopting  $A_V = 0.21$  mag, we could estimate mass of  $^{56}\text{Ni}$  synthesized during the explosion as  $0.05 \pm 0.01 M_{\odot}$ .
5. Our  $\text{H}\alpha$  observation taken about 560 days after the explosion indicates that the event took place in a low luminosity star forming arms, very close to a H II region. The emission kink of this H II region is also seen in  $\text{H}\alpha$  line near zero velocity of the Doppler corrected spectra of SN.

# Chapter 4

## The subluminous Type IIP SN 2008in

### 4.1 Introduction

The Observational signatures of Type IIP events have already been discussed in the previous chapter. The IIP SNe show a wide range of plateau luminosities, plateau durations, expansion velocities and nickel masses [Hamuy, 2003] and these observational properties are connected with the explosion mechanism as well as the physical properties of the progenitor star such as ejected mass, explosion energy and pre-SN radius [Nadyozhin, 2003; Smartt et al., 2009]. They are thought to be a result from progenitor masses in the range  $8 - 25 M_{\odot}$  [Heger et al., 2003] (it may extent upto  $30 M_{\odot}$ ) with an extended hydrogen envelope necessary to maintain the plateau phase.

A detailed study of optical light curves and spectra of only a few nearby IIP SNe has been done so far and there exists a discrepancy in estimating the mass of

#### 4. THE SUBLUMINOUS TYPE IIP SN 2008IN

---

their progenitors, e.g, for the three well studied events (namely 1999em, 2005cs and 2004et), the determination of progenitor mass from the hydrodynamical modeling of their light curve is found to be higher than that estimated from pre-SN imaging [Bersten et al., 2011; Utrobin et al., 2010].

Recently, a number of Type IIP events have been discovered which show ‘low luminosity’ than the usually found normal Type IIP events. Some of them are SNe 1999br, 1999eu, 1994N, 2001dc, 2005cs [Pastorello et al., 2009, 2004], 2008bk [Van Dyk et al., 2012] and 2009md [Fraser et al., 2010]. These events have explosion energy ( $\sim 10^{50}$  erg) and ejected  $^{56}\text{Ni}$ -mass ( $2-7 \times 10^{-3} M_{\odot}$ ), both lower by a factor of 10 than normal, and low expansion velocity  $\sim 1000 \text{ km s}^{-1}$  [Pastorello et al. 2009 and references therein]. The low-luminosity IIP SNe are debated because of the unknown nature of their progenitors. The first reported faint SN was SN 1997D [Benetti et al., 2001; Turatto et al., 1998], and the observed properties of its light curves and spectra were explained in terms of significant fallback of ejected material on a newly formed black hole (BH), created through the core collapse of a massive progenitor [ $M \gtrsim 20 M_{\odot}$ , Zampieri et al. 2003, 1998]. Alternatively, SN 1997D was interpreted as the explosion of a less massive progenitor [ $8 - 12 M_{\odot}$ , Chugai and Utrobin 2000], close in mass to the lower limit for stars that can undergo core-collapse. Heger et al. [2003] suggested that low-luminosity Type IIP events are electron capture SNe produced by low-mass progenitors giving rise to ONeMg cores. This is further supported through investigations of pre-explosion images [Maund and Smartt, 2005; Maund et al., 2005], though Eldridge et al. [2007] have ruled out the possibility of such a mechanism for the low-luminosity SN 2005cs. According to the formalism of Heger et al. [2003] and Eldridge and Tout [2004], no star having initial mass less than  $22 M_{\odot}$  can form a BH, which can quench the ejected material and produce a

---

low luminosity SN. Stars with masses above  $25M_{\odot}$ , formed in metal-poor or slightly sub-solar metallicity regions can produce low-luminosity, BH-forming Type IIP SNe. Type IIL/b events can be produced through this process from stars having masses  $> 25M_{\odot}$  and generated in regions with solar (or super-solar) metallicity. So, the metallicity information at the SN location and the estimation of the initial mass are essential to constrain the triggering mechanisms of these explosions.

SN 2008in was discovered in the nearby galaxy M 61 (NGC 4303). The first unfiltered CCD images of SN 2008in were taken by Koichi Itagaki on 2008 December 26.79 (all times in UT hereafter) and 27.69 at a magnitude of 14.9. Independent observations of this event by K. Kadota showed the transient at an unfiltered mag of 15.1, In addition W. Wells recorded the SN on 2008 December 28.46 at  $V$  and  $R$  band magnitudes of 14.3 and 13.2, respectively [Nakano et al., 2008c]. Low and mid-resolution spectroscopic observations indicate an early discovery for SN 2008in (within 1–2 weeks after core-collapse). The spectra showed highly blueshifted  $H_{\alpha}$  and  $H_{\beta}$  absorptions (by  $\sim 9000 \text{ km s}^{-1}$ ) with weaker emission components [Chakraborti et al., 2008; Foley, 2008; Stritzinger, 2008]. The presence of prominent P-Cygni profiles of Balmer lines leads to its classification as a Type II SN.

The broadband light curve and the initial spectral evolution of SN 2008in were similar to those of normal Type IIP SNe. However, from mid-plateau, the SN started to show a few spectral features (like  $H_{\alpha}$ ) which are similar to under-luminous events. SN 2008in was also observed in the radio with the Very Large Array (VLA) on 2008 December 31.40 UT in two frequency bands at 8.4601 and 22.4601 GHz [Stockdale et al., 2008]. Observation for the second epoch was further reported by Stockdale et al. [2009] on 2009 January 27. Interacting Type II SNe, like Type IIn events

## 4. THE SUBLUMINOUS TYPE IIP SN 2008IN

---

and a few Type IIP events (e.g. SN 2004et) are supposed to be strong sources of radio emission [for review see [Weiler et al. 2002](#)]. However, both VLA observations produced null results for this proximate event.

In this chapter optical and near-infrared photometric and optical spectroscopic observations of SN 2008in will be presented. The photometric data cover a time span of about 410 days since the discovery. The *Swift*/XRT [[Burrows et al., 2005b](#)] and *Swift*/UVOT [[Roming et al., 2005](#)] data covering a time span of 60 days are also presented. The epoch of explosion  $\text{JD} = 2454825.6$  (§4.3) is considered throughout this present work and the times of pre-/post-explosion are referred with  $-/+$  signs respectively.

## 4.2 observation and data reduction

### 4.2.1 Photometric Observation

The prompt follow-up of the event was carried out by the ground-based ROTSE-IIIb telescope<sup>1</sup> having sensitivity in the wavelength region from 0.35 to 1.0  $\mu\text{m}$  with a peak around 0.6  $\mu\text{m}$  [[Quimby et al., 2007b](#)]. The SN was first detected in the ROTSE-IIIb images on 2008 December 24.45 and it was monitored at 58 phases until +115d. The initial detections of the SN evaded the automated pipeline identification due to poor image quality and low signal-to-noise ratio (S/N). The data reduction is as explained in [Roy et al. \[2011a\]](#). The unfiltered instrumental magnitudes were calibrated using the USNO B1.0 *R*-band magnitudes of about 15 isolated stars. The

---

<sup>1</sup>The Robotic Optical Transient Search Experiment (ROTSE-III) is a set of four 45 cm fully robotic optical telescopes, installed at Siding Spring Observatory, Australia (ROTSE-IIIa), McDonald Observatory, Texas (ROTSE-IIIb), H.E.S.S. site, Namibia (ROTSE-IIIc) and TUBITAK National Observatory, Turkey [ROTSE-IIId; [Akerlof et al. 2003](#); [Yuan 2010](#)].

---

light curve thus produced was found to be 0.15 mag off from the Cousins  $R$  band light curve produced by multi-band observation carried out at ARIES (described below) and the ROTSE magnitudes were scaled accordingly.

The SN 2008in was also monitored with the Ultraviolet Optical Telescope (UVOT) on board *Swift* from +5d to +60d. The UVOT filters  $uvw2$ ,  $uvm2$ ,  $uvw1$ ,  $u$ ,  $b$ , and  $v$  have their effective wavelength at 2030, 2231, 2634, 3501, 4329, and 5402 Å, respectively (Poole et al. 2008). For the present work archival UVOT data was used. The UVOT data reduction was performed following the prescriptions of Brown [2009]. A 5'' aperture is used to measure the counts for the coincidence loss correction whereas a 3'' aperture was used for the photometry. For the filters  $uvw2$ ,  $uvm2$ , and  $uvw1$ , the last epoch (obtained about 60 days after explosion when the UV flux was very weak) data were used to subtract the galaxy light, while in the optical the SN remains much brighter than the underlying light so contamination was negligible. An aperture correction (based on an average PSF in *Swift* CALDB) as well as zero-points from Poole et al. [2008] was applied to put the magnitudes on the UVOT photometric system. The UVOT magnitudes are listed in Table 4.1.

From +5d to +416d, the follow-up of SN 2008in in optical broadband Johnson  $UBV$  and Cousins  $RI$  was performed with the 1-m Sampurnanand Telescope (ST) at ARIES, Nainital. The observation procedure is as mentioned in §2.2. An identification chart showing the field of the galaxy M61 along with the locations of SN 2008in as well as the local standards is presented in Figure 5.1. The photometry is performed using standard tasks of IRAF and *DAOPHOT* as described in §2.3. As the SN lies in the outskirts of the galaxy on a relatively faint and smooth background, the photometry at the initial phases (mostly during the plateau phase when the SN is bright) is estimated using the profile fitting method. During nebular phases,

## 4. THE SUBLUMINOUS TYPE IIP SN 2008IN

---

when the SN becomes faint, the true SN flux is estimated using the galaxy template subtraction method was applied to get the true SN flux. As a galaxy template, we used post-explosion (+600d) images observed on 2011 January 04 under good seeing conditions. Figure 4.2 shows the effect of template subtraction and demonstrates its importance, even to remove very faint background impression. The field of SN 2008in was calibrated using Landolt [2009] standard stars of the field SA98 observed on the same night as the SN. A sample of 10 bright and isolated non-variable stars in the field of SN 2008in was used as local standards to derive the zero points for the SN at each epoch. The location and magnitudes of these local standards are listed in Table 4.2. The entire time span of photometric observation is about 410 days and in Table 4.3, we report the *UBVRI* photometry of the event.

From +4d to +116d, the SN 2008in was also observed in *JHK* near-infrared (NIR) bands with the 0.6-m REM/REMIR at La Silla [Zerbi et al., 2004]. The object was clearly visible in the *J* and *H* passbands, while it remained undetected in *K*. The instrumental magnitudes were standardized using the 2MASS standards available in the field of SN 2008in. The calibrated *JH* magnitudes are listed in Table 4.4.

### 4.2.2 X-ray Observations

The archival data of *Swift*/XRT observations were used for this work. The extraction process is explained in Roy et al. [2011a]. No X-ray source is detected in the merged 27.1 ks XRT data obtained in photon-counting mode. The  $3\sigma$  upper limit to the XRT net count rate is  $7.2 \times 10^{-4}$  cts s $^{-1}$ , corresponding to an unabsorbed (0.2–10 keV band) X-ray flux of  $f_{0.2-10} < 3.4 \times 10^{-14}$  erg cm $^{-2}$  s $^{-1}$  and a luminosity

Table 4.1. The *swift*/UVOT photometric observations of SN 2008in.

UT Date (yy/mm/dd)	JD 2454000+	Phase <sup>a</sup> (day)	<i>uvw2</i> (mag)	<i>uvm2</i> (mag)	<i>uvw1</i> (mag)	<i>u</i> (mag)	<i>b</i> (mag)	<i>v</i> (mag)
2008/12/30.08	830.58	5.00	14.97±0.05	14.65±0.04	14.45±0.05	14.12±0.04	15.24±0.04	15.20±0.04
2008/12/30.60	831.11	5.53	15.13±0.05	14.85±0.04	14.54±0.04	14.16±0.04	15.20±0.04	15.13±0.05
2008/12/31.96	832.46	6.88	15.53±0.05	15.28±0.09	14.84±0.05	14.32±0.04	15.25±0.04	15.15±0.06
2009/01/01.83	833.30	7.72	15.72±0.05	15.47±0.05	15.01±0.05	14.34±0.04	15.30±0.04	15.17±0.04
2009/01/03.54	835.05	9.47	16.23±0.05	16.07±0.05	15.51±0.05	14.52±0.04	15.35±0.04	15.25±0.04
2009/01/07.79	839.29	13.71	17.87±0.08	17.88±0.11	16.96±0.07	15.15±0.04	15.49±0.04	15.25±0.05
2009/01/11.15	842.64	17.06	18.81±0.11	18.66±0.14	17.80±0.09	15.74±0.04	15.62±0.04	15.27±0.04
2009/01/19.79	851.30	25.72	—	—	18.67±0.16	16.67±0.05	16.00±0.04	15.36±0.05
2009/01/22.00	884.53	58.95	—	—	—	17.92±0.07	16.77±0.05	15.69±0.04
2009/01/22.73	885.23	59.65	—	—	—	18.02±0.09	16.75±0.05	15.68±0.05

<sup>a</sup>With reference to the explosion epoch JD 2454825.6

of  $L_{0.2-10} < 7.0 \times 10^{38} \text{ erg s}^{-1}$  for an adopted thermal plasma spectrum with a temperature of  $kT = 10 \text{ keV}$  [see Fransson et al. 1996 and references therein], a Galactic foreground column density of  $N_{\text{H}} = 1.67 \times 10^{20} \text{ cm}^{-2}$  [Dickey and Lockman, 1990] and a distance of 13.19 Mpc (§4.5).

### 4.2.3 Optical Spectroscopic Observation

Long-slit low-resolution spectra ( $\sim 6$  to  $14 \text{ \AA}$ ) in the optical range ( $0.33 - 1.0 \mu\text{m}$ ) were collected at eleven phases from +7d to +143d, including five phases from the 2-m IGO, three phases from the 9.2-m HET, two phases from the 6-m BTA and one epoch from the 3.6-m NTT. A journal of spectroscopic observations is given in Table 5.7. The spectroscopic data acquired from IGO, NTT and HET were reduced under the IRAF environment as demonstrated in §2.4. All the data obtained from the BTA were reduced using programs in the IDL software environment. The instrumental FWHM resolution of 2-m IGO spectra as measured from the [O I]  $\lambda 5777$  emission skyline was found to lie between 6 and  $10 \text{ \AA}$  ( $\sim 322 - 510 \text{ km s}^{-1}$ ). Flux calibration was done using standard spectrophotometric fluxes from Hamuy et al.

#### 4. THE SUBLUMINOUS TYPE IIP SN 2008IN

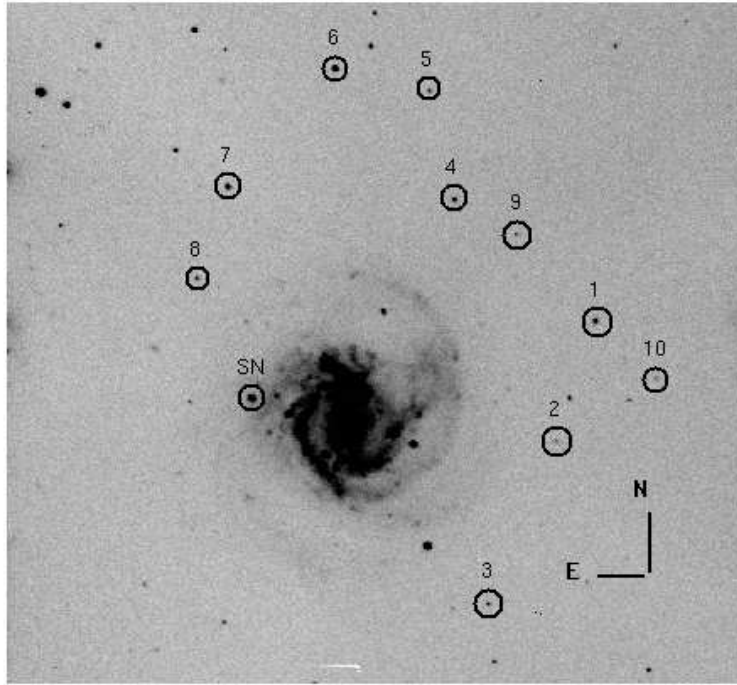


Figure 4.1 SN 2008in in M 61. A 600 s  $V$ -band image taken at phase +32d from the 1-m ST ARIES, India and covering an area of about  $10' \times 10'$  is shown. The location of SN 2008in as well as the local standard stars are marked with circles. North is up and east is to the left.

Table 4.2. The photometric magnitudes of secondary standard stars in the field of SN 2008in.

Star ID	$\alpha_{J2000}$ (h m s)	$\delta_{J2000}$ ( $^{\circ} ' ''$ )	$U$ (mag)	$B$ (mag)	$V$ (mag)	$R$ (mag)	$I$ (mag)
1	12 21 38	04 30 26	$16.99 \pm 0.03$	$17.69 \pm 0.03$	$17.33 \pm 0.05$	$16.96 \pm 0.06$	$16.59 \pm 0.05$
2	12 21 40	04 28 18	—	$19.49 \pm 0.05$	$18.38 \pm 0.04$	$17.85 \pm 0.01$	$17.40 \pm 0.02$
3	12 21 44	04 25 24	$17.91 \pm 0.04$	$18.09 \pm 0.02$	$17.65 \pm 0.01$	$17.30 \pm 0.02$	$16.94 \pm 0.01$
4	12 21 48	04 32 27	$18.38 \pm 0.11$	$17.61 \pm 0.01$	$16.02 \pm 0.01$	$15.10 \pm 0.01$	$14.34 \pm 0.01$
5	12 21 50	04 34 20	$19.10 \pm 0.21$	$18.45 \pm 0.04$	$17.25 \pm 0.01$	$16.55 \pm 0.01$	$15.99 \pm 0.01$
6	12 21 57	04 34 38	$16.06 \pm 0.01$	$15.72 \pm 0.00$	$14.88 \pm 0.00$	$14.36 \pm 0.01$	$13.94 \pm 0.00$
7	12 22 04	04 32 30	$16.66 \pm 0.02$	$16.30 \pm 0.00$	$15.48 \pm 0.01$	$15.00 \pm 0.01$	$14.61 \pm 0.01$
8	12 22 05	04 30 51	$18.05 \pm 0.06$	$18.17 \pm 0.01$	$17.60 \pm 0.04$	$17.25 \pm 0.03$	$16.93 \pm 0.01$
9	12 21 43	04 31 54	$19.56 \pm 0.41$	$19.20 \pm 0.05$	$17.55 \pm 0.01$	$16.53 \pm 0.01$	$15.51 \pm 0.01$
10	12 21 33	04 29 29	$19.11 \pm 0.43$	$18.96 \pm 0.02$	$18.55 \pm 0.02$	$18.21 \pm 0.05$	$17.89 \pm 0.02$

Note. — Errors in magnitude represent RMS scatter of the night-to-night repeatability over entire period of SN monitoring.

Table 4.3. The *UBVRI* photometry of SN 2008in.

UT Date (yy/mm/dd)	JD 2454000+	Phase <sup>a</sup> (day)	<i>U</i> (mag)	<i>B</i> (mag)	<i>V</i> (mag)	<i>R</i> (mag)	<i>I</i> (mag)	Seeing <sup>c</sup> ( $''$ )
2008/12/30.00	830.50	+5	14.23±0.01	15.33±0.01	15.07±0.01	14.86±0.01	14.86±0.01	2.9
2009/01/01.98	833.48	+8	14.39±0.01	15.54±0.01	15.17±0.01	14.65±0.01	14.98±0.01	1.3
2009/01/09.02	840.52	+15	15.47±0.02	15.76±0.02	15.21±0.02	14.89±0.02	14.87±0.03	2.5
2009/01/23.95	855.45	+30	16.85±0.04	16.36±0.01	15.38±0.02	15.00±0.01	14.85±0.01	2.1
2009/01/26.02	857.52	+32	16.90±0.04	16.41±0.02	15.39±0.01	14.98±0.01	14.85±0.02	3.1
2009/01/27.01	858.33	+33	16.81±0.02	16.41±0.01	15.39±0.01	15.00±0.01	14.83±0.01	2.8
2009/01/28.83	860.33	+35	16.83±0.03	16.48±0.01	15.43±0.01	15.04±0.01	14.89±0.01	2.2
2009/01/30.88	862.38	+37	17.16±0.04	16.53±0.01	15.43±0.01	15.02±0.01	14.85±0.01	2.4
2009/02/02.89	864.39	+39	17.11±0.04	16.53±0.01	15.42±0.01	14.99±0.01	14.78±0.01	2.0
2009/02/15.82	878.32	+53	17.58±0.05	16.87±0.01	15.43±0.02	14.76±0.01	14.82±0.01	2.8
2009/02/16.96	879.46	+54	17.74±0.06	16.84±0.01	15.54±0.01	15.09±0.02	14.83±0.01	3.1
2009/02/17.79	880.29	+55	17.79±0.05	16.87±0.01	15.55±0.01	15.10±0.02	14.85±0.01	3.1
2009/02/20.87	883.37	+58	17.92±0.07	16.94±0.01	15.59±0.02	15.09±0.01	14.84±0.01	3.1
2009/02/23.77	886.27	+61	18.05±0.04	17.08±0.01	—	15.13±0.01	14.89±0.01	3.1
2009/02/25.81	888.31	+63	18.13±0.05	17.05±0.01	15.60±0.01	15.14±0.01	14.92±0.01	2.9
2009/02/26.80	889.30	+64	—	—	15.62±0.01	15.15±0.01	—	3.8
2009/03/02.78	893.28	+68	—	17.08±0.01	15.63±0.01	15.17±0.01	14.90±0.00	4.4
2009/03/04.77	895.27	+70	—	17.15±0.01	15.66±0.01	15.18±0.01	14.94±0.01	2.4
2009/03/09.76	900.27	+75	18.72±0.14	17.31±0.02	15.68±0.01	—	15.08±0.01	2.3
2009/03/15.27	905.77	+80	—	17.20±0.02	—	15.21±0.01	14.92±0.01	2.2
2009/03/24.80	915.30	+90	18.73±0.08	17.42±0.01	15.94±0.01	15.48±0.01	15.15±0.01	2.5
2009/04/03.75	925.25	+100	19.28±0.15	17.66±0.02	16.10±0.01	15.57±0.01	15.31±0.01	2.2
2009/04/05.61	927.22	+102	—	—	—	15.67±0.01	15.41±0.01	2.5
2009/04/10.67	932.33	+107	—	18.38±0.06	16.76±0.01	16.20±0.01	15.84±0.02	2.7
2009/04/17.60	939.25	+114	—	19.83±0.06	17.91±0.01	17.13±0.01	16.68±0.01	2.8
2009/04/22.68	944.11	+118	—	20.30±0.16	18.10±0.03	17.21±0.03	16.85±0.04	3.5
2009/04/28.71	950.17	+125	—	20.40±0.09	—	17.24±0.01	16.74±0.01	2.2
2009/05/01.72	953.10	+127	—	20.22±0.11	18.06±0.04	17.27±0.04	16.70±0.04	2.7
2009/05/23.69	975.18	+150	—	—	18.30±0.04	17.47±0.02	17.00±0.03	2.7
2009/05/25.70	977.21	+152	—	20.21±0.12	18.35±0.02	17.45±0.01	—	2.6
2009/05/26.71	978.22	+153	—	20.15±0.17	18.33±0.04	17.49±0.02	17.06±0.03	2.8
2009/06/14.69	997.19	+172	—	—	18.39±0.04	—	—	2.9
2010/01/17.98	1214.49	+389	—	—	—	19.69±0.07	19.27±0.13	1.9
2010/01/19.91	1216.42	+391	—	21.47±0.12	20.34±0.05	19.76±0.05	19.52±0.07	2.3
2010/02/13.91	1241.42	+416	—	—	20.57±0.07	19.77±0.06	—	2.2

<sup>a</sup>With reference to the explosion epoch JD 2454825.6.

<sup>c</sup>FWHM of the stellar PSF at *V* band. The nights for which we do not have any observation in *V* band, PSF is found through interpolation.

Note. — The photometric observations are taken with the 1-m Sampurnanand Telescope, ARIES, Nainital. Errors in magnitude denote  $1\sigma$  uncertainty.

#### 4. THE SUBLUMINOUS TYPE IIP SN 2008IN

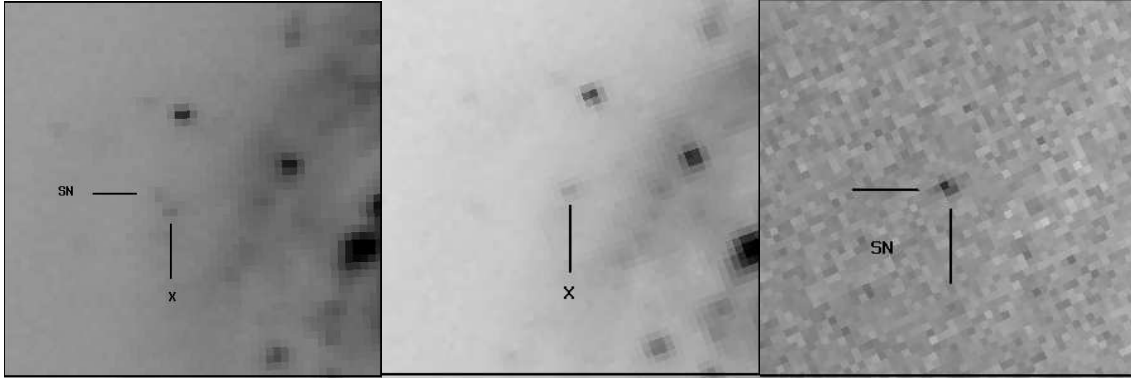


Figure 4.2 Measurement procedure of the true SN flux in the nebular phase. Each image shows  $76'' \times 76''$  around SN location. North is up and east is to the left. The leftmost panel shows  $V$ -band image observed on 2010 January 20 with a SN in it. The middle panel shows the template image taken on 2011 January 04, with no SN in it. A small flux enhancement marked with a cross ( $\times$ ) symbol is probably due to a star forming region. This is also present in the pre-SN SDSS image. The rightmost panel shows the subtracted image, where only SN is present.

Table 4.4. The REM near-infrared observation of SN 2008in.

UT Date (yy/mm/dd)	JD 2454000+	Phase <sup>a</sup> (day)	$J$ (mag)	$H$ (mag)
2008/12/29.85	830.36	4.78	$14.66 \pm 0.054$	$14.55 \pm 0.064$
2009/01/03.87	835.37	9.78	$14.60 \pm 0.077$	$14.38 \pm 0.058$
2009/01/09.73	841.23	15.65	$14.39 \pm 0.059$	$14.16 \pm 0.072$
2009/01/14.73	846.23	20.65	$14.47 \pm 0.107$	$14.32 \pm 0.150$
2009/01/19.78	851.24	25.66	$14.54 \pm 0.150$	—
2009/01/24.76	856.26	30.67	$14.25 \pm 0.077$	$14.11 \pm 0.087$
2009/01/29.87	861.37	35.79	$14.37 \pm 0.050$	$14.14 \pm 0.065$
2009/02/05.66	868.16	42.58	$14.43 \pm 0.067$	$14.24 \pm 0.107$
2009/02/11.69	874.19	48.61	$14.20 \pm 0.107$	$14.59 \pm 0.241$
2009/02/16.72	879.22	53.64	$14.43 \pm 0.050$	$14.35 \pm 0.097$
2009/02/21.75	884.25	58.67	—	$14.18 \pm 0.063$
2009/02/27.75	890.25	64.67	—	$14.44 \pm 0.077$
2009/03/04.89	895.40	69.82	$14.40 \pm 0.074$	$14.12 \pm 0.085$
2009/03/10.74	901.24	75.66	—	$14.36 \pm 0.190$
2009/03/21.71	912.21	86.63	—	$14.50 \pm 0.090$
2009/03/26.73	917.23	91.65	—	$14.41 \pm 0.073$
2009/04/05.79	927.29	101.71	—	$15.00 \pm 0.147$
2009/04/10.80	932.30	106.71	—	$14.94 \pm 0.171$
2009/04/15.80	937.30	111.72	—	$14.86 \pm 0.173$
2009/04/20.52	942.02	116.44	—	$15.23 \pm 0.232$

<sup>a</sup>With reference to the explosion epoch JD 2454825.6.

Table 4.5. Journal of spectroscopic observations of SN 2008in.

UT Date (yy/mm/dd/hh.hh)	JD 2454000+	Phase <sup>a</sup> (days)	Range $\mu\text{m}$	Telescope <sup>b</sup>	Grating (gr mm <sup>-1</sup> )	Slit width ( $''$ )	Dispersion ( $\text{\AA pix}^{-1}$ )	Exposure (s)	S/N <sup>c</sup> (pix <sup>-1</sup> )
2008/12/31/22.80	832.45	+7	0.45–1.00	HET	300	1.0	5.0	600	45
2009/01/07/22.31	839.43	+14	0.45–1.00	HET	300	1.0	5.0	600	43
2009/02/17/19.74	880.32	+54	0.38–0.68	IGO	600	1.5	1.4	1800	34
2009/02/22/22.50	885.44	+60	0.45–1.00	HET	300	1.0	5.0	600	35
2009/03/22/20.45	913.35	+87	0.38–0.68	IGO	600	1.5	1.4	1800	38
2009/03/25/22.13	916.42	+90	0.38–0.68	IGO	600	1.5	1.4	2700	35
2009/04/03/19.14	925.26	+99	0.38–0.68	IGO	600	1.5	1.4	1800	35
2009/04/03/20.98	925.33	+99	0.60–1.00	BTA	550	2.1	3.5	3×900	60
2009/04/22/15.49	944.14	+118	0.38–0.68	IGO	600	1.5	1.4	1800	11
2009/04/23/18.00	945.25	+119	0.38–0.79	BTA	600	2.1	3.5	3×900	65
2009/05/17/02.38	968.10	+143	0.33–0.80	NTT	300	1.0	4.0	2700	59

<sup>a</sup>With reference to the explosion epoch JD 2454825.6.

<sup>b</sup>HET : LRS on 9.2-m Hobby Eberly Telescope; IGO : IFOSC on 2-m IUCAA Girawali Observatory, India; BTA : SCORPIO on 6-m Big Telescope Alt-azimuth, Special Astrophysical Observatory, Russia; NTT : EFOSC2 on 3.6-m New Technology Telescope, ESO, Chile.

<sup>c</sup>At 0.6  $\mu\text{m}$ .

[1994], assuming a mean extinction for the site. For HET, BTA and NTT, the resolution near 6000 $\text{\AA}$  is about 10 $\text{\AA}$ , 14 $\text{\AA}$ , and 12 $\text{\AA}$  respectively.

## 4.3 Light Curve Evolution

According to theoretical interpretation, the entire broadband evolution of Type II SNe can be segmented into three phases: the rising phase, the plateau phase and the nebular phase.

### 4.3.1 The Rising Phase

The rising phase of the light curve is associated with the shock breakout phenomenon having been theoretically predicted for an SN explosion, in which, the radiation-dominated shock wave, generated through the reversal of iron core-collapse, starts to propagate outward through the onion shell-like layers of the progenitor; when

#### 4. THE SUBLUMINOUS TYPE IIP SN 2008IN

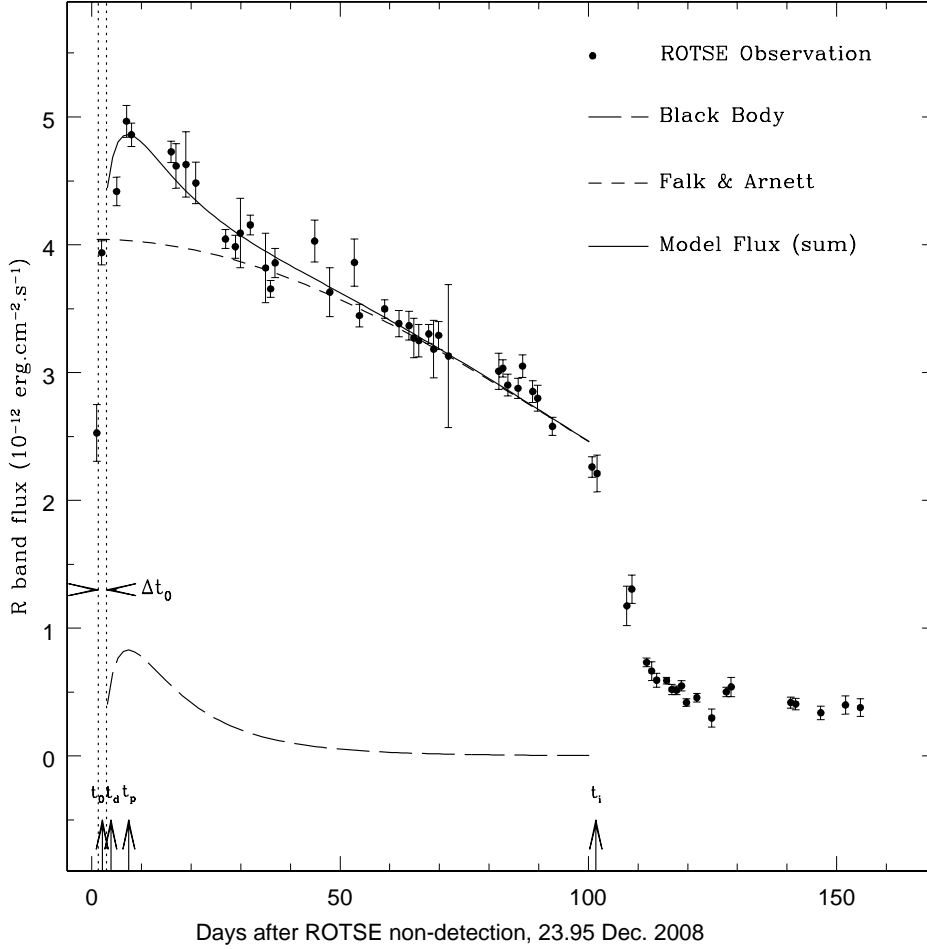


Figure 4.3 The ROTSE  $R$ -band light curve of SN 2008in. Reference time for x-axis is the epoch of ROTSE non detection on 2008 December 23.95. The evolution of post shock breakout flux has been modeled by using the simple analytical expressions given in Cowen et al. [2010] and Arnett [1980]. The best fit time for shock breakout is marked with  $t_0$  while the  $\Delta t_0$  shows the duration of uncertainty. The  $t_d$  is the time of discovery reported by Nakano et al. 2008. The  $t_p$  is the time when  $R$  light shows the peak. The  $t_i$  is the time of inflection obtained using the procedure of Elmhamdi et al. [2003a].

---

the shock reaches regions with an optical depth of a few tens to unity, the radiation behind the shock escapes the outer surface giving rise to a hot ( $T > 10^5$  K) fireball which emits quasi-black body radiation in UV and soft-Xrays. This phenomenon is called shock breakout and depending on envelope mass, density structure and wind properties of the progenitor, the breakout light curve may last from a few hours to few a days [Chevalier 1976; Falk and Arnett 1977; Grassberg et al. 1971]. Due to the short timescale, the detection of shock breakout is rare, and only recently were, the UV light curves of the entire shock breakout phase lasting several hours was reported for two Type IIP SNe – SNLS-04D2dc and SNLS-06D1jd [Gezari et al. 2008; Schawinski et al. 2008]. Observation of the earliest UV and optical light curves of IIP SNe is crucial to model the shock breakout light curves and constrain the properties of SN progenitors [Tominaga et al., 2009]. The earliest SNe IIP optical light curves have been studied in the past for SN 2005cs by Pastorello et al. [2009] and for SN 2006bp by Quimby et al. [2007b] and the optical rising phase is rarely observed.

We model the early optical (ROTSE-IIIb *R*-band) light curves of SN 2008in using a simple model and put an observational constraint on the epoch and duration of shock breakout. Following the formulation of Waxman et al. [2007], it can be shown that just after the shock breakout, the intensity of the SN light at a fixed wavelength is proportional to the intensity of blackbody radiation at that wavelength [see Equation 1 of Cowen et al. 2010], while for the plateau phase Arnett [1980] derived an analytical expression (Equation 39 of that paper) and hence by combining these two equations one can approximate the overall intensity profile of a Type II SN during the rising phase through the plateau with the following expression :

#### 4. THE SUBLUMINOUS TYPE IIP SN 2008IN

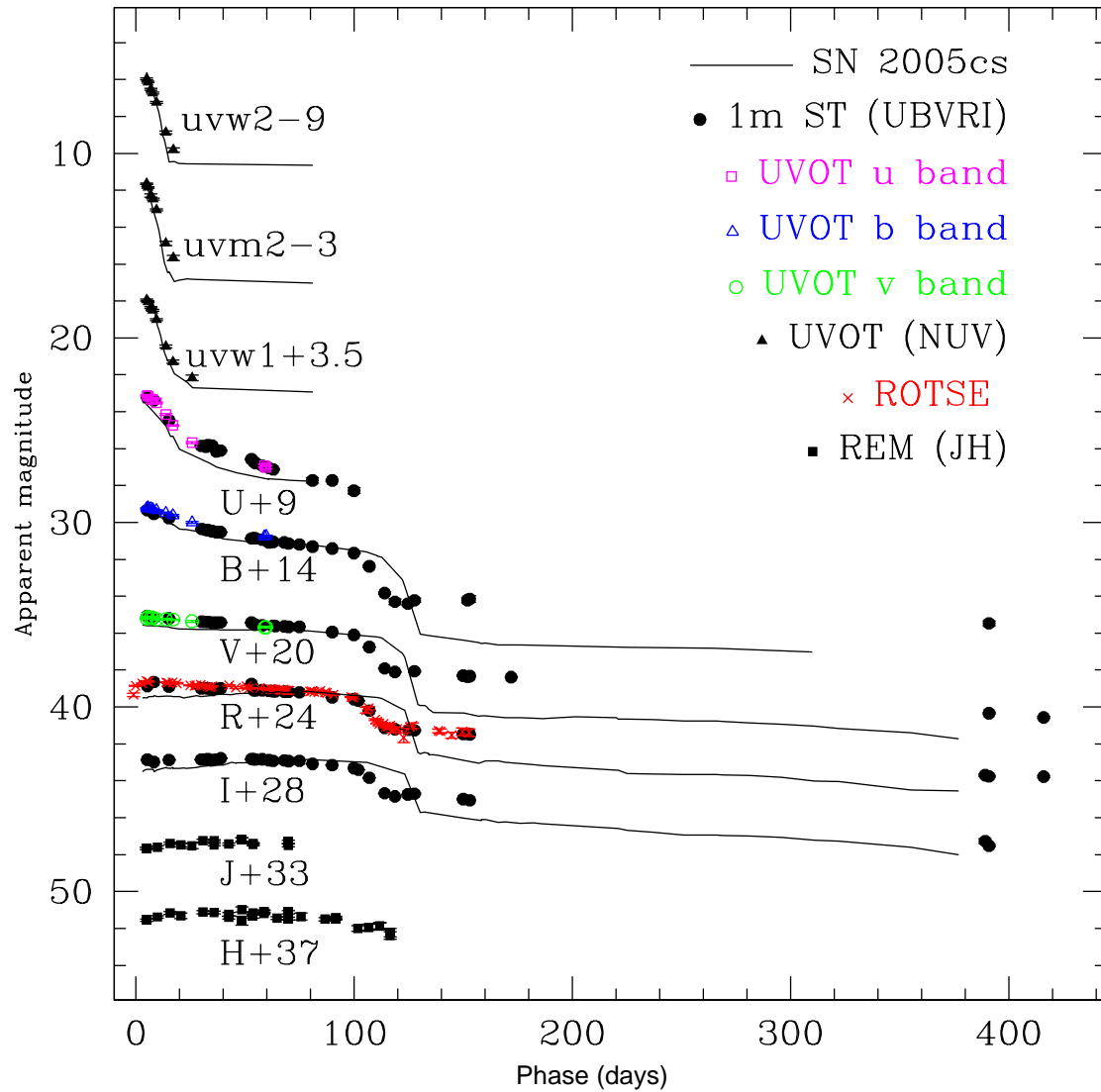


Figure 4.4 Light curves of SN 2008in in the UV, optical and NIR bands. The light curves of archetypal low-luminosity SN 2005cs are overplotted for comparison [data are taken from [Brown et al., 2009](#); [Pastorello et al., 2009](#)]. The light curves of SN 2005cs are scaled in magnitude to match the light curves of SN 2008in.

---


$$I_{SN}(t) = \frac{A}{\exp[B \times (t-t_0)^{0.5}] - 1} \times (t - t_0)^{1.6} + C \times \exp[-\{(t/D) + (t/E)^2\}] \quad (4.1)$$

Here, the first term represents the phase associated with the shock breakout while the second term represents the plateau phase. Here ‘ $t$ ’ is the time measured in days since 2008 December 23.95 (JD = 2454823.5), the epoch when ROTSE had a non-detection of the SN with limiting magnitude 16.16 in the  $R$  band. The time of shock breakout, ‘ $t_0$ ’ along with the constants  $A, B, C, D$  and  $E$  are free parameters of the fit. The values of these constants depend on the nature of the progenitor and the kind of explosion. The above model is fitted to the ROTSE data using the  $\chi$  minimization technique [Press et al., 1992] and the fit is shown in Figure 4.3. We obtained a value of the shock breakout time as  $t_0 = 2.13 \pm 0.83$  day. This value of  $t_0$  is consistent with the first data point observed from ROTSE. We shall adopt  $t_0$ , corresponding to JD = 2454825.6 as the explosion epoch for all the phases of SN 2008in. It is noted that at  $V$  and  $R$  bands, the SN was detected by Nakano et al. [2008c], just 2.4 d after the shock breakout. We note, however, that depending on the extent of the envelope the true core reversal marking the SN explosion would have occurred a few hours earlier (e.g., SN 1987A) or a few days earlier for a red supergiant envelope  $\sim 50000R_{\odot}$  [Quimby et al., 2007b].

In Figure 4.3, ‘ $t_p$ ’ (+5.3 d) corresponds to the peak of the ROTSE  $R$ -band light curve. A similar peak in the UV light curves of the post-shock breakout phase of the Type IIP supernova SNLS-04D2dc lasting several days was identified as a secondary peak and this peak was explained as the shift of the spectral energy distribution toward longer wavelengths due to the rapid fall in temperature during free adiabatic

## 4. THE SUBLUMINOUS TYPE IIP SN 2008IN

---

expansion of optically thick plasma lead by a collisionless shock [Schawinski et al. 2008; Tominaga et al. 2009]. For SN 2008in we identify the peak in the ROTSE *R*-band curve as a secondary peak and also speculate that for a few other type IIP SNe such as 1999em, 1999gi and 2005cs, where very tiny peaks before the plateau light curve were observed, such features are basically the footprints of the secondary peaks which could be a consequence of shock breakout.

### 4.3.2 The Plateau and Nebular Phase

The entire UV, optical and NIR light curves of SN 2008in are shown in Figure 4.4 and for comparison, the light curves of the archetypal low-luminosity SN 2005cs [Brown et al., 2009; Pastorello et al., 2009] are also plotted by scaling them in magnitude to match it with the observed plateau of SN 2008in. In the early plateau phase, a rapid drop in the UV flux and a slowly declining or constant optical and NIR flux are clearly apparent. The *uvm2* magnitude declined from about 14.7 to 18.7 mag within 12 days. The decline rates of the SN 2008in flux in UVOT, *U*, *B*, and *V* bands are almost identical with that of SN 2005cs. Starting from the *uvw2* until the *R* band, the measured decline rates from shock breakout to the plateau phase are approximately 0.32, 0.34, 0.25, 0.13, 0.04, 0.01 and 0.01 mag d<sup>-1</sup>. The *IJH* light curves are almost flat even at early phases of the plateau. For this SN, the plateau is well sampled in the *BVRI* bands, so we can accurately determine the plateau duration. As discussed in §4.3.1, the secondary peak ( $t_p \sim +5.3$  d) in the prompt light curve is generated by the gradually cooling shock heated SN atmosphere and after that the plateau mechanism starts to dominate. On the other hand, between the plateau and the nebular phase there is another transitional state,

---

when an inflection in the light curve can be seen (§4.7.1). Hence the plateau duration is precisely the time span between the secondary peak and the inflection. The inflection ( $t_i$ ) in the  $V$  band light curve is observed to occur nearly 103.2 days after the shock breakout. Hence the time interval between the  $t_i$  and  $t_p$  is assumed as the duration of the plateau i.e.  $(103.2 - 5.3) \sim 98$  days.

Once the hydrogen envelope is fully recombined and the ejecta becomes optically thin, the light curve enters into the nebular phase and it is sustained mainly by the energy output from the radioactive decays of the iron-group elements. During the plateau to nebular transition phase, the  $V$ -band magnitude drops from  $\sim 16.0$  mag at around +90d (still in the plateau) to 18.1 mag at +122d (in the exponential light curve tail), i.e.  $\sim 2$  mag in about one month. This drop is remarkably smaller than that of SN 2005cs, but consistent with the 2-3 mag drop observed in normal Type IIP SNe [Olivares E. et al., 2010]. A linear fit to the tail from +120d to +400d gives the following decline rates [in mag  $(100\text{d})^{-1}$ ]:  $\gamma_B \sim 0.44$ ,  $\gamma_V \sim 0.84$ ,  $\gamma_R \sim 0.91$ ,  $\gamma_I \sim 1.03$  at  $B, V, R$ , and  $I$  bands which are similar to the values found in normal IIP SNe and comparable with the decay slope of  $^{56}\text{Co}$  to  $^{56}\text{Fe}$ , i.e.  $0.98$  mag  $(100\text{d})^{-1}$ .

## 4.4 Spectroscopic Evolution

The spectra of SN 2008in at 10 phases from +7d to +143d are shown in Figure 4.5. The spectra are corrected for the recessional velocity of the host galaxy ( $\sim 1567 \pm 3$  km s $^{-1}$ )<sup>1</sup>. Spectral features are mainly identified as per previously published line identifications for IIP SNe [Leonard et al., 2002a; Pastorello et al., 2004]. The two earliest spectra (+7d and +14d) show the blue continuum of blackbody emission

---

<sup>1</sup><http://leda.univ-lyon1.fr/>

#### 4. THE SUBLUMINOUS TYPE IIP SN 2008IN

---

and have broad P-Cygni profiles of  $H\alpha$ ,  $H\beta$  and  $He\text{I } \lambda 5876$ . The next two spectra (+54d and +60d) represent the mid-plateau phase and are marked by a decrease in the continuum and the appearance of more number of P-Cygni profiles for the permitted metallic ( $Fe\text{II}$ ,  $Sc\text{II}$ ,  $Ti\text{II}$ ,  $Ba\text{II}$ ,  $Mg\text{II}$ ),  $O\text{I } \lambda 7773$ ,  $Na\text{I D}$ , and  $Ca\text{II IR triplet}$  lines similar to other normal Type IIP SNe [see Chapter 3 and references therein]. The spectra at phases +87d, +90d and +99d represent the end stages of the plateau and these are marked by a redder continuum and decreasing line widths of hydrogen lines. The +118d, +119d and +143d spectra represent the nebular phase having negligible continuum and are marked by pronounced emissions of forbidden lines [ $Ca\text{II } \lambda\lambda 7291, 7323$ , and fading of the absorption features of hydrogen and metallic lines.

In Figure 4.6, we compare the +99d spectrum of SN 2008in with the spectra of other Type IIP SNe observed at similar phases that is at roughly the time when the light curve changes from the photospheric plateau to the nebular phase. The phases quoted for each event are with reference to the moment of inflection ( $t_i$ ; see Figure 4.3). The narrow P-Cygni  $H\alpha$  profile and the presence of strong lines of  $Ba\text{II}$  at  $\lambda 6142$  and  $\lambda 6497$  of SN 2008in show striking resemblance to the low-luminosity SNe 1997D, 1999br, 1999eu, 2001dc and 2005cs. On the other hand, the normal Type IIP SNe 2004et, 2008gz show broader profiles of  $H\alpha$  and weaker lines of  $Ba\text{II}$ . It is noted that in the blue wing of  $H\alpha$  more metallic lines get resolved than that in the normal IIP SNe and this arises due to smaller line widths of hydrogen lines seen in low-luminosity IIP SNe [Fraser et al. 2010 and references therein]. In addition, the  $Ba\text{II}$  line in the low-luminosity SNe show stronger absorption components due to lower ejecta temperature than that in the normal luminosity Type IIP SNe 2004et and 2008gz [Turatto et al., 1998]. In Figure 4.7, we have identified the spectral

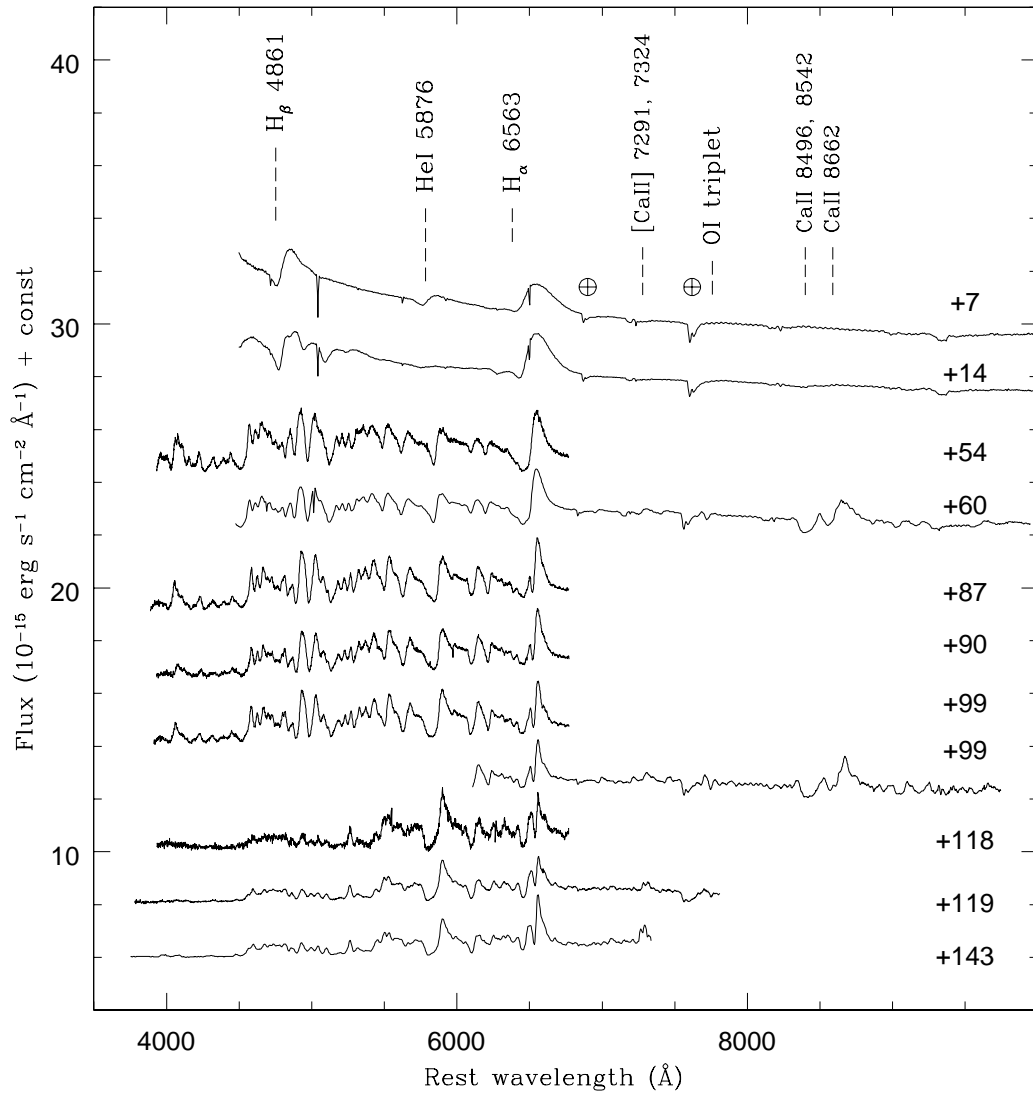


Figure 4.5 Doppler corrected flux spectra of SN 2008in observed during +7 d to +143 d. Prominent lines are marked. Telluric features are marked with  $\oplus$  symbol. The sharp absorption dips seen near 5000 Å and 6500 Å in the +7d and +14d spectra are artifacts. The spectra signify the early photospheric phase (+7d,+14d), mid-plateau phase (+54d, +60d), late-plateau phase (+87d, +90d, and +99d) and nebular phase (+118d, +119d, and +143d).

#### 4. THE SUBLUMINOUS TYPE IIP SN 2008IN

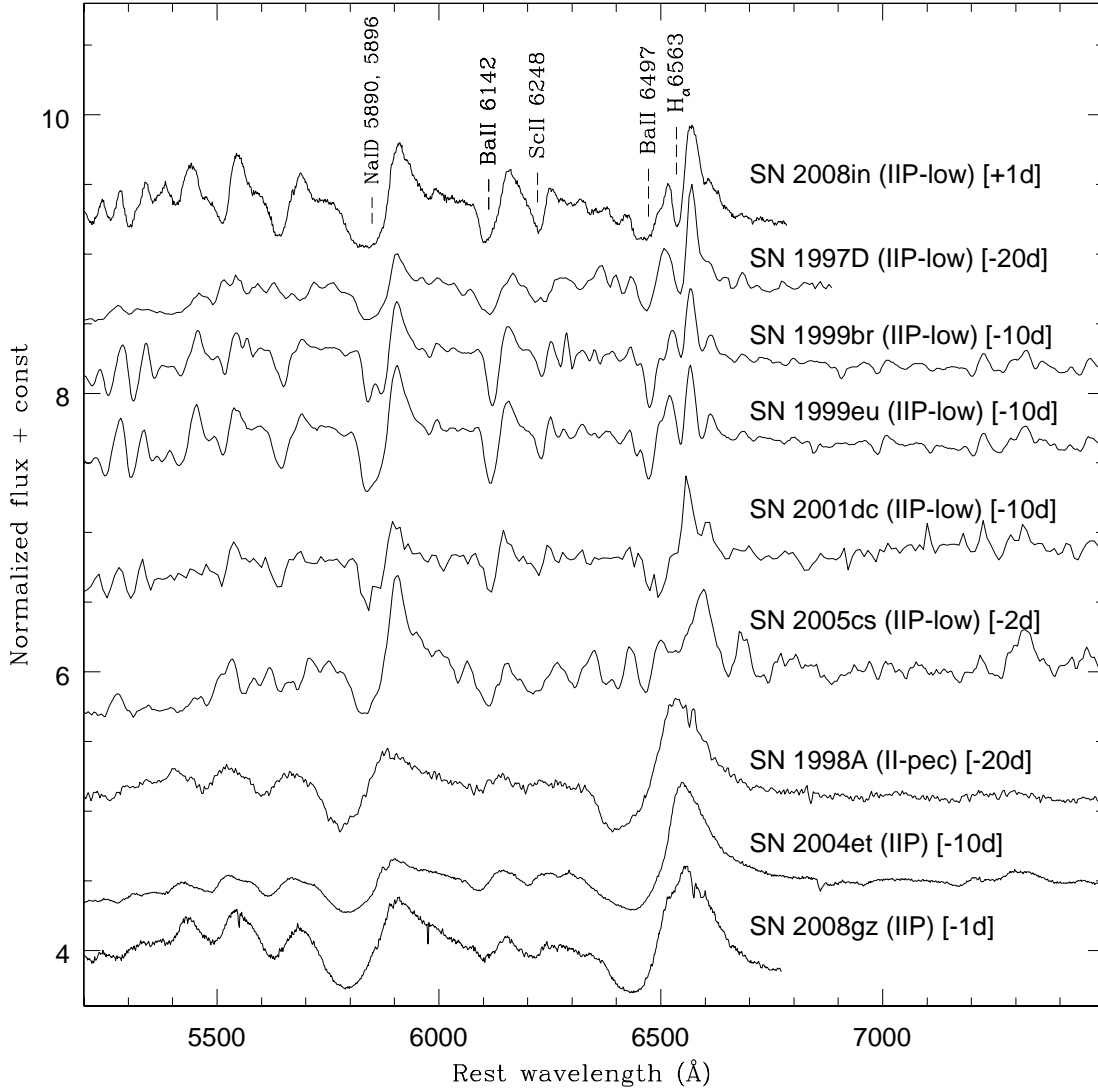


Figure 4.6 The end plateau spectrum (+99d) of SN 2008in, is compared with five low-luminosity SNe 1997D, 1999br, 1999eu, 2001dc, 2005cs (Pastorello et al. 2009 and references therein); two normal SNe 2004et [Misra et al., 2007b], 2008gz [Roy et al., 2011b] and a peculiar Type II SN 1998A [Pastorello et al., 2005], observed at comparable epochs. The phases quoted for each event are with reference to the moment of inflection ( $t_i$ ; see Left panel of Figure 4.12), which marks the highest rate of decline in the  $V$ -band light curve during the end of the plateau and the beginning of nebular phase [Elmhamdi et al., 2003a]. All the spectra have low spectral resolution ( $\sim 10 \text{ \AA}$ ). The P-Cygni features of Na I D, Ba II  $\lambda$  6142, Sc II  $\lambda$  6248, Ba II  $\lambda$  6497 and  $H\alpha$  are marked.

---

features in a late-plateau phase (+99d) spectrum which covers the full wavelength range from 0.4 to 0.95  $\mu\text{m}$ . For line identification we have followed [Pastorello et al. \[2004\]](#), where different spectral lines were identified for the +102d spectrum of a low-luminosity SN 1999br. We are able to identify all the features and the spectral profiles of all the elements are similar to the archetypal low-luminosity IIP SNe 1997D, 2005cs and 1999br [[Pastorello et al. 2004](#) and references therein].

Figure 4.8 shows the spectral evolution of  $\text{H}\alpha$ ,  $\text{H}\beta$ ,  $\text{Na I D}$ ,  $\text{Fe II}$ ,  $\text{Ba II}$ , and  $\text{Sc II}$  lines. In Figure 4.9 (upper panel), we show the expansion velocities of the ejecta derived from Balmer and  $\text{Fe II}$  lines. The later is a good indicator of photospheric velocity. The expansion velocities of the H-envelope are estimated using absorption minima of the P-Cygni profiles and at the two earliest phases (+7d and +14d)  $\text{H}\alpha$  and  $\text{H}\beta$  show a broad P-Cygni profile which, with time, becomes narrower at later phases keeping the position of the emission peak centered near zero velocity. The  $\text{H}\alpha$  line velocity starts at about  $7000 \text{ km s}^{-1}$  at +10d, reaches  $4000 \text{ km s}^{-1}$  at +50d and flattens at a level of  $1200 \text{ km s}^{-1}$  in the nebular phases. It can be seen from the lower panel of Figure 4.9 that in the comparable phases, the  $\text{H}\alpha$  line velocities of low-luminosity SNe are less than half those of normal IIP SNe 1999em and 2004et, whereas the SN 2008in velocities are more like low-luminosity SN 2005cs. To estimate the photospheric velocity of the transient we have computed the velocities of different  $\text{Fe II}$  lines  $\lambda 4924$ ,  $\lambda 5018$ , and  $\lambda 5169$  at different phases. The first marginal detection of these lines is in the +14d spectrum and they became prominent in later stages of evolution. For SN 2008in, the average velocity of these lines (and hence roughly the photospheric velocity) at +14d is about  $4450 \text{ km s}^{-1}$ , which is comparable with that of low luminosity SNe and much less than ordinary Type IIP events [see Figure 12 of [Pastorello et al. 2009](#)].

#### 4. THE SUBLUMINOUS TYPE IIP SN 2008IN

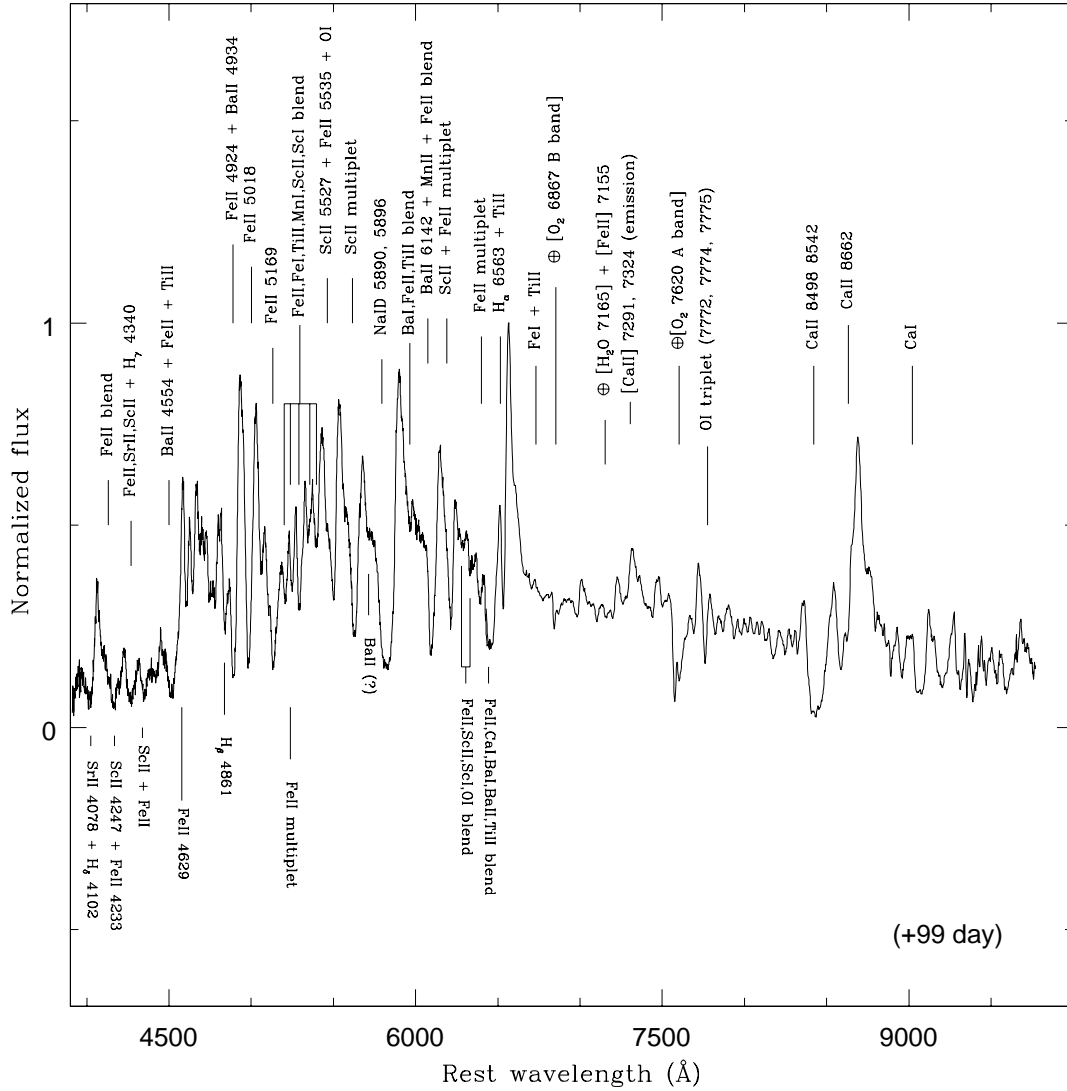


Figure 4.7 The spectral line identifications in a late-plateau phase (+99d) spectra are shown. Spectral features are mainly identified as per previously published line identifications for IIP SNe [Leonard et al., 2002a; Pastorello et al., 2004]. Telluric features are marked with  $\oplus$  symbol.

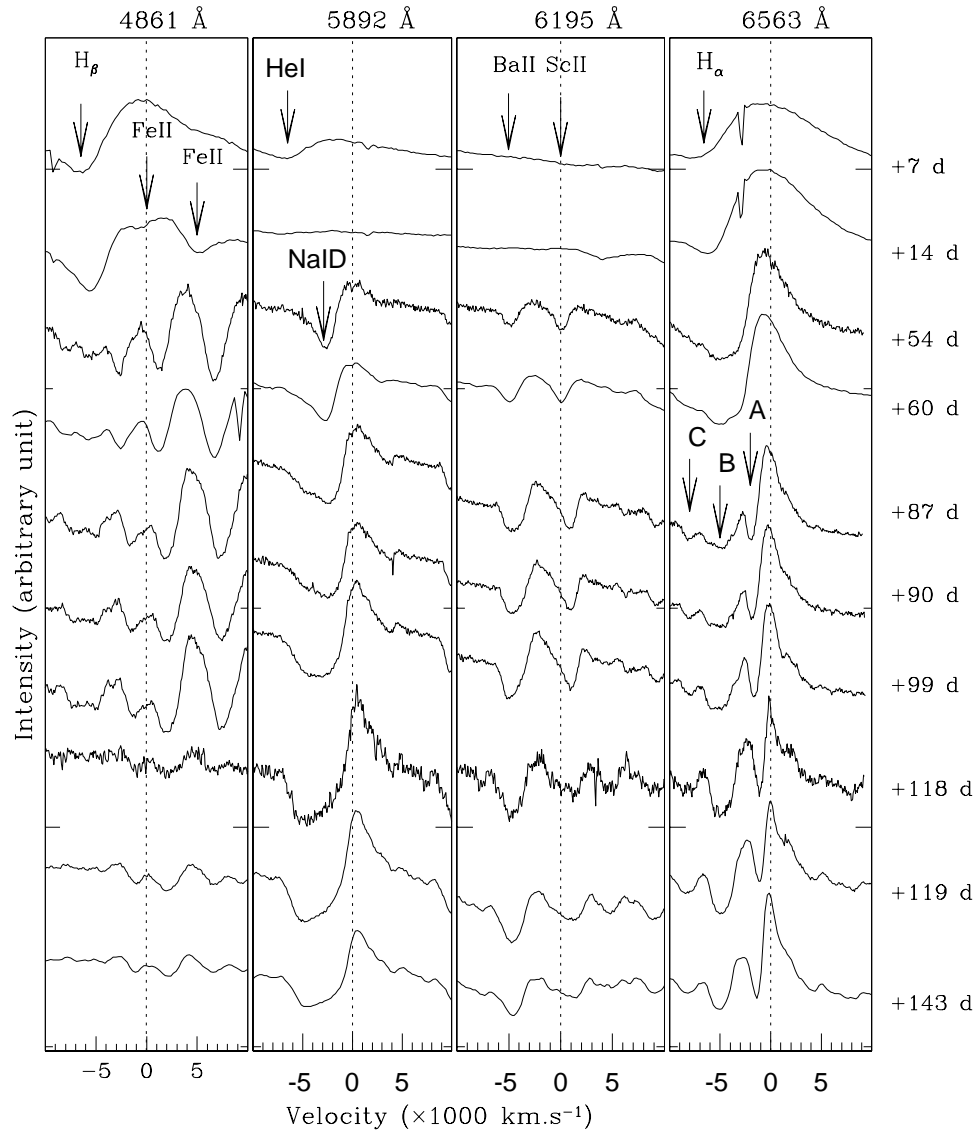


Figure 4.8 Spectral evolution of  $H\beta$ ,  $FeII \lambda 4924$ ,  $FeII \lambda 5018$ ,  $HeI \lambda 5876$ ,  $NaI D \lambda \lambda 5890, 5896$ ,  $BaII \lambda 6148$ ,  $ScII \lambda 6248$ ,  $BaII \lambda 6497$  and  $H\alpha$  lines of SN 2008in during its transition from plateau to nebular phase. The dotted line at zero velocity corresponds to the rest wavelength, marked at the top of each panel. The sharp absorption dips seen in the  $H\alpha$  profile for +7d and +14d spectra are artefacts.

#### 4. THE SUBLUMINOUS TYPE IIP SN 2008IN

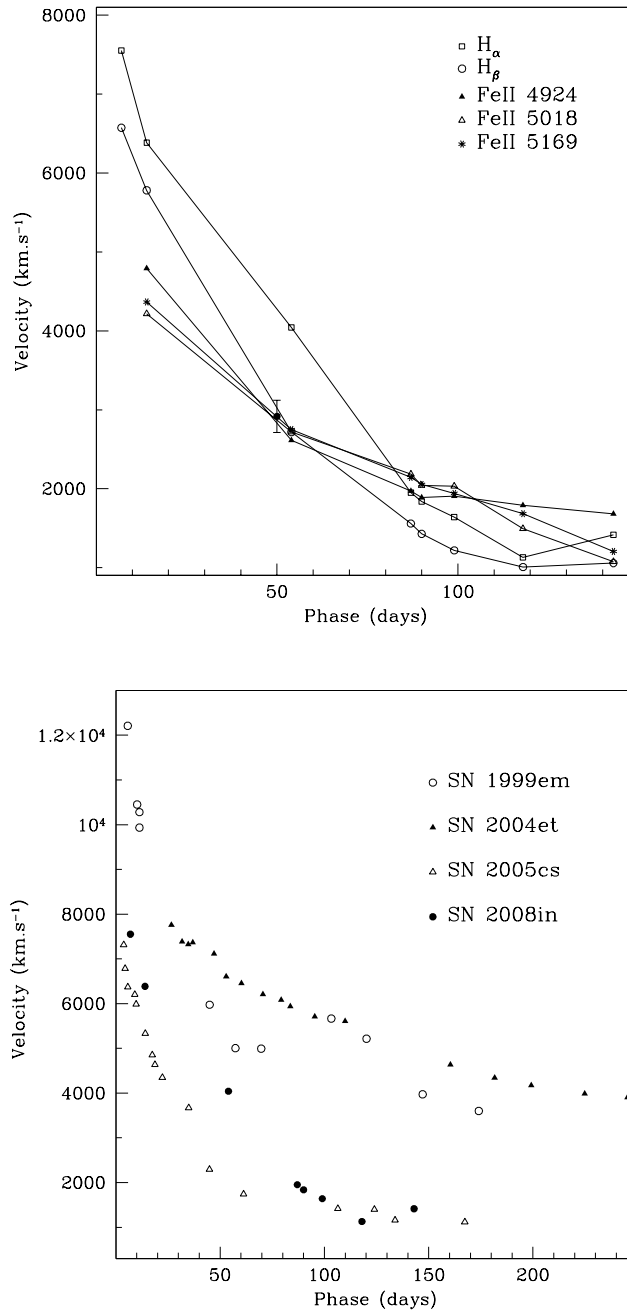


Figure 4.9 Evolution of expansion velocity of SN 2008in. The upper panel shows the velocity of different elements in the ejecta of SN 2008in. The black filled circle shows the estimated value of mid-plateau photospheric velocity, calculated using the relation mentioned in Roy et al. [2011b]. The lower panel shows a comparison of velocity derived from H $\alpha$  with that of low-luminosity event like SN 2005cs [Pastorello et al., 2009] and normal Type IIP SNe 1999em [Elmhamdi et al., 2003b] and 2004et [Sahu et al., 2006].

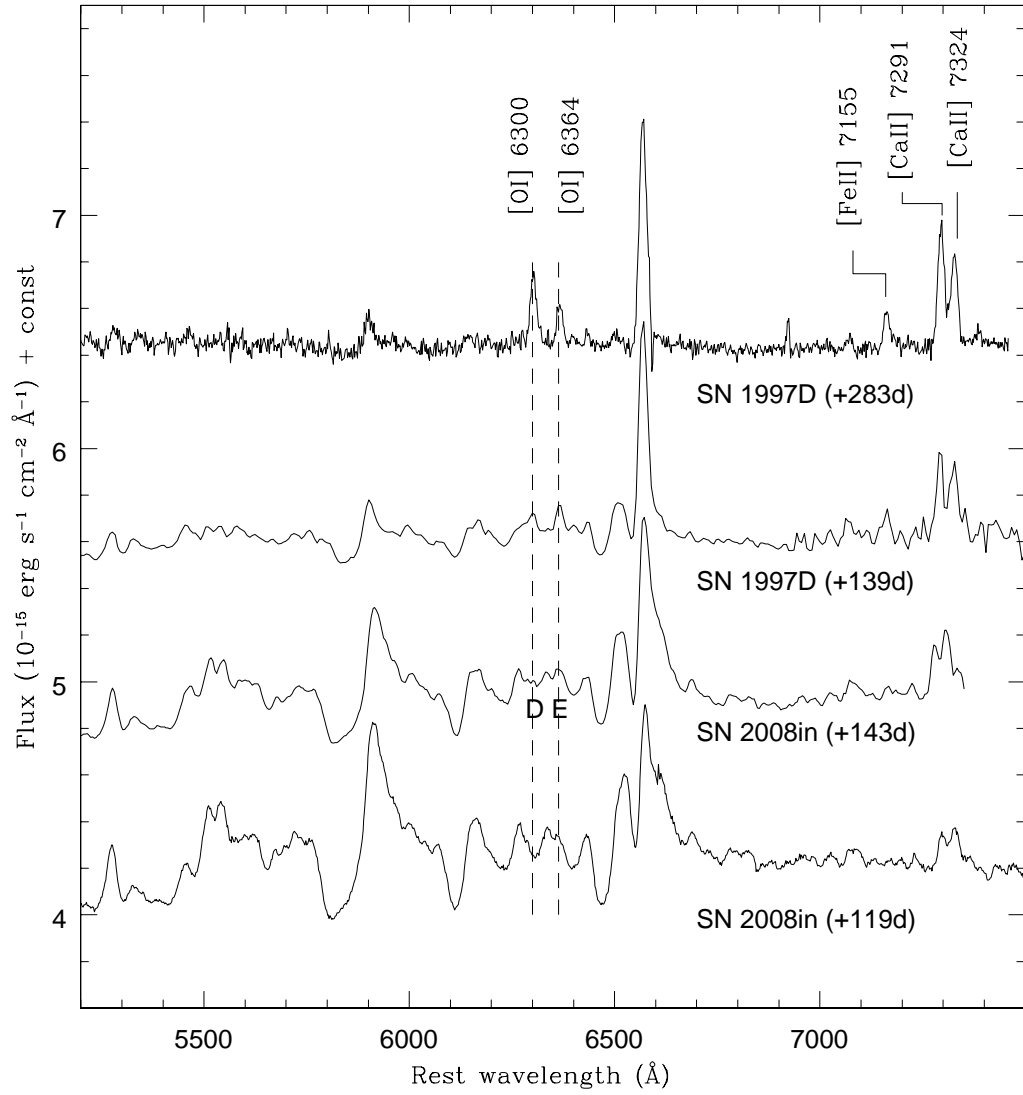


Figure 4.10 Forbidden lines during the nebular phases of SN 2008in are compared with the low-luminosity SN 1997D. The lines [O I], [Fe II] and [Ca II] are marked.

#### 4. THE SUBLUMINOUS TYPE IIP SN 2008IN

---

The emergence of absorption dips in the blue wings of  $H\alpha$  is clearly seen in the post +60d spectra <sup>1</sup> and the absorption dips have been marked with A, B and C in Figure 8. We distinguish ‘A’ as an absorption dip due to Ti II and  $H\alpha$  and its equivalent width (EW) increases from 12.85 Å at +60d to 19.45 Å at +143d. This progressively stronger absorption dip requires a steep deceleration of the  $H\alpha$  emitting zone along with its depletion by inner metal shells (like Ti II). The broader absorption dip ‘B’ is identified as a blend of Ba II  $\lambda$ 6497, Ba I, Ca I and Ti II. An exceptionally strong Ba II lines is quite typical for cooler ejecta of less energetic faint SNe. The segment ‘C’ is speculated to be a footprint of Fe II multiplets as the evolution of its linewidths seems to be correlated with the other Fe II lines. It is noted, however, that in a few normal Type IIP SNe 1999em, 2004et and 2008gz, the spectral feature near ‘C’ at early plateau phases was also identified as a signature of high velocity  $H\alpha$  component, and in the present spectra its presence cannot be completely ruled out.

The evolution of  $H\beta$  is similar to the evolution of  $H\alpha$ . The P-Cygni profile of  $H\beta$  is clearly visible in the +7d spectrum, and later on, the emission component is blanketed by various metal lines, mainly due to Fe II  $\lambda$ 4924,  $\lambda$ 5018 and  $\lambda$ 5169. Traces of  $H\beta$  and Fe II absorption dips indicate that from the beginning of the nebular phase H shells of ejecta and the regions containing Fe II ions move with a comparable velocity, reaching an asymptotic value  $\sim 1000 \text{ km s}^{-1}$  nearly 140 days after the explosion. In the +14d spectrum, Fe II lines are marginally detected while in the spectra between +60d and +99d they are prominent. We investigate the temporal change of EW of a relatively less blended Fe II  $\lambda$ 4924 and from the spectra

---

<sup>1</sup>This is the first time that the rapidly changing evolution of  $H\alpha$  profiles during the late plateau to nebular phase has been so densely covered in a low-luminosity SN

---

normalized to the  $H\alpha$  peak value, we found that at an  $EW \sim 0.67 \text{ \AA}$  at +14d, increased to  $17.45 \text{ \AA}$  at +54d and to  $26.53 \text{ \AA}$  in the +99d spectrum. Later on, the  $EW$  decreased to  $19.07 \text{ \AA}$  in the +118d spectrum and finally reaches to  $18.27 \text{ \AA}$  in the +143d spectrum. This rapid fall in the  $EW$  of inner metal-rich shells plausibly indicates a decrease in the opacity of the SN inner ejecta.

Traces of the  $\text{He I } \lambda 5876$  line are also seen in the +7d spectrum (Figure 4.8). The ratio of  $EW$ s between  $H\alpha$  and  $\text{He I}$  for this spectrum is  $EW(H\alpha)/EW(\text{He I}) \sim 1.99$ . In the +14d spectrum, this ratio has increased to 5.36. The steep decrement in  $EW$  of  $\text{He I}$  seems to be due to a quick recombination of  $\text{He I}$  ions as a result of the rapid fall in temperature of the constantly rarefying ejecta. From +54d, the emerging P-Cygni feature of  $\text{Na I D}$  becomes prominent. This feature seems to be a perfect P-Cygni throughout our entire spectral sequence. It simply indicates an uniform spherical distribution of  $\text{Na I}$  in the SN ejecta. In the three high S/N spectra labeled with +54d, +60d and +87d, a tiny absorption dip overlaid on the emission component of the  $\text{Na I D}$  P-Cygni is seen and since these spectra are redshift corrected, these dips are impressions of intervening interstellar matter present in the host galaxy. The absence of any similar absorption dip in the blue wing of the  $\text{Na I D}$  profile, expected from the Galactic interstellar matter, confirms that there is little absorption from the Milky Way in the line of sight of SN 2008in.

The spectral evolution of  $\text{Sc II } \lambda 6248$  and the s-process element  $\text{Ba II } \lambda 6142$  is clearly seen in SN 2008in. In the +7d and +14d spectra, there is no clear evidence for the presence of these two elements; however in the +54d spectrum they are prominent. The absorption components become stronger with time and persist until the +143d spectrum. In contrast, in the normal Type IIP SNe 2004et [Sahu et al., 2006], 1999em [Elmhamdi et al., 2003b] and 2008gz (Chapter 3) these features

## 4. THE SUBLUMINOUS TYPE IIP SN 2008IN

---

disappeared at  $\sim 170$  day after the explosion. The ejecta of underluminous Type IIP SNe expand at a lower velocity than those of normal ones. So, the Ba lines in low luminosity events persist for a longer time just because the ejecta takes more time to cool-down. As a result it takes longer time to become optically thin.

In the nebular phase, the forbidden lines: [Ca II]  $\lambda\lambda 7291, 7323$ , [O I]  $\lambda\lambda 6300, 6364$  and [Fe II]  $\lambda 7155$  are among the strongest features visible in the spectra. Also, the line ratios of emission lines of Ca II and the O I doublet in late nebular phases is a good indicator of the progenitor mass [Fransson and Chevalier, 1987]. In Figure 4.10, we compare the +139d and +283d spectra of SN 19997D (Benetti et al. 2001) with the nebular phase spectra of SN 2008in. The [Ca II] doublet is seen in the +99d, +119d and +143d spectra of SN 2008in, whereas a small footprints of the O I doublet can be seen in the +143d spectrum. Presence of [Fe II] line is not seen in our spectra. Considering that the explosion epoch of SN 1997D was quite uncertain, it is likely that the spectral evolution of  $H\alpha$  and forbidden lines of SN 2008in is quite similar to that of SN 1997D.

### 4.5 extinction and distance toward SN 2008in

In order to determine the bolometric light curve and other physical parameters, a correct estimate of the extinction and distance toward the SN is essential. We adopt the Galactic reddening along the line-of-sight of SN 2008in as derived from the  $100 \mu\text{m}$  all sky dust extinction map [Schlegel et al., 1998], i.e.  $E(B - V) = 0.0224 \pm 0.0003$  mag. In order to estimate reddening due to the host galaxy M61, we used the spectrum of SN 2008in taken on 2009 February 17 from the 2-m IGO telescope having good S/N ( $\sim 40$ ) and corrected for mean heliocentric radial velocity

---

of the host ( $cz \approx 1567 \pm 3 \text{ km s}^{-1}$ ). Near the zero velocity, the spectrum showed a tiny absorption feature overlaid on the emission component of the P-Cygni profile of Na I D (§ 4.4). The EW of this absorption feature was computed as  $0.535 \pm 0.713 \text{ \AA}$ . The error in EW is estimated using Equation 6 of [Vollmann and Eversberg \[2006\]](#). It is known that the EW of the interstellar absorption bands is well correlated with the reddening  $E(B - V)$  estimated from the tail of SN Ia color curve [[Barbon et al., 1990](#); [Richmond et al., 1994](#); [Turatto et al., 2003](#)] and hence using the empirical relation  $E(B - V) = -0.01 + 0.16\text{EW}$  (EW in  $\text{\AA}$ ), given by [Turatto et al. \[2003\]](#), we obtain the host contribution as  $E(B - V) \approx 0.076 \pm 0.104$ , which is considerably higher than the Galactic contribution. This is consistent with the absence of any absorption feature due to Galactic interstellar matter in the blue wing of the emission component of Na I D profile. Consequently, we adopt  $E(B - V)$  (estimated as a sum of Galactic and host galaxy reddening) of  $0.0984 \pm 0.104$  mag for SN 2008in. This corresponds to a visual extinction ( $A_V$ ) of  $0.305 \pm 0.322$ . Considering the uncertainty in the  $E(B - V)$  estimated using Na I D lines, a lower value of  $E(B - V)$  of  $0.0448 \pm 0.0006$  mag (twice the Galactic reddening) and the corresponding  $A_V$  of  $0.139 \pm 0.002$  cannot be ruled out. We will discuss its implication for the derived properties of the SN.

The Hubble flow distance of the host galaxy M 61, after correction for the Virgo infall, is estimated as  $13.7 \pm 1.1 \text{ Mpc}$ <sup>1</sup>. The distance estimated through the Tully-Fisher method is  $12.1 \pm 2.7 \text{ Mpc}$ <sup>2</sup>. Additionally, we also calculated the distance following the Standard Candle Method for Type II SNe [[Hamuy, 2005](#); [Hamuy and](#)

---

<sup>1</sup>The cosmological model with  $H_0 = 70 \text{ km s}^{-1} \text{ Mpc}^{-1}$ ,  $\Omega_m = 0.3$  and  $\Omega_\Lambda = 0.7$  is assumed throughout this work and the uncertainty corresponds to a local cosmic thermal velocity of  $208 \text{ km s}^{-1}$  [[Terry et al., 2002](#)].

<sup>2</sup><http://nedwww.ipac.caltech.edu/>

## 4. THE SUBLUMINOUS TYPE IIP SN 2008IN

---

Pinto, 2002; Hendry et al., 2005]. It is found that there is a strong correlation between the distance of Type IIP SNe along with their mid-plateau apparent  $V$  and  $I$  band magnitudes and the mid-plateau photospheric velocity, for a given cosmological model. For SN 2008in we estimate the mid-plateau ( $\sim +50$ d) apparent magnitudes  $\sim 15.56 \pm 0.05$  mag for  $V$  and  $\sim 14.77 \pm 0.06$  mag for the  $I$  band. Considering the  $V$  and  $I$  band extinctions toward the SN,  $0.305 \pm 0.322$  mag and  $0.183 \pm 0.193$  mag respectively, we derive a distance of  $\sim 12.23 \pm 1.87$  Mpc. The adopted value of mid-plateau photospheric velocity is  $2694.67 \pm 70$  km s $^{-1}$  (see §4.7.2). Combining the above three measurements, we adopt the weighted mean distance of  $13.19 \pm 1.09$  Mpc, which corresponds to a distance modulus of  $30.6 \pm 0.2$ .

### 4.6 Color Evolution and Bolometric Flux

Figure 4.11 shows the temporal evolution of the reddening-corrected broadband colors of SN 2008in. For comparison, we overplot the color curves for well studied SNe 1987A [Suntzeff and Bouchet, 1990], 1999em [Elmhamdi et al., 2003b], 2004et [Maguire et al., 2010; Sahu et al., 2006], 2005cs [Pastorello et al., 2009] and SN 2008gz [chapter 3]. After small differences during the initial phases, the plateau phase color evolution of all Type II SNe is more or less similar. The  $(U - B)_0$  and  $(B - V)_0$  colors are blue during early photospheric phases and they become redder by about 1-2 mag in the plateau phase while the  $(V - R)_0$  and  $(V - I)_0$  colors evolves slowly and become red only by about 0.5 mag. The  $(J - H)_0$  color remains constant at  $\sim 0.25$  mag. During the transition phase from plateau to nebular, the low luminosity SN 2005cs showed a striking red peak in the  $(B - V)_0$ ,  $(V - R)_0$  and  $(V - I)_0$  colors. For SN 2008in, this red peak is not present and its color evolution

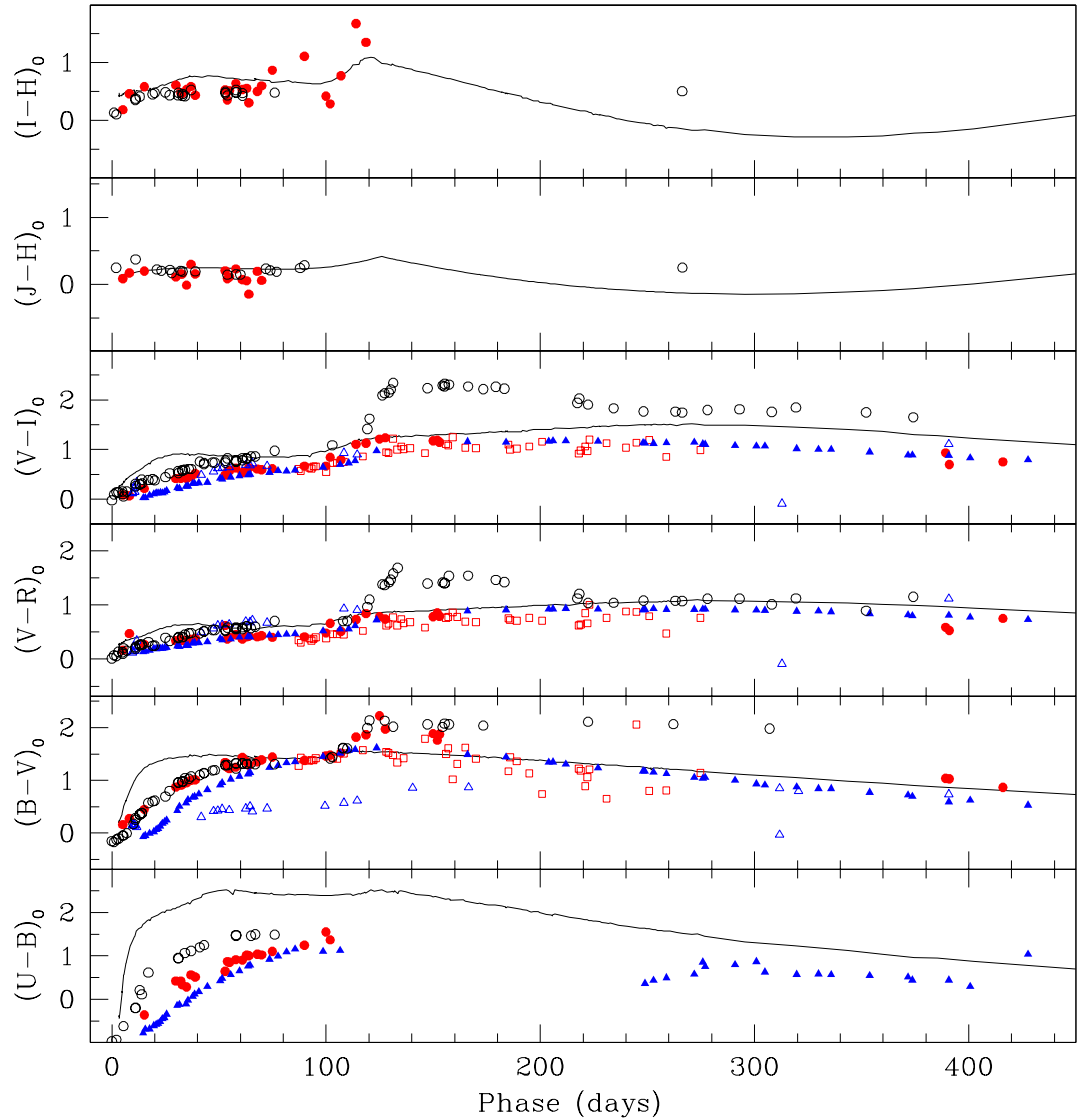


Figure 4.11 Colour curve of SN 2008in is shown with filled circles. Also shown are the SNe 1987A (solid line), 1999em (open triangle), 2004et (filled triangle), 2005cs (open circle) and 2008gz (open square).

#### 4. THE SUBLUMINOUS TYPE IIP SN 2008IN

---

is found to be consistent with the normal Type IIP SNe.

The quasi-bolometric light curve estimated from the UV, optical and IR broad-band (*UVOIR*) magnitudes of SN 2008in is shown in the right panel of Figure 4.12 along with those of other Type II SNe. The extinction-corrected magnitudes are first converted into fluxes using zero-points given by Bessell et al. [1998] and then the total flux in *UVOIR* bands is obtained after a linear interpolation and integration between 0.203 and 1.67  $\mu\text{m}$ . The fluxes were calculated on those nights for which we had complete observations in *UBVRI* bands. For the initial two weeks the SN was detected by *Swift*/UVOT in near ultraviolet bands with a significant flux density. This contribution has been accounted for while measuring the net *UVOIR* flux. It has been assumed that contribution in the *U* band is mainly important during the plateau and decreases rapidly to about 5% in the nebular phase [see Misra et al. 2007b; Roy et al. 2011b and references therein]. From the light curve it is noticeable that the near ultraviolet flux is almost negligible beyond 20 days after explosion. The *JH* contribution during the plateau is calculated from our data, whereas for the nebular phase, due to lack of data, we are not able to make any direct measurement. For most low luminosity SNe IIP, the NIR flux contribution in the nebular phase is about 50% of the total flux [Pastorello et al., 2009]. We have therefore increased the net flux by 55% to account for the maximal contributions from the *U* and NIR bands at phases later than +140d. The spectroscopic and bolometric comparison clearly demonstrate that spectroscopically SN 2008in appears to be like low-luminosity SNe IIP, but photometrically it appears quite normal. In the following section, the *UVOIR* curve is used to estimate the amount of radioactive  $^{56}\text{Ni}$  and other physical parameters that characterize the explosion and the progenitor star.

---

## 4.7 Physical Parameters

The physical entities that seem to govern the entire scenario are mainly associated with the nature of the progenitor and the radioactive elements (mainly  $^{56}\text{Ni}$ ), generated inside the inner portion of the ejecta during the explosion.  $^{56}\text{Ni}$  is synthesized by the explosive burning of Si and O during the shock breakout [Arnett, 1996, 1980]. Over time this material is eventually converted to  $^{56}\text{Co}$  and then to  $^{56}\text{Fe}$  by means of radioactive transitions having decay times of 8.77 and 111.3 days respectively. The  $\gamma$ -rays and neutrinos emitted during this process sustain the nebular phase light curve and consequently, the observed tail luminosity becomes a good tracer for the ejected synthesized  $^{56}\text{Ni}$ .

### 4.7.1 Produced Radioactive Nickel

We use different methods to estimate mass of  $^{56}\text{Ni}$ . Hamuy [2003] proposed a relation between bolometric tail luminosity and the synthesized  $^{56}\text{Ni}$  during core collapse SNe, by considering the underlying assumption that all  $\gamma$ -rays emitted during the radioactive decay make the ejecta thermalised. For SN 2008in, the time interval spanned by the observations is about 416 days, where the first  $\sim 100$  days are reserved for photospheric evolutionary processes. The average  $V$  band magnitude during the nebular phase calculated using the data between +114d and +416d is  $\sim 18.91$ , which corresponds to the  $V$  magnitude at  $\sim +222$ d. Taking the extinction correction as ( $A_V = 0.305 \pm 0.322$  mag; §4.5), a bolometric correction of  $0.26 \pm 0.06$  mag [Hamuy, 2001] and a distance modulus  $30.6 \pm 0.2$ , the derived tail luminosity at this fiducial time is  $(3.02 \pm 1.95) \times 10^{40}$  erg s $^{-1}$ . Within the errors, this value is consistent with the bolometric flux at a comparable epoch, determined in §4.6. This

#### 4. THE SUBLUMINOUS TYPE IIP SN 2008IN

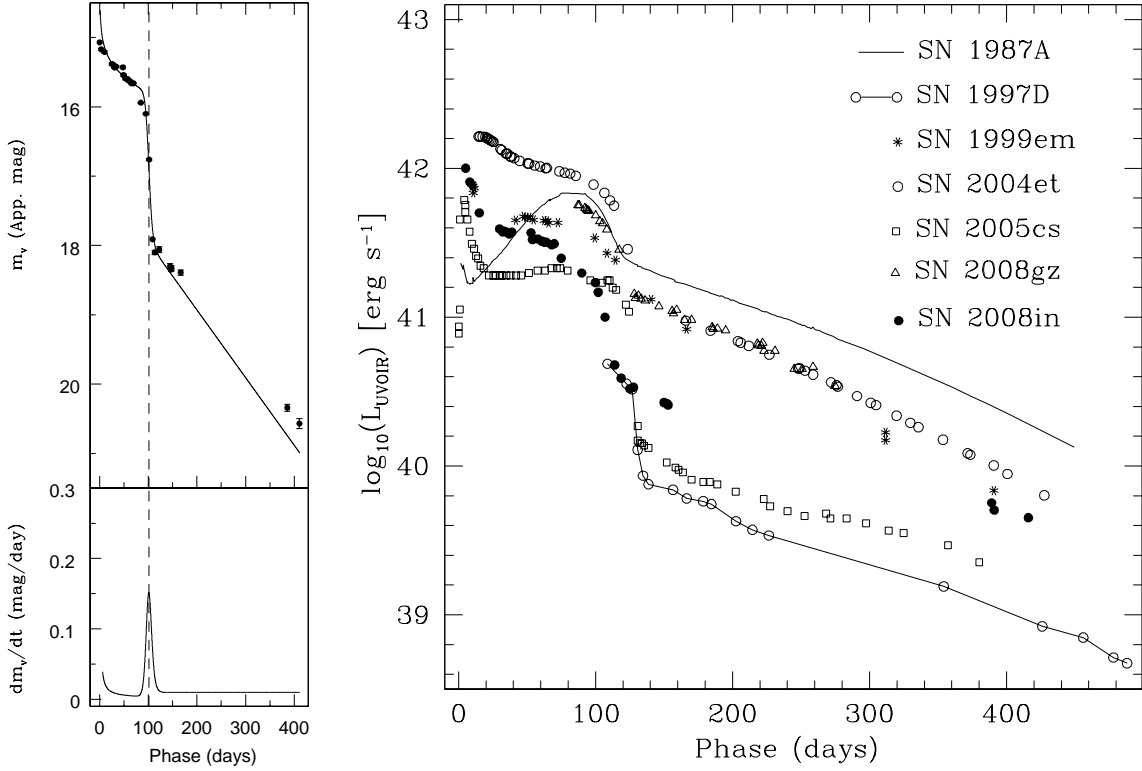


Figure 4.12 **Left:** Determination of steepness parameter from the apparent  $V$ -band light curve of SN 2008in. See text for details. **Right:** Comparison of the quasi-bolometric light curve of SN 2008in with the low-luminosity SNe 1997D, 2005cs; the normal SNe 1999em, 2004et, 2008gz; and the peculiar Type II SN 1987A.

implies that the amount of  $^{56}\text{Ni}$  produced in this process is  $M_{\text{Ni}} = 0.0157 \pm 0.0102 M_{\odot}$ .

All Type IIP SNe show an inflection in the light curve during the transition from the plateau to the nebular phase. Statistically it has been shown that the steepness of the  $V$ -band light curve slope (defined as  $S = dm_V/dt$ ) at the inflection time ( $t_i$ ) is anti-correlated with  $^{56}\text{Ni}$  mass [Elmhamdi et al., 2003a]. For SN 2008in, the  $V$  band light curve with its well-sampled transition phase, shows a value of steepness  $S = 0.151 \pm 0.044 \text{ mag d}^{-1}$  (The left panel of Figure 4.12) and the epoch

---

of inflection is  $t_i \approx +101.5\text{d}$  with respect to date of discovery. This corresponds to  $M_{\text{Ni}} = 0.0175 \pm 0.002M_{\odot}$ . This result is consistent with the value measured using the Hamuy [2003] scheme. According to Elmhamdi et al. [2003a], the amount of  $^{56}\text{Ni}$  can also be derived from the plateau absolute  $V$ -band magnitude using the relation  $\log M_{\text{Ni}} = -0.438M_V(t_i - 35) - 8.46$ . Here  $M_V(t_i - 35)$  is the absolute  $V$  magnitude 35 days prior to the day of inflection. For SN 2008in,  $M_V(t_i - 35) \approx -15.23$ , which again corresponds to a  $^{56}\text{Ni}$  mass around  $0.016M_{\odot}$ .

Comparison of the tail luminosity with that of SN 1987A – a well studied proximate event, is also used for estimation of the  $^{56}\text{Ni}$  mass. A linear least square fit on the nebular light curve tail shows that at +222d the luminosity of SN 2008in is about  $1.54 \times 10^{40} \text{ erg s}^{-1}$ , while SN 1987A had a luminosity  $\sim 1.10 \times 10^{41} \text{ erg s}^{-1}$  (right panel of figure 4.12). Since the  $^{56}\text{Ni}$  mass produced by SN 1987A is about  $0.075M_{\odot}$ , the amount of  $^{56}\text{Ni}$  in the case of SN 2008in is  $[(1.54/1.10) \times 10^{-1}] \times 0.075 \approx 0.0105M_{\odot}$ .

The above estimates are consistent with each other and hence we adopt a mean value for  $^{56}\text{Ni}$  mass as  $0.015 \pm 0.003M_{\odot}$ .

## 4.7.2 Explosion Energy and Mass of Progenitor Star

We use the radiation-hydrodynamical simulations of core-collapse IIP SNe by Dessart et al. [2010] to infer the explosion energy ( $E_0$  - kinetic plus thermal, expressed hereafter in units of  $10^{51} \text{ erg}$  or foe). These simulations suggest that in a given progenitor larger explosion energies yield larger ejecta velocities and this implies that the ejecta kinematics can be used to put constraint on  $E_0$ . For SN 2008in, the expansion rate of the H-rich progenitor envelope as derived from absorption minima in  $\text{H}\alpha$  at 15d after shock breakout is about  $6300 \text{ km s}^{-1}$  (see Figure 4.8), which is higher than

#### 4. THE SUBLUMINOUS TYPE IIP SN 2008IN

---

4700 km s<sup>-1</sup> [for SN 2005cs; [Pastorello et al. 2009](#)] and lower than 8800 km s<sup>-1</sup> [for SN 1999em; [Elmhamdi et al. 2003b](#)]. For the SNe 2005cs and 1999em, the simulation results (for explosion of a non-rotating solar metallicity pre-SN stars) predicted  $E_0 \sim 0.3$  foe and  $\gtrsim 1$  foe respectively and these values are found to be consistent with that determined from the actual hydrodynamical modeling of the SN light curves, e.g. 0.4 foe [[Utrobin and Chugai, 2008](#)] and 0.3 foe [[Pastorello et al., 2009](#)] for SN 2005cs; 1.3 foe [[Utrobin, 2007](#)] and 1.25 foe [[Bersten et al., 2011](#)] for SN 1999em. For SN 2008in, the simulations suggest  $E_0 \sim 0.5$  foe.

Accurate determinations of explosion parameters such as  $E_0$ , the ejected mass ( $M_{\text{ej}}$ ) and the pre-SN radius ( $R_0$ ) of the progenitor require detailed hydrodynamical modeling of the light curves and spectra and this being a non-trivial task has only been attempted for a few SNe. In order to have an estimate of explosion parameters of SN 2008in here, we employ the analytical relations derived by [Litvinova and Nadezhin \[1985\]](#) correlating the observed parameters ( $M_{V_{mp}}$  - the mid-plateau absolute magnitude at  $V$ ,  $v_{mp}$  - the mid-plateau photospheric velocity and  $\Delta t_p$  - the plateau duration) with the physical parameters ( $E_0$ ,  $M_{\text{ej}}$  and  $R_0$ ) based on a grid of hydrodynamical models for different values of physical parameter for Type IIP SNe. We note, however, that these approximate formulae have limitations owing to the poorly-measured observables and the simplified physical conditions such as non-inclusion of the effect of nickel heating, use of old opacity tables, neglecting the effect of line opacity and using outdated pre-SN models [[Bersten et al. 2011](#); [Smartt et al. 2009](#) and references therein]. As a result, only approximate values of the physical parameters can be derived using these relations. Fortunately, the observed parameters are derived very accurately for SN 2008in. The  $\Delta t_p$  is  $\sim 98$  days

---

(§4.3.2), the  $v_{mp}$  is  $2694 \pm 70^1$  km s<sup>-1</sup> and the  $M_{V_{mp}}$  is estimated as  $-15.32 \pm 0.38$  mag<sup>2</sup> Now, employing analytical relations, we estimate  $E_0 \sim 0.54$  foe,  $M_{ej} \sim 16.7$   $M_\odot$  and  $R_0 \sim 127R_\odot$ . The explosion energy derived in this way is consistent with that predicted from the hydrodynamical simulations of the ejecta kinematics.

The explosion energy of SN 2008in indicates that the event was less energetic than the standard IIP SNe 1999em, 2004et and more energetic than SN 2005cs. Assuming a net mass loss  $\sim 0.5M_\odot$  due to stellar wind <sup>3</sup> and accounting for a compact remnant with mass  $\sim 1.5 - 2M_\odot$  [Sahu et al., 2006], we find that the initial mass of the progenitor to be  $\leq 20M_\odot$ .

## 4.8 Discussion in context of other Type IIP SNe

In Figure 4.13, we compare the light curve of SN 2008in in absolute  $V$ -band magnitude with a sample of 13 other well studied Type II SNe taken from the literature [see Misra et al. 2007b and Roy et al. 2011b for the references]. The sample includes two low-luminosity Type IIP SNe 1997D, 2005cs; nine normal Type IIP SNe 1990E, 1992H, 1999gi, 1999em, 2003gd, 2004A, 2004dj, 2004et, 2008gz and two peculiar Type II SNe 1987A, 1998A. It is seen that the Type II SNe show a wide range of mid-plateau luminosity, i.e. from  $-14$  to  $-17$  mag. The data on low luminosity

---

<sup>1</sup>This is the mean value of the velocities computed from the lines of Fe II  $\lambda 4924$ ,  $\lambda 5018$  and  $\lambda 5169$  in the +54d spectrum.

<sup>2</sup>These observed values of  $M_{V_{mp}}$  and  $v_{mp}$  can be compared with the estimates derived empirically between the mass of <sup>56</sup>Ni, and the  $v_{mp}$  and  $M_{V_{mp}}$  for a larger sample of IIP SNe [see Section §3.8.3]. Using the <sup>56</sup>Ni mass of  $0.015 \pm 0.003M_\odot$  we find  $v_{mp} = 2916 \pm 220$  km s<sup>-1</sup> and  $M_{V_{mp}} = -15.37 \pm 0.23$  mag which are consistent with those measured observationally.

<sup>3</sup>SN 2008in was not detected in X-ray. The lack of X-ray emission can be used to constrain the mass-loss rate of the progenitor system that could be heated by the outgoing shock to X-ray emitting temperatures. Following the discussion in Immler et al. [2007] and references therein, an upper limit to the pre-SN mass-loss rate of  $5 \times 10^{-6} M_\odot \text{ yr}^{-1}$  ( $v_w/10$  km s<sup>-1</sup>) with an uncertainty of a factor of two to three is obtained.

#### 4. THE SUBLUMINOUS TYPE IIP SN 2008IN

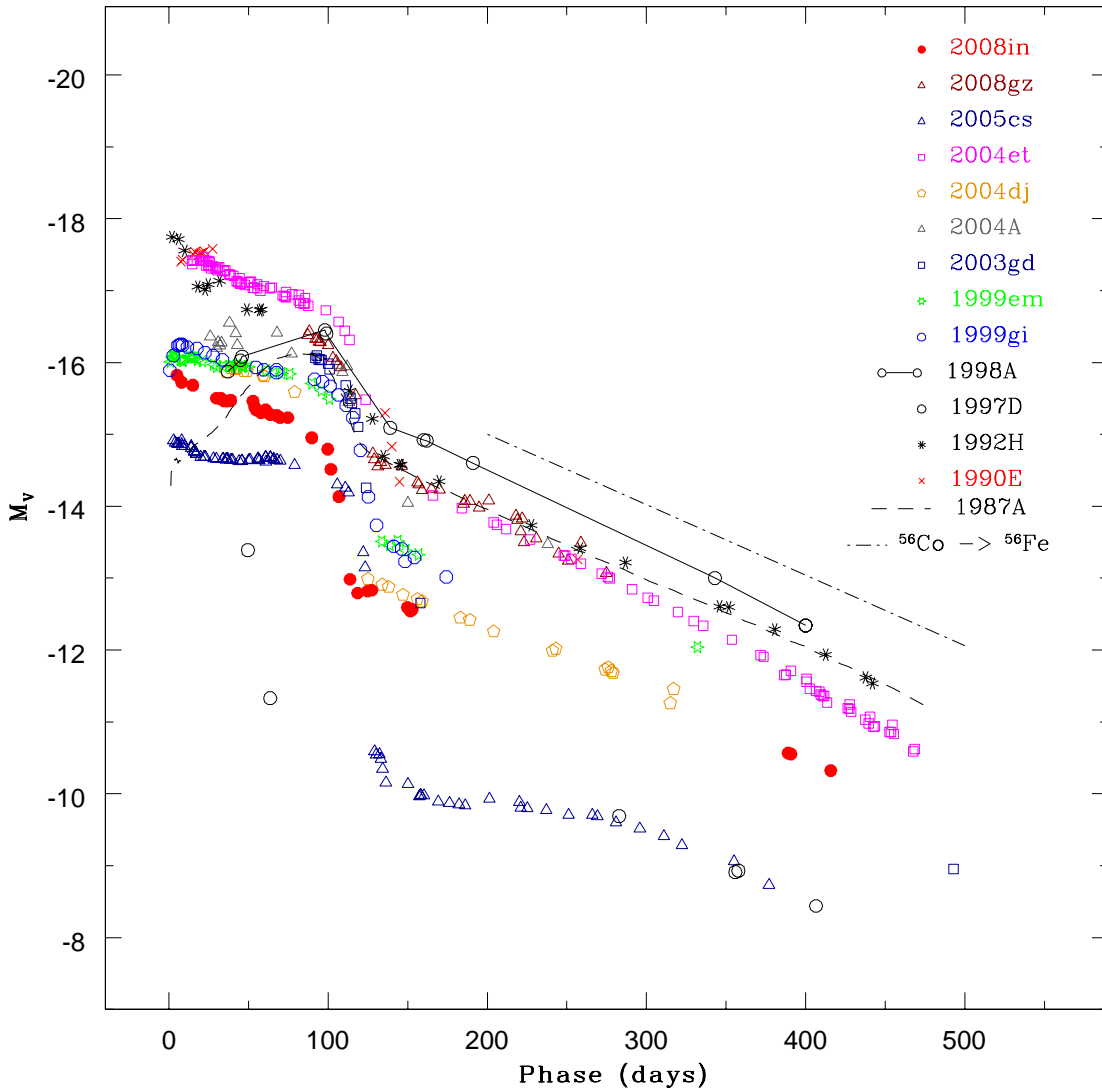


Figure 4.13 A comparison of the absolute  $V$ -band light curve of SN 2008in with the low-luminosity SNe 1997D, 2005cs; the normal SNe 1999em, 2004et, 2008gz, 2004dj, 2004A, 2003gd, 1999em, 1999gi; and the peculiar Type II SNe 1987A, 1998A. The decline rate of emission expected from radioactive decay of  $^{56}\text{Ni}$  to  $^{56}\text{Co}$  to  $^{56}\text{Fe}$  is shown with dot-dashed line.

---

SNe [see also Table 4 in [Pastorello et al. 2006](#)] indicate that their  $M_{Vmp}$  lie between  $-14$  and  $-15$  mag, with the only exception of SN 2002gd, whereas the other SNe are seen to lie between  $-16$  and  $-17$  mag. With the  $M_{Vmp}$  of  $-15.32$  mag<sup>1</sup>, the SN 2008in present another case which occupies the gap between a low and normal luminosity Type IIP events.

The tail luminosity is an important indication of ejected nickel mass. The average tail luminosity of SN 2008in ( $M_v \sim -12.16$ ) is nearly 2.3 mag brighter than those of the low luminosity SNe 1997D and 2005cs ( $\sim -9.6$  mag), and about 1.3 mag fainter than the normal Type IIP SNe 1992H, 2004et and 2008gz ( $\sim -13.5$  mag). A close inspection shows that the average tail luminosity of SN 2008in is roughly similar to Type IIP SNe 2004dj in NGC 2403 and 2003gd in M74, whereas their plateau is brighter ( $\sim 0.5 - 0.8$  mag at mid-plateau) than SN 2008in. These comparison of nebular phase luminosities with other SNe are consistent with a quite modest radioactive  $^{56}\text{Ni}$  production for SN 2008in (§4.7.1).

The luminosity and shape of the tail depend on the  $^{56}\text{Ni}$  mass and the radiant energy per unit ejected mass ( $E/M_{ej}$ ). The first parameter determines the absolute magnitude, while the second determines its decay rate [see [Turatto et al. 1998](#) and references therein]. The measured value of ejected  $^{56}\text{Ni}$  mass for SNe 2003gd, 2004dj and SN 2008in are respectively  $\sim 0.016$  [[Hendry et al., 2005](#)],  $0.017$  [[Vinkó et al., 2006](#)] and  $0.015M_{\odot}$ . These are more than twice the  $^{56}\text{Ni}$  amount synthesized by the low-luminosity SNe 1997D [ $\sim 0.002M_{\odot}$ , [Turatto et al. 1998](#)] and 2005cs [ $0.003 - 0.004M_{\odot}$ , [Pastorello et al. 2009](#)], although at least three times less than the  $^{56}\text{Ni}$  produced by normal Type IIP SNe such as 1992H [ $\sim 0.075M_{\odot}$ , [Clocchiatti et al. 1996](#)], 2004et [ $\sim 0.06M_{\odot}$ , [Maguire et al. 2010](#); [Sahu et al. 2006](#)] and 2008gz [ $\sim$

---

<sup>1</sup>Considering a lower value of  $A_V = 0.139 \pm 0.002$ , we get  $M_{Vmp} = -15.1 \pm 0.2$

## 4. THE SUBLUMINOUS TYPE IIP SN 2008IN

---

$0.05M_{\odot}$ , Roy et al. 2011b]. Similarly, the measured value of  $E/M_{\text{ej}}$  ratio for SN 2008in is larger than that for the low-luminosity SN 1997D and lower than other Type IIP events <sup>1</sup>.

Though we have an approximate value of the pre-SN radius ( $128 R_{\odot}$ ), it can be seen that the progenitor radius of SN 2008in is smaller than or comparable to that of low-luminosity SNe 1997D [ $\sim 300R_{\odot}$ , Turatto et al. 1998], 2005cs [ $100 - 600R_{\odot}$ , Pastorello et al. 2009, Utrobin and Chugai 2008], 1999br [ $114R_{\odot}$ , Zampieri et al. 2003] and much smaller than that of normal Type IIP SNe like 1992H [ $>600R_{\odot}$ , Clocchiatti et al. 1996], 2004et [ $\sim 530R_{\odot}$ , Misra et al. 2007b]. We also note that SN 2008in progenitor is only slightly larger than the blue supergiant progenitors of SNe 1987A and 1998A [Pastorello et al., 2005].

Information about the metallicity of the SNe location is essential to constrain the triggering mechanism of the SN explosion [Heger et al., 2003]. The oxygen abundance [O/H] of SN 2008in is about 8.44 dex <sup>2</sup> which is marginally lower than the solar value of 8.65 dex [Asplund et al., 2009]. A comparison <sup>3</sup> of [O/H] of all

---

<sup>1</sup> The measured value of the  $E/M$  ratio for SN 2008in is  $3.5 \times 10^{49} \text{erg } M_{\odot}^{-1}$ , which is twice the  $E/M$  ratio measured for SNe 1997D [ $1.7 \times 10^{49} \text{erg } M_{\odot}^{-1}$ , Turatto et al. 1998], but it is half those of SN 2008gz [ $7.3 \times 10^{49} \text{erg } M_{\odot}^{-1}$ , Roy et al. 2011b], SN 2004dj [ $7.3 \times 10^{49} \text{erg } M_{\odot}^{-1}$ , Vinkó et al. 2006] and SN 2004et [ $7.5 \times 10^{49} \text{erg } M_{\odot}^{-1}$ , Sahu et al. 2006]. Finally, it is barely a third the  $E/M$  ratios of SNe 1987A [ $11.3 \times 10^{49} \text{erg } M_{\odot}^{-1}$ , Hamuy 2003] and 2003gd [ $13.0 \times 10^{49} \text{erg } M_{\odot}^{-1}$ , Hendry et al. 2005], and about seven times smaller than the luminous event like SN 1998A [ $25.4 \times 10^{49} \text{erg } M_{\odot}^{-1}$ , Pastorello et al. 2005].

<sup>2</sup> Derived from the  $[O/H](= 12 + \log(N_O/N_H)) - M_B$  relation given by Pilyugin et al. [2004] for a given deprojected radius and galaxy type. The host of SN 2008in is a spiral galaxy of SBbc Type and the SN location is  $\sim 1.8'$  away from the center of the host. This corresponds to a deprojected distance  $\sim 7.03$  kpc.

<sup>3</sup> We have taken the [O/H] value from Smartt et al. [2009], though for a few cases the values are estimated using the [O/H]– $M_B$  relation mentioned in Pilyugin et al. [2004]. The [O/H] for normal Type IIP SNe 2008gz, 1999em and low-luminosity SNe 1999eu, 2005cs is about 8.6. For the low-luminosity SNe 1994N, 1999br, 2001dc, 2003gd and 2004dj, 1997D and the normal SN 2004et, it is about 8.4. In many cases, we have adopted the [O/H] value from Smartt et al. [2009]. For some cases we have estimated the value by adopting the [O/H]– $M_B$  relation mentioned in Pilyugin et al. [2004].

---

the events in our sample indicate that there is no clear trend in the type of event and the metallicity.

The photometric and spectroscopic comparisons of SN 2008in with some Type II SNe covering a wide range of physical parameters puts observational constraints on the nature of the progenitor of this event, pointing toward a star that was more compact than a typical M-Type red supergiants, and closer to a blue supergiant, may be an yellow supergiant. However, the direct detection of the progenitors of a few faint SNe IIP in pre-explosion archive *Hubble Space Telescope* images seems to contradict this conclusion [see [Smartt et al. 2009](#) for a review]. Our spectroscopic study suggests that in SN 2008in the hydrogen envelope ejected by the explosion is smaller than in most Type II events but larger than that ejected in low luminosity events (such as SN 1997D, SN 1999br and SN 1999eu). This may be due to a significant mass loss of the parent star in the latest stages of its life. This conclusion is also partially supported by the upper limit mass loss rate of the progenitor revealed from the X-ray study (§4.7.2). In view of the upper mass limit of  $20 M_{\odot}$  progenitor, occurrence of the event in a sub-solar metallicity region and following the evolution of a single massive star as a function of metallicity [[Heger et al., 2003](#)], we rule out the possibility of “fall back of ejecta to BH” scenario in case of SN 2008in, supporting the scenario of a weak explosion of a relatively compact progenitor.

## 4.9 conclusion

Low-luminosity Type IIP SNe belong to a poorly known class of events due to the unknown nature of their progenitors as well as the explosion mechanism. Spectroscopic as well as photometric characteristics of these events are significantly different

#### 4. THE SUBLUMINOUS TYPE IIP SN 2008IN

---

from the normal and peculiar Type IIP SNe. The number of such underluminous events discovered so far is relatively small. This could plausibly be a selection effect. If we confine the search of core-collapse SNe to a small volume, the majority of SNe discovered in the local universe are of Type IIP [ $\sim 48.2\%$ , [Smith et al. 2011a](#)] and probably a large fraction of them would turn out to be underluminous. Incidentally SN 1999br, SN 2005cs and SN 2009md are the only events of this group to have been discovered soon after the core-collapse and whose data are publicly available.

In this study we have reported the results of an extensive photometric and spectroscopic follow-up campaign for SN 2008in in the ultraviolet, optical and near-infrared domains. The SN was also observed (although not detected) at X-ray and radio wavelengths. The SN was observed soon after its explosion, during the fast rise of the light curve to the optical maximum. Evidence for a shock breakout in SN 2008in was primarily derived through the analysis of the ROTSE-IIIb *R*-band light curve. An upper limit of 16.16 mag in the *R*-band was estimated about two days before the discovery.

Modeling the *R*-band light curve allowed us to estimate a reliable epoch of the shock breakout, with an uncertainty of about two days. The plateau phase in SN 2008in lasts about 98 days which is marginally shorter than in normal Type IIP SNe. The evolution of the bolometric light curve indicate that the event is somewhat in between the normal and faint Type IIP event. The luminosity of the nebular phase light curve indicates an ejected  $^{56}\text{Ni}$  mass of  $\sim 0.015M_{\odot}$ , a factor two higher than that derived for low-luminosity IIP SNe. The spectroscopic evolution of SN 2008in is similar to those of low-luminosity IIP SNe (1997D, 1999br and 1999eu), indicated particularly by the strong presence of Ba II lines, the narrow line widths of  $\text{H}\alpha$  lines, and the expansion velocities of SN during the photospheric phases ( $\sim 3000 \text{ km s}^{-1}$ )

---

and the nebular phases ( $\sim 1200 \text{ km s}^{-1}$ ). The ejecta kinematics of SN 2008in are consistent with less-energetic ( $\sim 5 \times 10^{50} \text{ erg}$ ) Type IIP SNe.

Spectroscopically SN 2008in appears to be like low-luminosity SNe IIP, but photometrically it appears close to a normal type IIP event.

From the light curve and spectra of SN 2008in, we could determine quite accurate values of the observed properties such as plateau duration, mid-plateau luminosity as well as the photospheric velocity and this has helped us to comment on the properties of the explosion and the progenitor star. Using semi-analytical formulae by [Litvinova and Nadezhin \[1985\]](#), we could estimate approximate values of the explosion energy  $\sim 5.4 \times 10^{50} \text{ erg}$ , the ejected mass  $\sim 17M_{\odot}$  and the pre-SN radius  $\sim 127R_{\odot}$ . The explosion energy of SN 2008in is smaller than the normal ( $\geq 10^{51} \text{ erg}$ ) Type IIP events, although higher than that estimated in underenergetic ( $\sim 10^{50} \text{ erg}$ ) SNe IIP. We could provide an upper limit to the mass loss rate of the progenitor as  $5 \times 10^{-6} M_{\odot} \text{ yr}^{-1} (v_w/10 \text{ km s}^{-1})$  whereas the upper limit for the main-sequence mass of the progenitor star is estimated as  $20 M_{\odot}$ .

#### 4. THE SUBLUMINOUS TYPE IIP SN 2008IN

---



**Petroglyph of Crab explosion – The SN of AD1054 :** It was first discovered in the year 1970s at the Chaco Canyon site (New Mexico), which was occupied at around 1000 AD by the *Anasazi* civilization. On the vertical surface plane there are representations of a hand, and a crescent moon which is facing a star at the bottom-left. The drawing on the ground in front of the petroglyph is possibly showing the core and tail of a comet. This petroglyph may also represents the configuration of the moon and supernova that happen in the morning of 5 July 1054, the epoch which corresponds to the period of the Anasazi civilisation. [Source: 1) Kelley, D. H. & Milone, E. F., 2004, *Exploring Ancient Skies: An Encyclopedic Survey of Archaeoastronomy* (1st ed), Springer, 2) Wikinedia]

# Chapter 5

## The stripped envelope SNe 2007uy and 2008D

### 5.1 Introduction

In previous chapters we have discussed about the CCSNe which are generated from progenitors having initial mass  $8-30 M_{\odot}$  having an extended Hydrogen (H) envelope and shows a prolonged plateau in optical light curve along with strong  $H\alpha$  in their spectra. More evolved stars may not have thick H layer in their outer shell and during their death, they show the impression of Helium (He) (in Type Ib) or not even that (in Type Ic) in the optical spectra. In fact the explosion of these evolved stars are believed to be associated with the highly energetic cosmic explosions like long duration GRB (LGRB) (see chapter 1) [[Galama et al. 1998](#); [Olivares E. et al. 2012](#); [Sonbas et al. 2008](#) and references therein].

With a volumetric sample of nearby CCSNe discovered by the Lick Observatory SN Search (LOSS) program, [Smith et al. \[2011a\]](#) found that only about 7% of total

## 5. THE STRIPPED ENVELOPE SNE 2007UY AND 2008D

---

nearby CCSNe are of Type Ib nature. Further-more they argued that most of the Ib are formed through mass transfer in a binary system rather than through progenitor's wind and the true progenitors of SNe Ib must extend to a much lower range of initial masses than classical WR stars. So the bright Type Ib events, having better proximity and good coverage in different wavebands should be scrutinized to establish a finer statistics in this regard.

NGC 2770, a relatively nearby galaxy ( $z \sim 0.007$ , distance  $\sim 29.5$  Mpc) probably providing a clue to reveal the explosions in evolved stars. After 1999, this host experienced two similar marvelous explosions within a gap of  $\sim 10$  days, located at two opposite side with respect to the host centre. Several space and ground based telescopes were able to catch these two events from very beginning. Through a single set of observation we were able to monitor two events. This opportunity is rare indeed.

SN 2007uy, a Type Ib event, was first discovered by Yoji Hirose on 2007, December 31.669 UT at an unfiltered magnitude 17.2 [Nakano et al., 2008a]. There are numerous intervening host galaxy H II regions along the direction of the SN [Gorobabel et al., 2011] and no object was found at the transient location in the red band DSS image observed between 1998 and 2000. Blondin and Calkins [2008] report the first optical spectroscopic observation of this event taken on 2008, January 3.40 UT that ascribed this transient as a type Ib event similar to SN 2004gq and discovered nearly one week before its maximum. The properties of the host galaxy and SN 2007uy are provided in Table 5.1. A detail description of the host can also be found elsewhere [Thöne et al., 2009]. The SN 2007uy was also detected in radio bands at +10d [Soderberg, 2008] with a X-band (8.46 GHz) flux density  $0.29 \pm 0.03$  mJy. The high resolution X-ray observation with Chandra/ACIS-S was also reported by

---

Pooley and Soderberg [2008].

Meanwhile, on 2008 January 09 a bright X-ray transient was located by *Swift*/XRT when it was monitoring SN 2007uy in the same galaxy [Berger and Soderberg, 2008a,b]. A significant steepening was observed in the X-ray spectrum within 400 sec after the outburst but no  $\gamma$ -ray emission was detected during the outburst and pre-outburst stages [Soderberg et al., 2008]. A long term fading X-ray counterpart was detected by *Swift* and *Chandra* during the follow up observations. Pooley and Soderberg [2008] reported the high resolution observation of SN 2008D along with SN 2007uy conducted on 19.85 UT January, 2008 through ACIS-S instrument on-board the Chandra X-ray observatory. Although the X-ray spectrum of SN 2008D shows a significant amount of dust along line of sight, UVOT detected a bright NUV-optical counterpart in 2030 – 5400 Å wavelength range (though later, NUV component was disappeared). The presence of broad absorption lines, superposed on the blue continuum with lack of H and He [Valenti et al., 2008b], in the early spectra of SN 2008D classifies it as a Type Ic event which later underwent a transition to Type Ib similar to SN 2005hg [Modjaz et al., 2008a]. The observed properties of X-ray outburst are distinct from all other known X-ray transients and was initially supposed to be an X-ray flash XRF 080109. Soderberg et al. [2008] report that the estimated peak X-ray luminosity of XRF 080109 is 4 orders of magnitude larger than the Eddington Luminosity of a solar mass object, 3 orders of magnitude brighter than that of a type I X-ray burst, 2 orders of magnitudes brighter than ULX outbursts but more than 3 orders of magnitudes fainter than GRBs/XRFs luminosity.

In this chapter, we discuss the optical broad-band evolution of SN 2007uy and SN 2008D. The *BVRI* optical broad band evolution of SN 2008D will be described.

## 5. THE STRIPPED ENVELOPE SNE 2007UY AND 2008D

---

Table 5.1 Properties of the host galaxy NGC 2770 and SN 2007uy.

Parameters	Value	Ref. <sup>a</sup>
<b>NGC 2770:</b>		
Type	SABc	1
RA (J2000)	$\alpha = 09^{\text{h}}09^{\text{m}}33.^{\text{s}}68$	1
DEC (J2000)	$\delta = +33^{\circ}07'24.''7$	1
Abs. Magnitude	$M_B = -20.78$ mag	1
Distance	$D = 29.72 \pm 0.45$ Mpc	§5.6
Distance modulus	$\mu \sim 32.4$	
Apparent radius	$r_{25} = 1.'73$ ( $\sim 15.09$ kpc)	1
Inclination angle	$\Theta_{\text{inc}} = 82.3^{\circ}$	1
Position angle	$\Theta_{\text{maj}} = 146.1^{\circ}$	1
Heliocentric Velocity	$cz_{\text{helio}} = 1947 \pm 2$ km s <sup>-1</sup>	1
<b>SN 2007uy:</b>		
RA (J2000)	$\alpha = 09^{\text{h}}09^{\text{m}}35.^{\text{s}}40$	2
DEC (J2000)	$\delta = +33^{\circ}07'09.''9$	2
Location	20'' .6 E, 15'' .5 S	2
Deprojected radius	$r_{\text{SN}} = 42.''44$ ( $\sim 5.3$ kpc)	§5.6
Discovery date (UT)	31.7 December 2007 (JD 2454466.17)	2
Explosion epoch:	$\sim 4$ days prior the discovery	§5.1

<sup>a</sup>(1) HyperLEDA - <http://leda.univ-lyon1.fr>; (2) from [Nakano et al. \[2008a\]](#).

---

In addition to that, Near Ultra-violet (NUV), Optical and Near infrared (NIR) photometric and optical spectroscopic observations of SN 2007uy will be discussed. Optical coverage of span of  $\sim 120$  days is performed using 1–4m class telescopes whereas for NUV follow-up *Swift*/UVOT archival data has been utilized. NIR monitoring is performed from 2m class United Kingdom Infrared Telescope (UKIRT). The VLA archival radio data along with other literature data have been used to interpret the radio properties. Spectroscopic analysis has been done using the archival data obtained from ESO-VLT. The distance and extinction along the line of sight is also discussed. A preliminary information regarding the properties of the host and that of the transient is provided in Table 5.1.

The discovery of SN 2007uy corresponds to  $\text{JD} = 2454466.17$ . According to initial spectroscopy [Blondin and Calkins, 2008] the explosion happened within 7 days prior to the discovery. Modeling of radio data (§5.9) also claims that the event was discovered at about 3.6 days after the burst. Here we adopt a conservative value and constrain the explosion epoch about 4 days prior to the detection. Hence  $\text{JD}_{2007uy} = 2454462.17$  is assumed as the explosion epoch of SN 2007uy. In the rest of the work, if not mentioned, all the phases will be quoted with respect to the date of burst. On the other hand, the burst time of SN 2008D is very precisely known due to its serendipitous discovery by *Swift*. Hence in this case the date of discovery is precisely equivalent to the date of burst. For SN 2008D the explosion epoch is assumed to be  $\text{JD}_{2008D} = 2454475.06$  [Berger and Soderberg, 2008b].

### 5.2 Observation and data reduction

The field contains two transients. In this present work we have used the optical *BVRI* observations of SN 2007uy and SN 2008D along with NUV, optical *U*, NIR and radio observation of SN 2007uy along with optical spectroscopic observations of SN 2007uy. Here the data acquisition and reduction are briefly discussed.

### 5.3 Multiband photometry

#### 5.3.1 SN 2007uy:

The field of SN 2007uy was monitored from several ground-based Optical and radio telescopes as well as using space-based Optical and NUV telescopes.

We obtained the UVOT data from the *Swift* Data Archive. The photometry was done using standard processes, using HEASOFT routines along with the standard calibration data. The photometry was calibrated to the UVOT photometric system following the procedure described in [Poole et al. \[2008\]](#). To remove the contribution from the underlying host galaxy we measured the host galaxy flux at the position of the SN from late UVOT observations, where there was no longer a contribution from the SN. This additional flux was then subtracted from SN photometric measurements. For all observations the source was close to the centre of the field-of-view, and differences in the PSF between observations were, therefore, negligible. The UVOT photometry is given in [Table 5.2](#). The optical broadband Johnson *UBV* and Cousins *RI* follow-up observations were performed between  $\sim +16$ d to  $+130$ d using 104-cm Sampurnanand Telescope (ST)+imaging CCD camera at Nainital, In-

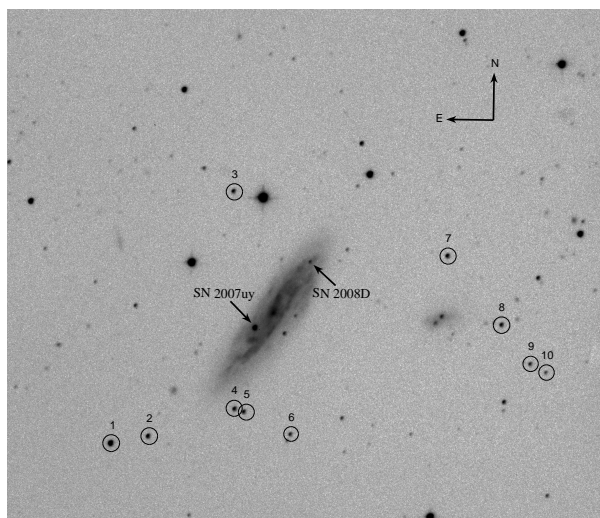


Figure 5.1 Identification chart of SN 2007uy field along with SN 2008D. The image is about 10x10 arcmin taken in V-band with the 104-cm Sampurnanand telescope (ST) at ARIES, Nainital. The SNe locations are marked along with the secondary stars used for calibration. North is up and East is to the left.

dia and 2.56 m Nordic optical telescope (NOT)+ALFOSC<sup>1</sup> at La Palma, Spain. The field of SN 2007uy (Figure 5.1) was monitored at 16 epochs from ST and at 11 epochs from NOT. Several exposures (100s to 300s) were taken and in order to increase the signal to noise ratio, photometry was performed on the co-added frames. The raw data was cleaned using standard data reduction software *IRAF* and the photometry was performed using the stand alone version of *DAOPHOT*. The reduction process is as mentioned in Chapter 2.

---

<sup>1</sup>Andalucia Faint Object Spectrograph and Camera (ALFOSC) mounted at the cassegrain focus of the telescope was used for photometric and spectroscopic observation.

Table 5.2 The *swift*/UVOT photometry of SN 2007uy.

UT Date (yy/mm/dd)	JD 2454000+	Phase <sup>a</sup> (day)	uvw2 (mag)	uvm2 (mag)	uvw1 (mag)	u (mag)	b (mag)	v (mag)
2008/01/06.15	471.65	+9	21.45	24.33	18.61±0.18	16.89±0.06	17.28±0.06	16.62±0.08
2008/01/06.49	471.99	+10	20.29±0.39	21.31±4.25	18.45±0.10	16.93±0.04	17.02±0.03	16.47±0.04
2008/01/09.71	475.21	+13	20.05±0.35	20.15±0.58	18.23±0.10	16.78±0.04	16.81±0.03	16.09±0.04
2008/01/11.38	476.88	+14	20.33±0.27	20.69±0.65	18.37±0.06	16.69±0.02	16.79±0.02	15.96±0.02
2008/01/11.99	477.49	+15	21.28±0.82	>20.57	18.51±0.07	16.72±0.02	16.81±0.02	15.93±0.02
2008/01/12.57	478.07	+15	20.48±0.40	21.40±3.72	18.45±0.09	16.76±0.03	16.77±0.02	15.85±0.03
2008/01/13.21	478.71	+16	20.59±0.47	22.63	18.50±0.09	16.76±0.03	16.80±0.03	15.93±0.03
2008/01/13.89	479.39	+17	20.34±0.29	20.81±0.68	18.41±0.07	16.78±0.03	16.81±0.02	15.81±0.02
2008/01/14.73	480.23	+18	21.41±0.87	>20.59	18.61±0.08	16.88±0.03	16.77±0.02	15.80±0.02
2008/01/15.49	480.99	+18	21.32±1.00	>20.36	18.95±0.12	17.03±0.04	16.81±0.02	15.79±0.02
2008/01/16.29	481.79	+19	20.77±0.47	>20.36	18.85±0.11	17.04±0.04	16.81±0.02	15.78±0.02
2008/01/17.14	482.64	+20	21.43	>19.88	18.93±0.09	17.15±0.03	16.90±0.03	15.77±0.02
2008/01/17.81	483.31	+21	21.53±0.96	22.97	18.94±0.08	17.27±0.03	16.89±0.02	15.73±0.02
2008/01/18.85	484.35	+22	>20.87	22.19	—	—	—	—
2008/01/21.12	486.62	+23	22.92	24.98	19.62±0.11	18.07±0.05	17.26±0.03	15.89±0.02
2008/01/21.76	487.26	+25	—	—	19.71±0.40	18.30±0.17	17.25±0.07	15.94±0.07
2008/01/25.17	490.67	+28	—	—	>20.64	—	—	—
2008/01/26.41	491.91	+29	—	—	20.84±0.29	19.33±0.10	17.88±0.03	16.28±0.02
2008/01/27.98	493.48	+31	—	—	>20.91	—	—	—
2008/01/29.35	494.85	+32	—	—	>20.78	—	—	—
2008/01/30.81	496.31	+35	—	—	22.04±0.50	20.78±0.58	18.51±0.06	16.66±0.03
2008/02/01.93	498.43	+37	—	—	>20.87	21.59±1.57	18.53±0.06	16.86±0.03
2008/02/03.93	500.43	+39	—	—	19.90±1.25	—	—	—
2008/02/08.95	505.45	+43	—	—	22.39±0.50	—	—	—
2008/02/10.89	507.39	+45	—	—	—	—	19.05±0.10	—
2008/02/13.03	509.53	+47	—	—	—	—	18.95±0.09	17.27±0.05
2008/02/16.11	512.61	+50	—	—	—	—	—	—
2008/02/22.30	518.80	+57	—	—	—	—	—	—
2008/02/25.79	522.29	+60	—	—	—	—	18.96±1.04	17.72±0.09
2008/03/12.60	538.10	+75	—	—	—	—	—	17.84±0.12

<sup>a</sup>With reference to the epoch of burst JD 2454462.17

Table 5.3 Photometry of Secondary Standard stars in the field of SN 2007uy and SN 2008D

Star ID	$\alpha_{2000}$ (h m s)	$\delta_{2000}$ (deg m s)	$B$ (mag)	$V$ (mag)	$R$ (mag)	$I$ (mag)
1	09:09:42.48	33:05:07.1	$16.37 \pm 0.002$	$15.56 \pm 0.006$	$15.06 \pm 0.013$	$14.64 \pm 0.016$
2	09:09:44.25	33:05:11.8	$17.64 \pm 0.003$	$16.98 \pm 0.002$	$16.62 \pm 0.005$	$16.27 \pm 0.007$
3	09:09:37.26	33:09:34.9	$17.85 \pm 0.009$	$17.34 \pm 0.012$	$17.01 \pm 0.010$	$16.69 \pm 0.002$
4	09:09:36.84	33:05:46.0	$18.00 \pm 0.011$	$17.26 \pm 0.010$	$16.84 \pm 0.013$	$16.43 \pm 0.009$
5	09:09:36.12	33:05:42.9	$18.11 \pm 0.014$	$17.48 \pm 0.016$	$17.13 \pm 0.005$	$16.81 \pm 0.011$
6	09:09:31.93	33:05:19.5	$19.01 \pm 0.012$	$17.93 \pm 0.011$	$17.26 \pm 0.006$	$16.74 \pm 0.003$
7	09:09:18.95	33:08:33.4	$17.54 \pm 0.012$	$17.15 \pm 0.011$	$16.87 \pm 0.006$	$16.57 \pm 0.003$
8	09:09:14.29	33:07:16.0	$18.85 \pm 0.012$	$17.49 \pm 0.011$	$16.63 \pm 0.006$	$15.92 \pm 0.003$
9	09:09:11.82	33:06:34.6	$19.09 \pm 0.012$	$18.02 \pm 0.011$	$17.36 \pm 0.006$	$16.86 \pm 0.003$
10	09:09:10.49	33:06:25.6	$19.83 \pm 0.012$	$18.72 \pm 0.011$	$17.97 \pm 0.006$	$17.37 \pm 0.003$

**Note**— The U band data is standardized with respect to the field standards mentioned in [Malesani et al. \[2009\]](#)

Both SNe were surrounded by a star forming knot and the host galaxy is highly inclined ( $\sim 82.3^\circ$ ) with respect to the line of sight. Hence, the SNe fluxes are highly contaminated by the background and in order to account this the post-explosion ( $\sim 36$  months) high S/N images of the host galaxy in *UBVRI* bands, obtained from NOT under good photometric sky condition, were used as a template to map the galaxy flux. Template subtraction technique (as described in §2.3.1) has been adopted to remove the galaxy contribution. Before flux subtraction, both NOT and ST images were bring to a common ‘plate-scale platform’ using the ‘magnify’ task provided in *IRAF* package. The instrumental magnitudes of SN were derived from the template subtracted SN frames using profile (Point Spread Function, PSF) fitting method. The field of NGC 2770 was calibrated in *BVRI* bands using [Landolt \[1992\]](#) standard stars of the fields of PG1633+009 and PG1047+003 observed on the night of March 02, 2008 under good seeing (FWHM  $\sim 2''$  in R band) and transparent sky condition. We used mean values of atmospheric extinction coefficients of the site viz 0.28, 0.17, 0.11 and 0.07 mag per unit airmass for the *B*, *V*, *R* and *I* bands

## 5. THE STRIPPED ENVELOPE SNE 2007UY AND 2008D

---

[Kumar et al., 2000] with a typical standard deviations between transformed and standard magnitudes of Landolt stars as 0.04, 0.02, 0.02, 0.01 in  $B$ ,  $V$ ,  $R$  and  $I$  bands respectively. A sample of 10 bright and isolated non-variable stars in the field of SN 2007uy was used as local standards to derive the zero points for the SN at each epoch. For  $U$  band observation we have used the calibrated stars mentioned by Malesani et al. [2009]. The location and magnitudes of these local standards are listed in Table 5.3. Figure 5.1 shows the SNe and the secondary standards of the field. Table 5.4 lists the magnitudes of SN 2007uy in  $UBVRI$  bands.

Table 5.4 The *UBVRI* photometry of SN 2007uy.

UT Date (yyyy/mm/dd)	JD 2454000+	Phase <sup>a</sup> (day)	<i>U</i> (mag)	<i>B</i> (mag)	<i>V</i> (mag)	<i>R</i> (mag)	<i>I</i> (mag)	Telescope <sup>b</sup>
2008/01/12.94	478.44	+16	16.64±0.01	16.78±0.01	15.79±0.01	15.54±0.01	–	NOT
2008/01/13.99	479.71	+17	–	16.77±0.02	15.81±0.03	15.51±0.03	15.53±0.03	ST
2008/01/14.85	480.58	+18	–	16.74±0.03	15.78±0.03	15.46±0.02	15.43±0.04	ST
2008/01/15.19	480.69	+18	16.69±0.03	16.71±0.02	15.76±0.01	15.38±0.02	15.31±0.01	NOT
2008/01/15.99	481.72	+19	–	16.78±0.02	15.74±0.02	15.44±0.01	15.36±0.03	ST
2008/01/17.19	482.69	+20	16.95±0.01	16.80±0.01	15.81±0.01	15.40±0.01	15.21±0.01	NOT
2008/01/28.94	494.44	+32	–	17.98±0.01	16.45±0.01	15.72±0.01	15.50±0.01	NOT
2008/01/29.84	495.57	+33	–	18.19±0.02	16.44±0.02	15.81±0.02	15.59±0.02	ST
2008/01/30.19	495.69	+33	–	–	16.53±0.02	15.79±0.01	15.58±0.01	NOT
2008/01/31.94	497.44	+35	19.08±0.02	18.22±0.01	16.60±0.01	15.89±0.01	15.62±0.02	NOT
2008/01/31.87	497.60	+35	–	18.28±0.03	16.54±0.03	15.91±0.03	15.62±0.04	ST
2008/02/01.94	498.44	+36	19.20±0.03	18.29±0.02	16.66±0.02	15.96±0.02	15.66±0.02	NOT
2008/02/03.94	500.44	+38	19.32±0.03	18.41±0.03	16.86±0.02	16.08±0.02	15.77±0.02	NOT
2008/02/04.88	501.61	+39	–	18.50±0.06	16.82±0.02	16.11±0.02	15.83±0.03	ST
2008/02/09.75	506.48	+44	–	18.70±0.03	17.07±0.03	16.40±0.03	15.97±0.04	ST
2008/02/05.86	512.59	+50	–	18.84±0.03	17.33±0.01	–	16.18±0.03	ST
2008/02/18.94	515.44	+53	19.75±0.04	19.01±0.03	17.33±0.03	16.66±0.03	16.26±0.03	NOT
2008/02/23.65	520.37	+57	–	19.27±0.05	17.64±0.04	16.84±0.03	16.53±0.07	ST
2008/02/24.62	521.35	+58	–	–	17.52±0.02	16.88±0.02	16.44±0.03	ST
2008/02/29.94	526.44	+64	–	–	17.58±0.03	–	16.48±0.03	NOT
2008/03/02.75	529.45	+66	–	19.22±0.07	–	–	–	ST
2008/03/03.72	531.53	+67	–	19.28±0.06	17.66±0.04	17.05±0.03	16.54±0.05	ST
2008/03/05.80	533.61	+69	–	19.29±0.03	–	17.05±0.04	16.53±0.06	ST
2008/03/17.69	543.19	+81	–	19.31±0.04	17.81±0.03	17.29±0.03	16.76±0.03	NOT
2008/03/05.80	587.36	+124	–	–	18.67±0.02	18.32±0.03	18.02±0.06	ST
2008/05/02.61	589.34	+126	–	–	–	18.51±0.05	–	ST
2008/05/05.62	592.35	+129	–	–	18.84±0.03	–	–	ST

<sup>a</sup>With reference to the epoch of burst JD 2454462.17.

<sup>b</sup>The photometric observations are taken with the 1-m Sampurnanand Telescope (ST), ARIES, Nainital and 2.6-m Nordic Optical Telescope (NOT) with ALFOSC detector. Errors in magnitude denote  $1\sigma$  uncertainty.

## 5. THE STRIPPED ENVELOPE SNE 2007UY AND 2008D

Table 5.5 The near-infrared *JHK* photometry of SN 2007uy.

UT Date (yyyy/mm/dd)	JD 2454000+	Phase <sup>a</sup> (day)	<i>J</i> (mag)	<i>H</i> (mag)	<i>K</i> (mag)
2008/01/12.67	478.17	+16	14.48±0.25	14.98±0.25	14.98±0.17
2008/01/14.68	480.18	+18	14.32±0.19	14.80±0.24	14.71±0.14
2008/01/15.66	481.16	+19	14.26±0.19	14.73±0.24	14.67±0.15
2008/01/17.69	483.19	+21	14.12±0.32	14.64±0.28	14.51±0.22
2008/01/23.67	489.17	+27	14.13±0.25	14.60±0.25	14.51±0.25
2008/02/15.92	512.42	+50	15.76±0.07	15.38±0.02	15.06±0.18
2008/02/24.92	521.42	+59	16.07±0.06	15.58±0.03	15.32±0.19
2008/03/23.92	549.42	+87	17.03±0.07	16.36±0.03	16.21±0.19

<sup>a</sup>With reference to the epoch of discovery JD 2454466.16899.

The field was also monitored in *JHK* NIR bands at 8 epochs spanning between +16d and +87d using UKIRT at Hawaii with ‘WFCAM’ as a backend detector [Hirst et al., 2006]. The dithered images were processed with standard tasks in *IRAF* and photometry was performed with *DAOPHOT* routines. The field has been calibrated with respect to nearby 2MASS stars. The calibrated *JHK* magnitudes of SN 2007uy is given in Table 5.5.

### 5.3.2 SN 2008D:

The optical photometry of SN 2008D is done at the same stroke while doing photometry of SN 2007uy. For the present work we have only used the Optical *BVRI* observations of SN 2008D, we have mainly used the results obtained through the observations of NGC 2770 field. We have also used the literature data for this event. The *BVRI* photometry of SN 2008D is presented in Table 5.6.

Table 5.6 The *BVRI* photometry of SN 2008D.

UT Date (yyyy/mm/dd)	JD 2454000+	Phase <sup>a</sup> (day)	<i>B</i> (mag)	<i>V</i> (mag)	<i>R</i> (mag)	<i>I</i> (mag)	Telescope <sup>b</sup>
2008/01/13.92	479.44	+4	19.30 ± 0.03	18.38 ± 0.03	17.95 ± 0.02	17.92 ± 0.03	ST
2008/01/14.83	480.34	+5	19.29 ± 0.06	18.38 ± 0.04	17.84 ± 0.04	17.36 ± 0.04	ST
2008/01/15.87	481.41	+6	19.11 ± 0.03	18.18 ± 0.02	17.66 ± 0.02	17.17 ± 0.02	ST
2008/01/29.83	495.35	+20	18.47 ± 0.02	17.39 ± 0.02	16.76 ± 0.03	16.04 ± 0.02	ST
2008/01/31.87	497.38	+22	18.59 ± 0.04	17.44 ± 0.03		16.04 ± 0.04	ST
2008/02/04.87	501.38	+26	19.18 ± 0.07	17.71 ± 0.03	16.86 ± 0.03	16.15 ± 0.03	ST
2008/02/09.71	506.25	+31	19.38 ± 0.04	17.82 ± 0.03	17.05 ± 0.03	16.21 ± 0.04	ST
2008/02/15.83	512.37	+37	20.00 ± 0.09	18.26 ± 0.02		16.48 ± 0.03	ST
2008/02/23.62	520.13	+45	20.47 ± 0.12	18.64 ± 0.03	17.70 ± 0.03	16.84 ± 0.07	ST
2008/02/24.58	521.12	+46		18.65 ± 0.02	17.80 ± 0.03	16.77 ± 0.02	ST
2008/03/02.71	528.24	+53	20.76 ± 0.19	18.89 ± 0.06	17.91 ± 0.05		ST
2008/03/03.71	529.23	+54	20.49 ± 0.15			16.90 ± 0.05	ST
2008/03/05.79	531.30	+56			17.90 ± 0.05	16.88 ± 0.06	ST
2008/04/29.67	586.17	+111			19.15 ± 0.04	17.93 ± 0.06	ST
2008/04/30.62	587.13	+112		19.87 ± 0.03			ST
2008/05/02.58	589.11	+114			19.59 ± 0.07		ST
2008/05/05.58	592.12	+117		19.96 ± 0.04			ST

<sup>a</sup>With reference to the epoch of discovery JD 2454475.06. <sup>b</sup>The photometric observations are taken with the 1-m Sampurnanand Telescope (ST), ARIES, Nainital. Errors in magnitude denote  $1\sigma$  uncertainty.

## 5.4 Optical Spectroscopy of SN 2007uy

The spectroscopic observations of SN 2007uy was carried out at 7 epochs between +17d to +392d. The spectral data for +17d was observed from NOT/ALFOSC on January 13, 2008. The spectra for the epochs +32d, +58d, +122d & +392d are based on the archival data obtained through ‘ESO Science Archive Portal’ which were acquired using 8m VLT and 3.6m NTT. The spectral data for +96d and +162d were taken from [Milisavljevic et al. \[2010\]](#). These were primarily acquired on 1st April and 6th June, 2008 using the ‘MMTBLUECHANNEL’ detector at MMT. The journal of spectroscopic observations is presented in Table 5.7.

All the raw optical data were processed using the standard tasks in *IRAF*. Bias and flatfielding were performed on each frames. Cosmic ray rejection on each frame was done by using Laplacian kernel detection [[van Dokkum, 2001](#)]. Images were coadded to improve the signal-to-noise ratio and one-dimensional spectra were

## 5. THE STRIPPED ENVELOPE SNE 2007UY AND 2008D

Table 5.7 Journal of spectroscopic observations of SN 2007uy<sup>a</sup>.

UT Date (yy/mm/dd)	Phase <sup>b</sup> (days)	Range $\mu\text{m}$	Telescope <sup>c</sup>	Grating (gr mm <sup>-1</sup> )	Slit width ( $''$ )	Dispersion ( $\text{\AA pix}^{-1}$ )	Exposure (s)	S/N <sup>d</sup> ( $\text{\AA}^{-1}$ )
2008/01/13	+17	0.32–0.91	NOT	300	1.3	3.0	1200	45
2008/01/28	+32	0.38–0.92	NTT	300	1.0	1.7	1200	43
2008/02/22	+58	0.45–0.87	VLT	300	1.3	1.7	900	34
2008/04/01	+96	0.32–0.80	MMT	300	1.0	2.0	600×4	50
2008/04/26	+122	0.35–0.87	VLT	300	1.3	1.7	2940	38
2008/06/06	+162	0.38–0.68	MMT	300	1.0	2.0	900	35
2009/01/20	+392	0.33–0.87	VLT	300	1.3	1.7	3600	59

<sup>a</sup>The spectra for +32, +58, +122 & +392d are based on data obtained from the ESO Science Archive Facility. The spectra for +96 & +162d are taken from [Milisavljevic et al. \[2010\]](#). <sup>b</sup>With reference to the epoch of explosion JD 2454466.17. <sup>c</sup>NOT : ALFOSC on 2.6-m Nordic Optical Telescope (NOT), la Palma; NTT : EMMI on 3.6-m New Technology Telescope, la Silla; VLT : FORS2 on 8.2-m ESO-VLT-UT1 telescope, Paranal Observatory; MMT : Blue Chanel spectrograph on 6.5-m MMT at Mt. Hopkins; <sup>d</sup>At 0.6  $\mu\text{m}$ .

extracted from coadded frames using the *apall* task in IRAF which is based on an optimal extraction algorithm by [Horne \[1986\]](#). Wavelength calibration was performed using the *identify* task and about 15 to 18 emission lines of He and Ar were used to find a dispersion solution. Fifth order fits were used to achieve a typical RMS scatter of 0.1 $\text{\AA}$  (i.e., 60 km s<sup>-1</sup> at 5000 $\text{\AA}$ ). The position of the O I emission skyline at 5577 $\text{\AA}$  was used to check the wavelength calibration and deviations were found between 0.5 to 1 $\text{\AA}$  and this was corrected with a linear shift in dispersion.

### 5.4.1 Radio observation of SN 2007uy

The transient was first detected in radio on 2008 January 6.18 UT, using the Very Large Array (VLA) at 8.46 GHz, with a flux density of  $290_{-30}^{+30} \mu\text{Jy}$  [[Soderberg, 2008](#)]. Though initially SN 2007uy was observed from VLA, but from January 10.2 UT it starts to observe the new bright transient SN 2008D. Due to larger primary beam size of VLA in L (30'), C (9') and X (5.4') bands<sup>1</sup>, locations of both transients were

<sup>1</sup>L band corresponds to 1.34-1.73 GHz, C band corresponds to 4.5-5.0 GHz and X band corresponds to 4.5-5.0 GHz radiation.

---

within VLA field of view. We used the NRAO archival facility to fetch these data sets and reduced the Radio data using standard routines from the dedicated software package – ‘Astrophysical Image Processing System (AIPS)’<sup>1</sup>. The transient was not detected in radio U band, but was prominent in the C and X band images. For further analysis we use the literature data [van der Horst et al., 2011] along with VLA archival data.

## 5.5 Photometric evolution of SN 2007uy & SN 2008D

The photometric evolutions of SNe 2007uy and 2008D have been examined intensively. For SN 2007uy we do it using NUV, Optical and NIR data while for SN 2008D it has been done with *BVRI* passband data acquired from ST telescope. In subsequent subsections this have been discussed.

### 5.5.1 Evolution of SN 2007uy: NUV, Optical and NIR

The calibrated light curves of SN 2007uy are presented in Figure 5.2. The data cadences of ground based Optical and NIR observations are  $N(U, B, V, R, I, J, H, K) = (7, 19, 23, 20, 22, 8, 8, 8)$ , while that for spaced based NUV and Optical observations are  $N(uvw2, uvm2, uvw1, u, b, v) = (14, 8, 18, 19, 28, 30)$  respectively. Since the host redshift is too small, ‘K-correction’ is not applied. From the peak, the SN light is mainly powered by the radioactive decay of <sup>56</sup>Ni and <sup>56</sup>Co. The energy of  $\gamma$ -ray and positrons emitted by radioactive decay processes are fully absorbed by the SN

---

<sup>1</sup> Astrophysical Image Processing System (AIPS) has been developed by the National Radio Astronomical Observatories (NRAO), USA

## 5. THE STRIPPED ENVELOPE SNE 2007UY AND 2008D

---

ejecta and is re-emitted as a blackbody radiation. Hence in early phase Type I events behave like ‘blackbody supernova’ [Arnett, 1982]. The emergence of a young Type I SN with its blackbody nature is clearly noticeable in all bands. At few phases, SN was not detected in some of the *Swift*/UVOT bands for which the corresponding upper limits are mentioned. During ground-based observation, the maximum sampling of SN light was done in V passband. Similarly, during space-based *Swift*/UVOT observation maximum sampling was done in *v* passband. Since the central wavelength and bandwidth of V passband (5448Å and 840Å respectively) is fairly similar to that of *v* passband (5468Å and 769Å respectively), we have treated the combined data of *V* and *v* bands as a single visual-data set for further analysis of photometric data and likewise the *B* and *b*-band data sets have been combined as a single blue-band data set. In contrast, a significant deviation between U and *u* passband light curves, starting from early epochs ( $\gtrsim 20$  days), is probably due to a considerable difference between their responses (for U band: central wavelength 3663Å bandwidth 650Å for *u* band: central wavelength 3465Å bandwidth 785Å respectively).

The evolution of supernova light can be segmented in three phases – (i) shock breakout phase (initial few days), (ii) photospheric phase (within first 40–50 days) and (iii) Nebular phase (beyond 50 days after explosion). For this particular event we discuss the photospheric and nebular evolution of SN light.

### 5.5.2 *BVRI* evolution of SN 2008D

SN 2008D was observed for 120 days with data frequency  $N(B, V, R, I) = (11, 14, 13, 13)$ . Figure 5.3 shows the time evolution of SN 2008D. The days on x-axis

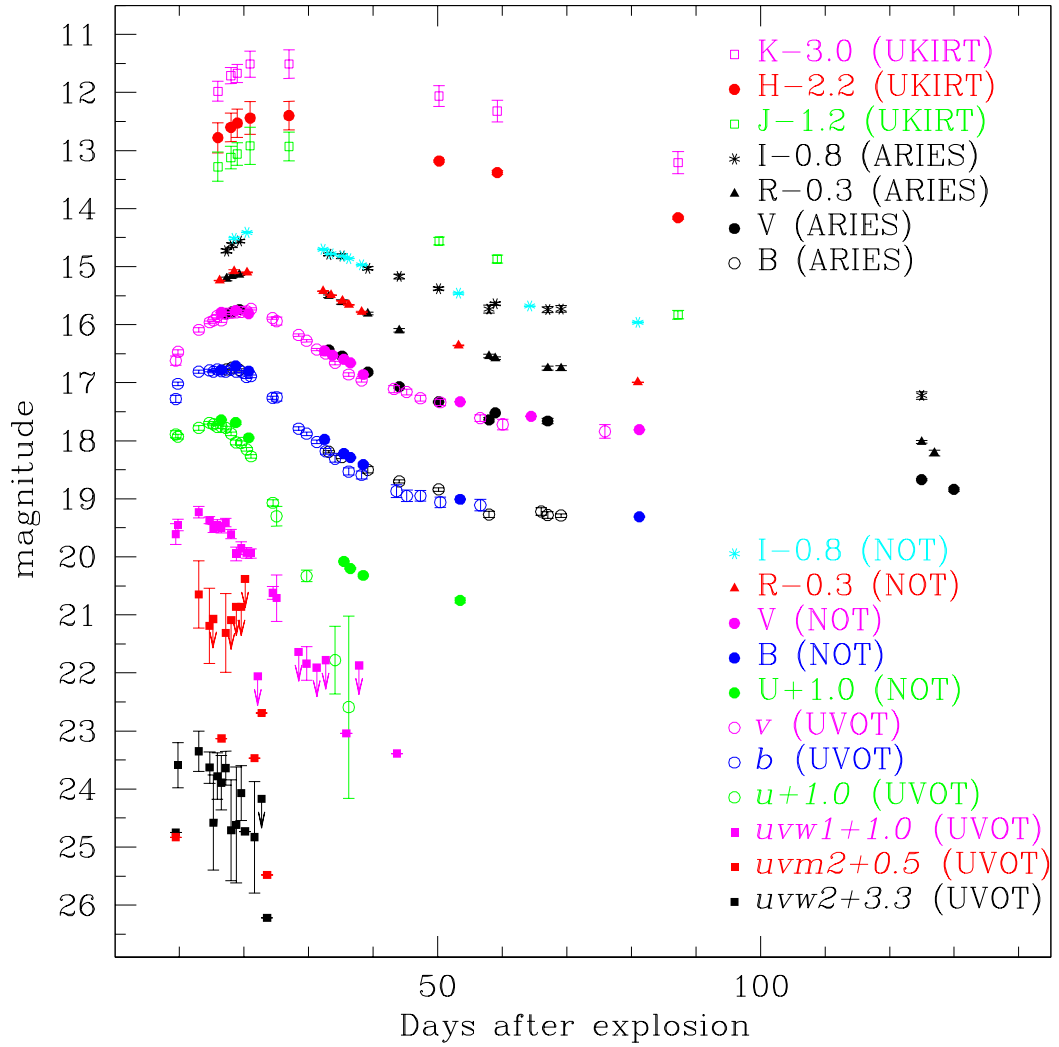


Figure 5.2 The light curves of SN 2007uy in NIR *JHK*, Optical *UBVRI* and *uvw2*, *uvm2*, *uvw1&u*, *b*, *v* NUV-Optical UVOT bands.

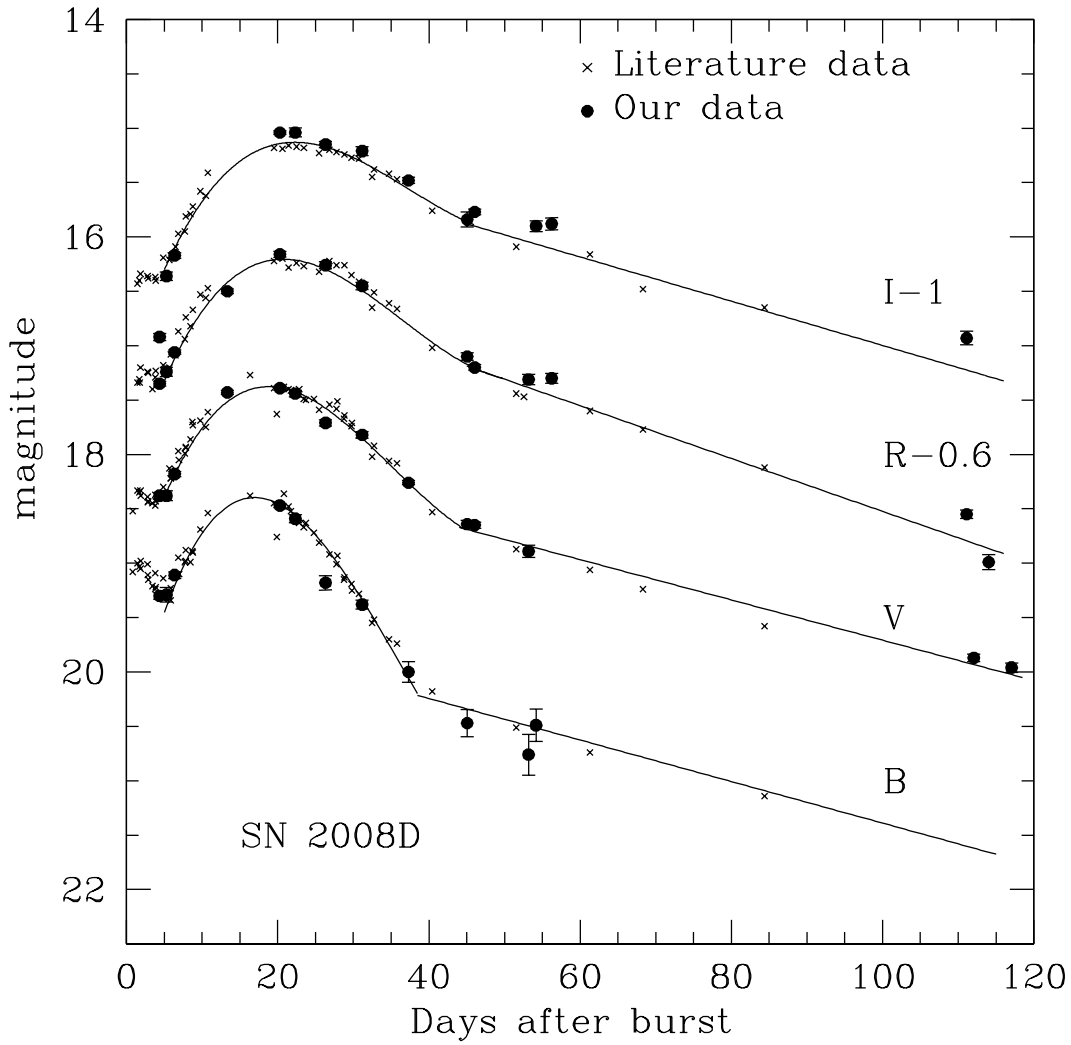


Figure 5.3 *BVRI* lightcurves of SN 2008D. Filled circles are our observations whereas crosses are taken from literature [Malesani et al., 2009; Mazzali et al., 2008; Modjaz et al., 2009]. Dates are given in days after the burst trigger time in the observers frame. The solid line in different bands represent the polynomial trace to the data points.

---

are counted since the time of burst in observer frame. To compare and construct a temporally dense light curve, we also plot the data from literature [Malesani et al., 2009; Mazzali et al., 2008; Modjaz et al., 2009]. Fig. 5.3 indicates that our photometry is consistent with the literature. For SN 2008D our points fill an important gap near maxima in  $V$  and  $R$  band.

The evolution of supernova light can be segmented in three phases – (i) shock breakout phase, (ii) photospheric phase and (iii) Nebular phase. For this particular event we discuss the photospheric and nebular evolution of SN light.

### 5.5.3 Early phase: first 40 days

Both apparent lightcurves illustrate that at shorter wavelengths (say in  $B$ ), the light curves peak at early time and have smaller peak width, whereas at longer wavelengths (in  $I$ ), it peaks at later time and have larger peak width. This trend is also observed in the light curves of type Ibc supernova like SN 2002ap [Pandey et al., 2003; Yoshii et al., 2003] and in the GRB-associated SN 1998bw [Galama et al., 1998].

The temporal variation of visual light roughly resembles the temporal variation of total UVOIR (NUV+Optical+NIR) light of the SN. The maxima of visual light also roughly corresponds the epoch of maxima of UVOIR bolometric light of the transient. The third order polynomial fitting of the early part ( $\lesssim 40$  days) of the visual light curve shows that the maxima occurred at +19.4d. Hence the rise time of SN 2007uy in visual band turns out to be roughly 19.4 day. This is comparable with the rise time derived for hypernova, Type Ic SN 1998bw ( $16.14 \pm 0.08$  days) and optically-normal Type Ib SN 2008D ( $18.82 \pm 0.24$  days), whereas, it is longer than

## 5. THE STRIPPED ENVELOPE SNE 2007UY AND 2008D

---

that of Type Ic SNe 2002ap ( $10.12 \pm 0.20$  days) and 2006aj ( $10.37 \pm 0.14$  days). The measured rise time of SN 2007uy in U band is  $15.13 \pm 0.4$  days whereas in I band it is  $23.09 \pm 1.44$  days. This shows that similar to other Ibc events, SN 2007uy also evolved faster and attains the maxima first in lower wavelength and than in higher wavelengths.

Peak width ( $\Delta d_{0.25}$ ), defined as the width of the light curve, when the SN is fainter by 0.25 mag from its maximum brightness, is also calculated for SN 2007uy. For visual band it is roughly 11 days. This is comparable to the V band peak width of SN 2006aj ( $\Delta d_{0.25} \sim 11.1$  days) and SN 2002ap ( $\Delta d_{0.25} \sim 10.6$  days), but less than engine driven SN 1998bw ( $\Delta d_{0.25} \sim 13.3$  days) and normal Type Ib event SN 2008D ( $\Delta d_{0.25} \sim 18.04$  days).

The post maxima decay rate of SN 2007uy in V and R bands are respectively  $0.058 \pm 0.002$  mag.d<sup>-1</sup> and  $0.042 \pm 0.002$  mag.d<sup>-1</sup>, which corresponds to a post maxima decay ( $\Delta m_{15}$ ) of  $0.87 \pm 0.003$  and  $0.63 \pm 0.03$  mag respectively in V and R band. Here  $\Delta m_{15}$  quantifies the decay in magnitude in 15 days after maxima. For B and U bands value of  $\Delta m_{15}$  are even higher, around 1.2 and 2.1 mag respectively. This is consistent with the predictions of models on SN evolution [Woosley et al., 1999b].

The V and R band decay rates are comparable with the decay rate of Type Ibc events studied by Drout et al. [2011]. However, in the same work it was also indicated that though this kind of exercise can bring the transient inside a larger frame of Type Ibc group, it can never conclude whether the event belongs to the Type Ib, Type Ic or in ‘broad-lined Type Ic’ (Type Ic-BL) category. On the other hand, the spectroscopic study (see §5.8) convinced us that the event neither belongs to the Type Ic nor to class Ic-BL.

Table 5.8 Light curve shape parameters of different core-collapse SNe, measured in *BVRI* photometric passbands. The post-maxima magnitude decay  $\Delta m_{15}$ , peak width  $d_{0.25}$ , pre- $(\alpha_1)$  and post- $(\alpha_2)$  flattening decay rates are derived from the absolute magnitude light curves. We quote uncertainties in rise time, peak magnitudes and decay rates arising from fitting polynomials. The errors are fitting error.

Supernova	Parameters	<i>B</i>	<i>V</i>	<i>R</i>	<i>I</i>	Ref.*
SN 1998bw	Rise time (day)	14.07±0.2	16.14±0.08	17.88±0.12	18.17±0.37	6
	Peak App. Mag.	14.27±0.46	13.74±0.22	13.68±0.29	13.72±0.71	6
	Peak Abs. Mag.	-18.67±0.46	-19.14±0.22	-19.17±0.29	-19.09±0.71	6
	Adopted Ext. (mag)	0.244	0.183	0.154	0.110	1,2
	$\Delta m_{15}$ (mag)	0.56	0.41	0.25	0.18	3
	$\Delta d_{0.25}$ (day)	11.3	13.3	14.4	18.0	3
	$\alpha_1$ (mag.day <sup>-1</sup> )	0.090±0.003	0.062±0.002	0.047±0.002	0.035±0.003	6
	$\alpha_2$ (mag.day <sup>-1</sup> )	0.015±0.001	0.019±0.001	0.020±0.001	0.018±0.001	3
SN 2002ap	Rise time (day)	8.36±0.20	10.12±0.20	13.25±0.14	14.95±0.15	6
	Peak App. Mag.	12.75±0.51	12.11±0.54	12.08±0.32	12.18±0.35	6
	Peak Abs. Mag.	-17.46±0.51	-17.49±0.54	-17.44±0.32	-17.27±0.35	6
	Adopted Ext. (mag)	0.369	0.279	0.209	0.135	3
	$\Delta m_{15}$ (mag)	0.99	0.87	0.73	0.47	3
	$\Delta d_{0.25}$ (day)	7.9	10.6	13.0	15.3	3
	$\alpha_1$ (mag.day <sup>-1</sup> )	0.09±0.003	0.064±0.002	0.047±0.002	0.033±0.002	6
	$\alpha_2$ (mag.day <sup>-1</sup> )	0.0163±0.0001	0.0206±0.0002	0.0177±0.0004	0.0207±0.0002	3
SN 2006aj	Rise time (day)	8.21±0.21	10.37±0.14	11.54±0.07	12.96±0.31	6
	Peak App. Mag.	17.99±0.41	17.50±0.25	17.23±0.11	16.95±0.60	6
	Peak Abs. Mag.	-18.48±0.41	-18.81±0.25	-18.98±0.11	-19.14±0.60	6
	Adopted Ext. (mag)	0.693	0.525	0.437	0.312	4,2
	$\Delta m_{15}$ (mag)	1.55	0.89	0.84	0.73	6
	$\Delta d_{0.25}$ (day)	8.0	11.1	12.9	15.2	6
	$\alpha_1$ (mag.day <sup>-1</sup> )	0.116±0.004	0.066±0.002	0.059±0.002	0.049±0.005	6
	$\alpha_2$ (mag.day <sup>-1</sup> )	--	--	--	--	
SN 2007uy	Rise time (day)	~13.5	15.35±0.23	18.01±0.58	19.09±1.44	6
	Peak App. Mag.	16.74±0.5	15.77±0.5	15.4±1.3	15.17±1.9	6
	Peak Abs. Mag.	-18.6±0.5	-18.8±0.6	-18.8±1.03	-18.5±0.9	6
	Adopted Ext. (mag)	2.95	2.22	1.85	1.32	6
	$\Delta m_{15}$ (mag)	1.2	0.87	0.63	0.60	6
	$\Delta d_{0.25}$ (day)	18.2	22.5	23.01	23.9	6
	$\alpha_1$ (mag.day <sup>-1</sup> )	0.089±0.003	0.049±0.002	0.037±0.004	0.027±0.003	6
	$\alpha_2$ (mag.day <sup>-1</sup> )	0.019±0.001	0.02±0.001	0.022±0.001	0.018±0.002	6
SN 2008D	Rise time (day)	16.93±0.17	18.82±0.24	20.73±0.24	21.67±0.23	6
	Peak App. Mag.	18.39±0.45	17.37±0.57	16.80±0.58	16.14±0.56	6
	Peak Abs. Mag.	-17.28±0.52	-17.51±0.63	-17.64±0.63	-17.74±0.62	6
	Adopted Ext. (mag)	3.303	2.503	2.0867	1.489	5,2
	$\Delta m_{15}$ (mag)	1.0	0.67	0.53	0.37	6
	$\Delta d_{0.25}$ (day)	14.16	18.04	19.01	23.95	6
	$\alpha_1$ (mag.day <sup>-1</sup> )	0.08±0.004	0.06±0.002	0.04±0.002	0.04±0.004	6
	$\alpha_2$ (mag.day <sup>-1</sup> )	0.021±0.001	0.018±0.001	0.022±0.001	0.018±0.002	6

\*References: (1) Schlegel et al. [1998]; (2) Cardelli et al. [1989]; (3) Pandey et al. [2003]; (4) Ferrero et al. [2006]; (5) Malesani et al. [2009]; (6) Present Work

5. THE STRIPPED ENVELOPE SNE 2007UY AND 2008D

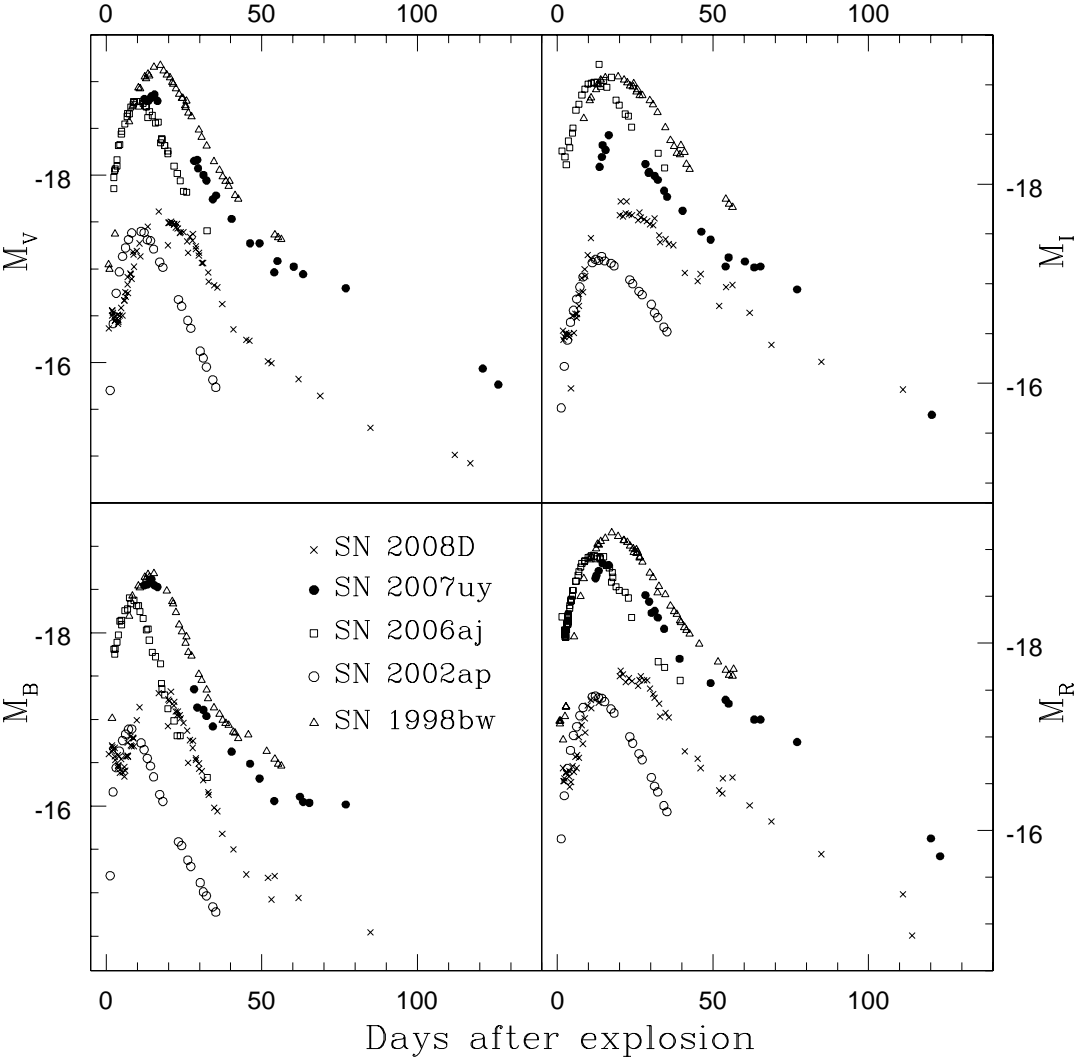


Figure 5.4 Absolute light curves of SN 2007uy. Comparison with SN 2008D and other Type Ibc events.

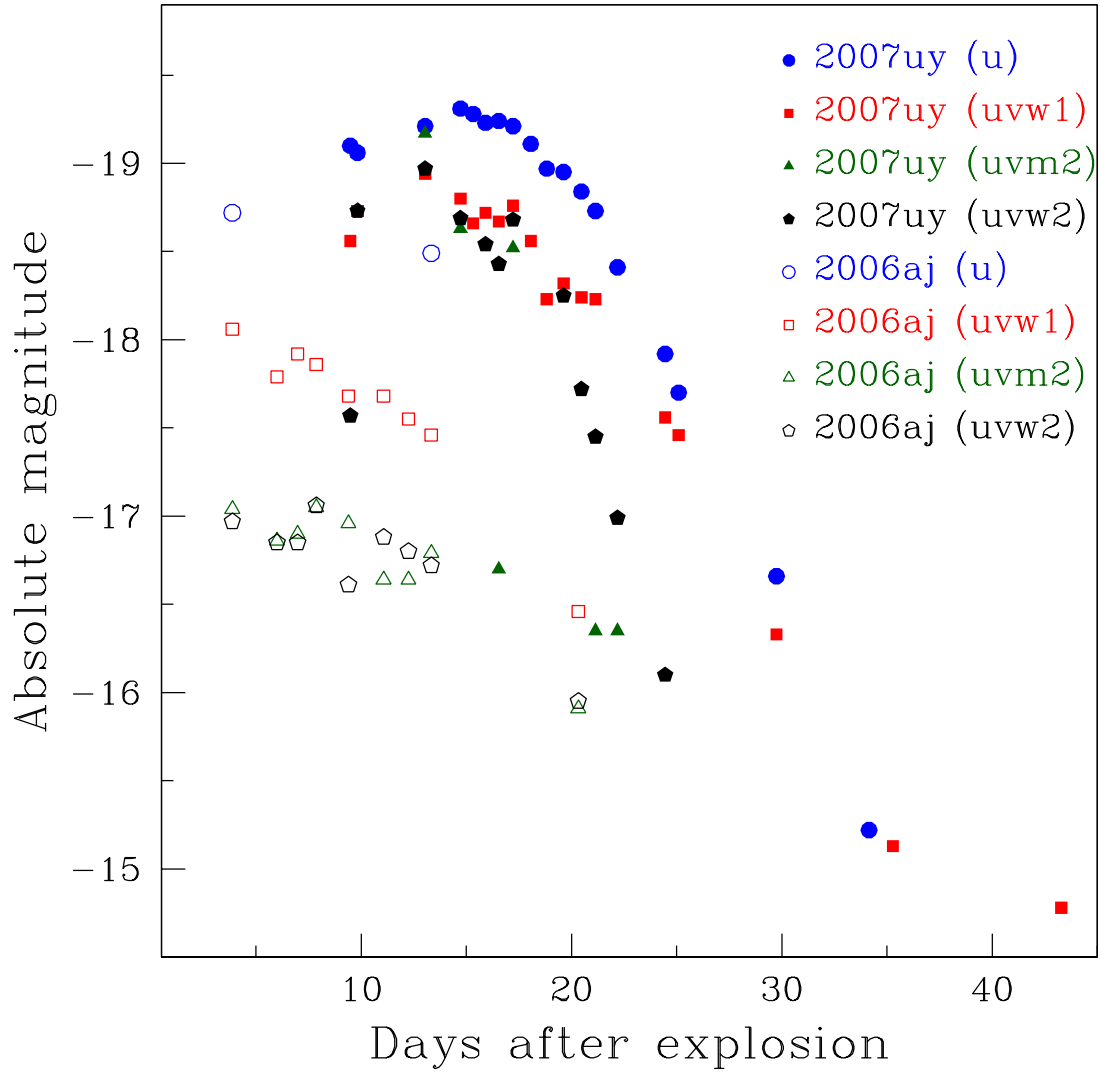


Figure 5.5 NUV and u band absolute light curves of SN 2007uy. Comparison with Type Ic event SN 2006aj. Data for SN 2006aj have been borrowed from Simon et al. (2010).

## 5. THE STRIPPED ENVELOPE SNE 2007UY AND 2008D

---

Adopting the distance modulus of SN 2007uy  $\sim 32.4$  mag and total reddening along the line of sight  $E(B - V) \sim 0.71$  mag (see §5.6) we have computed absolute magnitudes in  $BVRI$  passbands to compare it with other Type Ibc events (Figure 5.4). For relatively redshifted object, like SN 2006aj, the cosmological time dilation factor has been taken care into account to correct the corresponding time scale. In all bands SN 2007uy was intrinsically brighter than normal Type Ib event SN 2008D and Type Ic event SN 2002ap. Though in  $R$  and  $I$  passbands it was a little dimmer than GRB/XRF associated events SNe 2006aj and 1998bw, but in visual and blue bands its peak magnitude is comparable with those two energetic events.

SN 2007uy was luminous in NUV. It was detectable in *Swift*/*uvw2* and *uvm2* images until 24 days, while in *uvw1* and  $u$  filter systems it was detected until 44 days after the burst. In contrary, SN 2008D which was more luminous in X-ray and radio and happened in the same galaxy with almost similar environment [Thöne et al., 2009], was seldom detected in the *Swift* NUV bands. Interestingly XRF060218/SN 2006aj was detected by *Swift* in all NUV bands during same epochs. Figure 5.5 represents a comparison between the NUV and  $u$  absolute magnitudes of SN 2007uy with that of SN 2006aj. The UVOT data for SN 2006aj have been taken from Šimon et al. [2010]. SN 2006aj seems to be dimmer than SN 2007uy. The nature of evolving supernova is clearly visible in all absolute light curves of SN 2007uy. In case of SN 2006aj, nature of an evolving blackbody supernova is reflected in  $u$  and marginally in *uvw1* light curves, whereas photometry of *uvm2* and *uvw2* images show a very shallow linear decay of SN light in NUV range. Linear fit to these data sets shows that post maxima decay rates in these two bands are respectively  $-0.06$  mag.d $^{-1}$  and  $-0.04$  mag.d $^{-1}$ . If all kinds of optical photons are generated through blackbody radiation under similar condition of the ejecta, then post maxima decay

---

rates in these two bands should be much higher than this value (assuming the SN will be optically thick during first 20 days). It was also predicted by [Woosley et al. \[1999a\]](#) through modeling of SN 1998bw spectra in the spectral range between  $U$  and  $I$  passbands. For SN 2006aj, measured decay rate in  $I$  band  $\sim 0.05 \text{ mag.d}^{-1}$  while in  $B$  and  $uvw_1$  bands these are as high as  $\sim 0.10 \text{ mag.d}^{-1}$  and  $0.12 \text{ mag.d}^{-1}$  respectively. Hence the decay rate in NUV bands should be higher. This discrepancy was also noted by [Šimon et al. \[2010\]](#) and was explained as an effect of blackbody radiation [[Panagia, 2003](#)] largely extinct due to increase of opacity of the UV emitting area, which shrinks with time during evolution of the transient.

In contrast, blackbody fitting to the early part of SN 2007uy light, (See [Figure 5.6](#)) shows that envelope of this SN evolved more or less like a blackbody. Here we have plotted the flux, normalized with respect to V band flux, to nullify the effect due to time evolution of angular diameter of the transient. The effect due to dilution of SN envelope is also neglected under first approximation<sup>1</sup>. The temperature of each blackbody is mentioned inside the parenthesis, with a temperature scale 1000K. The one sigma uncertainties are measured by applying the ‘Monte Carlo’ method. The initial temperature of photosphere is  $\sim 8079\text{K}$ . During initial 5 days temperature slightly increased to  $\sim 11005\text{K}$  and then started to decrease with time through a power law with temporal decay index  $\sim 0.56$ , which is comparable with the theoretical prediction (0.5) by [Arnett \[1982\]](#). The initial increment in temperature, followed by a power law decay with time (decay index  $\sim 0.12$ ) was also observed in Type

---

<sup>1</sup>It is worth noting that the measurement of true Temperature of the SN envelope along with the measurement of its distance require a proper estimation of dilution factor through hydrodynamical modeling [[Eastman et al., 1996](#); [Kirshner and Kwan, 1974](#)]. This can only provide a colour temperature for the system along with a true estimation of distance independent of cosmology. The technique was properly applied by [Hamuy et al. \[2001\]](#); [Leonard et al. \[2002b\]](#) and others on Type IIP events. In the present work we provide a rough estimation of overall temperature of SN photosphere and adopted the value of distance obtained through a different approach (§5.6).

## 5. THE STRIPPED ENVELOPE SNE 2007UY AND 2008D

---

Ic SN 2002ap [Vinkó et al., 2004]. Thus we speculate that unlike XRF060218/SN 2006aj, SN 2007uy evolved roughly as a ‘blackbody supernova’ from very initial epoch.

### 5.5.4 Late phase: beyond 50 days

Normally 50 days beyond the explosion, the envelopes of most Type I events start to become optically thin, and hence the light curves start to flatten. In  $B$ ,  $V$ ,  $R$  and  $I$  bands decay rate of SN 2007uy is roughly  $0.017 - 0.018 \text{ mag d}^{-1}$ , whereas in  $U$  band it is  $\sim 0.03 \text{ mag d}^{-1}$ . This decay rate is well similar to the nebular decay rate of Type Ibc events and slightly higher than the decay rate of  $^{56}\text{Co} \rightarrow ^{56}\text{Fe}$  nuclear transition, which is typically  $0.0098 \text{ mag d}^{-1}$ . It is worth mentioning that in Type II SNe, mainly in normal Type IIP events, having huge H shell in the outer surface, the nebular decay rates are comparable with that of  $^{56}\text{Co}$  (Roy et al. 2011a,b and references therein). On the other hand, for low luminosity Type IIP events like SN 2005cs, decay rate during nebular phase ( $\sim 0.0046 \text{ mag d}^{-1}$  in V band during the period 140–320 days) is significantly lower than that of  $^{56}\text{Co}$  [Pastorello et al., 2009]. This was also observed by Elmhamdi et al. [2003b] in normal Type IIP event SN 1999em during its initial ( $\sim$  one month) nebular phase. Utrobin [2007] explained this as an effect due to radiation generated inside the inner warmed ejecta, that propagates through the cool, optically thin outer region and makes the nebular light relatively stable. Relatively high decay in very late epoch ( $t > 300$  days) during the evolution of SN 2005cs was explained as a result either due to (i) dust formation in the SN ejecta, (ii) a lower efficiency of  $\gamma$ -ray trapping due to the decreased density of the ejecta, or due to (iii) cooling of inner ejecta [Pastorello et al., 2009].

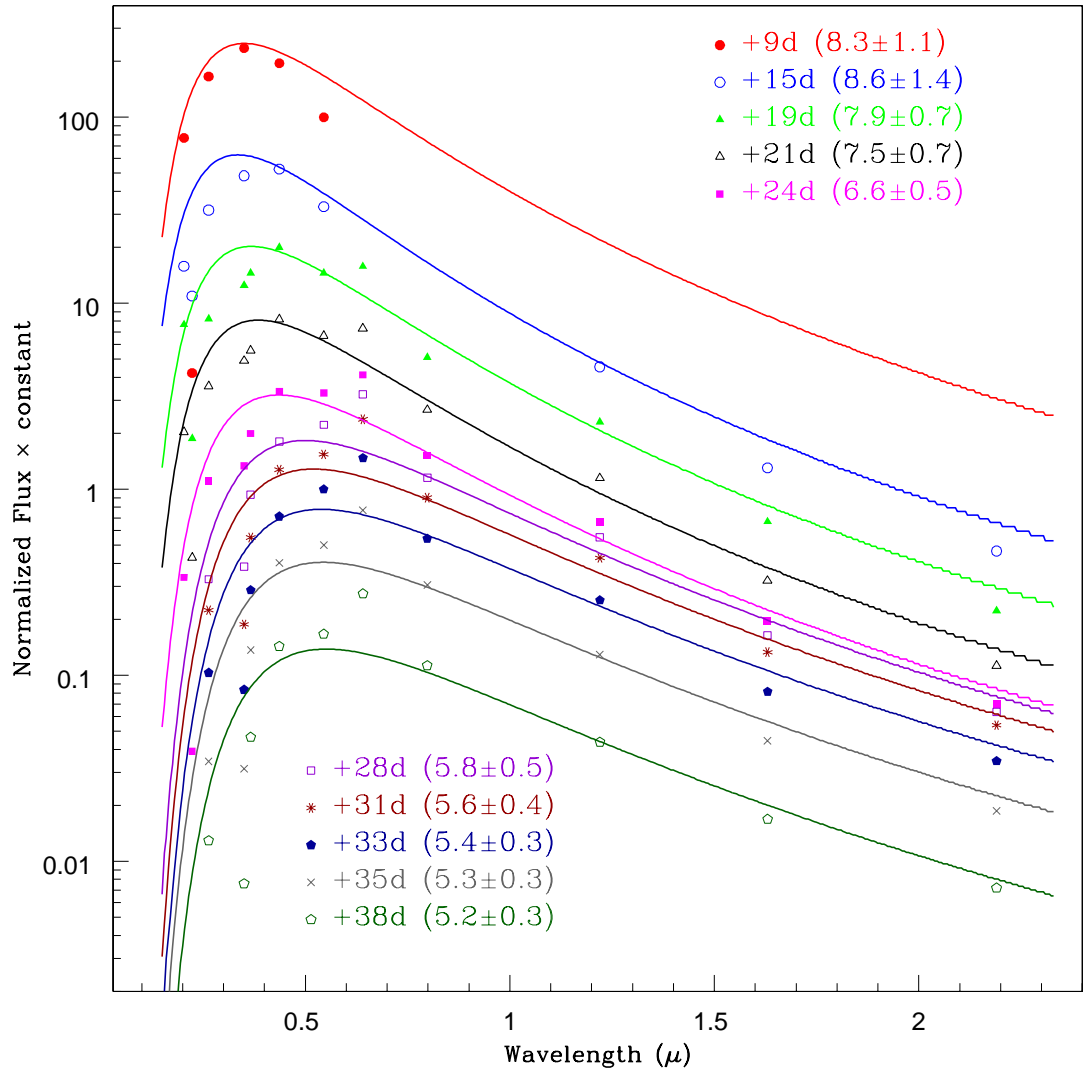


Figure 5.6 Temporal evolution of observed SED of SN 2007uy . The temperature of each blackbody is mentioned inside the parenthesis, with a temperature-scale 1000K. The one sigma uncertainties are measured by applying the ‘Monte Carlo’ method

## 5. THE STRIPPED ENVELOPE SNE 2007UY AND 2008D

---

The optical and NIR nebular light curves of SN 2007uy show sharper decay ( $\sim 0.02 - 0.03 \text{ mag.d}^{-1}$ ) than the canonical decay of radioactive  $^{56}\text{Co}$ . Similar decay rate was also noticed for SN 2002ap [Pandey et al., 2003; Vinkó et al., 2004], which was explained as a leakage of  $\gamma$ -photons from the transparent and less massive SN atmosphere. Dust formation may also be another cause. With increasing time, the newly formed small dust grains in the ejecta can progressively reduce the fluxes of SN in all bands. Though there is a possibility for creation of dust-grain of size  $\lesssim 0.01 \mu\text{m}$  within first 100–300 days in Type I SNe [Nozawa et al., 2011; Smith et al., 2008], this hot grains ( $T \sim 1600\text{K}$ ) would cause an IR excess in SN continuum spectra. Moreover, dust formation should manifest itself by creating a blueshift in the line, increasing with time. Neither excess in continuum, nor the temporal increment in the blueshifts of the spectral lines were observed for SN 2007uy (rather it decreases with time; see §5.8). In fact beyond +50d SN 2007uy started to become bluer (see §5.7), which does not support the dust formation during the period of observation. Thus the possibility of dust formation at the outer shell of the ejecta in early epoch is also unable to explain this deviation.

Here we propose that leakage of  $\gamma$ -photons is the principal cause for rapid decay in light curve of SN 2007uy, like other stripped envelope supernovae. We also admit that this simultaneously depends on the amount of ejected mass ( $M_{ej}$ ) and how fast it gets diluted (optically thin). If  $E_k$  is the kinetic energy of explosion then decay rate of nebular phase is roughly proportional to  $M_{ej}/E_k^{1/2}$  [Valenti et al., 2008a]. So, explosions with higher ejecta mass and kinetic energy or lower mass with low kinetic energy should show similar trend in nebular decay. For e.g., very late time ( $>150$  days after burst) evolutions of SNe 1998bw, 2006aj also show an almost identical decay rate in  $V$ ,  $R$ ,  $I$  bands  $\sim 0.02 \text{ mag.d}^{-1}$  and higher than the decay rate of  $^{56}\text{Co}$

---

[Misra et al., 2011; Patat et al., 2001]. The first one is an explosion with higher mass of ejecta and kinetic energy, while the second shows a lower ejecta mass with smaller amount of kinetic energy. Since nebular phase is powered by radioactive nuclei, the decay rate in nebular phase should be dependent on the amount of mixing of the radioactive nuclei within the ejecta. For Type Ibc events it may be possible that the fraction of radioactive nuclei mixed in the ejecta are comparable, which cause a similar decay rate in nebular phase.

## 5.6 Distance and extinction toward SN 2007uy and SN 2008D.

To determine the bolometric light curve and physical properties of the transient, a correct estimation of the distance and extinction toward the SN is essential.

The host NGC 2770 is a well studied star forming galaxy with 9 redshift independent distance estimations<sup>1</sup>. Out of them 8 measurements used ‘Tully Fisher’ technique and for one IRAS photometry was used. The measured values have a range between 26.1 Mpc and 36.0 Mpc, that corresponds to a weighted mean distance 29.97 Mpc with a standard deviation of 3.48 Mpc. The Hubble flow distance of the host<sup>2</sup>, after correction for the Virgo infall, is estimated as  $29.3 \pm 2.1$  Mpc. Combining the above two measurements, we adopt the weighted mean distance of  $29.5 \pm 1.8$  Mpc, which corresponds to a distance modulus of  $\sim 32.4$  mag.

The Galactic reddening along the line of sight of SN 2007uy as derived from the

---

<sup>1</sup><http://www.ned.ipac.caltech.edu/>

<sup>2</sup>The cosmological model with  $H_0 = 70 \text{ km s}^{-1} \text{ Mpc}^{-1}$ ,  $\Omega_m = 0.3$  and  $\Omega_\Lambda = 0.7$  is assumed throughout this work and the uncertainty corresponds to a local cosmic thermal velocity of  $208 \text{ km s}^{-1}$  [Terry et al., 2002].

## 5. THE STRIPPED ENVELOPE SNE 2007UY AND 2008D

---

100 $\mu$ m all sky dust extinction map [Schlegel et al., 1998] is  $E(B - V) = 0.022 \pm 0.0004$  mag. However, measurement of total extinction along the line of sight of SN 2007uy is a non-trivial task as its host galaxy NGC 2770 has a high inclination angle (see Table 5.1) and the line of sight also contains a large number (about 150) of H $\alpha$  emitters [Gorosabel et al., 2011] which are probably star forming regions making the transient highly extinct due to foreground host material. It was already pointed out by Drout et al. [2011], with sufficient number of Type Ib events, that by and large the more extincted SNe reside in more inclined host galaxies. SN 2007uy is also a highly extinct object which is hosted by a highly inclined ( $\sim 70^\circ$ ) galaxy, though there are exceptions like SN 2004ge.

The isophotal diameter of NGC 2770 is  $d_{25} = 3.567'$ <sup>1</sup>. This corresponds to an apparent radius  $r_{25} = 1.734'$  of the host. On the other hand since NGC 2770 is a spiral galaxy, assuming the star forming regions and SNe sites are distributed on the plane of the disk, the measured values of the deprojected distances of SNe 2007uy, 2008D and 1999eh from the centre of the host are roughly  $0.707'$  ( $\equiv 5.3$ kpc),  $1.210'$  ( $\equiv 9.1$ kpc) and  $1.262'$  ( $\equiv 9.5$ kpc) respectively. This implies  $r_{2007uy} \sim 0.408r_{25}$ ,  $r_{2008D} \sim 0.698r_{25}$  and  $r_{1999eh} \sim 0.728r_{25}$ . Thus all the SNe happen within half-light radius of the host. Moreover according to Thöne et al. [2009] the metallicities of these SNe sites are also comparable with each other ( $8.36 \pm 0.1$ , 8.53 and 8.37 dex respectively for SN 2008D, SN 2007uy, SN 1999eh). So, we can expect that the environments are comparable and the host extinctions should have nearby values. Though the extinction measured by Thöne et al. 2009 for the site of SN 2007uy ( $E(B - V) = 1.4$  mag) is relatively higher than that for SN 2008D ( $E(B - V) = 0.9$  mag) and SN 1999eh ( $E(B - V) = 0.7$  mag).

---

<sup>1</sup><http://leda.univ-lyon1.fr/>

---

The  $E(B - V)$  of the host can be measured from the equivalent width of non-contaminated Na I D absorption dip of the host [Barbon et al., 1990; Poznanski et al., 2012; Richmond et al., 1994; Roy et al., 2011a,b; Turatto et al., 2003] provided the absorption feature does not get saturated. For SN 2007uy we found a prominent impression ‘E’ of He I  $\lambda 5876$  due to associated star forming region, that may contaminate the Na I D absorption dip feature. The two Na I D features are not resolved in the moderate resolution spectra. Using four best spectra (+32d, +58d, +96d and +122d), where unresolved Na I D feature was prominent, we calculate the mean equivalent width of Na I D =  $0.66 \pm 0.04 \text{ \AA}$ . Using this value and applying the expression of Poznanski et al. [2012] for unresolved feature, the derived value of reddening  $E(B - V) = 0.08_{-0.02}^{+0.03}$  mag. This value is too low for a transient hosted by a highly inclined galaxy having large number of foreground intervening medium and only comparable with the line of sight reddening towards the face-on galaxies [Roy et al., 2011a].

The  $E(B - V)$  can also be measured by means of Balmer decrement, usually from  $H\alpha/H\beta$  ratio [Osterbrock, 1989]. Following this methodology Thöne et al. [2009] determined  $E(B - V) \sim 1.4$  mag for SN 2007uy site. This corresponds to total visual extinction  $\sim 4.34$  considering the ratio of total-to-selective extinction ( $R_V$ ) is 3.1. We note that with this value of visual extinction, peak absolute magnitude of SN 2007uy would be  $\sim -21$  mag. This is roughly 3.4 mag brighter than the average peak magnitude of Type Ibc events [Drout et al., 2011] and comparable with over-luminous events, though neither photometric nor spectroscopic evolution of this event matches with those of luminous SNe. It is needless to say that measurement of  $H\alpha/H\beta$  ratio is extensively dependent on the correct flux calibration that may arise as an issue during observation under even in a moderate sky condition and also

## 5. THE STRIPPED ENVELOPE SNE 2007UY AND 2008D

---

while using the average extinction for the site during flux calibration process.

To avoid this problem, we have used the line ratio between N II  $\lambda 6583$  and H $\alpha$  and adopted the empirical relation between  $E(B - V)$  and N II  $\lambda 6583$ /H $\alpha$  found by [Kong et al. \[2002\]](#) after noticing a strong anti-correlation between N II  $\lambda 6583$ /H $\alpha$  ratio and H $\alpha$  equivalent width in a sample of about 74 star forming blue galaxies. They found that since N II  $\lambda 6583$  and H $\alpha$  are two nearby lines, the strength ratio will be less affected due to galactic extinction while behaves like a moderate tracer of  $E(B - V)$  for highly reddened ( $E(B - V) \gtrsim 0.1$  mag) extra-galactic objects. Though this is inefficient for low reddened objects. The +392d spectrum, which has the least impression for SN and mostly contains the emission lines due to H $\alpha$  knots, has been used to calculate the  $E(B - V)$ . The measured value of  $E(B - V)$  by this relation is  $0.71^{+0.27}_{-0.17}$  mag. Since the galactic reddening is more than an order of magnitude less than this value, we anticipate that this is the total reddening along the line of sight. This is similar to the extinction along highly reddened SNe 2004ge and 2007D and also nearby to the mean extinction ( $E(B - V) \sim 0.65$ ) along SN 2008D [[Maud et al., 2009](#)].

From the extinction values of well studied nearby Type Ibc events, [Drout et al. \[2011\]](#) proposed an empirical relation to calculate the host extinction for Type Ibc events using the values of observed  $V - R$  colour of the transient at +10d after  $V$  and  $R$  band maxima. We adopt this formalism and calculate the host extinction for SN 2007uy. The values of host extinctions measured w.r.t the  $V$  and  $R$  band maxima are respectively  $0.79 \pm 0.18$  mag and  $0.82 \pm 0.21$  mag. These measurements are consistent with each other and also consistent with the extinction measured from N II  $\lambda 6583$ /H $\alpha$  ratio.

For this work, we will adopt the weighted average of these three measurements,

---

which implies that the host extinction for SN 2007uy is  $0.78 \pm 0.12$  mag. Since this is order of magnitude higher than the galactic extinction, we adopt this value as a total reddening along the line of sight of SN 2007uy. This corresponds to a total visual extinction ( $A_V$ ) of  $2.4 \pm 0.4$  mag with  $R_V = 3.1$ .

For SN 2008D many people have arrived at different results. For this present work we have adopted the results from [Malesani et al. \[2009\]](#) and it is as indicated in Table 5.8.

## 5.7 Colour Evolution and Bolometric Flux

The reddening-corrected colour evolutions of SNe 2007uy and 2008D are presented in Figure 5.7. For comparison, the colour curves of well-studied SNe 1998bw [[Galama et al., 1998](#)], 2002ap [[Foley et al., 2003](#)], 2006aj [[Ferrero et al., 2006](#); [Misra et al., 2007a](#)] have also been plotted. Though the trend in intrinsic colour evolution of SN 2007uy is similar to that of other events, it always appeared relatively bluer in comparison to other, especially in  $(U - B)_0$  and  $(V - I)_0$  colours. This shows that in overall SN 2007uy is hotter in optical bands. The  $(V - R)_0$  colour of the transient is almost similar to other transients during its photospheric evolution. The evolution of  $(V - R)_0$  colour is well matched with the expected intrinsic colours of Type Ibc events [[Drout et al., 2011](#)]. This shows that our estimation for the host galaxy extinction matches that obtained using the method by [Drout et al. \[2011\]](#). Like other events, SN 2007uy also shows a transition from blue to red during its initial evolution ( $\lesssim +40$ d) and turned bluish in comparison with other events during its nebular evolution ( $\gtrsim +50$ d). This is probably due to fast escape of high energy photons from a SN ejecta which is rapidly becoming optically-thin. The bolometric light curve is

## 5. THE STRIPPED ENVELOPE SNE 2007UY AND 2008D

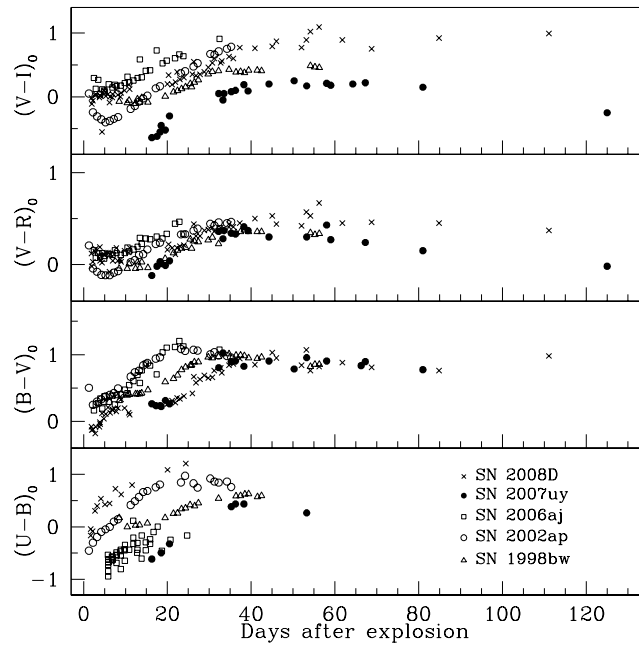


Figure 5.7 Color evolution of SN 2007uy. Comparison with other Type Ibc events

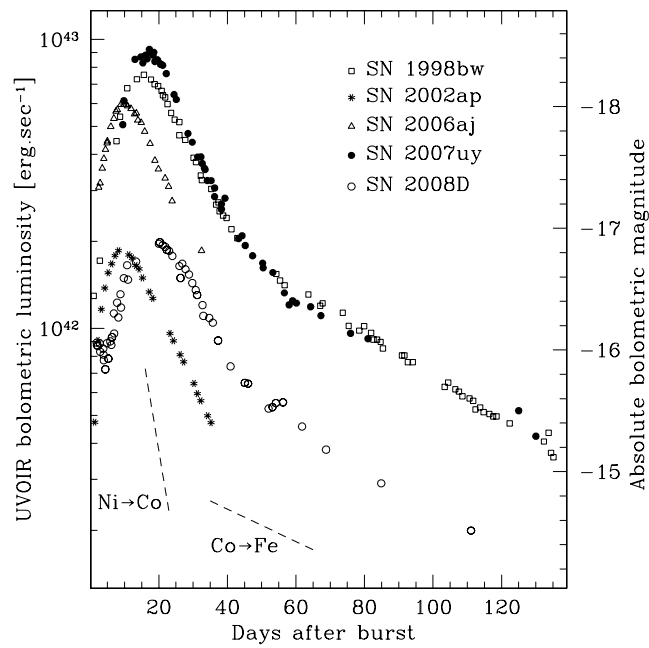


Figure 5.8 The UVOIR bolometric lightcurve of SN 2007uy. Comparison with other Type Ibc events

---

indispensable to calculate the synthesized radioactive  $^{56}\text{Ni}$ , the kinetic energy of the explosion, the amount of mass that was expelled during the burst and hence to understand the nature of the progenitor. The quasi-bolometric UVOIR light curve has been computed from UV, optical and NIR data of the event that is presented by the Figure 5.8. For comparison, UVOIR bolometric light curves of other Type Ibc events have also been plotted. Bolometric fluxes have been computed in those epochs for which visual magnitudes are available. The extinction-corrected magnitudes are first converted into fluxes using zero points given by [Bessell et al. \[1998\]](#) and then the total flux in the UVOIR bands is obtained after a linear interpolation and integration between  $0.203$  and  $2.19\mu\text{m}$ . The JHK contribution during the photospheric phase is calculated from our data, whereas beyond  $+80\text{d}$ , in the nebular phase, due to lack of UV and NIR data, we are not able to make any direct measurement. For many Type Ia supernovae it has been observed that NUV and NIR contribution at the nebular phase is roughly 20% [[Contardo et al., 2000](#); [Leloudas et al., 2009](#)]. So, for beyond 80 days we increase the bolometric flux by 20% to calculate the UVOIR quasi-bolometric light curve beyond  $+80\text{d}$ . Similarly, before the peak, there are few epochs for which we do not have any RI and JHK data. To calculate the magnitudes at those epochs, blackbody spectrum has been fitted to construct the SED for every day (see Figure 5.6) and synthetic magnitudes have been calculated from the SED.

The peak bolometric luminosity of SN 2007uy is about  $9.2 \times 10^{42} \text{ erg s}^{-1}$  which is comparable to that of engine driven hypernovae SN 1998bw ( $\sim 6.3 \times 10^{42} \text{ ergs}^{-1}$ ) and SN 2006aj ( $\sim 5.0 \times 10^{42} \text{ ergs}^{-1}$ ), whereas much higher than broad-lined Type Ic event SN 2002ap ( $\sim 1.9 \times 10^{42} \text{ ergs}^{-1}$ ) and optically-normal Type Ib event SN 2008D ( $\sim 2.0 \times 10^{42} \text{ ergs}^{-1}$ ). Since SN becomes optically thin in nebular phase and the radiation is mostly governed by radioactive power, the nebular luminosity is

## 5. THE STRIPPED ENVELOPE SNE 2007UY AND 2008D

---

expected to be a good tracer of synthesized radioactive nuclei. The nebular light of SN 2007uy is almost similar to that of SN 1998bw and hence the amount of synthesized radioactive nuclei should be comparable. The decay rate is comparable with radioactive decay of  $^{56}\text{Ni}$  to  $^{56}\text{Co}$ , though there is a slight deviation as mentioned in §5.5.4.

The bolometric light can rise due to many reasons such as the explosion of a high mass progenitor, the emergence of a magnetar, the interaction of ejecta with the circumstellar medium (CSM), or possibly due to a combination of these. The interacting feature of this SN with the CSM can be seen from the radio observations (see §5.9). Here we will try to understand, the probable mass of the progenitor, if the SN happen through the explosion in a single evolved star.

### 5.8 Spectroscopic Evolution of SN 2007uy

In order to proceed further with the spectral analysis, the calibrated wavelength of the spectra is converted into rest wavelength of the host galaxy using the prominent  $\text{H}\alpha$  emission line arising from the underlying H II regions of the host galaxy. In this way both the redshifts due to recession and rotation of the galaxy has been accounted for.

All the spectra have been normalized with respect to the peak flux of the underlying  $\text{H}\alpha$  feature and a constant offset has been applied to present them clearly. In Figure 5.9, the spectra of SN 2007uy is presented at 7 such epochs spanning between +17d and +392d post-explosion. The +17d spectrum was taken near maximum light, while +162d and +392d are late nebular phase spectra. The late time (+162d and +392d) spectra have been enlarged by a factor of 2 to clearly specify

---

their features. Spectral features are mainly identified as per previously published line identification lists for Type Ibc SNe (Cox 2000 and references therein), though high line-blending and line-blanketing affect the line detection. The dotted vertical line represents the position of  $H\alpha$ . The absence of Silicon (Si) feature at  $6315\text{\AA}$  as well as the absence of H lines indicate that the spectra of SN 2007uy resembles those of stripped envelope SNe. The lines are highly blended with each other and for most of the lines, the P-Cygni natures are affected by ‘line-blanketing’. The metallic lines like Fe II  $\lambda 4401$ , Mg II  $\lambda 4481$  as well as [Fe II]  $\lambda 5536$ , Na I D  $\lambda\lambda 5890, 5896$  and Ca II  $\lambda\lambda 8496, 8542$  are prominent from the early epochs. The O, Mg and Ca lines starts to appear nearly  $\sim 30$ d after the explosion. The spectra evolved faster than other SNe of Type Ibc’s and except [O I]  $\lambda\lambda 6300, 6364$ ; [Ca II] and [O II], all other features almost faded out within  $+162$ d. This is in contrast with normal Type Ibc SNe, where emission line profiles remain prominent even beyond  $+250$ d after the burst (see for e.g., Cox 2000; Milisavljevic et al. 2010; Modjaz et al. 2008b; Valenti et al. 2011).

The spectral features like [O I]  $\lambda 5577$  and [O I]  $\lambda\lambda 6300, 6364$  show highly blueshifted emission features in the early phase spectra that eventually move to their rest positions in the  $+92$ d phase and onwards. The high blueshift of the spectral features may be a signature of asymmetric explosion. The early blueshift of the spectral lines was also observed in other Type I events, especially in the case of Type Ia events [Maeda et al., 2010a, 2011, 2010b]. In Figure 5.10 we compare the  $+17$ d spectrum of SN 2007uy along with the spectra of Type Ia, Ia-pec, Ibc and Ic events, taken at similar phases. The blueshift in the bluer part of the spectra is clearly visible; and, interestingly the spectrum of SN 2007uy is highly similar to that of Type Ia and Ia-pec events (Maeda et al. 2010a,b; 2011). The characteristics that discriminate

## 5. THE STRIPPED ENVELOPE SNE 2007UY AND 2008D

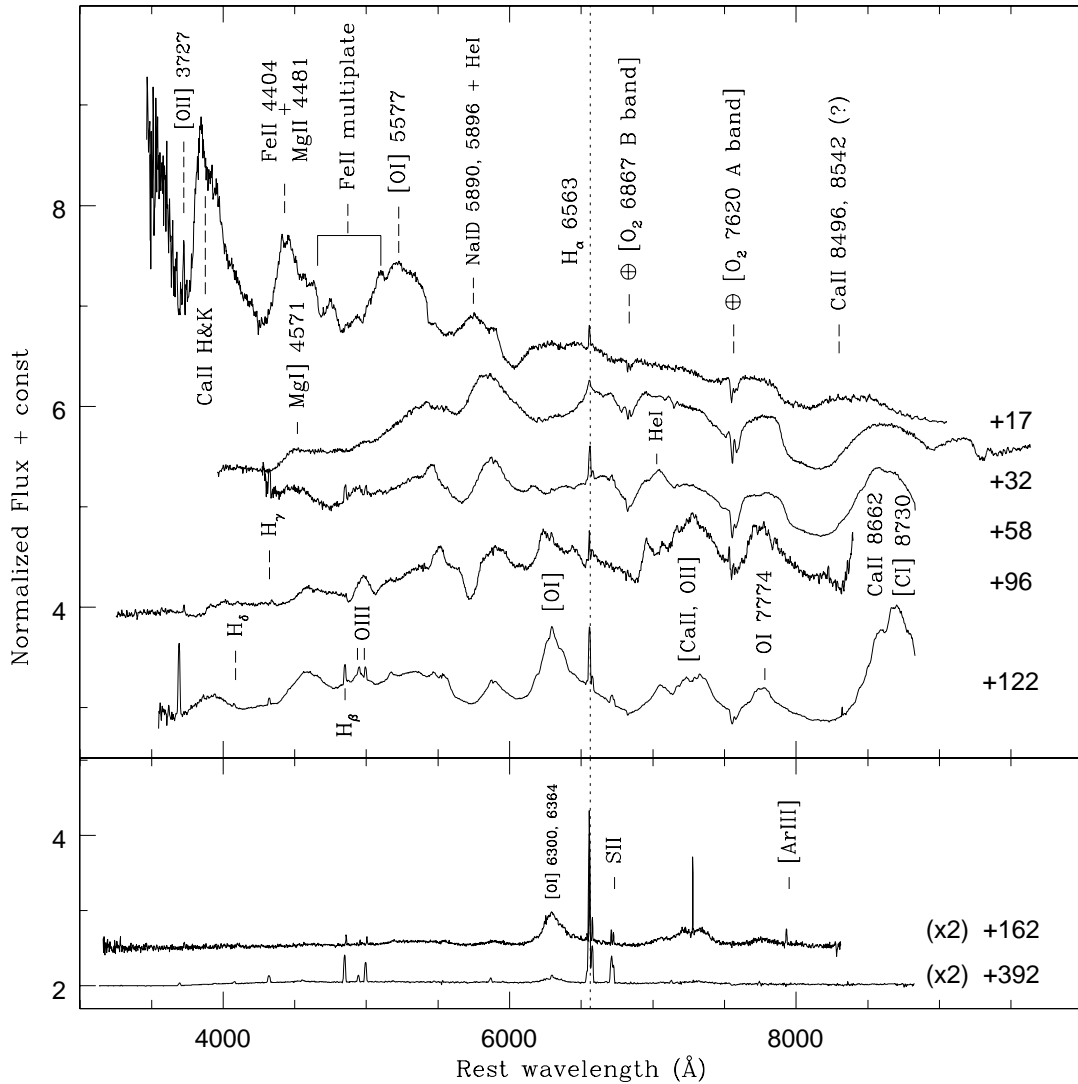


Figure 5.9 Spectroscopic evolution of SN 2007uy. The +162d and +392d spectra have been multiplied by a factor of 2 to enlarge several tiny features.

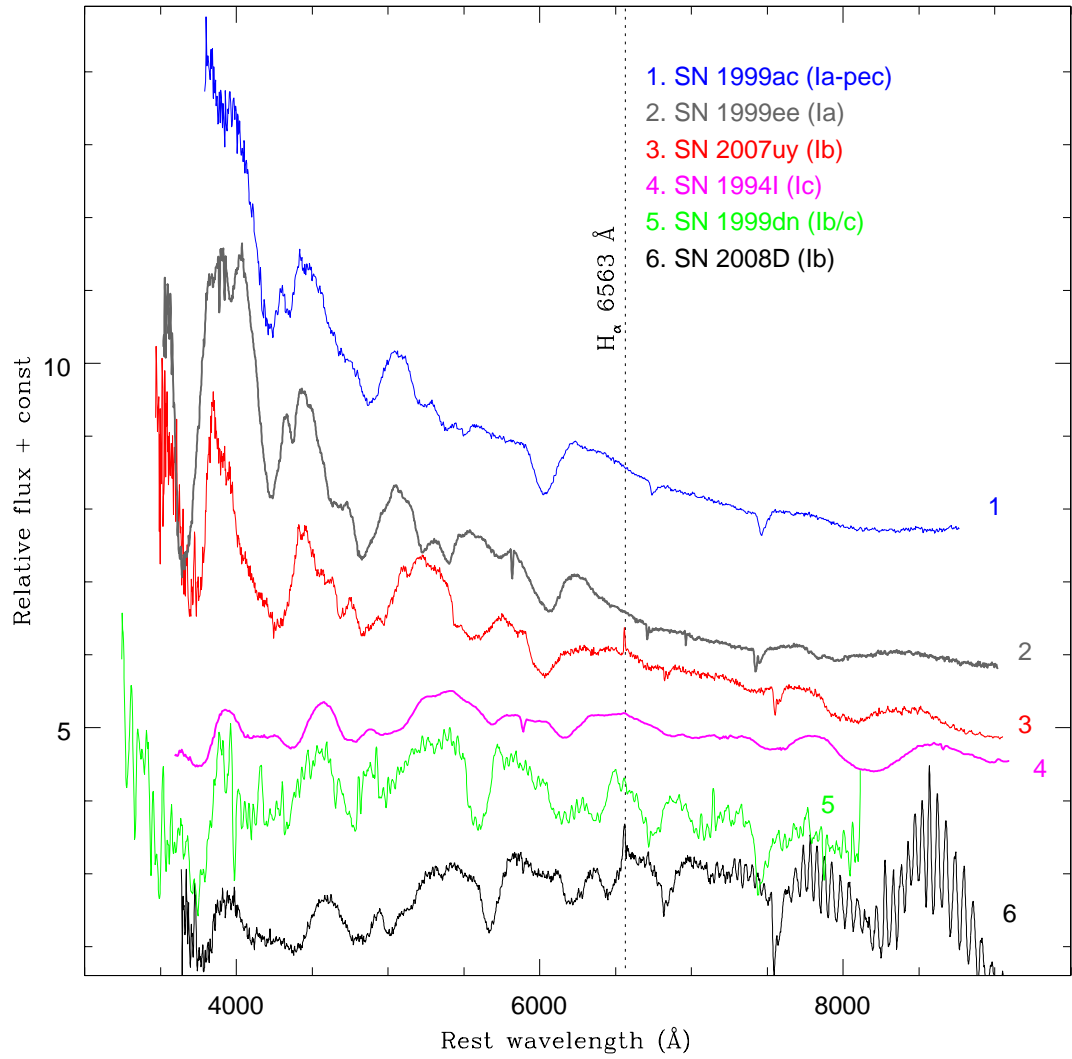


Figure 5.10 Spectroscopic comparison of SN 2007uy with other Type I events near maxima.

## 5. THE STRIPPED ENVELOPE SNE 2007UY AND 2008D

---

SN 2007uy from Type Ia events are the presence of He I lines as well as strong  $H\alpha$ , which indicates that the progenitor is associated with star forming regions which, are the common sites for Type Ibc events. Type Ia events are never found in the star forming regions and hence these two lines never appeared in their spectra. Moreover SN 2007uy is radio luminous (§5.4.1), which is the result of interaction of the SN shock with the circumburst medium. Type Ia progenitors are not surrounded by a dense circumstellar medium and hence very rarely observable in radio in the early epochs [Chomiuk et al., 2012; Weiler et al., 2002].

### 5.8.1 Evolution of some spectral lines: a message regarding asymmetry in SN 2007uy

Figure 5.11 represents the spectral evolution of [Mg I],  $\lambda 4571$ , [Fe II]  $\lambda 5536$ , Na I D  $\lambda 5890$ ,  $\lambda 5896$ , [O I]  $\lambda \lambda 6300, 6364$  and O I  $\lambda 7774$ , which are commonly found in Type Ibc events and in Type IIP SNe. During the initial epochs most of the features are highly asymmetric in reference to their rest velocities / wavelengths. With the exception O I  $\lambda 7774$ , the early blue-shift in the spectral lines is observed in all other line features presented in Figure 5.11.

The early and late phase blue-shifting of the spectral lines can arise for different reasons, e.g., (i) contamination due to other emission lines [Elmhamdi et al., 2003b], (ii) a torus or elongated ejecta with a sufficiently opaque inner portion [Chugai, 1992b; Wang and Hu, 1994] or (iii) due to dust formation [Danziger et al., 1989; Elmhamdi et al., 2003b; Lucy et al., 1989]. For the formation of dust which can block the red wings of the spectral lines, the presence of a cold SN shell is required whereas newly formed dust grains can only increase the continuum part (as discussed

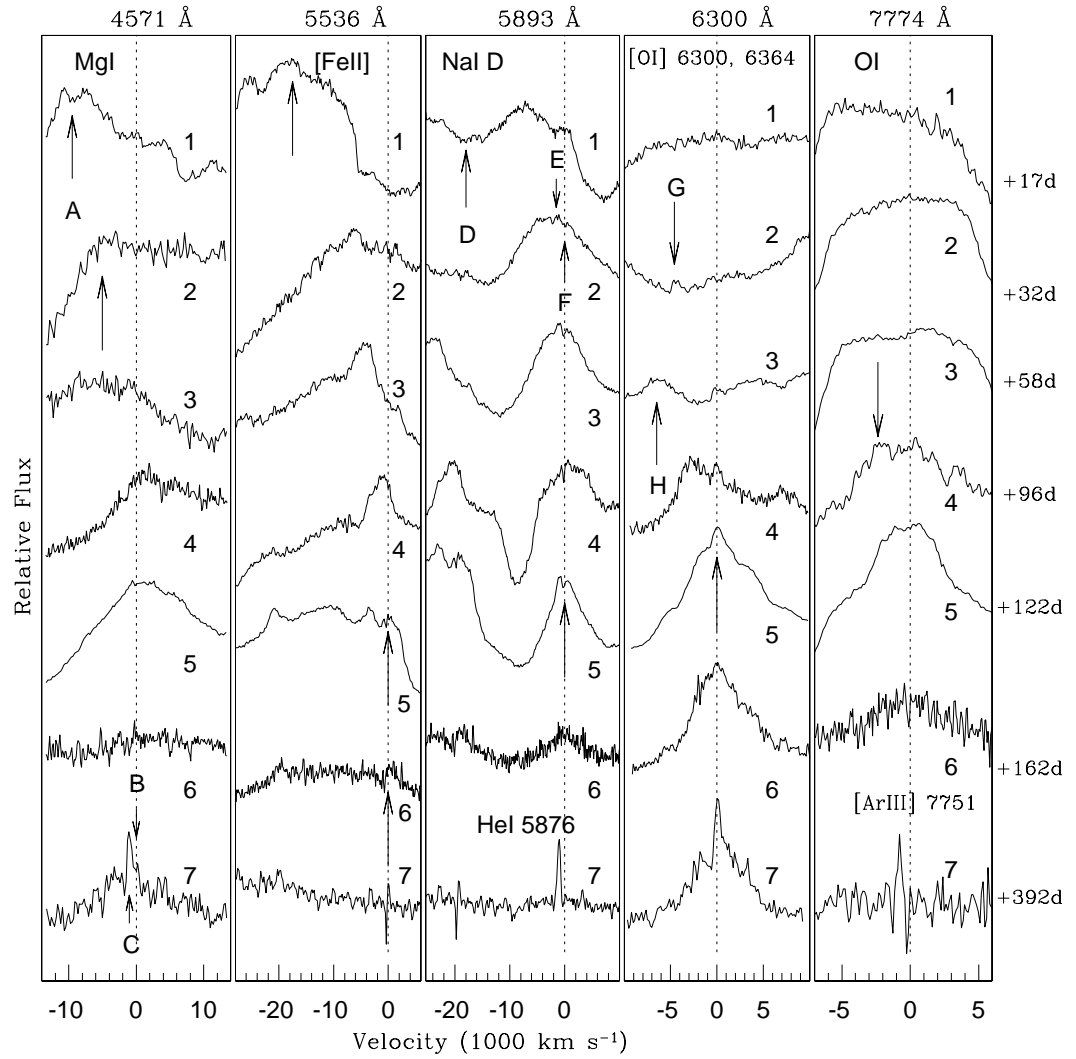


Figure 5.11 Temporal evolution of velocities some spectral lines of SN 2007uy .

## 5. THE STRIPPED ENVELOPE SNE 2007UY AND 2008D

---

in §5.5.4). With a Monte-Carlo simulation [Taubenberger et al. \[2009\]](#) showed that due to the residual opacity of the core ejecta the emission lines can be blueshifted by only about  $30 - 40 \text{ \AA}$ , which is much less than the blueshifts ( $\sim 70 - 100 \text{ \AA}$ ) observed for SN 2007uy. Thus, the third possibility can be ruled out for young ( $\lesssim 100\text{d}$ ) hot SN ejecta.

The lines can also be contaminated by several other lines. In fact there is a high probability that  $\text{Mg I } \lambda 4571$  is contaminated by Fe II multiplets, particularly by Fe II  $\lambda 6293$  [[Elmhamdi et al., 2003b](#)], though [Taubenberger et al. \[2009\]](#) argued against the emergence of this weak iron line.

Asphericity in the SN explosion with a torus or disk-like distribution of different elements, perpendicular to a semi bipolar jet could also be an explanation for the aspheric signature of the lines viz, double-horn emission profile of  $[\text{O I}] \lambda\lambda 6300, 6364$  [[Maeda et al. 2008](#); [Modjaz et al. 2008b](#) and references therein]. The residual opacity in the core of elongated ejecta may also be responsible for the observed blueshift. Optically thick inner ejecta could obstruct the light from the rear side of the SN, creating a flux deficit in the redshifted part of the emission lines [[Chugai, 1992b](#); [Wang and Hu, 1994](#)]. It is worth mentioning that symmetric double-peaked profiles can also be explained by the doublet nature of  $[\text{O I}] \lambda\lambda 6300, 6364$  seen under optically thick conditions leading to a intensity ratio close to one [[Milisavljevic et al., 2010](#)].

The  $[\text{Mg I}] \lambda 4571$  is seen clearly in +35d spectrum as a broad (FWHM  $\sim 185 \text{ \AA}$ ), highly blue shifted ( $\sim 71 \text{ \AA}$ ) emission peak that corresponds to  $\sim 4660 \text{ km s}^{-1}$  blueshifted velocity of the emitting region projected onto the line of sight. The ‘double-horn’ feature marked with **A** at the extreme blue end, is also noticed in +17d spectrum. The  $[\text{Mg I}]$  feature starts to move towards its rest wavelength after its first appearance at +32d and remains as a broad emission peak (FWHM  $\sim 205 \text{ \AA}$ ) until +122d

---

with the emission peak at zero velocity. This broad feature almost disappears in the +162d spectrum and remains as a tiny feature marked as B in the deep nebular spectrum obtained on +392d. The feature B is actually blended with a relatively blue shifted broad emission feature C. After deblending these two features, we marked the feature C as Ba II  $\lambda 4554$  [Cox, 2000].

The appearance of the extremely blueshifted (velocity  $\sim 17482 \text{ km s}^{-1}$ ) emission peak of the blended line of [O I]  $\lambda 5577$ , [Fe II]  $\lambda 5536$  and [Co II]  $\lambda 5526$  at +17d can be seen clearly. A similar blueshifted emission was initially identified as [O I]  $\lambda 5577$  for SN 1993J [Filippenko et al., 1994; Spyromilio, 1994; Wang and Hu, 1994] and for SN 2007uy [Milisavljevic et al., 2010], although the study of Houck and Fransson [1996] showed that this emission is a blend of [O I], [Fe II] and [Co II]. Over the time this feature developed and started to shift toward its rest wavelength from +122d onwards. This confirms the prediction of Houck and Fransson [1996] and establishes this emission line as a blend. Similar to [Mg I], [Fe II]  $\lambda 5536$  also showed a symmetric emission profile at around zero velocity in late epoch ( $\gtrsim 122$ d) spectra. Interestingly from the +122d (labeled by 5 in the second panel, from left, in Figure 5.11) the intensity of this blended line drastically dropped down. Like SN 2007uy, the blueshifted emission peak of [O I]  $\lambda 5577$  in the late time evolution of SN ejecta is commonly observed in many Type Ibc events, like SNe 1993J, 2004ao, 2006T, 2008D, 2008ax and 2008bo [Milisavljevic et al., 2010], but in none of the cases corresponding redshifted component was found.

The Na I D feature is more or less a perfect P-Cygni profile, nonetheless it also shows a highly blueshifted (velocity  $\sim 7697 \text{ km s}^{-1}$ ) emission peak, possibly blended with the He I  $\lambda 5876$  emission feature. The corresponding He I absorption dip is marked as D at +17d. The velocity drops down to about  $1933 \text{ km s}^{-1}$  at +32d and

## 5. THE STRIPPED ENVELOPE SNE 2007UY AND 2008D

---

the feature becomes almost P-Cygni from +58d. Na I D feature is absent in +392d spectrum and He I  $\lambda 5876$  emission feature of the underlying star forming region is clearly visible at its rest wavelength. A careful inspection shows the existence of a tiny emission peak E and an absorption dip F at ‘zero velocity’, starting from the initial epoch (+32d). We speculate E as an impression of He I, while F as a footprint of intervening Na I D gas of the host galaxy. There are two tiny absorption features around E – one is at right F and other at left, about  $2000 \text{ km s}^{-1}$  blueshifted w.r.t F that is equal to the redshift of the host. Hence the possibility of Na I D impressions due to host (feature F) and Milky Way (blueshifted feature) can not be ruled out.

The [O I]  $\lambda\lambda 6300, 6364$  is the most studied emission line in the context of asymmetric nature of Type Ibc explosions. Different geometries of oxygen ejecta have been proposed as origin of observed line profiles of the doublet – (i) a radially expanding spherical shell of oxygen gas produces a flat-topped profile, (ii) a filled uniform sphere produces a parabolic profile, while (iii) a cylindrical ring or torus, that expands in the equatorial plane along the line of sight gives rise to a ‘double horned’ profile where the bulk of the emitting gas is located at the projected expansion velocity ( $\pm v$ ) of the torus and a jet-like ejection of matter along the direction, perpendicular to the line of sight. The ‘ $\pm$ ’ sign represents respectively the red and blueshifted projected velocity of the torus (Maeda et al. 2008; Modjaz et al. 2008b and references therein). Alternatively it can be interpreted as an impression of doublet nature of [O I]  $\lambda\lambda 6300, 6364$ , seen under optically thick environment [Milisavljevic et al., 2010]. For SN 2007uy, we found that [O I]  $\lambda 6300$ , starts to develop from +32d spectrum as a tiny blueshifted (velocity  $\sim 5839 \text{ km s}^{-1}$ ) emission peak G. By +58d this peak moves to its rest wavelength as well as a second peak H is generated at the bluer end. Velocity of this emission peak with respect to rest

---

position of [O I]  $\lambda\lambda 6300, 6364$  is  $\sim 7732 \text{ km s}^{-1}$ . This corresponds to a wavelength separation of about  $163 \text{ \AA}$ . At +96d this separation has been reduced to about  $64 \text{ \AA}$ , but in +122d, +162d and +392d spectra the profile becomes almost symmetrical around ‘zero velocity’. This represents an uniform spherical distribution of [O I]  $\lambda\lambda 6300, 6364$  from +122d onward. Since G and H do not appear simultaneously, their internal separation is varying with time and the intensity ratio between blue and red wing of double horn feature does not approach toward 3:1 with time; we rule out the possibility of appearance of doublet nature of [O I]  $\lambda\lambda 6300, 6364$  in the form of a double horn profile, at least for this particular case. Since the features started to appear from very early phase, the The jet and disk/torus-like scenario [Maeda et al., 2008] will also not be able to explain the generation of symmetric [O I] profile from two separate [O I]  $\lambda 6300$  emitting regions. Similarly ‘Flat-top’ scenario is also not possible. The appearance of a blue shifted emission peak, keeping the other component at the zero velocity was also observed in the late time spectra of events like SNe 1990B, 1993J, 1996N, 1996cb, 2004dk, 2005bf, 2007gr, 2008bo and 2008D [Milisavljevic et al., 2010]. In many cases fragments in between two peaks were also observed. To explain it as a result of aspheric explosion velocity of the progenitor should be  $\sim 2000 \text{ km s}^{-1}$  preferentially toward the observer, which is hard to imagine for a large number of objects [Milisavljevic et al., 2010]. Although the fragmented O I  $\lambda\lambda 6300, 6364$  profile of SN 2009jf can be explained completely as a result of asymmetric explosion with an off-axis O I core surrounded by clumps in an uniformly distributed O I within SN ejecta [Valenti et al., 2011].

Unlike blended [O I]  $\lambda 5577$  and [O I]  $\lambda\lambda 6300, 6364$ ; O I  $\lambda 7774$  feature, shown in the right most panel of Figure 5.11, developed as a symmetrical flat-topped peak, centered around ‘zero velocity’. Though the present spectra do not cover the emer-

## 5. THE STRIPPED ENVELOPE SNE 2007UY AND 2008D

---

gence and development of O I  $\lambda 7774$  line explicitly, but they give a clear indication regarding the development of this particular line at around +96d from a completely featureless part of the spectrum. At +122d it became prominent, though it was not sustained in +162d spectrum. The flat-topped peak is a clear indication toward a shell-like structure of the line emitting region. A rapid dilution of the line emitting region is possibly responsible for the sudden decrease of line intensity. In +392d spectrum impression of O I  $\lambda 7774$  is completely absent, rather we found the impression of [Ar III]  $\lambda 7751$  at its rest wavelength, about  $1000 \text{ km s}^{-1}$  blue shifted with respect to O I  $\lambda 7774$  in velocity domain.

From above discussion it is clear that the velocity profiles of different line forming regions are not identical for SN 2007uy. Hence we propose that the distribution of  $^{56}\text{Ni}$  probably did not influence the distribution of different material inside the ejecta of SN 2007uy, otherwise the evolution of all material would be of similar. In the progenitors of Type Ib SNe the outer part of the ejecta are abundant with light elements, e.g., He ( $\gtrsim 95\%$ ) and O ( $\sim 1.6\%$ ) while relatively inner portion mostly contains the O ( $\sim 60\%$ ) along with relatively heavier ions like Mg and Na ( $\sim 10 - 11\%$ ), whereas the inner most core of the ejecta mainly contains the heavy elements like  $^{56}\text{Ni}$  ( $\sim 90\%$ ) [Shigeyama et al., 1990]. From the geometry of line profiles [Modjaz et al., 2008b], we propose that ions of O I  $\lambda 7774$  line were distributed inside the ejecta in the form of a shell whereas Na I D and Mg ions were concentrated toward the inner portion of the ejecta with a roughly spherical distribution. Evolution of blended [O II]  $\lambda 5577$  line and [O II]  $\lambda 6300$  line are especially interesting. The projected velocities of the features G and H show a power law profile with temporal decay index respectively  $-5.8$  and  $-1.6$  where as decay index of [Mg I], Na I D and [O II]  $\lambda 5577$  blend (rest wavelength  $\sim 5540 \text{ \AA}$ ) are respectively  $-1.5$ ,  $-1.6$ ,  $-1.3$ .

---

We also note that during the entire motion of **G**, its FWHM remain constant at  $\sim 20$  Å while that of **H** decreased from 66 Å at +58d to 41 Å at +96d. Interestingly, the [O II]  $\lambda 5577$  blend shows very tiny feature (FWHM  $\sim 41$  Å) at +32d, before the emergence of feature **H** and became prominent (FWHM  $\sim 63 - 68$  Å) in the +58d and +96d during the appearance of feature **H** and again shrink to the tiny feature with FWHM  $\sim 34$  Å at +122d when **G** and **H** merged together. This confirms that the regions which are forming the lines [O II]  $\lambda 5577$  blend, feature **H**, [Mg I] and Na I D are ‘attached’ with each other and may be originated from the core portion of the ejecta while the feature **G** is ‘detached’ from the core portion of the ejecta originated due to some other mechanism. Though beyond +122d **G** and **H** combined with each other.

Feature **G** is plausibly a high velocity component of [O I]  $\lambda 6300$  line forming region that was splinted-out from the outer surface of a rapidly rotating progenitor, during its death, with a projected velocity  $\sim 4400$  km s $^{-1}$  (at +32d) along the line of sight. With time the effect of rotation rapidly goes away as a power-law (with decay index  $\sim -5.8$ ) and the high velocity region started to get a roughly spherical symmetry and moves ahead with other shells of the ejecta. Since the FWHM of **G** did not change significantly during its evolution, the possibility of a continuous flow of matter along the direction of the motion of this high velocity component in a jet-like structure can not be ruled out. By the time ( $\sim +122$ d) **H** catches **G** (or both settle down to a constant velocity) and starts to move in a spherically symmetric manner, the ejecta becomes sufficiently cool. Our photometric calculation shows that temperature of this ejecta should asymptotically reach below 5000K (see Figure 5.6). In a simulation on forbidden lines in astrophysical-jets [Hartigan et al. \[2004\]](#) showed that below 5000K the strength of [O I]  $\lambda 5577$  becomes very little in

## 5. THE STRIPPED ENVELOPE SNE 2007UY AND 2008D

---

comparison to that of [O I]  $\lambda 6300$  ( $\lesssim 0.1$ ), even with a moderate electron number density (see Figure 9 of [Hartigan et al. 2004](#)). Here we speculate that this would be the reason for disappearance of [O I]  $\lambda 5577$  line at sometime in between +96 and +122d.

The spectral evolution at the locations of the most prominent He I lines is displayed in Figure 5.12. He I  $\lambda\lambda$  6678, 7065 and 7281 are the strongest and, at the same time, most isolated He lines in the optical spectrum of a SN and are thus often used to distinguish between a SN Ib and Ic. In contrast, He I  $\lambda$  5876 is often blended with Na I D (Figure 5.11), a line that also appears in SNe Ic, and He I  $\lambda$  4471 is in a region of the spectrum with other overlapping transitions, including Fe lines. Our spectrum at maximum light (+17d) does not show any trace of He in any reasonable velocities. He I  $\lambda$  7065 appears 15 days later at a velocity of  $\sim 12000$  km s $^{-1}$  (although the line is blended with the telluric B-band). In the same spectrum we do not see any other credible He feature. The same holds for the spectrum at +58d, where He I  $\lambda$  7065 has decelerated to 10000 km s $^{-1}$ . He I  $\lambda\lambda$  6678, 7281 finally appear in the +96d spectrum in a consistent velocity with He I  $\lambda$  7065 ( $\sim 7000$  km s $^{-1}$ ). Figure 5.12 also shows the region around 6000 Å. This region is dominated by an absorption feature that is usually attributed to Si II  $\lambda$  6355 in most Type I SNe. Adopting this identification, this line decelerates from  $\sim 15000$  km s $^{-1}$  at +17d to  $\sim 10000$  km s $^{-1}$  at +96d. What is striking, however, is the appearance of this feature in our second spectrum (+32d) where it has become very strong and broad. It is obvious that this absorption cannot be caused by Si only (it extends to negative velocities) but it must be a blend with more features. Attributing this to He I  $\lambda$  6678 is of course a possibility. However, this line would have to appear at very high velocities in order to appear blended with the Si line

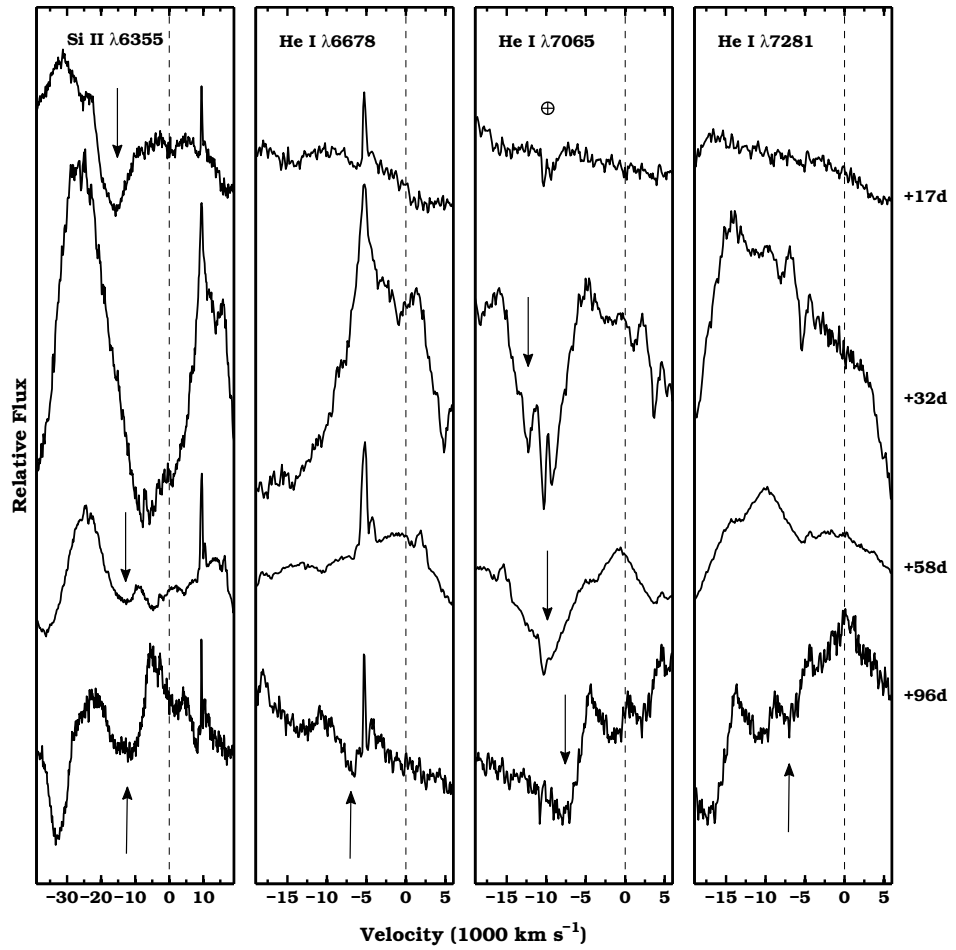


Figure 5.12 Temporal evolution of velocities of SiII and HeI spectral features in SN 2007uy .

(in most SNe Ib, these two features are clearly distinguishable). In addition, the line would have to be very strong and that appears to be in conflict both with the velocity and strength of the only other He I line detected in this spectrum (He I  $\lambda$  7065) and with the sudden disappearance of this feature in the next spectrum. If we attribute the (now weak) feature on the right of Si II  $\lambda$  6355 to He I  $\lambda$  6678 in the +58 spectrum, this would have to be at  $\sim 5000$  km/sec, i.e., a velocity inconsistent with the one inferred by He I  $\lambda$  7065 at the same epoch. In general, we note that the appearance and disappearance of this deep trough at  $6000 \text{ \AA}$  is rather unusual.

### 5.9 Modeling of SN 2007uy: Optical and Radio light curve

To determine the physical parameters of the exploding star, modeling of UVOIR bolometric light is essential. In addition to that, to quantify the interaction with circumstellar medium, modeling of radio data is also required.

#### 5.9.1 Optical data modeling

To derive the physical parameters, we have followed the methodology of [Valenti et al. \[2008a\]](#), i.e. the early and nebular phase have been modeled separately. For  $t \lesssim 30$  days past explosion, the ejecta is presumably optically thick and the model assumes a homologous expansion with a spherical symmetry and all radioactive  $^{56}\text{Ni}$  is located in the centre. It also assumes that the radius of the expanding shell is much higher than the radius of the progenitor, optical opacity  $\kappa_{opt}$  is  $\sim 0.06 \text{ cm}^2\text{g}^{-1}$  and remain constant through out its evolution [[Maeda et al., 2003](#)] and diffusion

---

approximation is valid for the photons [Arnett, 1982]. The theory was originally developed by Arnett [1982] for Type Ia events, after considering the heating only due to  $^{56}\text{Ni} \rightarrow ^{56}\text{Co}$  conversion, which was further improved by Valenti et al. [2008a] considering the contribution due to  $^{56}\text{Co} \rightarrow ^{56}\text{Fe}$  conversion and was also adopted to explain successfully the bolometric evolution of stripped envelope SNe [Benetti et al., 2011; Olivares E. et al., 2012; Pignata et al., 2011; Valenti et al., 2008a, 2011]. In the nebular phase (beyond  $\gtrsim 60$  days), ejecta becomes optically thin and the emitted luminosity is powered by three sources – instantaneous energy of the  $\gamma$ -rays generated during the  $^{56}\text{Co}$  decay, energy of the  $\gamma$ -rays coming from the electron-positron annihilation and due to the kinetic energy of the positrons [Cappellaro et al., 1997; Sutherland and Wheeler, 1984]. This information can be used to model the nebular light [Valenti et al., 2008a]. Moreover Maeda et al. [2003] noted the necessity of low and high  $\gamma$ -ray trapping at early and late time respectively, which was enabled by dividing the ejecta into two components – a high-density inner region and a low-density outer region. The outer region dominates the total emission mechanism at early epochs, i.e. in the optically thick regime, and emission from the inner region with higher  $\gamma$ -ray opacity, dominates the nebular phase. Adopting all these possibilities Valenti et al. [2008a] proposed the model for Type Ibc events.

Optical modeling, as mentioned above, returns the values of four free parameters used to fit the bolometric light curve of SN 2007uy. These are – the total mass of the ejected material ( $M_{ej}$ ), the total mass of  $^{56}\text{Ni}$  produced in the envelope ( $M_{Ni}$ ), the mass fraction of the inner ejecta component ( $f_M$ ) and the fraction of kinetic energy contributed by the inner component ( $f_E$ ). While fitting, the methodology of Olivares E. et al. [2012] was applied. To break the degeneracy between kinetic energy and ejected mass the expression for velocity at peak luminosity [Arnett, 1982] has

## 5. THE STRIPPED ENVELOPE SNE 2007UY AND 2008D

---

been used (also see the equation 2 of [Valenti et al. 2008a](#) and equation 3 of [Olivares E. et al. 2012](#)).

Velocity of the ejecta are measured from the blue shifts of the absorption dips of the P-Cygni profiles, but due to heavy line blanketing identification of photospheric lines are not trivial and also the possibility to get the undisturbed lines is very less. Our first spectrum, taken near maxima, contains the He I  $\lambda 5876$  line, with a considerable blue shifted absorption dip. The measured velocity corresponding to this blue shift is roughly  $15200 \text{ km s}^{-1}$ . Assuming the He shells to be marginally detached from the photosphere, we can constrain the upper limit of the photospheric velocity ( $v_{ph}$ ) within above value.

The parameters obtained after modeling the observed bolometric light of this event are respectively follows :  $M_{ej} \sim 2.0M_{\odot}$ ,  $M_{Ni} \sim 0.4M_{\odot}$ ,  $f_M \sim 0.26$  and  $f_E \sim 0.002$ . Since peak velocity and total ejected mass are related with Kinetic energy ( $E_K$ ) of entire ejecta by the expression:

$$E_K = [(5/6) M_{ej} (1 - f_M) v_{ph}^2]/(1 - f_E),$$

the kinetic energy of the ejecta turned out to be  $E_K \sim 5.7 \times 10^{51}$  ergs. The amount of ejected mass and the explosion energy are comparable with the events like SNe 1994I, 2002ap and 2006aj. The fitted model is presented in Figure 5.13. Using a statistically large number of samples [Drout et al. \[2011\]](#) showed that the absolute R-band magnitudes of Type Ibc events are directly related with the  $^{56}\text{Ni}$  production through some empirical relation. The absolute peak R-band magnitude of SN 2007uy is  $-18.8 \pm 1.3$  mag. Then, applying the above mentioned relation, we found that the produced Ni mass is  $0.26_{-0.18}^{+0.62}M_{\odot}$ . Hence the finding of Ni mass is consistent

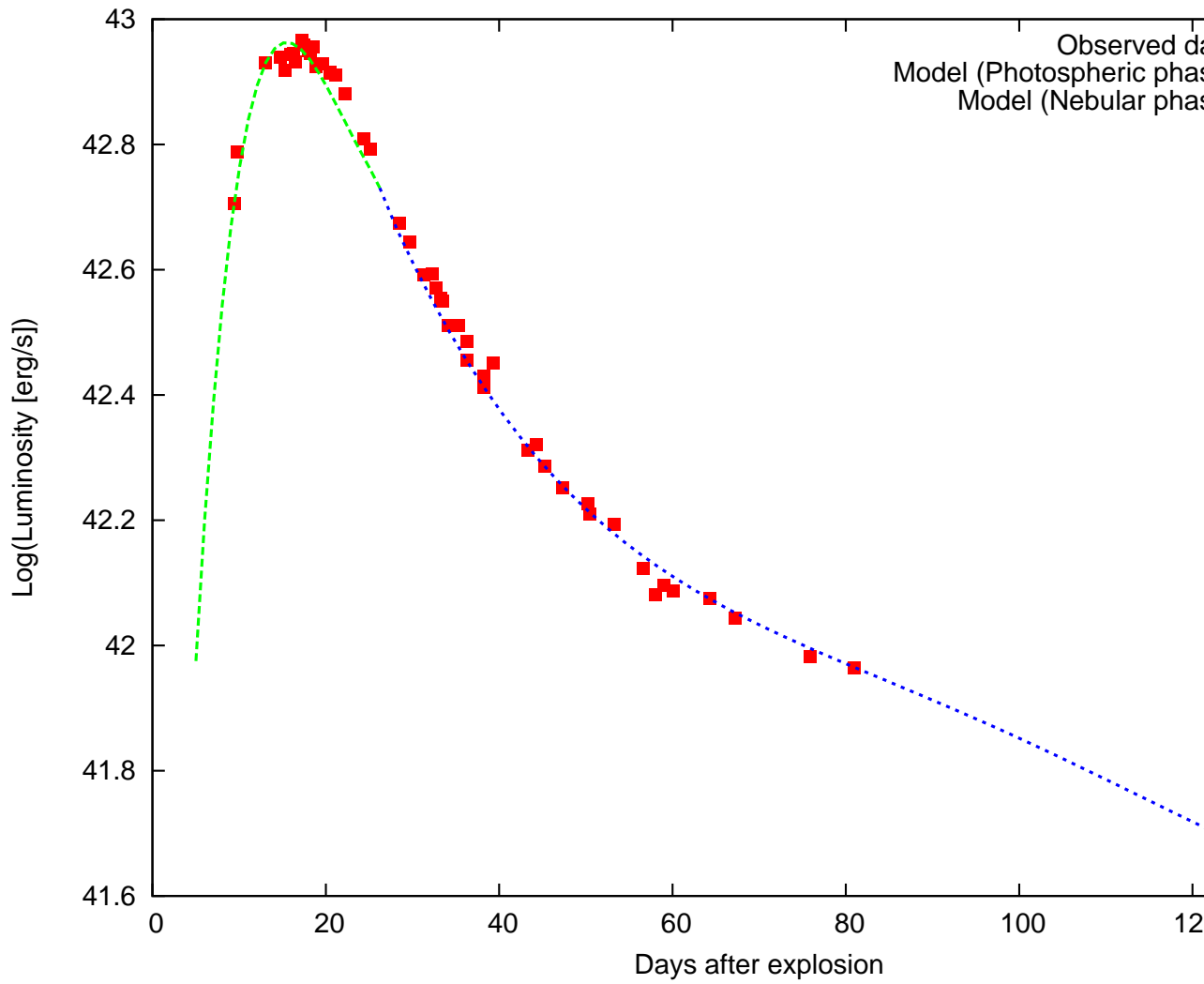


Figure 5.13 The modeled UVOIR bolometric light curve of SN 2007uy. The red dots are bolometric luminosity measured from UVOIR observation whereas the dotted curves are theoretical models. The green curve is for photospheric phase, while the blue curve is for nebular phase. See text for more detail.

with the larger sample.

### 5.9.2 Radio data modeling

The radio light curve can be explained in terms of evolution of the ejecta, which further determines the shape of the spectrum and evolution of its peak with time and hence the nature of the light curves [Sari et al., 1998; Wijers and Galama, 1999]. It can also be explained by Synchrotron Self Absorption (SSA) with high brightness temperature and/or by a Free Free Absorption (FFA) from the ambient medium which produce an exponential cutoff below the peak. A decrease in absorption with time, results a smooth, rapid turn-on, first at higher frequencies and later at lower frequencies. For each frequency, the peak flux corresponds to optical depth  $\sim 1$  and a power-law decline in light curve can be noticed. Finally, the spectral index approaches toward a constant negative value, which corresponds to a non-thermal radiation in an optically thin medium [Chevalier, 1998; Weiler et al., 1990, 1986].

For the present work, we will follow the second approach. Upper panel of Figure 5.14 shows the radio observations of SN 2007uy. The early time data is too sparse to determine spectral index ( $\alpha$ ) for early part of the light curve, during the optically thick regime. Radio follow-up of this event has already been reported by van der Horst et al. [2011]. Few initial data in 4.8 GHz and 8.4 GHz observed from VLA were not covered in previous literature. These data sets are analyzed using the reduction techniques of ‘*Astronomical Image Processing System*’ (AIPS)<sup>1</sup>. To model the light curves we have also included the literature data along with this new data set. The new VLA data set is presented in Table 5.9 and the modeled parameters

---

<sup>1</sup>Astrophysical Image Processing System (AIPS) has been developed by the National Radio Astronomical Observatories (NRAO), USA

---

are reported in Table 5.10. The notations of the parameters are as defined by Weiler et al. [2011]. The detail on modeling can be found from elsewhere [Weiler et al., 1990, 2011, 1986].

Out of the six frequencies of the data set, only three frequencies (8.4, 4.8 and 2.3 GHz) have been used to model the radio data through simultaneous fitting, while for other frequencies (1.28, 0.610 and 0.325 GHz) the expected theoretical light curves have been plotted along with observational data. Our best fitted model gives the value of overall reduced  $\chi^2 = 7.14$ . This is relatively higher than the value (4.42) mentioned by Weiler et al. [2011] for the well studied Type Ibc radio SN 1994I. This higher value corresponds to a relatively less coverage of SN 2007uy in radio band. Lower panel of Figure 5.14 represents the temporal evolution of  $\alpha$ . The field circles are the values of  $\alpha$  derived from observations using a set of two frequencies. The epochs for which we have observation in a given frequency, the probable flux for other frequency has been determined by interpolation through polynomial fitting of observed light curve. The theoretical curve shows that initially the source was extremely optically-thick with high +ve value of spectral index which turned to a constant -ve value  $\sim -1$  asymptotically, that clearly marks the transition from optically thick to thin state. A little lower value ( $\sim 2.0$ ) of  $\alpha$  than 2.5 in optically thick regime shows probably FFA is also responsible to govern the initial radio flux along with the SSA. The coefficient  $K_6 = 1.00085$ , which is associated with FFA is also sufficiently less than the coefficient  $K_5 = 1630.031$  responsible for SSA. Though the temporal evolution of both processes are almost similar ( $\delta'' = -4.602$  and  $\delta''' = -4.206$  respectively). Thus initial emission is mostly due to SSA in optically thick ejecta, though mild contribution due to FFA can not be ruled out. This result is consistent with the conclusion drawn by van der Horst et al. [2011].

## 5. THE STRIPPED ENVELOPE SNE 2007UY AND 2008D

Table 5.9 The log of radio observation of SN 2007uy from VLA in 4.8 & 8.4 GHz. The Flux errors are measured using the expression  $\sigma_f^2 = (\epsilon.S_0)^2 + \sigma_0^2 + \sigma_{S_0}^2$ . Here  $S_0$  is the observed flux density,  $\sigma_0$  is the RMS noise of the radio sky,  $\sigma_{S_0}$  is the error associated with  $\sigma_0$  and  $\epsilon$  is the fraction that accounts the error in VLA flux calibration. For 4.8 and 8.4 GHz observations value of  $\epsilon$  is 0.05. For the epochs where measured flux density is less than 3 times of the corresponding value of  $\sigma_f$ , we have considered the flux density as the upper limit for our measurement.

UT Date (yy/mm/dd)	JD 2454000+	Phase <sup>a</sup> (day)	Frequency (GHz)	Flux (mJy)	Flux error (mJy)
2008/01/06	471.76	+09	8.4	0.362	0.044
2008/01/07	473.11	+10	8.4	0.306	0.070
2008/01/11	476.82	+14	8.4	0.459	0.469
2008/01/14	479.76	+17	8.4	0.513	0.040
2008/01/16	481.80	+19	4.8	0.515	0.050
2008/01/16	481.83	+19	8.4	0.688	0.057
2008/01/17	482.90	+20	4.8	0.403	0.037
2008/01/17	482.92	+20	8.4	0.566	0.053
2008/01/20	485.66	+23	4.8	0.562	0.044
2008/01/21	486.66	+24	8.4	0.724	0.060
2008/01/21	486.67	+24	4.8	0.799	0.055
2008/01/23	488.66	+26	4.8	0.770	0.060
2008/01/23	488.67	+26	8.4	0.721	0.076
2008/01/25	490.67	+28	8.4	0.797	0.056
2008/01/25	490.68	+28	4.8	0.875	0.068
2008/01/27	492.92	+30	8.4	0.965	0.081
2008/01/27	492.93	+30	4.8	0.821	0.050
2008/01/30	495.82	+33	8.4	0.953	0.070
2008/02/01	497.73	+35	4.8	1.216	0.085
2008/02/01	497.74	+35	8.4	0.968	0.068
2008/02/03	499.70	+37	8.4	1.044	0.075
2008/02/03	499.71	+37	4.8	1.072	0.065
2008/02/08	504.72	+42	4.8	1.263	0.078
2008/02/08	504.73	+42	8.4	1.011	0.075
2008/02/14	510.79	+48	8.4	0.872	0.063
2008/02/14	510.80	+48	4.8	1.249	0.085
2008/02/21	517.92	+55	4.8	1.276	0.102
2008/02/21	517.93	+55	8.4	0.522	0.048
2008/02/24	520.65	+58	4.8	1.432	0.082
2008/02/24	520.66	+58	8.4	0.677	0.046
2008/03/07	532.60	+70	4.8	1.339	0.106
2008/03/07	532.62	+70	8.4	0.596	0.062
2008/03/21	546.58	+84	4.8	1.103	0.089
2008/03/22	547.65	+85	8.4	0.351	0.049
2008/04/14	570.53	+108	4.8	0.814	0.120
2008/05/04	591.36	+129	4.8	0.457	0.107

<sup>a</sup>With reference to the explosion epoch JD 2454466.17

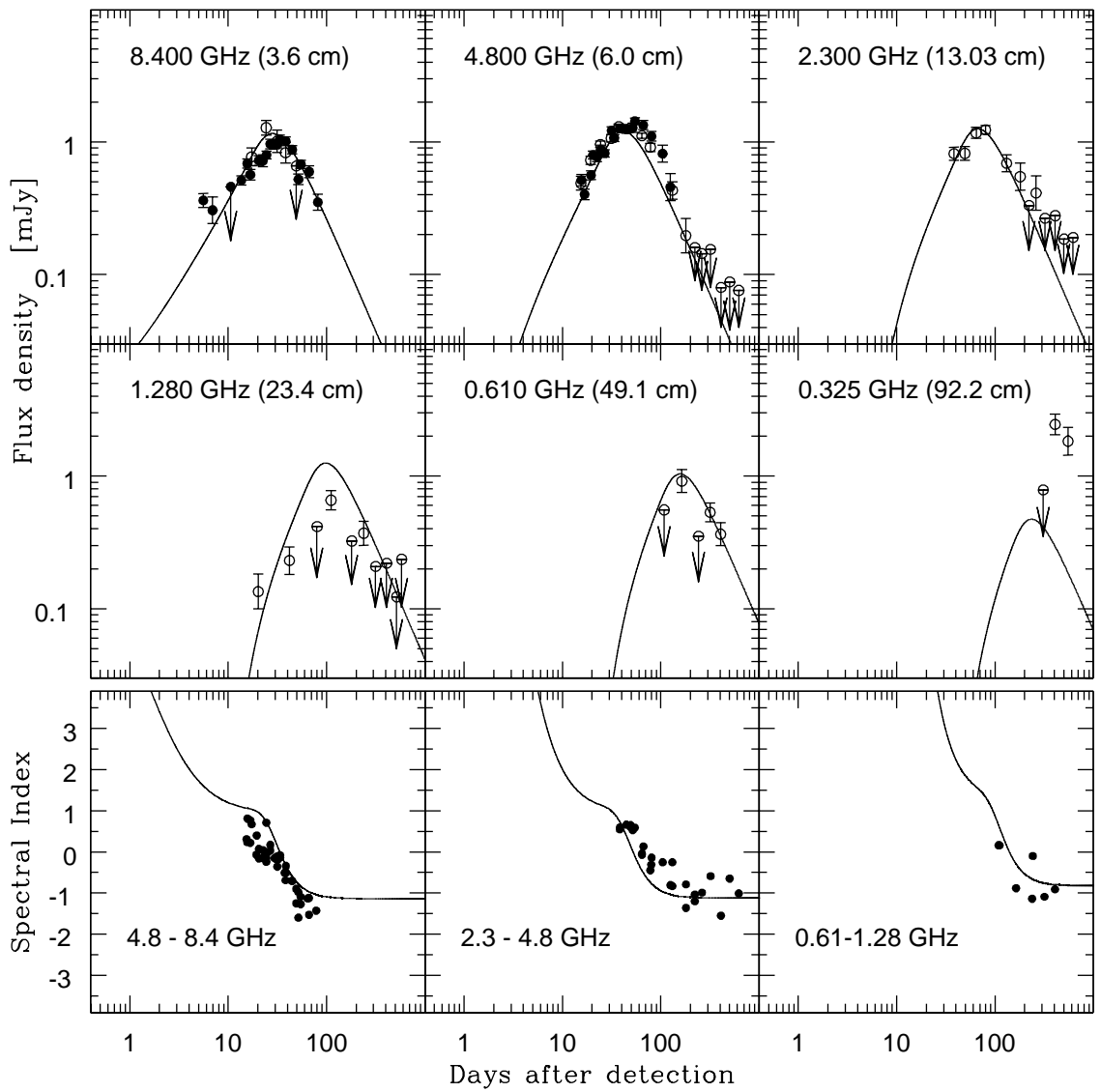


Figure 5.14 The modeled radio light curve of SN 2007uy. The upper panel shows the variation of radio wave with time. Open circles are the data obtained from literature [van der Horst et al., 2011], whereas the filled circles are VLA data acquired and processed during the present work. The solid curves represent the best fitted model. The lower panel shows the variation of spectral index with time.

## 5. THE STRIPPED ENVELOPE SNE 2007UY AND 2008D

---

Table 5.10 The parameters derived from the fitting of radio data

Parameters	Value
$K_1$	1500.75
$\alpha$	-1.1435
$\beta$	-1.734
$K_2$	91.38
$t_0$	-3.59 days
$\delta$	2.41
$K_3$	$5.408 \times 10^5$
$K_4$	0.0036
$\delta'$	-3.43
$K_5$	1630.03
$\delta''$	-4.60
$K_6$	$\sim 1.0008$
$\delta'''$	-4.20

The modeling of three frequencies shows that the radio flux of the source is moderate ( $K_1 = 1500.75$ ) with a temporal decay index ( $\beta$ ) roughly = -1.73 while the overall spectral index ( $\alpha$ ) is  $\sim -1.14$ , comparable with the optically thin condition. It predicts that the object was discovered about ( $t_0$ ) = -3.6 days after the burst, which is consistent with the optical follow-ups. Following [Chevalier \[1982a,c\]](#), we assumed that temporal decrement ( $\delta$ ) of opacity of uniform circumstellar medium (CSM) is roughly dependent on  $\alpha$  and  $\beta$  by the relation  $\delta = \alpha - \beta - 3$ . A sufficiently lower value of  $K_2$  (= 91.38), than  $K_3$  (=  $5.408 \times 10^5$ ) implies that the absorption processes in CSM is more due to its clumpy/structured form than its uniformity, but a relatively higher value of  $\delta'$  (= -3.43) than  $\delta$  (= -2.41) probably implies that the effect of clumpyness will not sustain for a longer time in comparison to the absorption due to uniform CSM and eventually the CSM starts to behave like a circumburst medium having statistically small number of clumps. The lower value of the term  $K_4$  (=  $3.6 \times 10^{-3}$ ) demands that the radio absorption due to distant H II

---

regions, which are in between the SN and us is quite low. In fact this is one order less than other events likes SNe 1978K, 1994I, 1998bw, but higher than SN 1993J [Weiler et al., 2002, 2011]. In contrast, the optical observation of SN 2007uy demands for a larger extinction. We speculate that along the line of sight of the SN, probably amount of fully ionized region is sufficiently low and the medium is relatively cooler with sufficient amount of dust grain. As a result, the radio absorption due to distant cloud is small but the optical extinction is high.

Finally, we find the mass loss rate during pre-SN phase using radio data, adopting the prescription of Weiler et al. [2001]. Assuming 50% of the CSM along the line of sight is clumpy and size of a clump is roughly 1/3 of the dimension of the expanding SN shock, then the volume filling factor by the blast wave is  $\phi \sim 0.22$ . Then the effective optical depth will be given by  $\langle \tau_{eff}^{0.5} \rangle \sim 0.204$  (using equations 5 and 16 of Weiler et al. 2001). Then assuming the wind velocity of the progenitor  $\sim 10 \text{ km s}^{-1}$  (the least possible value if the progenitor is a red super giant) and initial velocity ( $v_s$ ) and temperature ( $T_s$ ) of the shock are respectively of the order of  $10^4 \text{ km s}^{-1}$  and 20,000 K, we can quantify the mass loss rate by:

$$\dot{M} = 6.79 \times 10^{-7} (w_{wind}/10\text{km s}^{-1}).(v_s/10^4\text{km s}^{-1})^{1.5}.$$

$$\times (T_s/20,000\text{K})^{0.68} \text{ M}_{\odot} \text{ yr}^{-1}$$

Since the photospheric velocity and temperature, measured from spectroscopy and photometry at around optical peak are roughly  $15,200 \text{ km s}^{-1}$  and  $6,200 \text{ K}^1$

---

<sup>1</sup>This is important to mention that this is the Colour temperature of the photosphere and hence does not correspond to the effective temperature of the source but provides an approximate

## 5. THE STRIPPED ENVELOPE SNE 2007UY AND 2008D

---

respectively, then the mass loss rate should be  $\dot{M} \gtrsim 2.03 \times 10^{-7} (w_{wind}/10\text{km s}^{-1}) M_{\odot} \text{ yr}^{-1}$ . This value is comparable with the pre-SN mass loss rate for other Type Ibc events derived from radio data [Weiler et al., 2011]. Observations and theoretical studies predict that the progenitors of Type Ibc are WR stars, having extremely high wind velocity  $\gtrsim 10^3 \text{ km s}^{-1}$  [Willis, 1996; Yoon et al., 2012]. Then the mass loss rate of the progenitor of SN 2007uy during its WR phase was roughly  $\gtrsim 2.03 \times 10^{-5} M_{\odot} \text{ yr}^{-1}$ . Since the mass loss mainly happen in the WR state and having a time-scale of  $\sim 1 \text{ Myr}$  [Georgy et al., 2012], much larger than other eruptive state like LBV [Smith et al., 2012], then assuming that for SN 2007uy progenitor, the principal mass loss happen in WR state, we can say roughly that  $\gtrsim 20.3 M_{\odot}$  was liberated during the life time of the progenitor through wind. Since the ejecta mass  $\sim 2.0 M_{\odot}$  then assuming a neutron star with mass  $1.5 - 2.0 M_{\odot}$  was formed during this explosion, we can roughly constrain the lower limit of the progenitor as  $24.0 M_{\odot}$ .

### 5.10 Conclusion

Since the detection of progenitor of Type Ibc events in pre-SN images is rather a technically challenging task, rigorous observational follow-up along with theoretical interpretation is necessary to understand better these catastrophe.

Here we have presented an extensive follow-up of a normal Type Ib event SN 2007uy, using the data acquired in a wide range of wavelength – from NUV upto radio band along with optical spectroscopy. We also have investigated the *BVRI* optical photometric evolution of SN 2008D. The radio modeling predicts that the SN 2007uy was discovered within 4 days after the burst, while optical modeling

---

estimation of the source temperature.

---

predicts that probably the event was detected within a day after it triggered. The early spectral features also constrain the time difference between burst and detection within 7 days. Being conservative we have adopted a little higher value and assumed that the SN was discovered within 4 days after the burst.

The extinction ( $A_V = 2.2^{+0.84}_{-0.53}$  mag) along the line of sight is mainly dominated by the highly inclined host galaxy. The spiral arm of the host where SN 2007uy is located is receding and far away in comparison to the arm hosting SN 2008D. Hence SN 2008D is expected to be less extent in comparison to SN 2007uy.

The evolution of SN 2007uy was like a canonical ‘blackbody supernova’. The UV component is probably not due to shock breakout, rather it is a manifestation of radioactively heated, relatively less massive ejecta. As the ejecta become progressively optically thin, the optical photons starts to escape rapidly, causing a steepening in the late time optical light curve.

The spectral evolution of SN 2007uy is faster than other Type Ibc events. Most of the lines get diluted quickly in comparison to other archetypal events. We did not find any evidence of dependency of asymmetry on the distribution of radioactive Ni inside the ejecta, at least for this particular case. We propose for an initial asymmetry during this explosion. We speculate that rotational motion of the progenitor is mainly responsible for this initial asymmetry. Since it is the effect of rotation, material toward the outer shells of the ejecta will show relatively more asymmetry in early stage in comparison to the material concentrated toward the inner portion of the ejecta. In due course of time the explosion attain a large-scale spherical symmetry.

The colour evolution of SN 2007uy is similar to other stripped envelope SNe though this transient is intrinsically more bluish than other Type Ibc events. The

## 5. THE STRIPPED ENVELOPE SNE 2007UY AND 2008D

---

colour evolution of SN 2002ap and SN 2006aj follows roughly the same trend whereas the colour evolution of SN 1998bw and SN 2008D resemble each other remarkably. SN 2007uy remain bluish in compare to other Type Ibc events.

SN 2007uy is one of the luminous Type Ib event in respect to UVOIR bolometric flux. The peak flux is even higher than GRB associated SN 1998bw. The nebular flux of SN 2007uy is comparable with SN 1998bw. This implies that the production of radioactive  $^{56}\text{Ni}$  is similar in these two catastrophe.

The basic parameters of the burst have been derived from the optical and radio data modeling. The UVOIR optical data has been modeled assuming the event as a ‘point explosion’ after adopting the formalism of Arnett [1982], along with the modifications introduced by Valenti et al. [2008a]. Optical modeling predicts that about  $2.01 M_{\odot}$  was ejected with an explosion energy  $\sim 5.7 \times 10^{51}$  erg and roughly  $0.41 M_{\odot}$  was produced during this explosion. The radio data shows a SSA dominated light curve evolution of SN 2007uy, though the contribution of FFA during the early phase can not be ruled out. The line of sight is probably dominated by relatively cool gas and dust making the optical extinction high, but due to lack of free-electron content, absorption of radio wave through FFA is less. In fact it is one order less than that for other radio SNe. The pre-SN mass loss rate obtained through radio data is  $\dot{M} \gtrsim 2.03 \times 10^{-7} \cdot (w_{wind}/10\text{km.s}^{-1}) M_{\odot} \cdot \text{yr}^{-1}$ . This value is consistent with the results obtained for other Type Ibc radio SNe, though an order of magnitude lower than typical value of mass-loss rate derived from X-ray. Assuming the WR star as a progenitor with wind velocity  $\gtrsim 10^3 \text{km.s}^{-1}$ , we can constrain the lower limit of pre-SN mass loss rate at  $\dot{M} \gtrsim 2.03 \times 10^{-5} M_{\odot} \cdot \text{yr}^{-1}$  and the lower limit of the progenitor mass would be  $24.0 M_{\odot}$ , considering the compact remnant is a neutron star having mass  $1.5 - 2.0 M_{\odot}$ .

# Chapter 6

## The overluminous SNe – SN 2010jl, CSS 100217, SN 2010kd

### 6.1 Introduction

In the previous chapters I have mainly highlighted the consequences of core collapse in different kinds of evolved stars having mass range between 10–40  $M_{\odot}$ . The recent discoveries suggest an entirely new path for the death of massive stars and after a theoretical approach observations are also revealing the possibility of pair-instability process as more pronounced mechanism than core collapse in the stars having initial mass more than 60 $M_{\odot}$ . Research on SNe over the past decade has confirmed that there is a distinct class of events which are much more luminous than canonical CC-SNe. A few dedicated surveys like ‘*Catalina Real-Time Transient Survey*’ (CRTS), ‘*Lick Observatory Supernova Search*’ (LOSS), ‘*Robotic Optical Transient Search Experiment*’ (ROTSE), ‘*Palomar Transient Factory*’ (PTF) and ‘*Panoramic Survey Telescope & Rapid Response System*’ (PanSTARRS) discovered several such events

## 6. THE OVERLUMINOUS SNE – SN 2010JL, CSS 100217, SN 2010KD

---

in the past few years and found that they have an average absolute V-band peak magnitude of about 21 more than 2 mag brighter than normal stripped-envelope CC-SNe. Typically they show a broad peak with a shallower decline rate than normal events. Over-luminous supernovae (OLSNe) associated with faint and metal-poor host galaxies are the most spectacular recent discoveries [Drake et al., 2011; Gal-Yam et al., 2009; Gezari et al., 2009; Miller et al., 2009; Pastorello et al., 2010; Quimby et al., 2007a; Vinko et al., 2012; Young et al., 2010].

The number of luminous event detected in local ( $z \lesssim 0.01$ ) as well as at relatively distant universe is increasing with time. The larger luminosity may be due to enormous explosion in an extensively massive progenitor, producing huge amount of radioactive nuclei, it may be due to the emergence of magnetar or due to heavy interaction of the expanding ejecta with the circumburst medium. It may also be a combination of different processes. In this chapter I shall present the optical photometric follow-ups of three luminous events – nearby luminous Type IIn event SN 2010jl, relatively distant Type IIn over-luminous event CSS 100217 and over-luminous Type Ic SN 2010kd. Due to the unavailability of pre-SN images in the same *observing filters*, estimation of galaxy contribution is nontrivial for these cases and certainly the reduction procedures are different from other events. Here I shall at first briefly introduce these events and describe different photometric techniques to produce the light curves. Finally the consequences of these photometric observations and their implications toward the understanding of these events in context of other catastrophe will be discussed.

---

## 6.2 Luminous Type IIn SN 2010jl at redshift, $z = 0.0107$

SN 2010jl was discovered in the irregular galaxy UGC 5189A ( $z = 0.0107$ ) on November 02.06 UT (Benetti et al. 2010; Newton and Puckett 2010 and references therein). With a discovery magnitude of  $\sim 13.5$  mag, it was one of the brightest transient recorded in the year 2010. Location of the transient in the sky is  $\alpha = 09^{\text{h}} 42^{\text{m}} 53.33^{\text{s}}$ ,  $\delta = +09^{\circ} 29' 41.8''$ . The early spectroscopy revealed it as a Type IIn event in the relatively young phase, having distinguishable signatures of hydrogen Balmer emission lines in its spectrum. Early X-ray emission was also detected with a  $6.5\sigma$  significance label [Immler et al., 2010]. Using the archival WFPC2 images of HST taken about 10 years prior to explosion, Smith et al. [2011b] have proposed that the progenitor of SN 2010jl is consistent with a massive star with an initial mass above  $30M_{\odot}$ , though the exact nature of the progenitor is not conclusive. The optical linear spectropolarimetry of the event obtained two weeks after the discovery shows a continuum polarization at a level of 1.7%–2.0%, indicating that the explosion has a substantial asphericity [Patat et al., 2011]. Near-infrared observations, obtained at about 90 days past explosion revealed a significant infrared (IR) excess for SN 2010jl, suggesting that a large amount of dust may exist around this SN before explosion [Andrews et al., 2011]. An extensive optical coverage over 500 days past explosion revealed the heavily interacting feature of SN 2010jl [Zhang et al., 2012].

Figure 6.1 shows the supernova and its host galaxy. Optical photometric observations of SN 2010jl in the broad-band Johnson  $UBV$  and Cousins  $R_cI_c$  filters have also been carried out using the 1-m Sampurnanand Telescope (ST) at ARIES, Nainital and 2-m Himalayan Chandra Telescope (HCT) at Hanle under IIA, Ban-

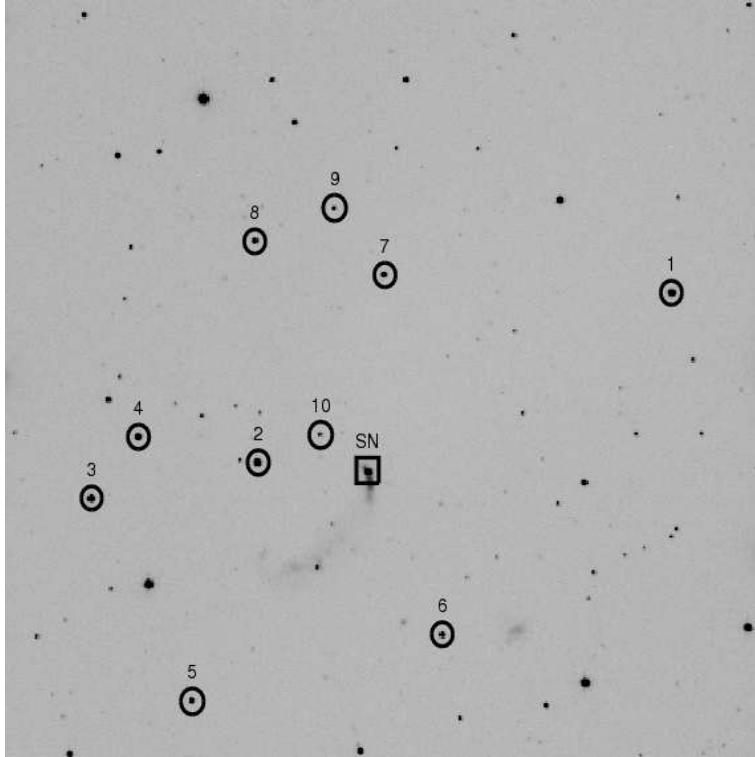


Figure 6.1 Identification chart of SN 2010jl field. The image is about 13x13 arcmin taken in V-band with the 1-m ST at ARIES, Nainital. The transient location is marked along with the secondary stars used for calibration. North is up and East is to the left.

galore. The event has been monitored photometrically in 22 epochs from ST while in 7 epochs from HCT.

### 6.2.1 Observational setup and reduction strategy

For observation from ST, we have used a  $2048 \times 2048$  CCD camera mounted at the f/13 Cassegrain focus of the telescope. The observational setup was canonical and the detector specification is as described in Chapter 2. Observations from HCT have also been conducted using a  $2048 \times 4096$  CCD camera, a part of HFOSC, which is the back-end instrument of 2-m telescope. The detail methodology is mentioned in

Table 6.1 Identification number (ID), coordinates ( $\alpha, \delta$ ) and calibrated magnitudes of stable secondary standard stars in the field of SN 2010jl.

Star ID	$\alpha_{J2000}$ (h m s)	$\delta_{J2000}$ (d m s)	$U$ (mag)	$B$ (mag)	$V$ (mag)	$R$ (mag)	$I$ (mag)
1	09 42 32	+09 32 24	14.20±0.01	14.23±0.01	13.72±0.02	13.40±0.01	13.10±0.02
2	09 43 01	+09 29 48	14.93±0.02	14.74±0.01	13.96±0.01	13.54±0.02	13.16±0.02
3	09 43 12	+09 29 17	14.65±0.01	14.68±0.01	14.09±0.02	13.72±0.01	13.35±0.02
4	09 43 09	+09 30 10	16.31±0.04	15.81±0.01	14.92±0.03	14.40±0.04	13.91±0.05
5	09 43 05	+09 26 16	15.72±0.02	15.73±0.01	15.15±0.01	14.79±0.01	14.43±0.02
6	09 42 48	+09 27 17	17.01±0.02	16.41±0.01	15.48±0.01	14.97±0.02	14.51±0.02
7	09 42 52	+09 32 39	16.62±0.02	16.33±0.01	15.53±0.01	15.07±0.02	14.64±0.02
8	09 43 01	+09 33 08	16.20±0.02	16.18±0.01	15.55±0.01	15.18±0.01	14.84±0.02
9	09 42 55	+09 33 38	17.71±0.05	17.79±0.02	17.19±0.02	16.86±0.02	16.54±0.02
10	09 42 57	+09 30 17	—	18.82±0.02	17.22±0.03	16.10±0.02	14.71±0.03

Chapter 2. Instrumental set-up is tabulated in Table 2.1.

Due to the extended nature of the SN host galaxy and high background, photometry of the SN location is non-trivial. The true flux of the transient is determined after subtracting the background contamination, computed from pre-SN SDSS images of the host galaxy. It has been discussed in detail in next section (i.e. 6.2.2). The photometry of all CCD frames have been performed using standard tasks of *IRAF* and *DAOPHOT* (see chapter 2).

In order to get the standard magnitudes of the transient, we calibrate the field of SN 2010jl on the night of 12 December, 2010 under a good and transparent sky condition (FWHM seeing  $\sim 2.3$  arcsec in  $R_c$  band) using Landolt [1992] field SA98. The instrumental magnitudes were converted into the standard photometric system using least-square linear regression procedures described by Stetson [1987]. For our calculation, we have used the mean values of atmospheric extinction coefficients of the site viz 0.57, 0.28, 0.17, 0.11 and 0.07 mag per unit airmass for the  $U$ ,  $B$ ,  $V$ ,  $R_c$  and  $I_c$  bands respectively [Kumar et al., 2000]. We obtain the following transformation coefficients for the night of standardization.

## 6. THE OVERLUMINOUS SNE – SN 2010JL, CSS 100217, SN 2010KD

---

$$u' = U + (8.242 \pm 0.008) + (-0.051 \pm 0.013)(U - B)$$

$$b' = B + (5.936 \pm 0.013) + (-0.062 \pm 0.018)(B - V)$$

$$v' = V + (5.519 \pm 0.015) + (-0.077 \pm 0.022)(B - V)$$

$$r' = R_c + (5.304 \pm 0.010) + (-0.088 \pm 0.027)(V - R_c)$$

$$i' = I_c + (5.706 \pm 0.005) + (-0.047 \pm 0.007)(V - I_c)$$

where  $U$ ,  $B$ ,  $V$ ,  $R_c$  and  $I_c$  are the standard magnitudes; and  $u'$ ,  $b'$ ,  $v'$ ,  $r'$  and  $i'$  are the corresponding instrumental magnitudes corrected for time and aperture. The RMS scatter between calibrated and Landolt standard stars are 0.029, 0.033, 0.028, 0.026 and 0.020 mag, respectively for  $U$ ,  $B$ ,  $V$ ,  $R_c$  and  $I_c$  passband. These are the calibration errors in corresponding bands.

To generate the local standards in the field of transient, we selected ten isolated stars in the field and construct the aperture growth curve using the DAOGROW program for determination of the difference between aperture and profile fitting magnitudes. These differences along with the differences in the exposure times and atmospheric extinction, were used to evaluate zero points for local standards in the transient-frame. The calibrated standard magnitudes of ten secondary stars in SN 2010jl field and their standard deviation are listed in Table 6.1. The Figure 6.1 shows the secondary stars and the SN.

Table 6.2 Photometric evolution of SN 2010jl. The Phase is measured in days w.r.t. JD = 2455504.06

Date (UT)	JD 2455000+	Phase (day)	<i>U</i> (mag)	<i>B</i> (mag)	<i>V</i> (mag)	<i>R</i> (mag)	<i>I</i> (mag)	Telescope
2010/11/06	507.444813	3.38	13.57±0.04	14.23±0.04	13.89±0.05	13.46±0.04	13.16±0.04	ST*
2010/11/07	508.461548	4.40	13.63±0.03	14.22±0.05	13.91±0.05	13.47±0.05	13.15±0.04	ST
2010/11/08	509.489858	5.43	13.68±0.03	14.28±0.05	13.95±0.05	13.53±0.05	13.23±0.04	ST
2010/11/09	510.446973	6.39	13.68±0.03	14.25±0.04	13.92±0.04	13.47±0.03	13.16±0.02	ST
2010/11/10	511.444468	7.38	13.63±0.03	14.27±0.05	13.95±0.05	13.50±0.04	13.20±0.03	ST
2010/11/11	512.457923	8.40	13.70±0.02	14.26±0.05	13.95±0.05	13.51±0.04	13.21±0.04	ST
2010/11/29	530.376813	26.32	14.07±0.05	—	14.22±0.04	13.70±0.04	13.40±0.04	ST
2010/12/01	532.475423	28.42	13.98±0.04	14.56±0.06	14.23±0.05	13.71±0.04	13.41±0.03	ST
2010/12/03	534.442083	30.38	14.01±0.03	14.59±0.03	14.26±0.04	13.74±0.03	13.48±0.03	ST
2010/12/06	537.344318	33.28	14.02±0.03	14.60±0.03	14.23±0.03	13.77±0.03	13.48±0.03	ST
2010/12/09	540.466158	36.41	14.09±0.03	14.68±0.03	14.32±0.05	13.79±0.05	13.49±0.05	ST
2010/12/12	543.469783	39.41	14.11±0.03	14.89±0.04	14.57±0.05	13.98±0.06	13.75±0.03	ST
2011/01/01	563.428878	59.37	14.28±0.03	14.95±0.04	14.60±0.03	14.02±0.03	13.83±0.02	ST
2011/01/09	571.458093	67.40	14.32±0.03	14.93±0.04	14.63±0.03	14.01±0.02	13.84±0.02	ST
2011/01/13	575.321400	71.26	14.38±0.03	14.89±0.04	14.63±0.03	14.03±0.03	13.92±0.02	ST
2011/01/24	586.423046	82.36	14.39±0.03	15.20±0.04	14.94±0.05	14.20±0.03	14.27±0.03	HCT <sup>⊕</sup>
2011/03/06	627.236928	123.18	14.51±0.02	15.17±0.04	14.95±0.06	14.13±0.04	14.20±0.04	ST
2011/03/12	633.105858	129.05	14.61±0.04	15.33±0.08	14.86±0.06	14.20±0.05	14.30±0.07	ST
2011/03/21	642.193393	138.13	14.53±0.05	15.31±0.08	15.07±0.06	14.27±0.05	14.33±0.05	ST
2011/03/23	644.113889	140.05	14.66±0.07	15.17±0.06	14.95±0.05	14.22±0.04	14.26±0.04	HCT
2011/03/24	645.129728	141.07	14.75±0.04	15.28±0.06	14.98±0.05	14.21±0.04	14.27±0.08	HCT
2011/03/31	652.184508	148.12	14.64±0.04	15.25±0.08	14.99±0.06	14.21±0.05	14.22±0.05	HCT
2011/04/01	653.188103	149.13	14.59±0.06	15.30±0.08	15.07±0.08	14.20±0.06	14.19±0.05	ST
2011/04/04	656.081944	152.23	14.75±0.07	15.31±0.07	15.10±0.05	14.23±0.05	14.24±0.05	HCT
2011/04/06	658.220038	154.16	14.69±0.04	15.35±0.04	15.14±0.06	14.21±0.04	14.27±0.03	ST
2011/04/15	667.176389	163.11	14.78±0.08	15.36±0.06	15.20±0.06	14.25±0.06	14.32±0.05	HCT
2011/04/20	672.308333	168.23	14.85±0.07	15.40±0.07	15.20±0.07	14.27±0.06	14.36±0.06	HCT
2011/04/21	673.108993	169.05	14.81±0.04	15.43±0.07	15.23±0.06	14.28±0.04	14.40±0.04	ST
2011/06/02	714.673628	210.61	14.83±0.05	15.41±0.06	15.18±0.06	14.25±0.04	14.36±0.04	ST

\* ST : 1.04 m Sampurnanand Telescope, ARIES, India;

⊕ HCT : 2.01 m Himalayan Chandra Telescope, Hanle, India;

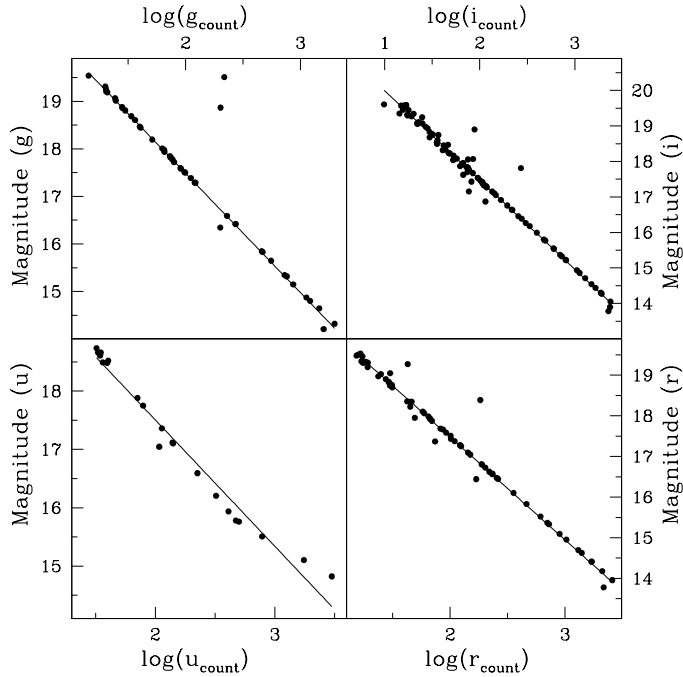


Figure 6.2 The correlation between counts and Gunn magnitudes of SDSS field of SN 2010jl.

### 6.2.2 Optical photometry and light curves

The transient occurred in the star forming region of the host galaxy with considerably intense background. SN background is computed from pre-SN SDSS images that provide Gunn magnitudes ( $u, g, r, i$ ) of the field stars. As our observations are in Bessell filter system, conversion of Gunn magnitudes to Bessell magnitudes is done following the relations reported in [Jester et al. \[2005\]](#). Background flux subtraction is a multi-step process. To bring the SDSS images in the platform, similar to our observation, ‘plate scale matching’ has been performed over all SDSS frames. After plate scale matching, all the images (including pre and post SN images) have been aligned with each other. In every aligned frame, two box areas, each of dimension  $25 \times 25$  squared pixel are precisely chosen – one at SN location and other at a

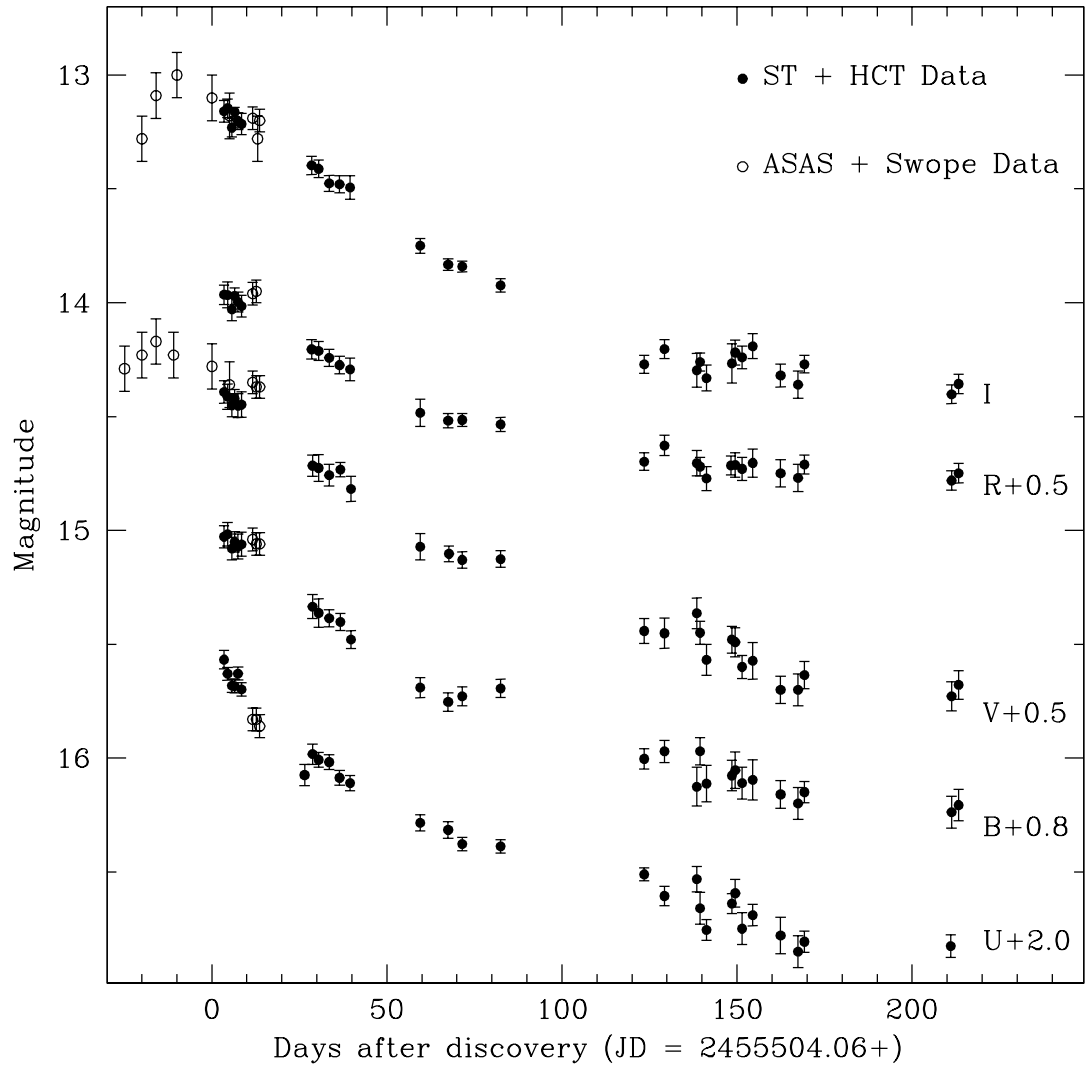


Figure 6.3 Light curves of SN 2010jl. Closed circles are the data observed from ST and HCT telescopes, while the open circles are the pre-discovery photometry taken from [Stoll et al. \[2011\]](#).

## 6. THE OVERLUMINOUS SNE – SN 2010JL, CSS 100217, SN 2010KD

---

star free region, near the SN position. For each frame, the entire counts of these two individual boxes are determined. Certainly, the median value of the counts of the star free region represents the ‘sky-value’ of the corresponding frame. For every frame the ‘sky-value’ has been subtracted from the entire counts of the box covering the SN region. In this way we obtain the sky-subtracted counts of the SN region for all frames in all bands.

Standard aperture photometry of the four pre-SN SDSS frames has been done to calculate the counts of the stars in those frame. From SDSS catalog the Gunn magnitudes of these objects have also been noted. To find out the positions of the field stars we have used ‘sky2xy’ package of the ‘wctool’. For every Gunn filter we found a very strong correlation between counts and corresponding magnitudes. Figure 6.2 represents this correlation and the following relations can be derived.

$$u = (-2.166 \pm 0.081) \times \log(u_{count}) + (21.837 \pm 0.181)$$

$$g = (-2.513 \pm 0.019) \times \log(g_{count}) + (22.510 \pm 0.041)$$

$$r = (-2.529 \pm 0.031) \times \log(r_{count}) + (22.535 \pm 0.065)$$

$$i = (-2.513 \pm 0.032) \times \log(i_{count}) + (22.501 \pm 0.067)$$

where  $u_{count}$ ,  $g_{count}$ ,  $r_{count}$  and  $i_{count}$  are the counts of the field stars in SDSS frames. After measuring the total sky-subtracted count of the box area covering the SN position of each SDSS frame we have computed the SDSS host galaxy magnitudes at the SN position by using above correlations. The host galaxy magnitudes for the SN positions are 16.04, 15.22, 15.09 and 15.10 in  $u$ ,  $g$ ,  $r$  and  $i$  band respectively. [Jester et al. \[2005\]](#), proposed sets of relations between SDSS Gunn magnitudes and

---

UBVR<sub>c</sub>I<sub>c</sub> Bessell Magnitudes. One of them is for stars ( $R_c - I_c < 1.15$  and  $U - B < 0$ ). Using this relation we calculate the host galaxy magnitudes as  $U = 15.22$ ,  $B = 15.47$ ,  $V = 15.13$ ,  $R_c = 14.94$  and  $I_c = 14.75$  and hence the corresponding Bessell fluxes. The rms residual of transformation is maximum  $\sim 0.04$  mag for  $(U - B)$  color and minimum ( $\sim 0.01$  mag) for  $(R_c - I_c)$  color [Jester et al., 2005].

For each epoch of our observation, we have computed the total count of the box area surrounding the SN position. This contains both SN counts and background counts due to host galaxy. Further we have converted these counts to magnitudes and used standard calibration tasks of *DAOPHOT* to get the calibrated magnitudes and hence the corresponding Bessell fluxes for each epoch. The true magnitude of the transient for each epoch has been determined after subtracting of host galaxy flux from that of all post-SN images. At every epoch, the error associate with the magnitude is determined after adding the corresponding profile error, calibration error and conversion error mentioned in Jester et al. [2005] in quadrature.

Figure 6.3 represents the optical light curve with respect to the observer frame.  $JD = 2455504.06$ , the epoch of discovery [Newton and Puckett, 2010] has been assumed as the origin of time axis. Table 6.2 summarizes the temporal variation of the object. We have also over-plotted the ASAS pre-discovery data produced by Stoll et al. [2011]. Within error, the data are consistent with each other. Figure shows a clear evidence of rising part in V and  $I_c$  bands. The shallow decay in  $R_c$  band during late time evolution (beyond 100 days) is presumably due to strong  $H_\alpha$  (6563 Å) emission.

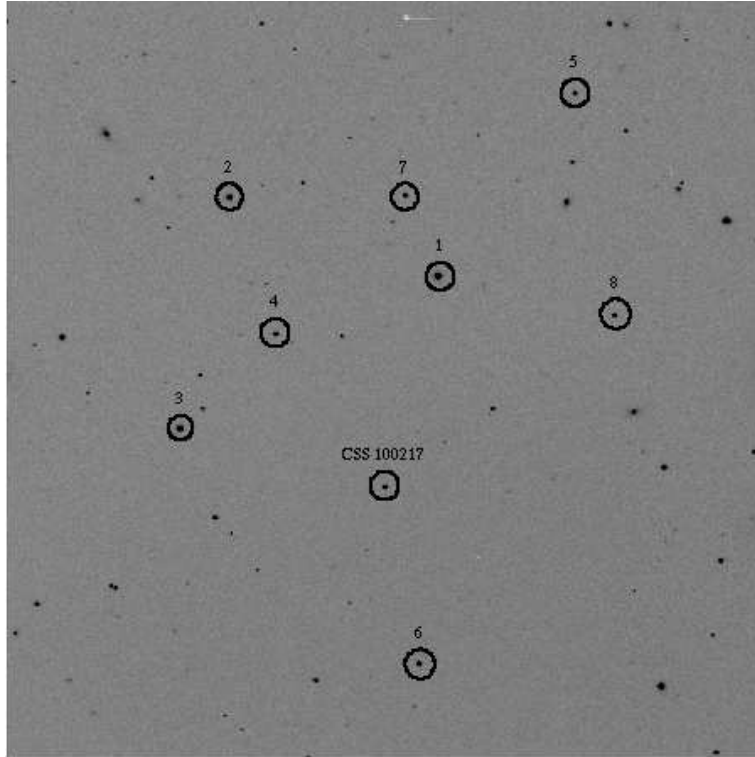


Figure 6.4 Identification chart of CSS 100217 field. The image is about 13x13 arcmin taken in V-band with the 1-m ST at ARIES, Nainital. The transient location is marked along with the secondary stars used for calibration. North is up and East is to the left.

### 6.3 Over-luminous event CSS 100217 at redshift, $z = 0.147$

On 17 February, 2010 CRTS discovered the transient event CSS100217:102913+404220 (CSS100217 hereafter) associated with the optical source J102912.58+404219.7 detected in Solan Digital Sky Survey (SDSS; [Sesar et al. 2007](#)). This event was categorized as unusual at discovery as the optical host had a past spectrum from the SDSS [[Abazajian et al., 2009](#)] that resembled a Seyfert, though the outburst was uncharacteristically rapid and larger than an AGN. Moreover, there was no detec-

Table 6.3 Identification number (ID), coordinates ( $\alpha, \delta$ ) and calibrated magnitudes of stable secondary standard stars in the field of CSS 100217.

Star ID	$\alpha_{J2000}$ (h m s)	$\delta_{J2000}$ (d m s)	$U$ (mag)	$B$ (mag)	$V$ (mag)	$R$ (mag)	$I$ (mag)
1	10 29 07.24	40 45 52.4	13.98±0.02	13.75±0.01	13.05±0.01	12.71±0.004	12.37±0.011
2	10 29 25.83	40 47 17.5	14.55±0.02	14.37±0.01	13.80±0.01	13.50±0.004	13.18±0.010
3	10 29 30.83	40 43 26.3	16.47±0.06	15.53±0.01	14.54±0.01	13.97±0.006	13.44±0.009
4	10 29 22.11	40 44 58.7	16.29±0.04	15.83±0.01	15.05±0.01	14.65±0.006	14.24±0.009
5	10 28 50.04	40 48 14.7	16.52±0.06	16.18±0.02	15.42±0.01	15.01±0.006	14.55±0.020
6	10 29 09.85	40 39 21.1	16.18±0.05	16.12±0.02	15.55±0.01	15.22±0.006	14.84±0.009
7	10 29 09.87	40 47 16.4	17.64±0.15	17.06±0.03	16.18±0.02	15.73±0.009	15.26±0.017
8	10 28 51.44	40 45 07.4	17.09±0.09	17.09±0.02	16.41±0.01	16.09±0.007	15.68±0.022

tion in archival *FIRST* and *NRAO VLA Sky Survey* (NVSS) radio data covering the objects location. The absence of any radio source implied that the variability was not due to a jet, and unlikely to be an optically variable blazars. Due to this unexpected nature of the event, immediate photometric and spectroscopic follow up had been conducted

The object had been monitored regularly from ARIES, starting from 11 April, 2010. It has been observed for more than two months. The observational setup was similar to other events and had been highlighted in chapter 2. Optical photometric observations in the broad-band Johnson *UBV* and Cousins *R<sub>c</sub>I<sub>c</sub>* filters have also been carried out using the 1-m ST at ARIES, Nainital. The supernova field has been shown in figure 6.4.

### 6.3.1 Reduction and calibration strategy

Photometry is performed using standard tasks of *IRAF* and *DAOPHOT*. Bias subtraction, flat fielding and cosmic ray removal in all the object frames were done to clean the raw frames. The PSF photometry is performed to measure the instrumental magnitudes of the CSS 100217. In order to get the standard magnitudes

## 6. THE OVERLUMINOUS SNE – SN 2010JL, CSS 100217, SN 2010KD

---

of the transient, we calibrate the field of CSS 100217 on the night of 2010, April 11 under a good and transparent sky condition (FWHM seeing  $\sim 2.3$  arcsec in R band) using Landolt [1992] standard star fields PG1047+003 and PG1323-085. The standard stars had a colour range of  $-0.290 \leq (B-V) \leq 0.688$  and brightness range of  $12.08 \leq V \leq 14.75$ . The instrumental magnitudes were converted into the standard photometric system using the tasks in *DAOPHOT* by applying least-square linear regression procedures proposed by Stetson [1992a]. The procedure is canonical. For our calculation, we have used the mean values of atmospheric extinction coefficients of the site viz 0.57, 0.28, 0.17, 0.11 and 0.07 mag per unit airmass for the  $U$ ,  $B$ ,  $V$ ,  $R_c$  and  $I_c$  bands respectively [Kumar et al., 2000]. We obtain the following transformation coefficients for the night of standardization.

$$u = U + (8.738 \pm 0.020) + (-0.065 \pm 0.040)(U - B)$$

$$b = B + (6.287 \pm 0.016) + (-0.022 \pm 0.034)(B - V)$$

$$v = V + (5.701 \pm 0.019) + (-0.025 \pm 0.032)(B - V)$$

$$r = R_c + (5.447 \pm 0.007) + (-0.052 \pm 0.022)(V - R_c)$$

$$i = I_c + (5.839 \pm 0.007) + (-0.052 \pm 0.022)(V - I_c)$$

where  $U$ ,  $B$ ,  $V$ ,  $R_c$  and  $I_c$  are the standard magnitudes; and  $u$ ,  $b$ ,  $v$ ,  $r$  and  $i$  are the corresponding instrumental magnitudes corrected for time and aperture. The scatter between photometric solution and Landolt standard stars are 0.021, 0.009, 0.005, 0.001 and 0.001 mag for  $U$ ,  $B$ ,  $V$ ,  $R_c$  and  $I_c$  bands respectively which represent the calibration error.

Table 6.4 Photometric evolution of CSS 100217. The Phase is measured in days w.r.t. JD = 2455256.0

Date (UT)	JD 2454000+	Phase (day)	<i>U</i> (mag)	<i>B</i> (mag)	<i>V</i> (mag)	<i>R</i> (mag)	<i>I</i> (mag)	Telescope
2010/04/11	098.24879	42.25	16.45±0.05	16.94±0.01	16.56±0.01	16.38±0.02	15.92±0.02	ST*
2010/04/12	099.28386	43.28	16.52±0.05	16.95±0.02	16.53±0.02	16.40±0.03	15.87±0.03	ST
2010/04/13	100.15244	44.15	16.41±0.06	16.93±0.05	16.52±0.02	16.36±0.02	—	ST
2010/04/14	101.16370	45.16	16.59±0.06	—	—	16.40±0.02	15.91±0.02	ST
2010/04/24	111.14610	55.15	16.55±0.03	—	—	16.47±0.02	15.90±0.02	ST
2010/04/25	112.15126	56.15	16.61±0.05	17.11±0.02	—	16.49±0.02	15.92±0.02	ST
2010/04/26	113.12707	57.13	16.72±0.05	17.11±0.03	16.67±0.03	16.59±0.02	15.94±0.03	ST
2010/04/30	117.12402	61.12	16.73±0.05	17.20±0.01	16.72±0.01	16.58±0.01	15.97±0.02	ST
2010/05/04	121.10514	65.10	16.68±0.14	—	—	16.61±0.02	16.03±0.02	ST
2010/05/07	124.16602	68.17	16.85±0.03	17.30±0.01	16.83±0.01	16.71±0.02	16.08±0.02	ST
2010/05/08	125.12100	69.12	16.89±0.04	17.30±0.02	16.83±0.01	16.69±0.02	16.09±0.02	ST
2010/05/13	130.12542	74.12	—	—	—	16.72±0.03	—	ST
2010/05/18	135.14788	79.15	16.92±0.03	17.41±0.03	16.97±0.02	16.85±0.03	16.18±0.05	ST
2010/05/30	147.11492	91.11	—	17.60±0.02	17.10±0.02	16.99±0.03	16.36±0.03	ST
2010/06/02	150.16341	94.16	17.28±0.07	17.65±0.05	17.14±0.03	17.01±0.04	16.29±0.03	ST
2010/06/09	157.14958	101.15	17.19±0.06	17.70±0.03	17.21±0.02	17.14±0.03	16.41±0.04	ST
2010/06/11	159.11546	103.11	17.25±0.04	17.82±0.03	17.21±0.03	17.23±0.05	16.49±0.04	ST
2010/06/15	163.14118	107.14	17.14±0.04	17.77±0.02	17.23±0.02	—	16.49±0.03	ST
2010/06/17	165.11897	109.11	—	17.80±0.06	17.19±0.05	—	16.49±0.04	ST

\* ST : 1.04 m Sampurnanand Telescope, ARIES, India;

## 6. THE OVERLUMINOUS SNE – SN 2010JL, CSS 100217, SN 2010KD

---

To generate the local standards in the field of transient, we selected ten isolated stars in the field and construct the aperture growth curve using the DAOGROW program for determination of the difference between aperture and profile fitting magnitudes. These differences along with the differences in the exposure times and atmospheric extinction, were used to evaluate zero points for local standards in the transient-frame. The calibrated standard magnitudes of eight secondary stars in CSS 100217 field and their standard deviation are listed in Table 6.3. The Figure 6.4 shows the secondary stars and the SN.

### 6.3.2 Optical photometry and light curves

As mentioned above, CSS 100217 is a transient discovered on 17<sup>th</sup> February, 2010, associated with the SDSS object J102912.58+404219.7. According to SDSS spectrum, this is a galaxy at a redshift of 0.147, with strong Balmer emission lines. This pre-SN spectrum available through SDSS survey is a composite spectrum of the whole object. On the other hand the brightness profile of this object is Gaussian with FWHM similar to the FWHM of other stars of the field.

The transient was not resolved from its host. This implies that there may be a projection effect and ‘*template subtraction*’ process to figure out the true SN flux would not be helpful in this case. Under this circumstances, the best way to estimate the true SN flux would be to subtract the flux of the host, when the transient was absent from the flux when the transient is present. SDSS provides the Gunn magnitudes of the host (according to pre-SN image). As our observations are in Bessell filter system, we followed the relations reported in Jester et al. [2005], to convert the Gunn magnitudes of the SDSS object to Bessell magnitudes.

---

Jester et al. [2005], proposed two sets of relations between SDSS Gunn magnitudes and UBV $R_c$ I $_c$  Bessell Magnitudes. One set is for stars ( $R_c - I_c < 1.15$  and  $U - B < 0$ ), while the other is for Quasars at redshift  $\leq 2.1$ . The Gunn magnitudes of this object are  $u = 18.24 \pm 0.01$ ,  $g = 17.90 \pm 0.01$ ,  $r = 17.70 \pm 0.01$ ,  $i = 17.38 \pm 0.01$ ,  $z = 17.45 \pm 0.01$ . Using the relations provided for stars we calculate the host magnitudes as  $U = 17.55$ ,  $B = 18.17$ ,  $V = 17.77$ ,  $R_c = 17.25$  and  $I_c = 16.71$ . The rms residual of transformation is maximum  $\sim 0.04$  mag for  $(U - B)$  color and minimum ( $\sim 0.01$  mag) for  $(R_c - I_c)$  color [Jester et al., 2005]. Using the expressions for Quasar, we got the following magnitudes of the host in the Bessell system :  $U = 17.51$ ,  $B = 18.07$ ,  $V = 17.77$ ,  $R_c = 17.38$  and  $I_c = 16.88$ . For this kind of objects, the rms scatter in transformation is maximum (0.09 mag) for  $(V - R_c)$  color and minimum (0.03 mag) for  $(U - B)$  color [Jester et al., 2005]. Further we note that the difference in magnitudes using two different methods, described above is maximum (0.17 mag) for  $I_c$  band and for  $V$  band both methods produce same result. In this work I adopt the expressions for star and note that use of other set of equations will only produce a small constant shift in the SN light curve and will not make any significant change in color evolution of the transient. Figure 6.5 represents the optical light curve with respect to the observer frame.  $JD = 2455256.0$  has been assumed as the origin of time axis. Table 6.4 summarizes the temporal variation of the object. We have performed differential photometry and applied profile and background fitting method , to find out the magnitudes of the optical transient. As the transient is not resolved from its host, the true magnitude of the transient for each epoch has been determined after subtracting of host flux from that of transient. At every epoch, the error associate with the magnitude is determined after adding the corresponding profile error and conversion error mentioned in Jester et al. [2005] in quadrature.

6. THE OVERLUMINOUS SNE – SN 2010JL, CSS 100217, SN 2010KD

---

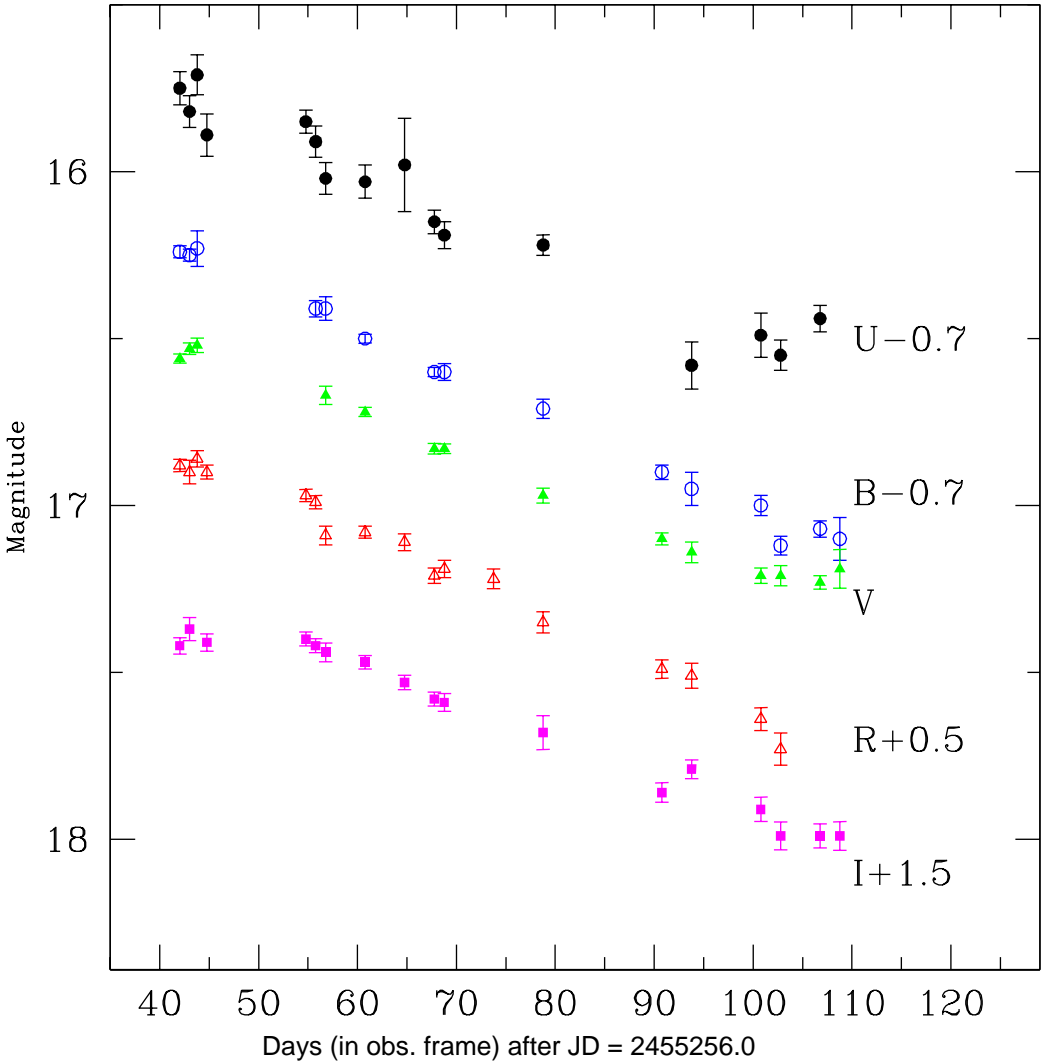


Figure 6.5 Optical photometric light curve of CSS 100217. The light curve is with respect to observer frame and hence not corrected for redshift. JD = 2455256.0 has been assumed as the origin of time axis for this event.

---

We did not include the calibration error, which is very small in comparison with other. The figure shows the SN nature of this transient with a prominent peak in V,  $R_c$  and  $I_c$  bands.

## 6.4 Over-luminous Type Ic event SN 2010kd at redshift, $z \sim 0.1$

SN 2010kd was discovered by *ROTSE collaboration* on 14.49 November, 2010 at about 17.5 mag in an anonymous galaxy [Vinko et al., 2010]. A cross-identification revealed a faint SDSS source J120800.89+491332.8 at the location of the transient and probably the host galaxy of the supernova. The coordinate of the transient is  $\alpha = 12\text{h}08\text{m}01.11\text{s}$ ,  $\delta = +49^\circ 13' 31.1''$ . A spectrum, obtained on November 22.51 UT with the 9.2-m HET (+ Marcario Low-Resolution Spectrograph) showed the broad, weak P-Cygni features superimposed on a blue continuum which was consistent with the features of an early type-II supernovae and the spectrum was most similar to the Type II SN 1999gi [Vinko et al., 2010]. Assuming the strongest broad feature to be  $H\alpha$ , the calculated redshift  $\sim 0.1$ , which implied that the absolute magnitude is brighter than  $-22.5$  mag. Interestingly in later spectra, the H or He lines were absent but a strong presence of CII, OI and OII, unveiled SN 2010kd as a peculiar Type Ic SN [Vinko et al., 2012]. A regular unfiltered imaging of the transient was conducted by ground based ROTSE III telescope and also by space based *Swift*/UVOT telescope to get the UV signature of the event. Long term spectroscopic monitoring was also carried-out to characterize the spectral signature and evolution [Vinko et al., 2012]. The object was also monitored regularly

## 6. THE OVERLUMINOUS SNE – SN 2010JL, CSS 100217, SN 2010KD

---

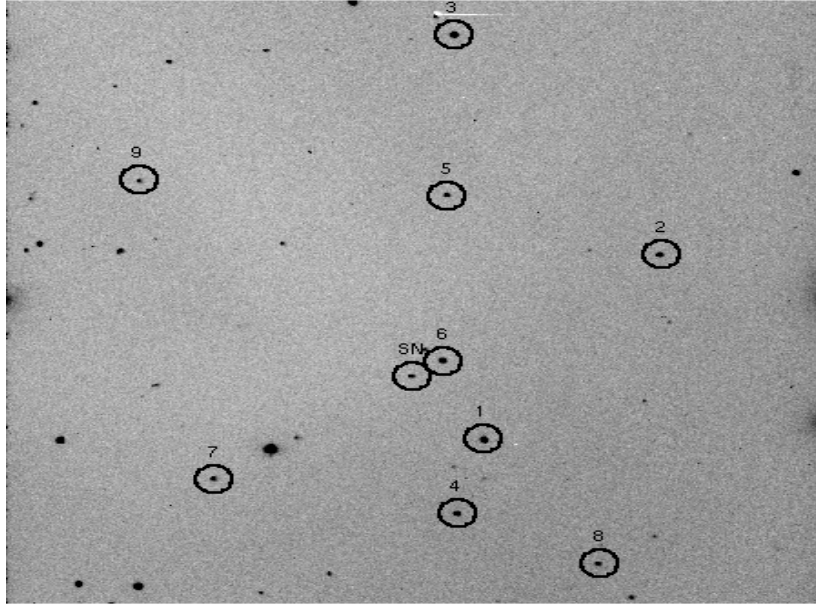


Figure 6.6 Identification chart of SN 2010kd field. The image is about 13x13 arcmin taken in B-band with the 1-m ST at ARIES, Nainital. The transient location is marked along with the secondary stars used for calibration. North is up and East is to the left.

Table 6.5 Identification number (ID), coordinates ( $\alpha, \delta$ ) and calibrated magnitudes of stable secondary standard stars in the field of SN 2010kd.

Star ID	$\alpha_{J2000}$ (h m s)	$\delta_{J2000}$ (d m s)	$U$ (mag)	$B$ (mag)	$V$ (mag)	$R$ (mag)	$I$ (mag)
1	12 07 54	+49 12 11	14.69±0.02	15.35±0.02	13.97±0.02	14.32±0.02	15.46±0.03
2	12 07 37	+49 16 09	14.82±0.01	15.74±0.01	13.79±0.01	14.25±0.01	16.35±0.02
3	12 07 57	+49 20 49	14.95±0.01	15.65±0.03	14.14±0.02	14.49±0.02	15.77±0.03
4	12 07 57	+49 10 37	15.32±0.02	16.02±0.02	14.53±0.02	14.90±0.01	16.32±0.03
5	12 07 58	+49 17 23	15.51±0.01	16.36±0.01	14.61±0.01	15.01±0.01	16.83±0.06
6	12 07 58	+49 13 51	15.54±0.01	16.53±0.02	14.52±0.02	14.98±0.02	17.19±0.04
7	12 08 20	+49 11 19	16.26±0.03	17.58±0.02	14.61±0.01	15.37±0.01	18.53±0.15
8	12 07 43	+49 09 33	17.22±0.02	17.75±0.03	16.50±0.02	16.86±0.01	17.62±0.06
9	12 08 14	+49 16 20	17.85±0.02	18.21±0.03	17.08±0.03	17.44±0.02	17.95±0.11

---

from ARIES, starting from 28 November, 2010. It was observed for a time span of about 160 days. The observational setup was similar to other events and have been highlighted in chapter 2. Optical photometric observations in the broad-band Johnson  $UBV$  and Cousins  $R_cI_c$  filters have also been carried out using the 1-m ST at ARIES, Nainital. Figure 6.6 represents the field of SN 2010kd.

### 6.4.1 Photometry and Calibration

During the entire period of observation, the transient was exceptionally bright in comparison to its host. Since the host was faint, regular PSF photometry is performed to measure the instrumental magnitudes of the optical transient.

In order to get the standard magnitudes of the transient, we calibrate the field of SN 2010kd on the night of 12 December, 2010, the same night when SN 2010jl was also calibrated. So the calibration process and the transformation equations are identical with the expressions mentioned for the calibration of SN 2010jl.

The local standards in the field of SN 2010kd has been generated using the standard routines of *DAOPHOT*. The calibrated standard magnitudes of nine secondary stars in SN 2010kd field and their standard deviation are listed in Table 6.5. The Figure 6.6 shows the secondary stars and the SN.

Table 6.6 Photometric evolution of SN 2010kd. The Phase is measured in days w.r.t. JD = 2455515.0

Date (UT)	JD 2455000+	Phase (day)	<i>U</i> (mag)	<i>B</i> (mag)	<i>V</i> (mag)	<i>R</i> (mag)	<i>I</i> (mag)	Telescope
2010/11/28.98	529.48	14.48	16.70±0.04	17.47±0.02	17.40±0.02	17.27±0.02	17.07±0.08	ST*
2010/11/29.94	530.45	15.45	16.72±0.06	17.50±0.01	17.35±0.01	17.26±0.02	17.07±0.02	ST
2010/12/02.02	532.52	17.52	16.65±0.03	17.44±0.03	17.37±0.04	17.27±0.02	17.11±0.03	ST
2010/12/04.02	534.52	19.52	–	17.42±0.02	–	17.27±0.04	17.09±0.03	ST
2010/12/04.96	535.46	20.46	16.61±0.03	17.42±0.02	17.29±0.01	17.22±0.01	17.05±0.03	ST
2010/12/06.92	537.41	22.41	16.62±0.03	17.41±0.02	17.30±0.02	17.19±0.03	16.99±0.04	ST
2010/12/13.02	543.52	28.52	16.53±0.03	17.31±0.02	17.19±0.01	17.15±0.02	16.96±0.03	ST
2011/01/02.02	563.52	48.52	16.63±0.02	17.40±0.01	17.25±0.01	17.12±0.01	16.95±0.02	ST
2011/01/03.96	565.45	50.45	16.77±0.04	17.41±0.01	17.27±0.01	17.15±0.01	16.96±0.02	ST
2011/01/05.03	566.53	51.53	16.84±0.05	17.40±0.03	17.22±0.04	17.17±0.01	16.98±0.02	ST
2011/01/10.02	571.52	56.52	16.86±0.05	17.51±0.02	17.28±0.02	17.20±0.01	17.00±0.02	ST
2011/01/24.95	586.47	71.47	17.15±0.02	17.67±0.02	17.42±0.01	17.28±0.02	17.07±0.02	ST
2011/02/04.00	596.50	81.50	17.54±0.12	17.89±0.04	17.50±0.02	17.33±0.02	17.08±0.02	ST
2011/03/08.71	629.22	114.22	18.56±0.08	18.80±0.04	18.22±0.02	17.89±0.02	17.51±0.02	ST
2011/03/12.64	633.15	118.15	18.35±0.09	18.83±0.08	–	17.95±0.03	17.62±0.06	ST
2011/03/22.72	643.22	128.22	18.76±0.09	18.84±0.06	18.28±0.03	18.02±0.02	17.64±0.02	ST
2011/04/09.01	661.18	146.18	–	19.36±0.08	18.71±0.05	18.39±0.04	–	ST
2011/04/19.60	671.10	156.10	–	19.48±0.08	18.73±0.05	18.53±0.06	18.12±0.06	ST
2011/04/22.68	674.18	159.18	–	19.51±0.09	18.87±0.04	18.54±0.05	18.08±0.07	ST

\* ST : 1.04 m Sampurnanand Telescope, ARIES, India;

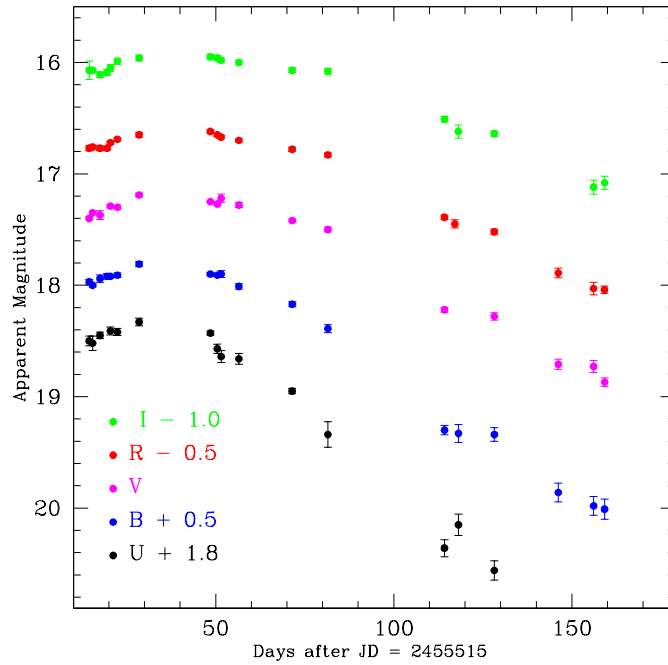


Figure 6.7 The multiband Light curves of SN 2010kd.

### 6.4.2 Optical light curve

The optical measurements, obtained after PSF photometry is listed in Table 6.6. The  $UBVR_cI_c$  light curves have been plotted in Figure 6.7. Like other two events, this also shows a shallow decline in the light curve along with a broad prolonged plateau in the light curve.

The light curves of three different kinds of over luminous events have been described in previous sections. On the basis of this the photometric properties will be discussed in the subsequent section.

## 6.5 Discussion on photometric properties, comparison with other events

To compare the intrinsic properties of the SNe lights with other events, the observed light have to be corrected for foreground extinction and distance.

In all three cases mentioned above the galactic extinctions were measured from the Schlegel-map [Schlegel et al., 1998]. To get the reddening due to host galaxy, spectroscopy is necessary. Neither for CSS 100217 [Drake et al., 2011] nor for SN 2010jl [Zhang et al., 2012] impression for host extinction were found. Also for SN 2010kd, host extinction is expected to be less [Vinko et al., 2012]. This is worth to mention that, according to literature, galaxies of these three SNe are extremely metal poor. So, the possibility for high reddening is low. Hence for the present work it has been assumed that the reddening properties of the hosts along the line of site are comparable at most with the properties of milky way along the line of site. So, after knowing the galactic extinction along those directions, the values have been doubled to account the total extinction along the line of site. The visual extinction according to Schlegel et al. [1998] along these directions are respectively 0.084 mag for SN 2010jl, 0.046 mag for CSS 100217 and 0.072 mag for SN 2010kd. Hence the total visual extinction along the line of site are 0.167, 0.092 and 0.144 mag respectively for SN 2010jl, CSS 100217 and SN 2010kd. The extinction in other optical bands were measured after using the relation proposed by Cardelli et al. [1989].

The hosts of CSS 100217 and SN 2010kd are relatively distant objects. The redshifts of these two objects are respectively 0.147 and 0.12 [Drake et al., 2011; Vinko et al., 2012]. Assuming standard cosmological model these corresponds to lu-

---

minosity distances of about 690 Mpc and 415 Mpc. On the other hand the distance of SN 2010jl host is about 48.53 Mpc [Zhang et al., 2012]. Using these measurements of extinctions and distances, the observed magnitudes have been corrected to the absolute magnitudes, which are the intrinsic properties of the SNe. This is also important to mention that  $k$ -correction have not been applied to the fluxes of relatively distant objects – CSS 100217 and SN 2010kd.

Figure 6.8 shows the time variation of absolute V-band magnitudes of these three transient and a comparison with other Types of SNe. The very broad plateau like light curve which shows the difference that probably a huge mass was ejected during this explosion. Through optical photometry and spectroscopy of SN 2010jl Zhang et al. [2012] speculated that probably  $30\text{--}40M_{\odot}$  amount of mass of the progenitor was loose during couple of decays before the explosion with a mass loss rate as high as  $1\text{--}2M_{\odot}.\text{yr}^{-1}$ . After the investigation of pre-SN image Smith et al. [2011b] also concluded that the initial mass of the progenitor was above  $30M_{\odot}$ . Similarly for SN 2010kd, the ejected mass is of the order of  $20\text{--}30 M_{\odot}$  [Vinko et al., 2012], though it is roughly factor of two less than the progenitor mass ( $\sim 65M_{\odot}$ ) expected for a ‘Pair-Instability’ supernovae [Chatzopoulos and Wheeler, 2012]. On the other hand CSS 100217 is the brightest event ever observed so far. Its luminosity was higher and peak was much broader than the well studied Type IIn event SN 2006gy [Kawabata et al., 2009; Miller et al., 2010; Smith et al., 2007; Smith and McCray, 2007]. SN 2006gy was speculated to be a death of a massive star similar to galactic massive star  $\eta$ -Carina, having mass  $\sim 120M_{\odot}$ . Then progenitor of CSS 100217 should be even higher than this limit. But, it is also true that this prolonged large luminosity may also arise from interaction of the ejecta with the dense surrounding. At least for SN 2006gy it was shown by Moriya et al. [2012] through light curve modeling

6. THE OVERLUMINOUS SNE – SN 2010JL, CSS 100217, SN 2010KD

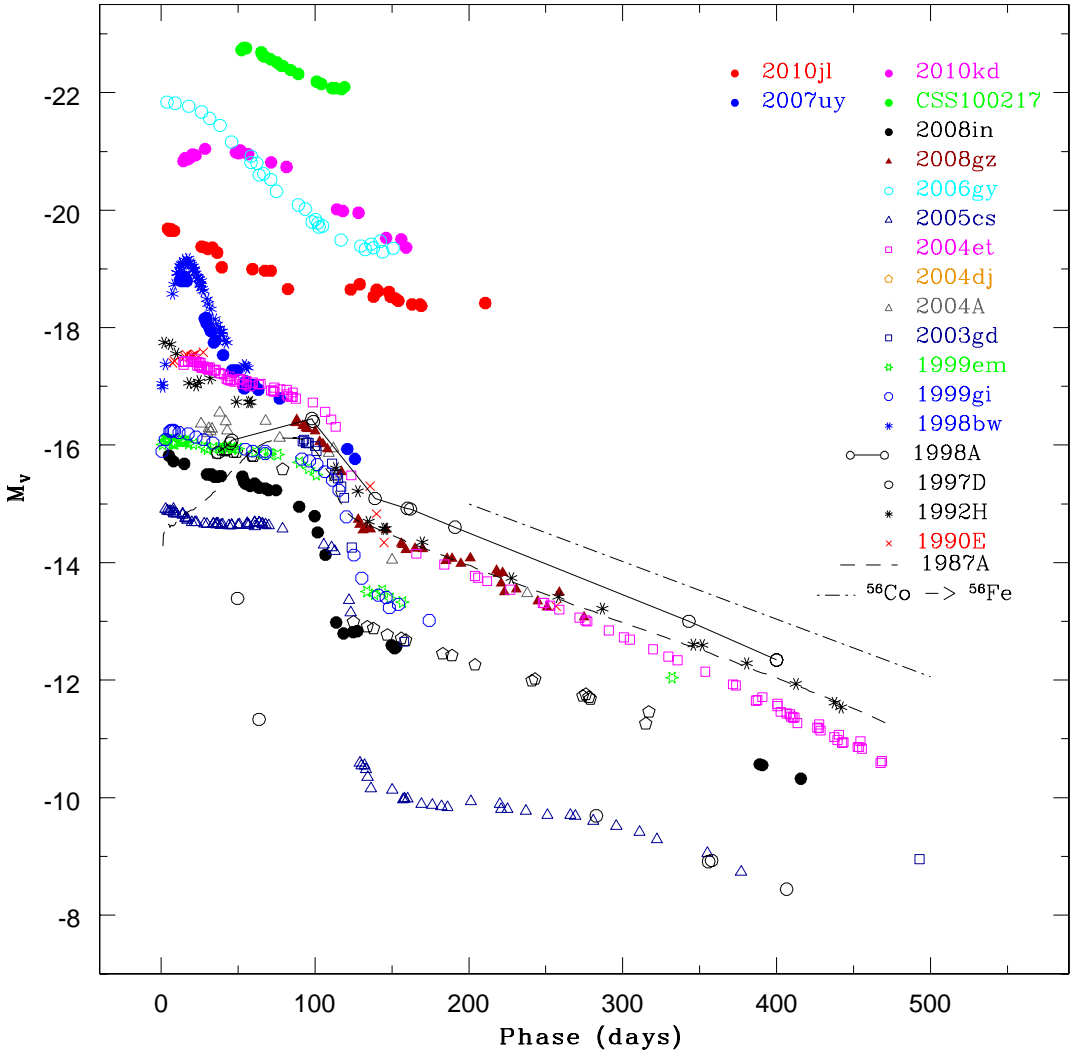


Figure 6.8 The comparison of V-band light of SN 2010jl, CSS 100217 and SN 2010kd with other Types of SNe. All these SNe shows a very high brightness in comparison with other events. A pronounced plateau like decline is noticeable

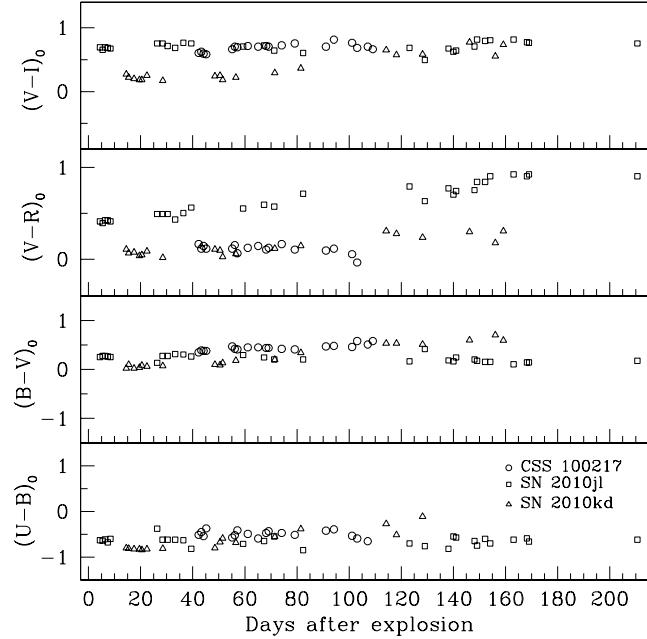


Figure 6.9 The colour evolution of luminous events. The phases are measured with respect to the observer frame.

and was also speculated for SN 2010jl [Zhang et al., 2012].

The colour evolution of these transients is shown in the figure 6.9. The difference between normal events and over luminous events in respect of colour is clearly understandable. Irrespective of supernova Types their colour evolution are almost similar – A linear progress in all colours with time can be noticed, though SN 2010jl shows a little jump at round 150 days in  $(V - R)_0$  colour. Most of the Type Ibc events get bluish within first 20–30 days and then become red and finally again start to become blue in the late nebular phase. Similar blue to red transition can also be noticed for normal Type IIP events. In contrary, we do not see such transition for over luminous events, during our time span of observation. Only a mild change is noticeable. This implies that probably the densities of the expanding shells are so huge that photons remain trapped inside these shells during the observing period.

6. THE OVERLUMINOUS SNE – SN 2010JL, CSS 100217, SN 2010KD  
2010KD

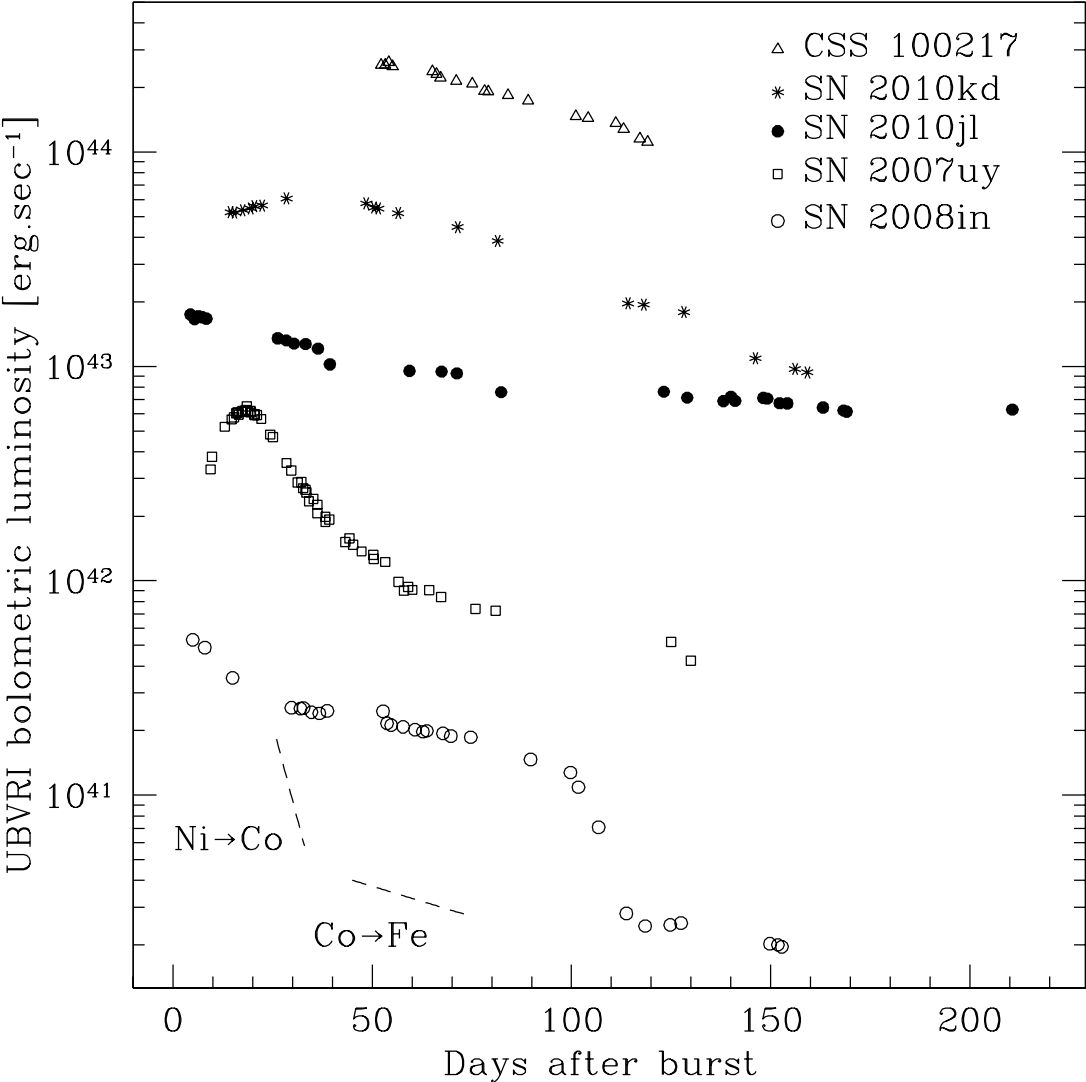


Figure 6.10 *UBVR* Bolometric light curve of over luminous events. Comparison with other Types of events. The phase axis is with respect to the observer rest frame.

---

Figure 6.10 represents the evolution of bolometric light of over luminous events and their comparison with normal supernovae. Since we have only optical band observation, so the figure represents the evolution of total optical light and will be marked as ‘*UBVRI bolometric light curve*’. SN 2007uy and SN 2008in which are respectively prototypes of Type Ibc and Type IIP events are also plotted. The bolometric luminosity of luminous events are typically 1–1.5 order brighter than normal events. Again, if we assume that only radioactive Ni is responsible for such brightness, then the amount of  $^{56}\text{Ni}$  should be extensively high than normal events. Comparing the luminosity of SN 2010kd with that of SN 1987A, it can be argued that the mass of  $^{56}\text{Ni}$  should be  $\sim 10 M_{\odot}$  [Vinko et al., 2012]. Similarly comparing the peak-luminosities of SN 2006gy and that of CSS 100217, revealed that the produced  $^{56}\text{Ni}$  for second event may be larger than  $22 M_{\odot}$ , Which was produced by SN 2006gy [Smith et al., 2007]. These values are more than 10–100 times larger than normal Type Ibc or Type IIP events.

In this chapter the basic photometric properties of few highly luminous events have been discussed. Certainly the origin of large luminosity and prolonged plateau is still not completely understandable. If the origin is a single progenitor, it demands for a high initial mass with a huge amount of  $^{56}\text{Ni}$  production, and the possibility of ‘Pair-Instability’ becomes more dominant. Alternatively, the spin-down of a newly emerged magnetar can be cause for the rise in peak luminosity (Woosley 2010 and references therein). The another possibility of interaction of ejecta with circumburst medium. For SN 2006gy and for SN 2010jl this possibility have already been proposed. In fact X-ray detection for SN 2010jl, year after the burst strongly supports the heavy interaction between circumstellar medium and SN shock [Chandra et al., 2012], but surprisingly these events are not very much radio luminous [Drake et al.,

2011].

This is needless to say that rigorous photometric and spectroscopic monitoring of these events along with proper theoretical interpretation is extremely valuable to reveal the nature of these events. There are other cosmic catastrophe such as GRBs, origin of which are also not properly understood. The difference in basic mechanisms of these two kinds of explosions are still almost unknown. For GRBs different systematic observations had already been devised with a gradual improvement in last couple of decays. The Afterglow physics has been developed to extent over last couple of years though the nature of central engine is still not clear. In the period of present thesis also several GRB events were observed. GRB 071010A is one of them. This event was detected in optical from ST and was also observed for almost a month in the Optical/near-Infrared (NIR) with various telescopes through out the world starting from about +2 min after the prompt burst. The X-ray follow-up was carried out from +0.4d onwards. A clear complexity in the light curve evolution was revealed during its study [Covino et al., 2008]. Few other GRB events which were also detected from ST during this period of Thesis are GRB 080430 and GRB 090424. Due to limited scope, in this present thesis discussion on this events are not possible, but the message that should be conveyed in this regard is that these high energy events are still not well resolved. So systematic monitoring of a large number of sources along with proper theoretical modeling is indispensable to understand these kinds of explosions.

# Chapter 7

## Summary, conclusions and future prospects

### 7.1 Summary and conclusions

In this present work, a multiwavelength investigation of energetic cosmic explosions have been carried out. Several issues like nature of Type Ibc and II progenitors, the asymmetry scenario in Type Ib burst and the interaction signature of Type Ibc events have been revisited. Essentially, this investigation have arose a possibility of new query – whether there is any subtype between two classes of SNe or not and the effect of rotation on the asymmetric explosion. We have found out the most energetic explosion ever known so far. The nature of these transients and how are they differ from canonical CCSNe have also been discussed. The conclusions regarding different events have been briefed below:

**SN 2008gz:** In this work, we have presented *BVRI* photometric and low-resolution

## 7. SUMMARY, CONCLUSIONS AND FUTURE PROSPECTS

---

spectroscopic investigation of a type II CCSN 2008gz, which occurred in a star forming arm and within a half-light radius (solar metallicity region) of a nearby spiral galaxy NGC 3672. The SN event was detected late, and a detailed investigation of its light curves and spectra spanning 200 days suggest that it is an event of type IIP similar to archetypal SNe 2004et and 1999em. However, in contrast to other events of its class, the SN 2008gz exhibits rarely observed  $V$  magnitude drop of 1.5 over the period of a month during plateau to nebular phase. Using 0.21 mag of  $A_V$  as a lower limit and a distance of 25.5 Mpc, we estimate synthesized  $^{56}\text{Ni}$  mass of  $0.05 \pm 0.01 M_\odot$  and a mid-plateau  $M_V$  of  $-16.6 \pm 0.2$  mag. The photospheric velocity is observed to be higher than that was observed for SN 2004et at similar epochs, indicating explosion energy was comparable to or higher than SN 2004et. Similar trend was also seen for the expansion velocity of H-envelopes. By comparing its properties with other well studied events as well as by using a recent simulation of pre-SN models of Dessart et al. [2010], we infer an explosion energy range of  $2 - 3 \times 10^{51}$  erg and this coupled with the observed width of the forbidden [O I] 6300-6364Å line at 275 days after the explosion gives an upper limit for the main-sequence (non-rotating, solar metallicity) progenitor mass of  $17 M_\odot$ . Our narrow-band H $\alpha$  observation, taken nearly 560 days after the explosion and the presence of an emission kink at zero velocity in the Doppler corrected spectra of SN indicate that the event took place in a low luminosity star forming H II region.

**SN 2008in:** In this work we have presented the optical photometric and low-resolution spectroscopic observations of the Type IIP SN 2008in, which occurred in the outskirts of the nearly face-on spiral galaxy M 61. Photometric data in the X-rays, ultraviolet and near-infrared bands have been used to characterize this event.

---

The SN field was imaged with the ROTSE-IIIb optical telescope about seven days before the explosion. This allowed us to constrain the epoch of the shock breakout to  $\text{JD} = 2454825.6$ . The duration of the plateau phase, as derived from the photometric monitoring, was  $\sim 98$  days. The spectra of SN 2008in show a striking resemblance to those of the archetypal low-luminosity IIP SNe 1997D and 1999br. A comparison of ejecta kinematics of SN 2008in with the hydrodynamical simulations of Type IIP SNe by [Dessart et al. \[2010\]](#) indicates that it is a less energetic event ( $\sim 5 \times 10^{50}$  erg). However, the light curve indicates that the production of radioactive  $^{56}\text{Ni}$  is significantly higher than that in the low-luminosity SNe. Adopting an interstellar absorption along the SN direction of  $A_V \sim 0.3$  mag and a distance of 13.2 Mpc, we estimated a synthesized  $^{56}\text{Ni}$  mass of  $\sim 0.015M_\odot$ . Employing semi-analytical formulae [[Litvinova and Nadezhin, 1985](#)], we derived a pre-SN radius of  $\sim 126R_\odot$ , an explosion energy of  $\sim 5.4 \times 10^{50}$  erg and a total ejected mass of  $\sim 16.7M_\odot$ . The latter indicates that the zero age main-sequence mass of the progenitor did not exceed  $20M_\odot$ . Considering the above properties of SN 2008in, and its occurrence in a region of sub-solar metallicity ( $[\text{O}/\text{H}] \sim 8.44$  dex), it is unlikely that fall-back of the ejecta onto a newly formed black hole occurred in SN 2008in. We therefore favor a low-energy explosion scenario of a relatively compact, moderate-mass progenitor star that generates a neutron star.

**SNe 2007uy & 2008D:** Here We have presented the results from a comprehensive analysis of two Type Ib SNe 2007uy and 2008D in a nearby galaxy NGC 2770 ( $\sim 29.5$  Mpc), using data from space-based *Swift*/UVOT observations along with ground-based follow-up at visible, infrared and radio wave bands. Our study was mainly focused on Type Ib event SN 2007uy. As a complementary part we have

## 7. SUMMARY, CONCLUSIONS AND FUTURE PROSPECTS

---

also explored the evolution of Type Ib event SN 2008D which occurred in the same galaxy within a gap of 10 days. Spectroscopically, SN 2007uy was not similar to broad lined energetic Type Ibc events, but its peak absolute visual magnitude was  $\sim -18.8$ , which is about 1 mag brighter than the mean value for Type Ibc events. From optical and radio data modeling we confirm that the event was discovered within a week after the burst. Due to large inclination angle ( $\sim 82.3^\circ$ ) of the host, the SN is heavily reddened,  $E(B - V) \sim 0.71$  mag. This measurement is consistent with the value quoted by other researchers and it is substantially higher than the galactic reddening ( $\sim 0.02$  mag) along this direction. This implies that the optical emission is mainly attenuated by the host galaxy. The study of optical spectroscopic follow-up shows a clear asymmetric evolution of several spectral lines. We did not find any evidence of dependency of asymmetry on the distribution of radioactive Ni inside the ejecta, at least for this particular case. Modeling of the optical bolometric light curve shows that about  $0.4 M_\odot$  radioactive  $^{56}\text{Ni}$  is produced and roughly  $2.01 M_\odot$  material was ejected during this catastrophe with liberated energy  $5.7 \times 10^{51}$  erg. This explosion parameters are comparable with that of XRF associated Type Ic event SN 2006aj. The radio data shows a SSA dominated light curve evolution of SN 2007uy, though the contribution of FFA during the early phase can not be ruled out. The line of sight is probably dominated by relatively cool gas and dust making the optical extinction high, but due to lack of free-electron content, absorption of radio wave through FFA is less. In fact it is one order less than that for other radio SNe. The pre-SN mass loss rate obtained through radio data is  $\dot{M} \gtrsim 2.03 \times 10^{-7} \cdot (w_{wind}/10\text{km.s}^{-1}) M_\odot \cdot \text{yr}^{-1}$ . This value is consistent with the results obtained for other Type Ibc radio SNe, though an order of magnitude lower than typical value of mass-loss rate derived from X-ray. Assuming the WR star

---

as a progenitor with wind velocity  $\gtrsim 10^3 \text{km.s}^{-1}$ , we can constrain the lower limit of pre-SN mass loss rate at  $\dot{M} \gtrsim 2.03 \times 10^{-5} M_{\odot} .\text{yr}^{-1}$  and the lower limit of the progenitor mass would be  $24 M_{\odot}$ , considering the compact remnant is a neutron star having mass  $1.5 - 2.0 M_{\odot}$ .

**Overluminous events:** These are a new class of transients discovered in last decade. We have very few information about these class of catastrophe. Many leading astronomical surveys are trying to catch more and more catastrophe of this kind. They are optically luminous and at least more than 2 mag brighter than normal catastrophe. Most of the time it is believed to be the end of a very massive star  $\gtrsim 60M_{\odot}$ , and the explosion mechanism is ‘pair-instability’ process, but recent investigations shows that emergence of heavy magnetar or shock interaction can also produce a prolonged luminous plateau like lightcurve during a collapsing star. Spectroscopically they may be of Type II or Type I nature. In this present work three this kind of events were observed and their Optical photometric behaviours have been illustrated. CSS 100217 is the most luminous event, whereas peak brightness of SN 2010kd is almost comparable with the CSS event. SN 2010jl is a relatively nearby event and most probably a heavily interacting supernova created from a high mass star (initial mass  $\gtrsim 40 M_{\odot}$ ).

## 7.2 Future Prospects

According to present understanding, kinetic energies of SNe explosion can be in between  $10^{50}$  and  $10^{51}$  ergs. Depending on the spectral and temporal behaviour, they are broadly categorized in two sub-classes – (i) Core collapse supernovae (CC-

## 7. SUMMARY, CONCLUSIONS AND FUTURE PROSPECTS

---

SNe) and (ii) Thermonuclear supernovae, which are further classified into smaller branches. Detail discussions on these events have already been done in previous sections. Recent discoveries of subluminoous and overluminous events is now again challenging our basic understanding of these kind of catastrophes. A few key research objective on SNe that fascinate me to continue my work in this area are as described below.

### 7.2.1 Nature of subluminoous and overluminous Type II events

Many candidates have been found, which show an intrinsic low luminosity during their light curve evolution. As already discussed in Chapter 4, that spectroscopically also they are distinct from normal events. SN 1997D, the first reported faint SN [Turatto et al., 1998], was explained in terms of significant fall-back of ejected material on a newly formed Black Hole (BH), created through the core-collapse of a massive progenitor [ $M \gtrsim 20M_{\odot}$ ; Zampieri et al. 1998] or as an explosion in a less massive progenitor [8–12 $M_{\odot}$ ; Chugai and Utrobin 2000]. The reason behind this serious disagreement between two results could be addressed and constrained through regular monitoring of numerous events of this kind and improved hydrodynamical modeling of spectra and light curves. In addition to these subclasses, there may be a new class of events, which would represent the upper-bound of low-luminosity category, an event that simultaneously posses the signatures of normal and low-luminosity events. The only example in this category is SN 2008in (chapter 4). The peculiarity of this object lies in its spectral resemblance with low luminosity events with a higher  $^{56}\text{Ni}$  production. Undoubtedly, detailed analysis of these events will enrich the supernova science – burst geometry and explosion mechanism would be

---

understood in a better way.

The origin of super luminous SNe (OLSNe) (2006gy, 2008fz, CSS100217, 2010kd) having an extreme luminosity in the optical, with  $L_{opt} \gtrsim 10^{51}$  erg.s<sup>-1</sup> is unknown to a large extent. They are probably associated with very massive progenitor ( $M \sim 100M_{\odot}$ ). Type IIn event CSS100217 [Drake et al. 2011, also in chapter 6] is the brightest event ever observed so far. Type Ibc event SN 2010kd [Vinko et al. 2012, also discussed in chapter 6] shows a little less absolute V band luminosity than CSS100217. It is being explained either as a shock interaction effect in a Type Ibc explosion or as a birth of heavy mass magnetar with an ejection of large amount of synthesized <sup>56</sup>Ni as a SN-yield, though the proper mechanism is still uncertain. An extensive investigation of these events both observationally and theoretically can only flourish the SN science in this direction.

### 7.2.2 Occurrence rate of peculiar Type IIP events & their progenitors

Though the overall spectroscopic and photometric nature of Type IIPs intended to classify them within a fairly homogeneous group, there are intriguing relatives to this class of objects. The well monitored object of this kind is SN 1987A, which was explained as an explosion in a Blue supergiant (BSG) star, more compact progenitor than RSGs [Arnett and Fu, 1989]. In due course of time many other events [like SN 1998A, Pastorello et al. 2005; SN 2000cb, Kleiser et al. 2011; SN 2009E, Pastorello et al. 2012] in this category were found. Meanwhile Utrobin and Chugai [2011] introduced a new terminology – ‘dome-like shape’ (Type-IIId) for 1987A like events, to distinguish them from ordinary IIPs. Their dome like part of the light curve

## 7. SUMMARY, CONCLUSIONS AND FUTURE PROSPECTS

---

is mainly powered by radioactive decay, while the thermal energy is completely exhausted within first 20 days; a different physics than that for normal Type IIP events, where plateau phases are generated through the deposition of bulk radiated energy as an internal energy during the shock propagation.

According to present observations (measured with limited sample inside the volume with distance  $\lesssim 30$  Mpc), nearly 58.7% of CCSNe belongs to IIP class, which is about 39.1% of all SNe explosions discovered in nearby universe [Smartt, 2009]. Chemical evolution of a galaxy is highly influenced by the rate and kind of supernovae occurring in that galaxy. If the explosions in BSGs are different from commonly observed explosions of RSGs, then observationally it will be important to figure-out the percentage of these new subclass among total observed CCSNe. The environment, where these kind of progenitors are formed, how are they differ from the environments of other Type II progenitors and how the SN-ejecta interacts with circumburst environment are also a subject of interest. Certainly, this problem has a direct implication toward the understanding of chemical enrichment of galactic environment due to SNe-yields and contribution of SNe to the cosmic chemical evolution.

### 7.2.3 Type II events as a source of cosmic dust

SNe-II, being the prime generators of Si- and Fe- group of elements, as well as light p-, r- and s-process elements, are the most likely source of dust, especially at intermediate and high red-shifts [Todini and Ferrara, 2001]. Empirical estimate of dust formation rate is proposed to be made via spectrophotometric studies of Type-IIP SNe. This is especially important as errors in the estimates of line-of-sight dust

---

concentration (especially at high red-shift) contribute significantly to the errors in measurements of Hubble constant from both SNe-Ia and SNe-II. For bright nearby events, high resolution Echelle spectroscopy can be performed to trace the early signature of dust formation [Smith et al., 2011a].

#### 7.2.4 Asymmetric nature of SN explosion

Investigation of extreme Shock physics is a challenging task in observational astronomy, especially to catch the event during shock breakout epoch. Though after Swift, GALEX and other X-ray & UV satellites, detection rate of young SNe at earliest epoch has been improved; in contemporary with space based observation, ground based observation is necessary to probe the explosion properties in detail. The leading aspect in this regard is the investigation of initial asymmetry. Various mechanisms that could be responsible for aspherical explosions are rotation of magnetic field [Takiwaki et al., 2004], convection [Janka and Mueller, 1996] or shock instability in ejected matter [Iwakami et al., 2008]. For bright (V mag  $\lesssim 16$ ) nearby events, spectropolarimetric observation during initial epochs is proposed for investigation of early asymmetry as well as to probe the early structure of the ejecta [Maund et al., 2009]. Normally Type Ib/c SNe, which are more energetic than Type IIP events, show larger asymmetry than later one. Under this context, spectropolarimetric investigation of bright shock dominated Type IIn events are being proposed to investigate their initial asymmetries as well as to understand the initial structure of the ejecta.

## **7. SUMMARY, CONCLUSIONS AND FUTURE PROSPECTS**

# Bibliography

- Abazajian K.N., Adelman-McCarthy J.K., Agüeros M.A. et al. *ApJS*, 182, 543 (2009). [254](#)
- Akerlof C., Amrose S., Balsano R. et al. *AJ*, 119, 1901 (2000). [15](#)
- Akerlof C.W., Kehoe R.L., McKay T.A. et al. *PASP*, 115, 132 (2003). [140](#)
- Aksenov A.G. and Imshennik V.S. *Astronomy Letters*, 20, 24 (1994). [33](#)
- Alard C. *A&AS*, 144, 363 (2000). [66](#)
- Alard C. and Lupton R.H. *ApJ*, 503, 325 (1998). [66](#), [96](#)
- Anderson J.P. and James P.A. *MNRAS*, 390, 1527 (2008). [91](#), [128](#)
- Anderson J.P. and James P.A. *MNRAS*, 399, 559 (2009). [128](#)
- Andrews J.E., Clayton G.C., Wesson R. et al. *AJ*, 142, 45 (2011). [245](#)
- Andrews J.E., Gallagher J.S., Clayton G.C. et al. *ApJ*, 715, 541 (2010). [99](#), [107](#)
- Arcavi I., Gal-Yam A., Cenko S.B. et al. *ApJL*, 756, L30 (2012). [13](#), [51](#)
- Arnett D. *Supernovae and nucleosynthesis. an investigation of the history of matter, from the Big Bang to the present* (Princeton University Press, 1996). [2](#), [125](#), [169](#)
- Arnett D., Fryxell B. and Mueller E. *ApJL*, 341, L63 (1989). [33](#)
- Arnett W.D. *ApJ*, 179, 249 (1973). [23](#)
- Arnett W.D. *ApJ*, 237, 541 (1980). [xxxiv](#), [30](#), [33](#), [125](#), [148](#), [149](#), [169](#)

## BIBLIOGRAPHY

---

- Arnett W.D. ApJ, 253, 785 (1982). [25](#), [30](#), [33](#), [35](#), [36](#), [196](#), [205](#), [231](#), [242](#)
- Arnett W.D. and Fu A. ApJ, 340, 396 (1989). [32](#), [279](#)
- Asplund M., Grevesse N., Sauval A.J. and Scott P. ARA&A, 47, 481 (2009). [129](#), [176](#)
- Atwood W.B., Abdo A.A., Ackermann M. et al. ApJ, 697, 1071 (2009). [15](#)
- Baars J.W.M., Genzel R., Pauliny-Toth I.I.K. and Witzel A. A&A, 61, 99 (1977). [89](#)
- Barbon R., Benetti S., Rosino L., Cappellaro E. and Turatto M. A&A, 237, 79 (1990). [121](#), [165](#), [211](#)
- Barkat Z., Rakavy G. and Sack N. Physical Review Letters, 18, 379 (1967). [47](#)
- Baron E., Nugent P.E., Branch D. and Hauschildt P.H. Turatto M., Benetti S., Zampieri L. and Shea W., (eds.) 1604-2004: Supernovae as Cosmological Lighthouses, volume 342 of Astronomical Society of the Pacific Conference Series, 351 (2005). [112](#)
- Barthelmy S.D., Barbier L.M., Cummings J.R. et al. Space Sci. Rev., 120, 143 (2005). [15](#)
- Benetti S., Boschin W. and Harutyunyan H. Central Bureau Electronic Telegrams, 1568, 1 (2008). [92](#), [99](#), [134](#)
- Benetti S., Bufano F., Vinko J. et al. Central Bureau Electronic Telegrams, 2536, 1 (2010). [245](#)
- Benetti S., Turatto M., Balberg S. et al. MNRAS, 322, 361 (2001). [105](#), [109](#), [138](#)
- Benetti S., Turatto M., Valenti S. et al. MNRAS, 411, 2726 (2011). [231](#)
- Berger E. and Soderberg A. The Astronomer's Telegram, 1353, 1 (2008a). [183](#)
- Berger E. and Soderberg A.M. GRB Coordinates Network, 7159, 1 (2008b). [183](#), [185](#)

- Bersten M.C., Benvenuto O. and Hamuy M. *ApJ*, 729, 61 (2011). [33](#), [138](#), [172](#)
- Bessell M.S., Castelli F. and Plez B. *A&A*, 333, 231 (1998). [124](#), [168](#), [215](#)
- Bethe H.A. and Wilson J.R. *ApJ*, 295, 14 (1985). [18](#), [21](#)
- Bionta R.M., Blewitt G., Bratton C.B., Casper D. and Ciocio A. *Physical Review Letters*, 58, 1494 (1987). [21](#)
- Blinnikov S., Lundqvist P., Bartunov O., Nomoto K. and Iwamoto K. *ApJ*, 532, 1132 (2000). [31](#)
- Blinnikov S.I. and Bartunov O.S. *A&A*, 273, 106 (1993). [33](#)
- Blinnikov S.I., Eastman R., Bartunov O.S., Popolitov V.A. and Woosley S.E. *ApJ*, 496, 454 (1998). [31](#)
- Blondin J.M. and Ellison D.C. *ApJ*, 560, 244 (2001). [xxx](#), [28](#), [29](#)
- Blondin S. and Calkins M. *Central Bureau Electronic Telegrams*, 1191, 2 (2008). [182](#), [185](#)
- Bode M.F. and Evans A. *Classical Novae* (Cambridge University Press, 2008). [3](#)
- Branch D. *ArXiv Astrophysics e-prints* (1999). [41](#)
- Branch D., Baron E.A. and Jeffery D.J. Weiler K., (ed.) *Supernovae and Gamma-Ray Bursters*, volume 598 of *Lecture Notes in Physics*, Berlin Springer Verlag, 47–75 (2003). [112](#), [116](#)
- Branch D., Benetti S., Kasen D. et al. *ApJ*, 566, 1005 (2002). [xxx](#), [39](#), [40](#), [112](#)
- Bromm V., Yoshida N. and Hernquist L. *ApJL*, 596, L135 (2003). [4](#)
- Brown P.J. *The ultraviolet properties of supernovae*. Ph.D. thesis, The Pennsylvania State University (2009). [80](#), [141](#)
- Brown P.J., Holland S.T., Immler S. et al. *AJ*, 137, 4517 (2009). [xxxiv](#), [150](#), [152](#)
- Burrows A. *ArXiv e-prints* (2012). [xxx](#), [17](#)

## BIBLIOGRAPHY

---

- Burrows A., Hayes J. and Fryxell B.A. *ApJ*, 450, 830 (1995). [18](#)
- Burrows A., Walder R., Ott C.D. and Livne E. Humphreys R. and Stanek K., (eds.) *The Fate of the Most Massive Stars*, volume 332 of *Astronomical Society of the Pacific Conference Series*, 350 (2005a). [33](#)
- Burrows A.S. Petschek A.G., (ed.) *Supernovae*, 143–181 (1990). [21](#)
- Burrows D.N., Hill J.E., Nousek J.A. et al. *Space Sci. Rev.*, 120, 165 (2005b). [140](#)
- Buzzoni B., Delabre B., Dekker H. et al. *The Messenger*, 38, 9 (1984). [60](#)
- Campana S., Mangano V., Blustin A.J. et al. *Nature*, 442, 1008 (2006). [23](#)
- Cano Z., Bersier D., Guidorzi C. et al. *ApJ*, 740, 41 (2011). [23](#)
- Cappellaro E., Danziger I.J., della Valle M., Gouiffes C. and Turatto M. *A&A*, 293, 723 (1995). [107](#)
- Cappellaro E., Evans R. and Turatto M. *A&A*, 351, 459 (1999). [91](#)
- Cappellaro E., Mazzali P.A., Benetti S. et al. *A&A*, 328, 203 (1997). [36](#), [231](#)
- Cardelli J.A., Clayton G.C. and Mathis J.S. *ApJ*, 345, 245 (1989). [122](#), [201](#), [266](#)
- Chakraborti S., Prabhu T., Anupama G.C. et al. *Central Bureau Electronic Telegrams*, 1638, 1 (2008). [139](#)
- Chakraborty P., Das1 H.K. and Tandon S.N. *Bulletin of the Astronomical Society of India*, 33, 513 (2005). [100](#)
- Chan L.W. and Lingenfelter R.E. *ApJL*, 318, L51 (1987). [32](#)
- Chandra P., Chevalier R.A., Irwin C.M. et al. *ApJL*, 750, L2 (2012). [271](#)
- Chatzopoulos E. and Wheeler J.C. *ApJ*, 748, 42 (2012). [267](#)
- Chevalier R.A. *ApJ*, 207, 872 (1976). [22](#), [33](#), [149](#)
- Chevalier R.A. *ApJL*, 259, L85 (1982a). [238](#)

- Chevalier R.A. ApJ, 258, 790 (1982b). [23](#), [26](#), [27](#)
- Chevalier R.A. ApJ, 259, 302 (1982c). [238](#)
- Chevalier R.A. ApJ, 499, 810 (1998). [43](#), [234](#)
- Chevalier R.A., Fransson C. and Nymark T.K. ApJ, 641, 1029 (2006). [134](#)
- Chomiuk L., Soderberg A.M., Moe M. et al. ApJ, 750, 164 (2012). [220](#)
- Chugai N.N. Soviet Astronomy Letters, 14, 334 (1988). [107](#)
- Chugai N.N. sovast, 36, 63 (1992a). [33](#)
- Chugai N.N. Soviet Astronomy Letters, 18, 168 (1992b). [220](#), [222](#)
- Chugai N.N. Astronomy Letters, 26, 797 (2000). [33](#)
- Chugai N.N. and Utrobin V.P. A&A, 354, 557 (2000). [138](#), [278](#)
- Clark J.D. NASA STI/Recon Technical Report N, 83, 31710 (1983). [1](#)
- Clocchiatti A., Benetti S., Wheeler J.C. et al. AJ, 111, 1286 (1996). [175](#), [176](#)
- Clocchiatti A. and Wheeler J.C. ApJ, 491, 375 (1997). [35](#), [37](#)
- Colgate S.A. and McKee C. ApJ, 157, 623 (1969). [xxx](#), [30](#), [31](#), [32](#)
- Contardo G., Leibundgut B. and Vacca W.D. A&A, 359, 876 (2000). [215](#)
- Covino S., D'Avanzo P., Klotz A. et al. MNRAS, 388, 347 (2008). [272](#)
- Cowen D.F., Franckowiak A. and Kowalski M. Astroparticle Physics, 33, 19 (2010). [xxxiv](#), [148](#), [149](#)
- Cox A.N. Allen's astrophysical quantities (Springer Press, 2000). [217](#), [223](#)
- Cutispoto G., Zerbi F.M., Chincarini G. and REM/Ross Team. Baltic Astronomy, 13, 307 (2004). [15](#)
- Danziger I.J., Gouiffes C., Bouchet P. and Lucy L.B. IAU Circ., 4746, 1 (1989). [220](#)

## BIBLIOGRAPHY

---

- Danziger I.J., Lucy L.B., Bouchet P. and Gouiffes C. Woosley S.E., (ed.) *Supernovae*, 69 (1991). [110](#)
- De Donder E. and Vanbeveren D. *A&A*, 333, 557 (1998). [43](#)
- De Donder E. and Vanbeveren D. *New A*, 8, 817 (2003). [43](#)
- Dessart L. and Hillier D.J. *MNRAS*, 383, 57 (2008). [30](#)
- Dessart L. and Hillier D.J. *MNRAS*, 405, 2141 (2010). [41](#)
- Dessart L., Hillier D.J., Livne E. et al. *MNRAS*, 414, 2985 (2011). [33](#)
- Dessart L., Livne E. and Waldman R. *MNRAS*, 408, 827 (2010). [33](#), [117](#), [131](#), [135](#), [171](#), [274](#), [275](#)
- Dickey J.M. and Lockman F.J. *ARA&A*, 28, 215 (1990). [143](#)
- Drake A.J., Djorgovski S.G., Mahabal A. et al. *ApJ*, 696, 870 (2009). [13](#)
- Drake A.J., Djorgovski S.G., Mahabal A. et al. *ApJ*, 735, 106 (2011). [4](#), [48](#), [244](#), [266](#), [271](#), [279](#)
- Drout M.R., Soderberg A.M., Gal-Yam A. et al. *ApJ*, 741, 97 (2011). [200](#), [210](#), [211](#), [212](#), [213](#), [232](#)
- Eastman R.G., Schmidt B.P. and Kirshner R. *ApJ*, 466, 911 (1996). [29](#), [205](#)
- Eastman R.G., Woosley S.E., Weaver T.A. and Pinto P.A. *ApJ*, 430, 300 (1994). [33](#)
- Ebisuzaki T., Shigeyama T. and Nomoto K. *ApJL*, 344, L65 (1989). [33](#)
- Eldridge J.J., Mattila S. and Smartt S.J. *MNRAS*, 376, L52 (2007). [138](#)
- Eldridge J.J. and Tout C.A. *MNRAS*, 353, 87 (2004). [43](#), [138](#)
- Elmhamdi A., Chugai N.N. and Danziger I.J. *A&A*, 404, 1077 (2003a). [xxxiv](#), [xxxv](#), [34](#), [97](#), [127](#), [148](#), [156](#), [170](#), [171](#)
- Elmhamdi A., Danziger I.J., Branch D. et al. *A&A*, 450, 305 (2006). [116](#)

- Elmhamdi A., Danziger I.J., Chugai N. et al. MNRAS, 338, 939 (2003b). [xxxv](#), [97](#), [99](#), [105](#), [107](#), [109](#), [122](#), [160](#), [163](#), [166](#), [172](#), [206](#), [220](#), [222](#)
- Falk S.W. and Arnett W.D. ApJS, 33, 515 (1977). [xxx](#), [22](#), [31](#), [32](#), [149](#)
- Fassnacht C.D. and Taylor G.B. AJ, 122, 1661 (2001). [88](#)
- Ferrero P., Kann D.A., Zeh A. et al. A&A, 457, 857 (2006). [201](#), [213](#)
- Filippenko A.V. ARA&A, 35, 309 (1997). [xxix](#), [6](#), [11](#), [91](#)
- Filippenko A.V., Matheson T. and Barth A.J. AJ, 108, 2220 (1994). [223](#)
- Foley R.J. Central Bureau Electronic Telegrams, 1638, 2 (2008). [139](#)
- Foley R.J., Papenkova M.S., Swift B.J. et al. PASP, 115, 1220 (2003). [213](#)
- Fraley G.S. Ap&SS, 2, 96 (1968). [47](#)
- Frank J., King A. and Raine D.J. Accretion Power in Astrophysics: Third Edition (Cambridge University Press, 2002). [3](#)
- Fransson C. A&A, 111, 140 (1982). [xxx](#), [22](#), [23](#), [25](#)
- Fransson C. and Chevalier R.A. ApJL, 322, L15 (1987). [164](#)
- Fransson C., Lundqvist P. and Chevalier R.A. ApJ, 461, 993 (1996). [143](#)
- Fraser M., Ergon M., Eldridge J.J. et al. ArXiv e-prints (2010). [138](#), [154](#)
- Fraser M., Ergon M., Eldridge J.J. et al. MNRAS, 417, 1417 (2011). [13](#)
- Frieman J., Prasad R.R., Li W. et al. IAU Circ., 8754, 1 (2006). [48](#)
- Fryer C.L., Woosley S.E. and Hartmann D.H. ApJ, 526, 152 (1999). [49](#)
- Fryer C.L., Woosley S.E. and Heger A. ApJ, 550, 372 (2001). [4](#)
- Fu A. and Arnett W.D. ApJ, 340, 414 (1989). [32](#)
- Gal-Yam A., Mazzali P., Ofek E.O. et al. Nature, 462, 624 (2009). [48](#), [244](#)

## BIBLIOGRAPHY

---

- Galama T.J., Vreeswijk P.M., van Paradijs J. et al. *Nature*, 395, 670 (1998). [181](#), [199](#), [213](#)
- Georgy C., Ekström S., Meynet G. et al. *A&A*, 542, A29 (2012). [240](#)
- Gezari S., Dessart L., Basa S. et al. *ApJL*, 683, L131 (2008). [30](#), [149](#)
- Gezari S., Halpern J.P., Grupe D. et al. *ApJ*, 690, 1313 (2009). [244](#)
- Gorosabel J., de Ugarte Postigo A., Castro-Tirado A.J. et al. *Advances in Space Research*, 47, 1421 (2011). [182](#), [210](#)
- Grasberg E.K. and Nadezhin D.K. *Ap&SS*, 44, 409 (1976). [23](#)
- Grassberg E.K., Imshennik V.S. and Nadyozhin D.K. *Ap&SS*, 10, 28 (1971). [149](#)
- Green D.A. and Stephenson F.R. Weiler K., (ed.) *Supernovae and Gamma-Ray Bursters*, volume 598 of *Lecture Notes in Physics*, Berlin Springer Verlag, 7–19 (2003). [5](#)
- Gupta R. *Bull. Astron. Soc. India*, 30, 785 (2002). [100](#)
- Gurugubelli U.K., Sahu D.K., Anupama G.C. and Chakradhari N.K. *Bulletin of the Astronomical Society of India*, 36, 79 (2008). [109](#)
- Habergham S.M., Anderson J.P. and James P.A. *ApJ*, 717, 342 (2010). [92](#)
- Hadjiyska E., Rabinowitz D., Baltay C. et al. *The Astronomer’s Telegram*, 3812, 1 (2011). [13](#)
- Hakobyan A.A., Mamon G.A., Petrosian A.R., Kunth D. and Turatto M. *A&A*, 508, 1259 (2009). [91](#)
- Hamuy M. *ApJ*, 582, 905 (2003). [34](#), [35](#), [92](#), [125](#), [130](#), [137](#), [169](#), [171](#), [176](#)
- Hamuy M. Marcaide J.M. and Weiler K.W., (eds.) *IAU Colloq. 192: Cosmic Explosions, On the 10th Anniversary of SN1993J*, 535 (2005). [165](#)
- Hamuy M. and Pinto P.A. *ApJL*, 566, L63 (2002). [92](#), [165](#)

- Hamuy M., Pinto P.A., Maza J. et al. *ApJ*, 558, 615 (2001). [30](#), [205](#)
- Hamuy M., Suntzeff N.B., Heathcote S.R. et al. *PASP*, 106, 566 (1994). [77](#), [143](#)
- Hamuy M.A. Type II supernovae as distance indicators. Ph.D. thesis, The University of Arizona (2001). [169](#)
- Hanuschik R.W. and Dachs J. *A&A*, 182, L29 (1987). [107](#)
- Hardie R.H. and Ballard C.M. *PASP*, 74, 242 (1962). [74](#)
- Hartigan P., Edwards S. and Pierson R. *ApJ*, 609, 261 (2004). [227](#), [228](#)
- Harutyunyan A.H., Pfahler P., Pastorello A. et al. *A&A*, 488, 383 (2008). [92](#)
- Hashimoto M., Iwamoto K. and Nomoto K. *ApJL*, 414, L105 (1993). [33](#)
- Hauschildt P.H. and Baron E. *Journal of Computational and Applied Mathematics*, 109, 41 (1999). [41](#)
- Heger A., Fryer C.L., Woosley S.E., Langer N. and Hartmann D.H. *ApJ*, 591, 288 (2003). [xxxix](#), [43](#), [44](#), [92](#), [137](#), [138](#), [176](#), [177](#)
- Hendry M.A., Smartt S.J., Crockett R.M. et al. *MNRAS*, 369, 1303 (2006). [127](#)
- Hendry M.A., Smartt S.J., Maund J.R. et al. *MNRAS*, 359, 906 (2005). [166](#), [175](#), [176](#)
- Hirata K., Kajita T., Koshiha M., Nakahata M. and Oyama Y. *Physical Review Letters*, 58, 1490 (1987). [21](#)
- Hirst P., Casali M., Adamson A., Ives D. and Kerr T. *Society of Photo-Optical Instrumentation Engineers (SPIE) Conference Series*, volume 6269 of *Society of Photo-Optical Instrumentation Engineers (SPIE) Conference Series* (2006). [62](#), [192](#)
- Hodapp K.W., Kaiser N., Aussel H. et al. *Astronomische Nachrichten*, 325, 636 (2004). [15](#)

## BIBLIOGRAPHY

---

- Höflich P., Straniero O., Limongi M., Dominguez I. and Chieffi A. Cantó J. and Rodríguez L.F., (eds.) *Revista Mexicana de Astronomia y Astrofisica Conference Series*, volume 10 of *Revista Mexicana de Astronomia y Astrofisica*, vol. 27, 157–162 (2001). [133](#)
- Högbom J.A. *A&AS*, 15, 417 (1974). [90](#)
- Horne K. *PASP*, 98, 609 (1986). [77](#), [194](#)
- Horváth I. *ApJ*, 508, 757 (1998). [50](#)
- Horváth I., Balázs L.G., Bagoly Z., Ryde F. and Mészáros A. *A&A*, 447, 23 (2006). [50](#)
- Houck J.C. and Fransson C. *ApJ*, 456, 811 (1996). [223](#)
- Howell S.B. *Handbook of CCD astronomy* (Cambridge University Press, 2006). [63](#)
- Hoyle F. and Fowler W.A. *ApJ*, 132, 565 (1960). [18](#)
- Immler S., Brown P.J., Milne P. et al. *ApJ*, 664, 435 (2007). [173](#)
- Immler S., Milne P. and Pooley D. *The Astronomer’s Telegram*, 3012, 1 (2010). [245](#)
- Ivezic Z., Axelrod T., Brandt W.N. et al. *Serbian Astronomical Journal*, 176, 1 (2008). [15](#)
- Iwakami W., Kotake K., Ohnishi N., Yamada S. and Sawada K. *ApJ*, 678, 1207 (2008). [281](#)
- Jahoda K., Swank J.H., Giles A.B. et al. Siegmund O.H. and Gummin M.A., (eds.) *Society of Photo-Optical Instrumentation Engineers (SPIE) Conference Series*, volume 2808 of *Society of Photo-Optical Instrumentation Engineers (SPIE) Conference Series*, 59–70 (1996). [15](#)
- James P.A. and Anderson J.P. *A&A*, 453, 57 (2006). [128](#)
- Janka H.T. Giovannelli F. and Mannocchi G., (eds.) *Frontier Objects in Astrophysics and Particle Physics*, 345 (1993). [18](#)

- Janka H.T. and Mueller E. *A&A*, 306, 167 (1996). [281](#)
- Janka H.T. and Müller E. Suzuki Y. and Nakamura K., (eds.) *Frontiers of Neutrino Astrophysics*, 203–217 (1993). [18](#)
- Jeffery D.J. *ArXiv Astrophysics e-prints* (1999). [33](#), [35](#)
- Jester S., Schneider D.P., Richards G.T. et al. *AJ*, 130, 873 (2005). [250](#), [252](#), [253](#), [258](#), [259](#)
- Kann D.A., Klose S., Zhang B. et al. *ApJ*, 720, 1513 (2010). [50](#)
- Kasliwal M.M. *Bulletin of the Astronomical Society of India*, 39, 375 (2011). [xxix](#), [4](#)
- Kawabata K.S., Tanaka M., Maeda K. et al. *ApJ*, 697, 747 (2009). [267](#)
- Kelly P.L., Kirshner R.P. and Pahre M. *ApJ*, 687, 1201 (2008). [128](#)
- Kirshner R.P. and Kwan J. *ApJ*, 193, 27 (1974). [205](#)
- Klebesadel R.W., Strong I.B. and Olson R.A. *ApJL*, 182, L85 (1973). [49](#)
- Kleiser I.K.W., Poznanski D., Kasen D. et al. *MNRAS*, 415, 372 (2011). [279](#)
- Kong X., Cheng F.Z., Weiss A. and Charlot S. *A&A*, 396, 503 (2002). [212](#)
- Kouveliotou C., Meegan C.A., Fishman G.J. et al. *ApJL*, 413, L101 (1993). [49](#)
- Kulkarni S.R., Ofek E.O., Rau A. et al. *Nature*, 447, 458 (2007). [4](#)
- Kumar B., Sagar R., Rautela B.S., Srivastava J.B. and Srivastava R.K. *Bulletin of the Astronomical Society of India*, 28, 675 (2000). [97](#), [190](#), [247](#), [256](#)
- Landau L.D. and Lifshitz E.M. *Fluid mechanics* (Oxford: Pergamon Press, 1959). [20](#)
- Landolt A.U. *AJ*, 104, 340 (1992). [75](#), [189](#), [247](#), [256](#)
- Landolt A.U. *AJ*, 137, 4186 (2009). [96](#), [142](#)

## BIBLIOGRAPHY

---

- Leaman J.F., Li W., Filippenko A. and LOSS. American Astronomical Society Meeting Abstracts 214, volume 214 of American Astronomical Society Meeting Abstracts, 316 (2009). [13](#)
- Leloudas G., Stritzinger M.D., Sollerman J. et al. *A&A*, 505, 265 (2009). [215](#)
- Lennarz D., Altmann D. and Wiebusch C. *A&A*, 538, A120 (2012). [xxix](#), [14](#), [15](#)
- Leonard D.C., Filippenko A.V., Gates E.L. et al. *PASP*, 114, 35 (2002a). [xxxv](#), [30](#), [97](#), [100](#), [105](#), [153](#), [158](#)
- Leonard D.C., Filippenko A.V., Li W. et al. *AJ*, 124, 2490 (2002b). [205](#)
- Li W., Leaman J., Chornock R. et al. *MNRAS*, 412, 1441 (2011). [xxix](#), [14](#)
- Li W., Van Dyk S.D., Filippenko A.V. and Cuillandre J.C. *PASP*, 117, 121 (2005). [105](#)
- Litvinova I.Y. and Nadezhin D.K. *Soviet Astronomy Letters*, 11, 145 (1985). [33](#), [34](#), [130](#), [172](#), [179](#), [275](#)
- Lucy L.B., Danziger I.J., Gouiffes C. and Bouchet P. Tenorio-Tagle G., Moles M. and Melnick J., (eds.) *IAU Colloq. 120: Structure and Dynamics of the Interstellar Medium*, volume 350 of *Lecture Notes in Physics*, Berlin Springer Verlag, 164 (1989). [220](#)
- Lucy L.B., Danziger I.J., Gouiffes C. and Bouchet P. Woosley S.E., (ed.) *Supernovae*, 82 (1991). [110](#)
- Maeda K., Benetti S., Stritzinger M. et al. *Nature*, 466, 82 (2010a). [217](#)
- Maeda K., Kawabata K., Mazzali P.A. et al. *Science*, 319, 1220 (2008). [222](#), [224](#), [225](#)
- Maeda K., Leloudas G., Taubenberger S. et al. *MNRAS*, 413, 3075 (2011). [217](#)
- Maeda K., Mazzali P.A., Deng J. et al. *ApJ*, 593, 931 (2003). [33](#), [35](#), [38](#), [230](#), [231](#)
- Maeda K., Taubenberger S., Sollerman J. et al. *ApJ*, 708, 1703 (2010b). [217](#)

- Maguire K., di Carlo E., Smartt S.J. et al. *MNRAS*, 404, 981 (2010). [166](#), [175](#)
- Malesani D., Fynbo J.P.U., Hjorth J. et al. *ApJL*, 692, L84 (2009). [xxxvi](#), [189](#), [190](#), [198](#), [199](#), [201](#), [213](#)
- Martin D.C., Fanson J., Schiminovich D. et al. *ApJL*, 619, L1 (2005). [15](#)
- Massey P., Strobel K., Barnes J.V. and Anderson E. *ApJ*, 328, 315 (1988). [77](#)
- Matheson T., Filippenko A.V., Barth A.J. et al. *AJ*, 120, 1487 (2000). [107](#)
- Matheson T., Garnavich P.M., Stanek K.Z. et al. *ApJ*, 599, 394 (2003). [50](#)
- Maund J.R. and Smartt S.J. *MNRAS*, 360, 288 (2005). [138](#)
- Maund J.R., Smartt S.J. and Danziger I.J. *MNRAS*, 364, L33 (2005). [138](#)
- Maund J.R., Wheeler J.C., Baade D. et al. *ApJ*, 705, 1139 (2009). [212](#), [281](#)
- Mazzali P.A., Valenti S., Della Valle M. et al. *Science*, 321, 1185 (2008). [xxxvi](#), [23](#), [31](#), [198](#), [199](#)
- McCray R., Shull J.M. and Sutherland P. *ApJL*, 317, L73 (1987). [32](#)
- Mészáros P. *ARA&A*, 40, 137 (2002). [50](#)
- Milisavljevic D., Fesen R.A., Gerardy C.L., Kirshner R.P. and Challis P. *ApJ*, 709, 1343 (2010). [193](#), [194](#), [217](#), [222](#), [223](#), [224](#), [225](#)
- Miller A.A., Chornock R., Perley D.A. et al. *ApJ*, 690, 1303 (2009). [244](#)
- Miller A.A., Smith N., Li W. et al. *AJ*, 139, 2218 (2010). [267](#)
- Minkowski R. *PASP*, 53, 224 (1941). [6](#)
- Misra K., Bhattacharya D., Sahu D.K. et al. *A&A*, 464, 903 (2007a). [213](#)
- Misra K., Fruchter A.S. and Nugent P. McEnery J.E., Racusin J.L. and Gehrels N., (eds.) American Institute of Physics Conference Series, volume 1358 of American Institute of Physics Conference Series, 299–302 (2011). [209](#)

## BIBLIOGRAPHY

---

- Misra K., Pooley D., Chandra P. et al. MNRAS, 381, 280 (2007b). [xxxv](#), [97](#), [124](#), [133](#), [156](#), [168](#), [173](#), [176](#)
- Modjaz M., Chornock R., Foley R.J. et al. GRB Coordinates Network, 7212, 1 (2008a). [183](#)
- Modjaz M., Kirshner R.P., Blondin S., Challis P. and Matheson T. ApJL, 687, L9 (2008b). [217](#), [222](#), [224](#), [226](#)
- Modjaz M., Li W., Butler N. et al. ApJ, 702, 226 (2009). [xxxvi](#), [198](#), [199](#)
- Moriya T.J., Blinnikov S.I., Tominaga N. et al. MNRAS, 132 (2012). [267](#)
- Moskvitin A.S., Fatkhullin T.A., Sokolov V.V. et al. Astrophysical Bulletin, 65, 230 (2010). [116](#)
- Mukherjee S., Feigelson E.D., Jogesh Babu G. et al. ApJ, 508, 314 (1998). [50](#)
- Müller E. Bludman S.A., Mochkovitch R. and Zinn-Justin J., (eds.) Supernovae, 393 (1994). [18](#)
- Myra E.S. and Bludman S.A. ApJ, 340, 384 (1989). [18](#), [21](#)
- Nadezhin D.K. Ap&SS, 112, 225 (1985). [xxx](#), [23](#), [25](#), [26](#)
- Nadyozhin D.K. MNRAS, 346, 97 (2003). [xxx](#), [34](#), [130](#), [137](#)
- Nakano S., Kadota K., Itagaki K. and Corelli P. Central Bureau Electronic Telegrams, 1191, 1 (2008a). [182](#), [184](#)
- Nakano S., Kadota K. and Wells W. Central Bureau Electronic Telegrams, 1636, 1 (2008b). [94](#)
- Nakano S., Kadota K. and Wells W. Central Bureau Electronic Telegrams, 1636, 1 (2008c). [139](#), [151](#)
- Nakano S. and Martin R. Central Bureau Electronic Telegrams, 1566, 1 (2008). [92](#), [97](#)
- Narayan R., Paczynski B. and Piran T. ApJL, 395, L83 (1992). [50](#)

- Newton J. and Puckett T. Central Bureau Electronic Telegrams, 2532, 1 (2010). [245](#), [253](#)
- Nomoto K. and Hashimoto M. Phys. Rep., 163, 13 (1988). [23](#)
- Nomoto K., Hashimoto M., Arai K. and Kaminisi K. Kubono S., Ishihara M. and Nomura T., (eds.) Heavy Ion Physics and Nuclear Astrophysical Problems, 9 (1989). [23](#)
- Nomoto K. and Sugimoto D. Progress of Theoretical Physics, 48, 46 (1972). [23](#)
- Nozawa T., Maeda K., Kozasa T. et al. ApJ, 736, 45 (2011). [208](#)
- Olivares E. F., Greiner J., Schady P. et al. A&A, 539, A76 (2012). [23](#), [31](#), [181](#), [231](#), [232](#)
- Olivares E. F., Hamuy M., Pignata G. et al. ApJ, 715, 833 (2010). [92](#), [99](#), [153](#)
- Osterbrock D.E. Astrophysics of gaseous nebulae and active galactic nuclei (University Science Books, 1989). [211](#)
- Ostriker J.P. and McKee C.F. Reviews of Modern Physics, 60, 1 (1988). [26](#)
- Panagia N. Weiler K., (ed.) Supernovae and Gamma-Ray Bursters, volume 598 of Lecture Notes in Physics, Berlin Springer Verlag, 113–144 (2003). [205](#)
- Pandey S.B., Anupama G.C., Sagar R. et al. MNRAS, 340, 375 (2003). [199](#), [201](#), [208](#)
- Pastorello A., Baron E., Branch D. et al. MNRAS, 360, 950 (2005). [xxxv](#), [92](#), [96](#), [105](#), [107](#), [156](#), [176](#), [279](#)
- Pastorello A., Pumo M.L., Navasardyan H. et al. A&A, 537, A141 (2012). [279](#)
- Pastorello A., Sauer D., Taubenberger S. et al. MNRAS, 370, 1752 (2006). [23](#), [175](#)
- Pastorello A., Smartt S.J., Botticella M.T. et al. ApJL, 724, L16 (2010). [4](#), [48](#), [244](#)
- Pastorello A., Valenti S., Zampieri L. et al. MNRAS, 394, 2266 (2009). [xxxiv](#), [xxxv](#), [107](#), [138](#), [149](#), [150](#), [152](#), [156](#), [157](#), [160](#), [166](#), [168](#), [172](#), [175](#), [176](#), [206](#)

## BIBLIOGRAPHY

---

- Pastorello A., Zampieri L., Turatto M. et al. MNRAS, 347, 74 (2004). [xxxv](#), [13](#), [107](#), [109](#), [124](#), [138](#), [153](#), [157](#), [158](#)
- Patat F., Cappellaro E., Danziger J. et al. ApJ, 555, 900 (2001). [209](#)
- Patat F., Taubenberger S., Benetti S., Pastorello A. and Harutyunyan A. A&A, 527, L6 (2011). [245](#)
- Pignata G., Stritzinger M., Soderberg A. et al. ApJ, 728, 14 (2011). [231](#)
- Pilyugin L.S., Vílchez J.M. and Contini T. A&A, 425, 849 (2004). [128](#), [176](#)
- Pinto P.A. and Eastman R.G. ApJ, 530, 744 (2000). [30](#)
- Pinto P.A. and Woosley S.E. ApJ, 329, 820 (1988). [32](#)
- Piran T. Phys. Rep., 314, 575 (1999). [50](#)
- Piran T. Nuovo Cimento C Geophysics Space Physics C, 28, 373 (2005). [50](#)
- Poole T.S., Breeveld A.A., Page M.J. et al. MNRAS, 383, 627 (2008). [79](#), [80](#), [141](#), [186](#)
- Pooley D. and Soderberg A. The Astronomer's Telegram, 1368, 1 (2008). [183](#)
- Popov D.V. ApJ, 414, 712 (1993). [130](#)
- Portegies Zwart S.F. and van den Heuvel E.P.J. Nature, 450, 388 (2007). [48](#)
- Poznanski D., Butler N., Filippenko A.V. et al. ApJ, 694, 1067 (2009). [92](#)
- Poznanski D., Prochaska J.X. and Bloom J.S. ArXiv e-prints (2012). [211](#)
- Prabhu T.P., Mayya Y.D., Singh K.P. et al. A&A, 295, 403 (1995). [23](#)
- Press W.H., Teukolsky S.A., Vetterling W.T. and Flannery B.P. Numerical recipes in C. The art of scientific computing (Cambridge: University Press, 1992). [151](#)
- Priest E.R. Solar magneto-hydrodynamics (D. Reidel Publishing Company, 1984). [2](#)

- Pumo M.L. and Zampieri L. *ApJ*, 741, 41 (2011). [33](#)
- Quimby R.M., Aldering G., Wheeler J.C. et al. *ApJL*, 668, L99 (2007a). [48](#), [244](#)
- Quimby R.M., Wheeler J.C., Höflich P. et al. *ApJ*, 666, 1093 (2007b). [140](#), [149](#), [151](#)
- Rakavy G. and Shaviv G. *ApJ*, 148, 803 (1967). [47](#)
- Rau A., Kulkarni S.R., Law N.M. et al. *PASP*, 121, 1334 (2009). [13](#)
- Rees M.J. and Meszaros P. *ApJL*, 430, L93 (1994). [50](#)
- Richmond M.W., Treffers R.R., Filippenko A.V. et al. *AJ*, 107, 1022 (1994). [121](#), [165](#), [211](#)
- Ripero J., Garcia F., Rodriguez D. et al. *IAU Circ.*, 5731, 1 (1993). [23](#)
- Roming P., Pritchard T., Brown P. et al. American Astronomical Society Meeting Abstracts 215, volume 42 of Bulletin of the American Astronomical Society, 342.03 (2010). [23](#)
- Roming P.W.A., Kennedy T.E., Mason K.O. et al. *Space Sci. Rev.*, 120, 95 (2005). [140](#)
- Roy R., Kumar B., Benetti S. et al. *ApJ*, 736, 76 (2011a). [23](#), [140](#), [142](#), [206](#), [211](#)
- Roy R., Kumar B., Moskvitin A.S. et al. *MNRAS*, 414, 167 (2011b). [xxxv](#), [96](#), [156](#), [160](#), [168](#), [173](#), [176](#), [206](#), [211](#)
- Sahu D.K., Anupama G.C., Srividya S. and Muneer S. *MNRAS*, 372, 1315 (2006). [xxxv](#), [97](#), [100](#), [105](#), [109](#), [117](#), [122](#), [160](#), [163](#), [166](#), [173](#), [175](#), [176](#)
- Sari R., Piran T. and Narayan R. *ApJL*, 497, L17 (1998). [43](#), [234](#)
- Schawinski K., Justham S., Wolf C. et al. *Science*, 321, 223 (2008). [23](#), [30](#), [149](#), [152](#)
- Schlegel D.J., Finkbeiner D.P. and Davis M. *ApJ*, 500, 525 (1998). [121](#), [164](#), [201](#), [210](#), [266](#)
- Sedov L.I. *Similarity and Dimensional Methods in Mechanics* (Academic Press, 1959). [26](#)

## BIBLIOGRAPHY

---

- Sesar B., Ivezić Ž., Lupton R.H. et al. *AJ*, 134, 2236 (2007). [254](#)
- Shigeyama T., Nomoto K. and Hashimoto M. *A&A*, 196, 141 (1988). [32](#)
- Shigeyama T., Nomoto K., Tsujimoto T. and Hashimoto M.A. *ApJL*, 361, L23 (1990). [226](#)
- Shu F.H. *The physical universe. an introduction to astronomy* (University Science Books, 1982). [4](#), [24](#)
- Silvestri N.M., Balonek T.J., Wells L.A. et al. American Astronomical Society Meeting Abstracts, volume 26 of *Bulletin of the American Astronomical Society*, 1444 (1994). [23](#)
- Sivaram C. ArXiv e-prints (2007). [2](#)
- Smartt S.J. *ARA&A*, 47, 63 (2009). [92](#), [280](#)
- Smartt S.J., Eldridge J.J., Crockett R.M. and Maund J.R. *MNRAS*, 395, 1409 (2009). [91](#), [131](#), [137](#), [172](#), [176](#), [177](#)
- Smartt S.J., Wright D., Valenti S. et al. *The Astronomer's Telegram*, 3918, 1 (2012). [4](#)
- Smith N., Foley R.J. and Filippenko A.V. *ApJ*, 680, 568 (2008). [208](#)
- Smith N., Li W., Filippenko A.V. and Chornock R. *MNRAS*, 412, 1522 (2011a). [91](#), [178](#), [181](#), [281](#)
- Smith N., Li W., Foley R.J. et al. *ApJ*, 666, 1116 (2007). [267](#), [271](#)
- Smith N., Li W., Miller A.A. et al. *ApJ*, 732, 63 (2011b). [245](#), [267](#)
- Smith N., Mauerhan J.C., Silverman J.M. et al. *MNRAS*, 426, 1905 (2012). [240](#)
- Smith N. and McCray R. *ApJL*, 671, L17 (2007). [267](#)
- Soderberg A. *The Astronomer's Telegram*, 1350, 1 (2008). [182](#), [194](#)
- Soderberg A.M., Berger E., Page K.L. et al. *Nature*, 453, 469 (2008). [23](#), [30](#), [31](#), [183](#)

- Soker N. and Kashi A. ArXiv e-prints (2011). [xxix](#), [4](#)
- Sonbas E., Moskvitin A.S., Fatkhullin T.A. et al. *Astrophysical Bulletin*, 63, 228 (2008). [23](#), [116](#), [181](#)
- Spyromilio J. *MNRAS*, 253, 25P (1991). [110](#)
- Spyromilio J. *MNRAS*, 266, L61 (1994). [223](#)
- Stetson P.B. *PASP*, 99, 191 (1987). [67](#), [247](#)
- Stetson P.B. Worrall D.M., Biemesderfer C. and Barnes J., (eds.) *Astronomical Data Analysis Software and Systems I*, volume 25 of *Astronomical Society of the Pacific Conference Series*, 297 (1992a). [256](#)
- Stetson P.B. *J. R. Astron. Soc. Canada*, 86, 71 (1992b). [96](#)
- Stetson P.B., Davis L.E. and Crabtree D.R. Jacoby G.H., (ed.) *CCDs in astronomy*, volume 8 of *Astronomical Society of the Pacific Conference Series*, 289–304 (1990). [70](#), [72](#)
- Stockdale C.J., Weiler K.W., Immler S. et al. *The Astronomer's Telegram*, 1883, 1 (2008). [139](#)
- Stockdale C.J., Weiler K.W., Immler S. et al. *The Astronomer's Telegram*, 1912, 1 (2009). [139](#)
- Stoll R., Prieto J.L., Stanek K.Z. et al. *ApJ*, 730, 34 (2011). [xxxvii](#), [251](#), [253](#)
- Stritzinger M. *Central Bureau Electronic Telegrams*, 1638, 3 (2008). [139](#)
- Suntzeff N.B. and Bouchet P. *AJ*, 99, 650 (1990). [122](#), [166](#)
- Suntzeff N.B., Hamuy M., Martin G., Gomez A. and Gonzalez R. *AJ*, 96, 1864 (1988). [99](#)
- Sutherland P.G. and Wheeler J.C. *ApJ*, 280, 282 (1984). [36](#), [231](#)
- Takiwaki T., Kotake K., Nagataki S. and Sato K. *ApJ*, 616, 1086 (2004). [281](#)

## BIBLIOGRAPHY

---

- Taubenberger S., Valenti S., Benetti S. et al. MNRAS, 397, 677 (2009). [110](#), [222](#)
- Terry J.N., Patrel G. and Ekholm T. A&A, 393, 57 (2002). [120](#), [165](#), [209](#)
- Thompson A.R., Clark B.G., Wade C.M. and Napier P.J. ApJS, 44, 151 (1980). [80](#)
- Thöne C.C., Michałowski M.J., Leloudas G. et al. ApJ, 698, 1307 (2009). [182](#), [204](#), [210](#), [211](#)
- Todini P. and Ferrara A. MNRAS, 325, 726 (2001). [280](#)
- Tominaga N., Blinnikov S., Baklanov P. et al. ApJL, 705, L10 (2009). [31](#), [149](#), [152](#)
- Tominaga N., Morokuma T., Blinnikov S.I. et al. ApJS, 193, 20 (2011). [31](#)
- Tsvetkov D.Y., Volkov I.M., Sorokina E. et al. Peremennye Zvezdy, 32, 6 (2012). [23](#)
- Turatto M. Weiler K., (ed.) Supernovae and Gamma-Ray Bursters, volume 598 of Lecture Notes in Physics, Berlin Springer Verlag, 21–36 (2003). [xxix](#), [7](#), [12](#)
- Turatto M., Benetti S. and Cappellaro E. Hillebrandt W. and Leibundgut B., (eds.) From Twilight to Highlight: The Physics of Supernovae, 200 (2003). [121](#), [165](#), [211](#)
- Turatto M., Cappellaro E., Benetti S. and Danziger I.J. MNRAS, 265, 471 (1993). [107](#)
- Turatto M., Mazzali P.A., Young T.R. et al. ApJL, 498, L129 (1998). [13](#), [109](#), [138](#), [154](#), [175](#), [176](#), [278](#)
- Ueno S., Matsuoka M., Kawasaki K. et al. Society of Photo-Optical Instrumentation Engineers (SPIE) Conference Series, volume 7011 of Society of Photo-Optical Instrumentation Engineers (SPIE) Conference Series (2008). [15](#)
- Utrobin V., Chugai N., Müller E. and Hillebrandt W. Progenitors and Environments of Stellar Explosions (2010). [138](#)
- Utrobin V.P. A&A, 461, 233 (2007). [117](#), [172](#), [206](#)
- Utrobin V.P. and Chugai N.N. A&A, 491, 507 (2008). [172](#), [176](#)

- Utrobin V.P. and Chugai N.N. *A&A*, 506, 829 (2009). [117](#)
- Utrobin V.P. and Chugai N.N. *A&A*, 532, A100 (2011). [12](#), [279](#)
- Šimon V., Pizzichini G. and Hudec R. *A&A*, 523, A56 (2010). [204](#), [205](#)
- Valenti S., Benetti S., Cappellaro E. et al. *MNRAS*, 383, 1485 (2008a). [33](#), [35](#), [208](#), [230](#), [231](#), [232](#), [242](#)
- Valenti S., Fraser M., Benetti S. et al. *MNRAS*, 416, 3138 (2011). [217](#), [225](#), [231](#)
- Valenti S., Fugazza D., Maiorano E. et al. *Central Bureau Electronic Telegrams*, 1205, 2 (2008b). [183](#)
- van der Horst A.J., Kamble A.P., Paragi Z. et al. *ApJ*, 726, 99 (2011). [xxxvii](#), [195](#), [234](#), [235](#), [237](#)
- van Dokkum P.G. *PASP*, 113, 1420 (2001). [77](#), [193](#)
- Van Dyk S.D., Davidge T.J., Elias-Rosa N. et al. *AJ*, 143, 19 (2012). [138](#)
- Vinkó J., Blake R.M., Sárneczky K. et al. *A&A*, 427, 453 (2004). [206](#), [208](#)
- Vinkó J., Takáts K., Sárneczky K. et al. *MNRAS*, 369, 1780 (2006). [175](#), [176](#)
- Vinko J., Zheng W., Pandey S.B. et al. *American Astronomical Society Meeting Abstracts 219*, volume 219 of *American Astronomical Society Meeting Abstracts*, 436 (2012). [4](#), [48](#), [244](#), [261](#), [266](#), [267](#), [271](#), [279](#)
- Vinko J., Zheng W., Romadan A. et al. *Central Bureau Electronic Telegrams*, 2556, 1 (2010). [261](#)
- Vollmann K. and Eversberg T. *Astronomische Nachrichten*, 327, 862 (2006). [121](#), [165](#)
- Wagoner R.V. Rees M.J. and Stoneham R.J., (eds.) *NATO ASIC Proc. 90: Supernovae: A Survey of Current Research*, 253–266 (1982). [29](#)
- Waldman R. *ApJ*, 685, 1103 (2008). [48](#)

## BIBLIOGRAPHY

---

- Wang L. and Hu J. *Nature*, 369, 380 (1994). [220](#), [222](#), [223](#)
- Waxman E., Mészáros P. and Campana S. *ApJ*, 667, 351 (2007). [149](#)
- Weaver H.A., A’Hearn M.F., Arpigny C. et al. *Science*, 267, 1282 (1995). [2](#)
- Weaver T.A. and Woosley S.E. *Phys. Rep.*, 227, 65 (1993). [33](#)
- Weiler K., (Ed.). *Supernovae and Gamma-Ray Bursters*, volume 598 of *Lecture Notes in Physics*, Berlin Springer Verlag (2003). [2](#)
- Weiler K.W., Panagia N. and Montes M.J. *ApJ*, 562, 670 (2001). [239](#)
- Weiler K.W., Panagia N., Montes M.J. and Sramek R.A. *ARA&A*, 40, 387 (2002). [xxxi](#), [42](#), [140](#), [220](#), [239](#)
- Weiler K.W., Panagia N. and Sramek R.A. *ApJ*, 364, 611 (1990). [234](#), [235](#)
- Weiler K.W., Panagia N., Stockdale C. et al. *ApJ*, 740, 79 (2011). [235](#), [239](#), [240](#)
- Weiler K.W., Sramek R.A., Panagia N., van der Hulst J.M. and Salvati M. *ApJ*, 301, 790 (1986). [43](#), [234](#), [235](#)
- Whalen D.J., Even W., Frey L.H. et al. *ArXiv e-prints* (2012). [4](#)
- Wijers R.A.M.J. and Galama T.J. *ApJ*, 523, 177 (1999). [43](#), [234](#)
- Willis A.J. *Ap&SS*, 237, 145 (1996). [240](#)
- Wilson J.R. *Energy Technology Review*, 12–19 (1983). [18](#)
- Woosley S.E. Nomoto K., (ed.) *IAU Colloq. 108: Atmospheric Diagnostics of Stellar Evolution*, volume 305 of *Lecture Notes in Physics*, Berlin Springer Verlag, 361 (1988). [16](#)
- Woosley S.E. *ApJ*, 405, 273 (1993). [33](#)
- Woosley S.E. *ApJL*, 719, L204 (2010). [47](#), [271](#)
- Woosley S.E., Blinnikov S. and Heger A. *Nature*, 450, 390 (2007). [48](#)

- Woosley S.E., Eastman R.G. and Schmidt B.P. *ApJ*, 516, 788 (1999a). [205](#)
- Woosley S.E., Eastman R.G., Weaver T.A. and Pinto P.A. *ApJ*, 429, 300 (1994). [33](#)
- Woosley S.E., Heger A. and Weaver T.A. *Reviews of Modern Physics*, 74, 1015 (2002). [16](#)
- Woosley S.E., MacFadyen A.I. and Heger A. *ArXiv Astrophysics e-prints* (1999b). [200](#)
- Yoon S.C., Gräfener G., Vink J.S., Kozyreva A. and Izzard R.G. *A&A*, 544, L11 (2012). [240](#)
- Yoshii Y., Tomita H., Kobayashi Y. et al. *ApJ*, 592, 467 (2003). [199](#)
- Young D.R., Smartt S.J., Valenti S. et al. *A&A*, 512, A70 (2010). [244](#)
- Yuan F. Chasing the brightest cosmic explosions with ROTSE-III. Ph.D. thesis, University of Michigan (2010). [140](#)
- Zampieri L., Pastorello A., Turatto M. et al. *MNRAS*, 338, 711 (2003). [138](#), [176](#)
- Zampieri L., Shapiro S.L. and Colpi M. *ApJL*, 502, L149+ (1998). [138](#), [278](#)
- Zerbi F.M., Chincarini G., Ghisellini G. et al. Moorwood A.F.M. and Iye M., (eds.) *Society of Photo-Optical Instrumentation Engineers (SPIE) Conference Series*, volume 5492 of *Society of Photo-Optical Instrumentation Engineers (SPIE) Conference Series*, 1590–1601 (2004). [62](#), [142](#)
- Zhang T., Wang X., Wu C. et al. *AJ*, 144, 131 (2012). [245](#), [266](#), [267](#), [269](#)